Static and Dynamic Effects of Sterically Demanding Ligands

Sarah L. Hinchley

A thesis presented for the degree of
Doctor of Philosophy
in the Faculty of Science at the
University of Edinburgh, 2000

To Mum

For her love, support and never ending faith in me

Declaration

This thesis has not been submitted, in whole or in part, for any degree at this or any other university. The work is original and my own, carried out under the direction of Prof. D. W. H. Rankin; where this is not so credit has been duly given.

Acknowledgements

Firstly I must thank my supervisor, David Rankin, for his constant help, advice, encouragement, support and grammatical corrections over the last three years. Without his boundless enthusiasm, none of this would have been possible.

I also need to thank Drs. Bruce Smart, Paul Brain, Heather Robertson and Carole Morrison for all their help, guidance, patience and data collection. Although Bruce and Paul are no longer part of our group, their legacy lives on. Thanks are also due to Drs. Simon Parsons and Bob Coxall for trying to teach me crystallography, and for collection of data.

A lot of thank you's are directed around the chemistry department, firstly to Blair and Frank for making 106 a great place to work, to Mary, Mandy and Marie, for their hospitality and nights in the Subway. I must also thank Steve, Bob, Pammie and Elsp, again for nights in the Subway, Hilary, for nights in the Subway, and to Al, for being a fantastic vice-president and for nights in the Subway!

Many inorganic thanks to (organic) Mark and Dave (the dynamic duo) and Sander for being shoulders to whinge on when needed, and for all the laughs. I must thank Gareth, for all his encouragement and Friday afternoon humour, keeping my chin up and for telling me to get on with it.

Finally I must thank the University of Edinburgh for funding my research, and everyone in room 106 for putting up with me.

Abstract

This thesis is concerned with the determination of the gas-phase structures of large, asymmetric, sterically crowded molecules, with bulky alkyl ligands. Gas-phase electron diffraction is the best fluid phase technique available for the determination of structure. However, the many assumptions needed to refine these sterically encumbered molecules made complete structural determination impossible. In these cases, other fluid phase experimental data are called upon to fill in the structural detail, the main ones being liquid crystal nuclear magnetic resonance (LCNMR) and microwave spectroscopy. However, for the kind of systems under study in this thesis, it is not possible to collect data from these types of experiment.

The combination of gas-phase electron diffraction data and *ab initio* calculations, called the SARACEN method, has overcome these problems. It has opened up the possibility of studying compounds previously beyond our capabilities. Advances in computational power mean that we can now calculate the structures of larger molecules with ~ 70 atoms to reasonable accuracy, and that our computers can now refine experimental structures up to 100 atoms in size.

Previously, the SARACEN method has been applied to smaller systems of ~20 atoms. In this thesis, the method has been applied to much larger systems and many interesting features of the ligands, the effects they have on each other and the overall structures of molecules have been revealed. A series of disilanes with increasing steric bulk have been studied: 1,2-di-*tert*-butyltetrachlorodisilane, 1,1,2-tri-*tert*-butyldisilane, and 1,1,2,2-tetra-*tert*-butyldisilane. The structural results are surprising. The three-coordinate systems of tri(*tert*-butyl)sulfurtriimide and bis(trichlorosilyl)*tert*-butylphosphine have also been studied. Finally, the very unusual bis[bis(trimethylsilyl)methyl]phosphine and arsine radicals and the related dimers in the crystalline phase have been studied. Detailed analysis of the steric crowding of the solid structures has revealed the interesting new concept of ligands as energy reservoirs, which facilitate bond dissociation in the dimer.

Contents

List of Abbreviations Used

pm	picometer
mm	millimeter
nm	nanometer
Å	angstrom unit (10^{-10} m)
λ	wavelength
h	Planck's constant
p	momentum
kV	kilovolt
Z	atomic number
E	energy
Ψ	wavefunction
H	Hamiltonian
HF	Hartree-Fock
MP	Møller-Plesset perturbation series
DFT	density functional theory
MM	molecular mechanics
ECP	effective core potential
DZ	double zeta (ξ)
GED	gas-phase electron diffraction
SARACEN	strcuture analysis restrained by *ab initio* calculations for electron diffraction
DYNAMITE	dymanic interaction of theory and experiment
Gb	gigabyte
p_x	parameter
u	root mean square amplitude of vibration
k	perpendicular amplitude of vibration
K	Kelvin
NCA	normal coordinate analysis
PED	potential energy distribution
PES	potential energy surface
IR	infrared

Chapter 1

Introduction.

1.1 General Introduction

Chemists have always been interested in the structure of molecules. The ways that atoms connect to form molecules determine the very chemical and physical properties of those molecules. But the meaning of the word structure has changed greatly over the last century or so. Initially, chemists were concerned with the elemental composition of a compound. When it was realised that bonds held the atoms together, they wanted to know which atoms were connected to which. Nowadays, chemists would like to know the exact geometry of their compound, with accurate values for the bond lengths, angles and torsion angles. There are many techniques such as microwave spectroscopy, liquid crystal nuclear magnetic resonance, X-ray diffraction, and gas-phase electron diffraction, that can be used both in isolation and in synergy with each other to determine the geometrical structures of molecules in the solid, liquid and the gas phase.

Ideally, for accurate structural determination, molecules should be looked at in the gas phase. This is due to the fact that, in the gas phase, the molecules are free from the intramolecular interactions and packing forces that can distort the structure in the solid phase and even change the structure of the molecule completely. There are two main techniques available to the experimental chemists to study molecules in the gas-phase: rotational spectroscopy and electron diffraction. Geometrical information obtained from rotational spectroscopy is limited as the technique is really only applicable to rather small molecules, *e.g.* ring systems with up to twelve atoms. As this thesis is concerned with the determination of structures of larger molecules than can be studied satisfactorily with rotational spectroscopy, this technique can be disregarded as a source of experimental information. Gas-phase electron diffraction can be used to determine the structures of slightly larger molecules, but as will be demonstrated later, there are limitations to this technique as well. Thus we look elsewhere for information and turn to theoretical methods, which also relate to isolated molecules. *Ab initio* calculations have also until recently been restricted to smaller molecules (*ca.* 20 atoms). However, increased

computing power, for both theory and the interpretation of experimental data, has allowed the structural determination of larger (*ca.* 60 atoms), more complicated systems to be undertaken.

1.2 Theory of Electron Diffraction

The theory of electron diffraction is based on two important physical processes: (i) diffraction/interference of electromagnetic radiation and (ii) particle-wave duality theory.

1.2.1 Diffraction/Interference of Electromagnetic Radiation

In 1801, Thomas Young first demonstrated that light behaved as a wave in his classic 'Young's double slit experiment'. In his experiment, he proved that light, just like water waves, can be diffracted and show interference phenomena. The experimental set-up is shown in Figure 1.

Figure 1 Young's Double Slit Experiment

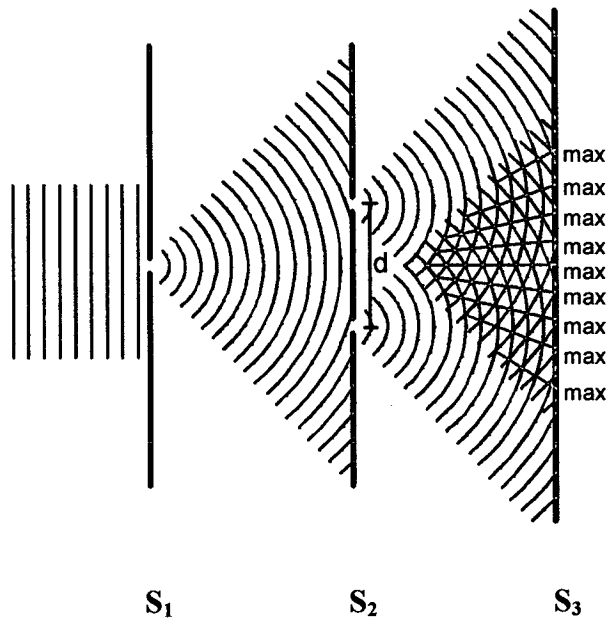

The first screen S_1 contains a narrow slit through which a wave of incident light diffracts to form a spherical wavefront that advances towards the second screen, S_2. This second screen contains two parallel slits, which cause the spherical wavefront to be diffracted, producing two identical spherical wavefronts. Both wavefronts will have the same phase since they originate from the same initial wave. The wavefronts then combine to produce an interference pattern at S_3, which consists of alternating bands of light and dark areas. The light areas arise from constructive interference, whereas the dark areas show destructive interference between the two (out-of-phase) wavefronts.

By measuring the distance between adjacent maxima (light areas) or minima (dark areas) the wavelength of the incident light can be calculated. If D is the distance between screens S_2 and S_3, and d is the slit separation on screen S_2, then the wavelength λ is given by Equation 1.1 below

$$\lambda = \frac{d\Delta_{max}}{D} \qquad 1.1$$

where Δ_{max} is the distance between adjacent maxima.

1.2.2 Wave-Particle Duality Theory

With the wave nature of light firmly established, in 1924 Louis de Broglie[1] first postulated that all moving particles will possess an associated wavelength, λ; given by Equation 1.2 below

$$\lambda = \frac{h}{p} \qquad 1.2$$

where h is Planck's constant and p is the momentum of the particle. Or, in other words, a photon of light can be thought of as existing as both a wave and a particle, and similarly, a particle, such as an electron, can also behave as a wave.

1.2.3 Diffraction of Electrons

The de Broglie hypothesis and Young's experiment can be applied to the technique of electron diffraction in the following way. When a beam of electrons is directed towards a molecule, every pair of atoms within the molecule will act like a pair of slits, in much the same way as those seen on the screen S_2. The electrons are diffracted by pairs of atoms as a result of their wave-like nature. The electrons diffracted by each pair of atoms then interfere, and the pattern produced by the summation of interference from the many molecules in the gas sample then consists of a series of concentric rings, due to the fact that the molecules in the gas are randomly orientated. This interference process occurs because the electrons have a wavelength of the order of a few picometers, which is comparable to the separation between the atoms in a molecule. Therefore, if the wavelength of the electrons is known, the distance between the atoms can be found from an analysis of the diffraction pattern obtained and hence the structure of the molecule can be determined.

1.3 The Electron Diffraction Experiment

1.3.1 Experimental Procedure

The general experimental set-up for an electron diffraction instrument is shown in Figure 2. The beam of electrons is accelerated from a cathode (a hot tungsten wire) towards an anode with an accelerating voltage of *ca.* 40 kV. The beam is then focused through a series of magnetic lenses and apertures to generate a narrow electron beam. The sample is introduced into the diffraction chamber through a fine nozzle and the beam of electrons intersects the molecular beam at right angles. The sample is then collected in a cold trap. The diffracted electrons continue through the diffraction chamber to the detector, usually a photographic plate (although this can be an electron counter), which records the scattered electron pattern. The intensity of the scattered electrons falls off as the fourth power of the scattering angle and the range of intensities is too large to be recorded on a

photographic plate. If a photographic detector is used, a rotating sector (which is cut so that the width of its opening increases as the fourth power of the distance from the centre of the sector) is placed in front of the plate, to reduce the effective exposure time towards the centre of the plate.[2] To prevent back reflection of any undiffracted electron beam, a beam stop consisting of a metal cylinder is placed at the centre of the sector. This prevents the collection of data at very small scattering angles but is necessary to avoid back scattering. Typically, data are collected at two nozzle-to-detector distances to increase the amount of structural information that can be obtained about the molecule, by widening the angular range over which the experimental data extend. Also, calibration of the apparatus (i.e. determining the wavelength of the electron beam and the camera distances) is usually performed using benzene as a standard, as the structure of this is known accurately.

Figure 2 Typical Electron Diffraction Apparatus

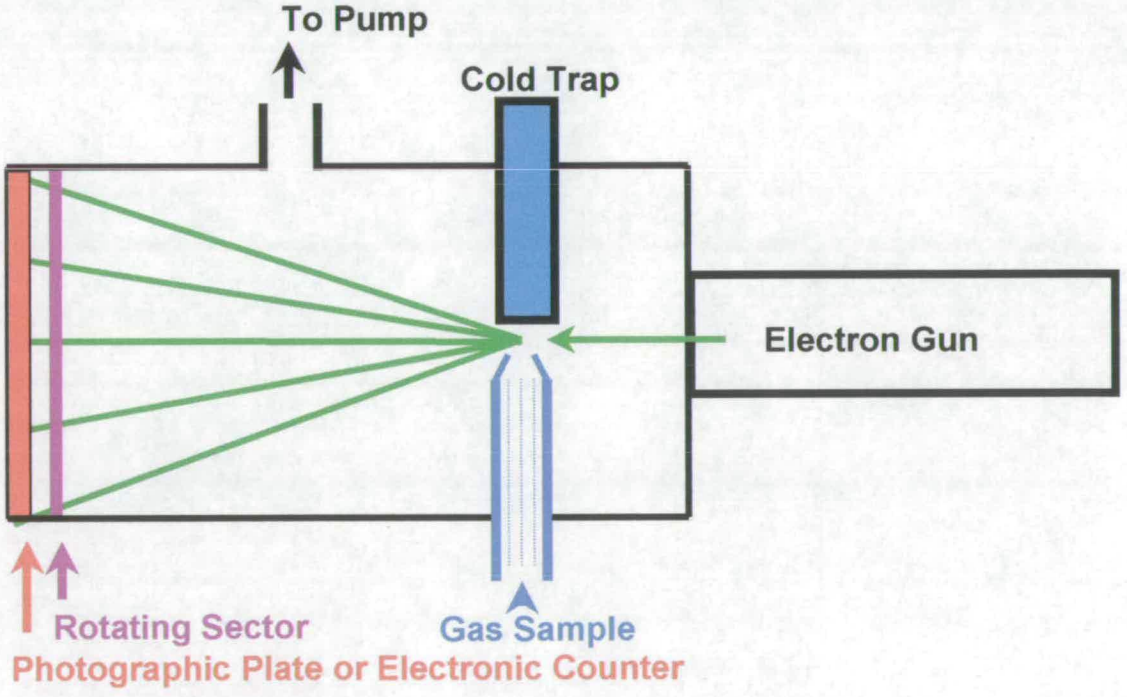

1.3.2 Data Analysis

The scattering intensities recorded in the electron diffraction experiment must be measured, and saved as a function of the scattering angle, for use in the structural refinement. This is done using a microdensitometer. Originally, a Joyce Loebl MDM6 at the EPSRC Daresbury laboratory was used,[3] but in the last three years, a PDS densitometer at the Institute of Astronomy in Cambridge has been used.[4] The microdensitometer reads intensities from the whole plate, and the software then determines mean intensities as a function of distance from the centre of the pattern, as shown in Figure 3.

Figure 3 Conversion of Data using the Cambridge Microdensitometer.

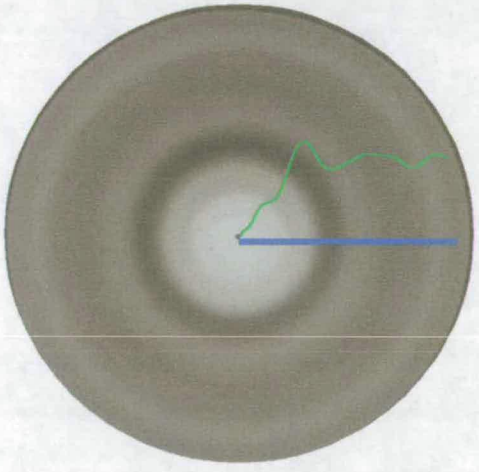

These optical data must then be converted into the total electron scattering (I_{total}) in a process that takes several factors into account including the flatness of the plate and the non-linearity of the photographic emulsion (the blackness correction). The total scattering intensity can be expressed as

$$I_{total} = I_{atomic} + I_{molecular} + I_{background} \qquad 1.3$$

The total scattering reveals little information. The top diagram in Figure 4 is a favourable example, and even in this case only one positive maximum can be seen. The examples used in the rest of Figure 4 would show no more than minor inflections in the total intensity curve. The molecular scattering intensity must then be separated from the background and atomic scattering. The atomic scattering is due to electrons being diffracted by single atoms, and thus does not give rise to an interference pattern because the diffracted electrons are coming from one source, not two. The atomic intensity can be calculated using tabulated scattering factors. The background scattering consists of incidental scattering due to the experimental conditions and is subtracted using a smooth spline function. A typical molecular intensity scattering curve is shown in Figure 4. Note that it is normal practice to refine using $s^4 I_{mol}(s)$.

Figure 4 From raw data to radial distribution curve

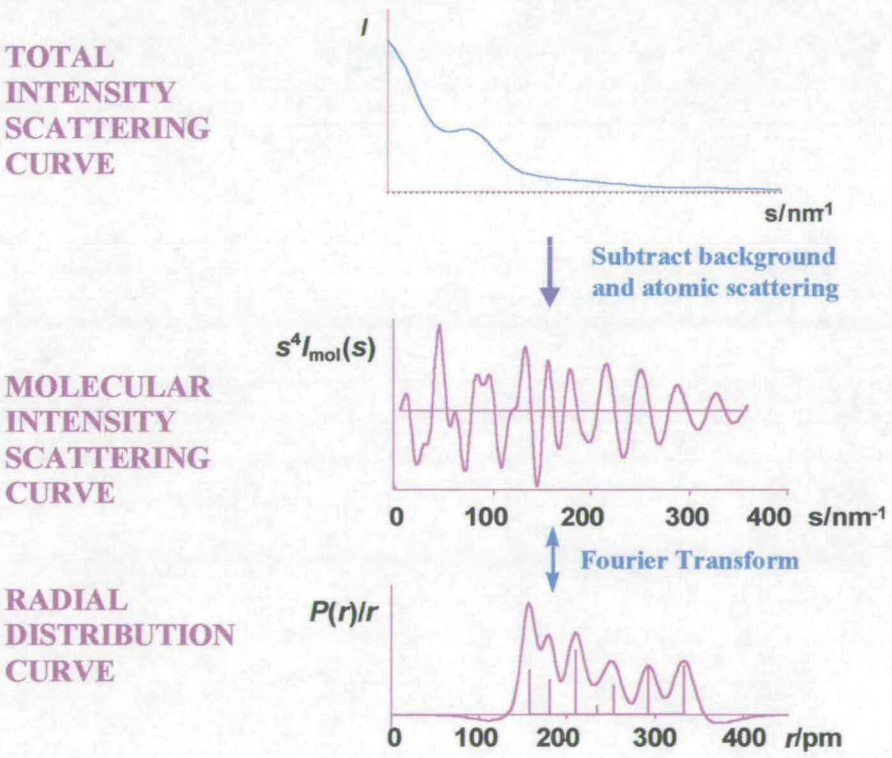

Looking at the molecular scattering curve, distances between atoms are not immediately obvious. However, if we sine Fourier transform this molecular scattering curve we get a radial distribution curve, which plots the probability $P(r)/r$ of finding distance r plotted against r. Therefore, we get a visual interpretation of all the bonded and non-bonded distances in the molecule. The plot consists of a series of broad peaks [actually they are Gaussian in $P/(r)$], each centred on the internuclear distance and with the peak width determined by the amplitude of vibration of the atom pair. The area under each peak is given by

$$Area \propto \frac{n_{ij} Z_i Z_j}{r_{ij}} \qquad 1.4$$

where n_{ij} is the multiplicity of r_{ij}, and Z_i and Z_j are the atomic numbers of atoms i and j respectively. One important thing to note about radial distribution curves is that if two atomic distances are very similar, then the distances will not be resolved in the composite peak.

An example of this can be seen in Figure 5, which is the radial distribution curve for triazine. The non-bonded C...C and N...N distances are very similar and are not resolved. C-H is close to C-N and is seen as a shoulder, as is N...H on the side of the C...C/N...N peak. Another feature of the curve is the size of the H...H peak in comparison to, for example the C-N bonded peak. From Equation 1.4 it can be seen that the atomic numbers of the atoms play an important part in determining the area under the peak. Therefore the area under the H...H peak will be much smaller than the area under the C-N peak.

Figure 5 Radial Distribution Curve for Triazine

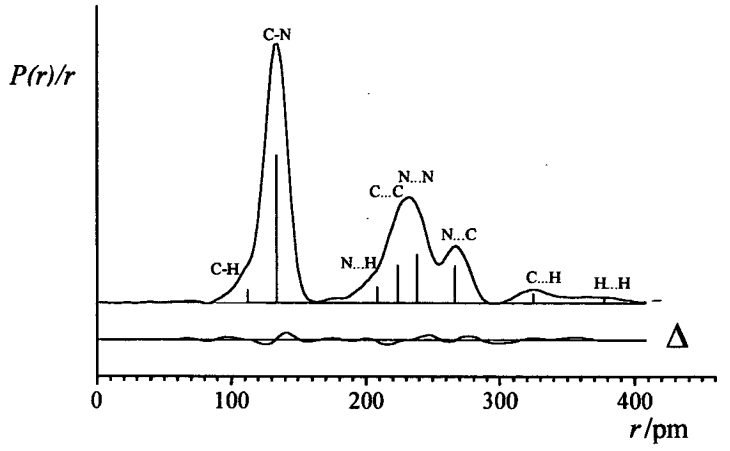

1.3.3 Limitations of Electron Diffraction

Electron diffraction is a very useful structural tool but it has its limitations, which in the past have led to restrictions on the types of molecules that were suited to the technique. We know from equation 1.4 that the area of the peak in the radial distribution curve depends on the atomic numbers of the atoms forming that peak. Thus the positions of light atoms are poorly defined in comparison to those for heavy atoms due to their poor scattering ability. This is a common theme to both electron diffraction and X-ray diffraction and can lead to incomplete structures being obtained because of the uncertainty of the positions of these light atoms.

Overlapping peaks on the radial distribution curve can also cause problems. If two distances within a molecule are very similar, then it can be impossible to deconvolute the Gaussian curves associated with both atom pairs. We have seen this in the triazine example above, and another good example of this is that of ClO_3F,[5] shown in Figure 6, which possesses C_{3v} symmetry.

Figure 6 Structure and radial distribution curve for ClO_3F

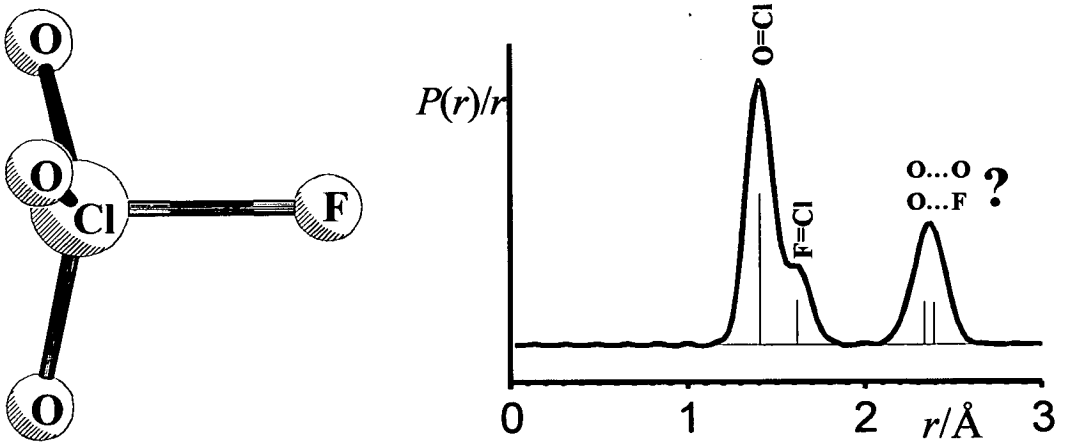

The O...F and O...O distances with in this molecule are very similar, both lying around 250 pm, under the peak to the right on Figure 6. If the distances are incorrectly assigned, the whole structure of the molecule is affected, and the wrong structure will be obtained. It can be seen how the problem could escalate very rapidly with increasing number of atoms within the molecule.

Another problem associated with electron diffraction is that of phase shifts. This can arise when there are light and unusually heavy atoms present in the molecule, e.g. in UF_6,[6] and leads to "beating" in the molecular intensity scattering curve. There is analogy with the sound made by Chinook helicopters. They have two large rotors, which rotate at slightly different frequencies to prevent massive destructive resonance that would effectively destroy the helicopter. When they fly, a distinctive beating sound is heard as the two frequencies come in and out of phase with each other, and the same effect is seen in the molecular scattering curve of UF_6. This leads to two peaks being observed in the experimental radial distribution curve (Figure 7) for the U-F distance (A) while the normal theoretical curve shows only one peak for the U-F distance (C). The single U-F distance is the correct one, but complex scattering factors must be used to calculate the

molecular scattering and therefore the radial distribution curve. This was done for (B) and it can be seen that this matches well with the experimental curve.

Figure 7 Phase shift effects in UF_6[6]

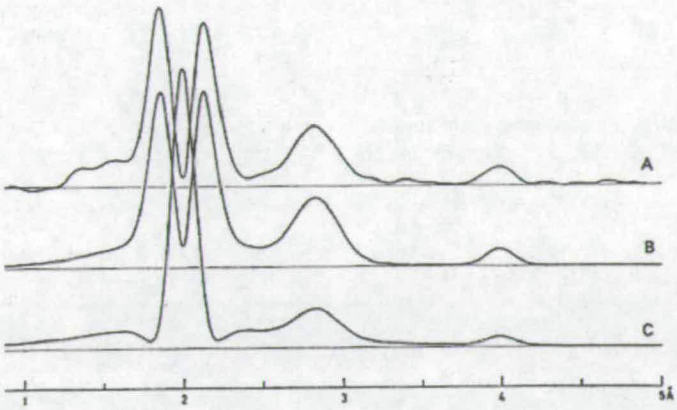

The final problem associated with gas-phase electron diffraction arises from the fact that the atoms are not stationary. The molecule is vibrating and an electron "sees" a picture of the molecule frozen at an instant in time. However, there are millions of electrons contributing to the overall picture, which leads to a vibrationally averaged structure being obtained. Figure 8 shows how a simple molecule can vibrate.

Figure 8 Vibration of a 3-atom molecule

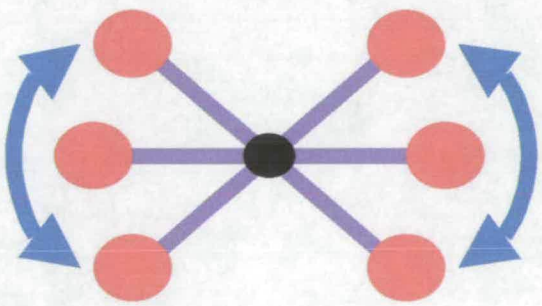

It can be seen from Figure 8 that the molecule spends all its time, except for an instant, bent. Therefore the distance between the outer two atoms is, on average, less than twice

the actual atom-atom distance. In this model, the bonded distance does not change. Thus, unless this vibration is corrected for, the molecule may be incorrectly deduced as being bent rather than linear. This problem is known as the shrinkage effect[7] and is more of a problem in larger molecules with low-frequency large-amplitude torsion angles.

1.4 *Ab Initio* Calculations

Ab initio calculations are the most sophisticated of the currently available computational methods. This quantum mechanical approach to solving molecular structure is based on finding a solution to the Schrödinger equation

$$E\Psi = \mathrm{H}\Psi \qquad 1.5$$

where **E** is the total molecular energy, Ψ is the total molecular wavefunction (describing the positions of nuclei and electrons) and **H** is the Hamiltonian operator (containing the electronic and nuclear kinetic and potential energy terms). The aim of solving the Schrödinger equation is to find all the stable structures and to locate the global minimum, from many possible starting geometries.

The Schrödinger equation suffers from one major problem: the equation can only be solved exactly for one-electron systems such as H or He^+. However, the systems that we want to study contain many electrons, and these electrons feel the electrostatic forces of one another in what is commonly termed the "many body perturbation theory". Simplifying **H** and Ψ so that approximate solutions can be obtained for larger systems circumvents this problem, although numerical methods must still be used.

The Hamiltonian operator is composed of five terms: the kinetic energy of the nuclei and the electrons, and the potential energy of nuclear repulsion, electronic repulsion and nuclear-electronic attraction. The first approximation adopted is the Born-Oppenheimer

approximation, which separates out the motion of the nuclei and the electrons. Effectively, because the mass of the nuclei is many thousands of times larger than the electrons, they are moving very slowly in relation to the electrons. Thus the Born-Oppenheimer approximation reduces this slow motion to assume that the heavy nuclei are stationary in a field of moving electrons. The main result of this is that the kinetic energy of the nuclei can be disregarded and the potential energy of nuclear repulsion is held constant in any one stage in the calculation. This leaves only the electronic Hamiltonian to be considered further.

1.4.1 Simplifying the Hamiltonian Operator (H): Levels of Theory

In the simplest approach to obtaining **H**, the electronic repulsion term in the Hamiltonian can be replaced by the Hartree-Fock potential. This treats each electron as if it were moving in a uniform field generated by the other electrons present in the molecule. Therefore, a series of one-electron Schrödinger equations can be solved generating a series of one-electron atomic orbitals for the molecule. Although this is an important assumption to make it provides a good starting geometry and can account for the bulk (~ 99%) of the energy in the molecule. The missing ~1% can be accounted for in terms of electron correlation energy, which is missing from these initial optimisations because, in reality, electrons do not move in a uniform field, but in one that is dependent upon the instantaneous positions of the other electrons. Higher *"levels of theory"* deal with this problem by still solving the Schrödinger equation in terms of one electron, but positioning the other electrons in a different region of space to the first. This can be thought of in terms of placing the electron in a different orbit, as in Figure 9.

Figure 9 General method for including electron correlation for a He atom ($1s^2$)

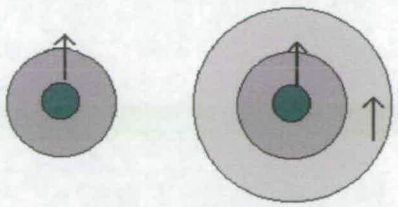

Second electron placed in a different region of space to prevent them coming too close together

Another approach to electron correlation is the Møller-Plesset (MP) perturbation series,[8] which adds higher excitations to Hartree-Fock theory as a non-iterative correction drawing on the many body perturbation theory. The most commonly used of these is the MP2 level of theory. This truncates the Møller-Plesset correlation energy correction at the second order (third order for MP3 etc). MP2 can be successfully used to model a wide range of systems and has been extensively used throughout this thesis.

1.4.2 Simplifying the Molecular Wavefunction (Ψ): Basis Sets

In the Born-Oppenheimer approximation, we have fixed the position of the nuclei in space so Ψ only considers the region of space for electron distribution. The wavefunction can be generated by a linear combination of Gaussian functions that are centred on atoms, and are used to approximate atomic orbitals in the molecule. A collection of these functions is called a basis set. In general, the larger the basis set the fewer the constraints on the location of the electrons in space. Ideally, a basis set would be composed of an infinite number of these functions to describe all space but, in reality, this is not practical, requiring a computer with an infinite supply of memory. Instead, a truncated series is used. Intuition tells us that the smaller the basis set used, the poorer the quality of the calculations will be. However, the time taken for calculations scales as about the fourth power of the number of functions, depending on the method. This places serious restrictions on the sizes of calculations that can be undertaken. Therefore, it is important that calculations start with a small basis set and build up to larger ones when more information has been obtained about the molecule.

Generally, calculations in this work were restricted to basis sets of approximately double-ξ quality such as 6-31G*[9-11] because of the size of systems being studied. Double-ξ basis sets form all molecular orbitals from linear combinations of two sizes of functions for each atomic orbital.[12] The 6-31G* basis set is a split-valence contracted Gaussian basis (6-31G) in which each inner shell function is represented by a linear combination of six s-type Gaussian functions and each valence shell by an inner set with a combination of three

Gausians and an outer set with a single Gaussian. To this basis is added a set of six polarisation functions for each heavy atom. Split valence basis sets allow the orbitals to change size but not to change shape. This is allowed for by the polarisation function which is denoted by the * in the 6-31G*. The easiest way to picture this is to think of it as adding *d* functions onto a carbon atom, thus describing more of the region of space around the carbon nucleus.

Diffuse functions can also be used to describe the space around the nucleus. They are larger versions of the s- and p-type functions that allow orbitals to occupy a larger region of space. This is important for systems where electrons are relatively far from the nucleus as in molecules with lone pairs, or with a negative charge.

Many different basis sets have been employed throughout this thesis. The D95 Dunning-Huzinaga[13] basis set is another example of the double-ξ basis set mentioned earlier. The cc-pVnZ[14-17] basis set series has also been employed where n is 2, 3, 4 or 5. This is Dunning's correlation consistent basis set where n represents double- to quintuple-ξ.

Ab initio calculations allow the user to calculate many properties of the molecule including molecular energies and structures, vibrational frequencies, IR and Raman spectra, atomic charges and thermochemical properties. Initially the total molecular energy of the system is calculated by solving the Schrödinger equation in terms of E. Once the total molecular energy has been calculated, the first derivative of the energy with respect to each nuclear coordinate will allow the location of stationary points on the potential energy surface to be determined. These stationary points correspond to a point of zero force on the surface i.e. an optimised geometry. Calculation of the second derivatives of the energy with respect to nuclear coordinates of the previously determined stationary point will reveal the nature of that stationary point. There are two possibilities, either a potential well where a small displacement will increase the total energy of the system, or a saddle point where a small displacement in one or more directions will lower

the total energy. Thus the optimised structure can be identified as a kinetically stable, real structure, or as a kinetically unstable structure, for example, a transition state. The calculation of the second derivatives of the energy also yields force constants, which can be used to calculate the normal modes of vibration. In this way, we can determine both the nature of the stationary point and gain vibrational information about the structure.

1.5 Other Calculations

Other types of calculations can also be used to determine the structure of molecules, and all of the following have been used to some extent to aid in the determination of the structures investigated.

1.5.1 Density Functional Theory Calculations

Density functional theory (DFT) calculations are attractive to computational chemists studying larger molecules. This empirical method is based on the electron density, rather than the wavefunction, and is ideal for relatively large systems. They use the same resources as the basic Hartree-Fock calculations described above, but electron correlation is accounted for within the calculations. In DFT calculations, the electron correlation is computed via functionals (which are functions of functions). Here the functionals are functions of the electron density which in itself is a function of coordinates in real space. Thus, for large systems for which MP2 calculations can be expensive and time consuming, DFT calculations offer a quicker route to a reliable structure. The main DFT method used in this thesis is the B3LYP method.[18-20] This is Becke's three-parameter hybrid functional using the LYP correlation functional of Lee, Yang and Parr. The basis sets used with this method are as for *ab initio* calculations.

1.5.2 Semi-Empirical Calculations

Semi-empirical calculations use parameters derived from experiments to simplify the calculation. Thus each atom within the molecule is parameterised, and an approximate form of the Schrödinger equation is solved. These calculations are a quick, cheap way of searching the potential energy surface for minima for further investigation using *ab initio* calculations employing higher levels of theory and larger basis sets. They rely on a good parameter set being present for each atom, with the AM1,[21-25] MNDO[22-31] and PM3[32-33] being the best known. The main difference between each of the methods is the type of Hamiltonian used, i.e. the AM1 Hamiltonian in AM1 calculations etc. The AM1 semi-empirical method was used in this thesis as this method is generally thought of as one of the best semi-empirical methods available to the computational chemist.

1.5.3 Molecular Mechanics

Molecular mechanics use the laws of classical physics to predict structures of molecules. They rely on the interactions between nuclei, rather than explicitly treating the individual electrons within molecules. Thus they can be thought of as "ball and spring" calculations, with the atoms being balls, and the bonds being the springs connecting the balls. There are many different molecular mechanical methods, each one characterised by its different force field. The force field contains equations defining how the potential energy surface varies with the location of atoms, a series of atom types defining the characteristics of an element within a chemical context, and parameter sets that fit the equations and atom types to experimental data.[12] The force field used in this thesis is the Universal Force Field,[34] in which each term has been designed for a specific atom *and* geometry, e.g. tetrahedral, square planar etc. Molecular mechanics calculations provide another reasonably quick, cheap and reliable method of initial structural investigation for large molecules which are basically organic, and for which more than one conformer is possible. An evaluation of molecular mechanics and semi-empirical methods as tools for conformational searches is given in Chapter 8, using the series $Bu^tX_2SiSiX_2Bu^t$ (X = F, Cl, Br or I) and $Bu^t_2HSiSiH_2Bu^t$ as examples.

1.6 Combining *Ab Initio* Calculations and GED Data

With electron diffraction looking at the structure of molecules in the gas phase, free from intramolecular interactions, and *ab initio* calculations performed on isolated molecules, the two techniques are complementary. In standard structural investigations *ab initio* molecular orbital calculations can be used to predict which conformers are present and to obtain theoretical harmonic force fields from which estimates of vibrational amplitudes can be obtained. This information is used to provide accurate starting values for parameters in the electron diffraction refinement. To solve the structure, a FORTRAN model is written to define the atomic coordinates of the molecule. The model is defined in terms of parameters (bond distances, angles and torsion angles) and takes into account any local and overall symmetry in the molecule. The parameters are then refined by a least-squares analysis until a satisfactory fit to the data is obtained. The parameters should refine to reasonable values with realistic standard deviations and the goodness of fit, the so-called R_G factor, should preferably be below 10% for most compounds. A feature of the electron diffraction program is that when the molecular scattering curve and radial distribution curve is generated, a difference curve is also generated between the experimental and theoretical data sets. This difference curve is marked as Δ on Figure 5 and should be as flat as possible for the best fit of the theoretical data to the modeled data.

Previously, it has been necessary to fix certain parameters that are poorly defined by the GED experiment to stop them refining to unreasonable values in the electron diffraction refinement. Such parameters could be differences between similar bond distances that are troubled by correlation effects, or parameters involving light atoms such as hydrogen, which tend to be poorly defined due to their low electron scattering ability. Fixing parameter values is undesirable because this assumes that the calculated values are absolutely correct, and leads to unrealistically low estimated standard deviations. This is particularly serious in the case of correlated parameters. A new technique has recently

been introduced to remove the necessity to make these assumptions. Instead of constraining (fixing) parameters that could not be refined freely using GED data alone, these parameters are included in the refinement, but subject to flexible restraints. These restraints have both a value (usually derived from the highest level *ab initio* or DFT calculations) and an uncertainty (based on the level of convergence achieved for that parameter or from experience of the accuracy of the adopted theoretical method on related compounds). This methodology has been coined SARACEN (Structure Analysis Restrained by *Ab initio* Calculations for Electron diffractioN)[35] and has allowed the refinement of previously unrefinable parameters and therefore the elucidation of more reliable structures.

This thesis is concerned with the determination of gas-phase structures of large molecules containing sterically demanding groups. Structures of this type have often previously proved to be unrefinable. A common feature of all the molecules studied is that of bulky ligands, either tertiary butyl groups, or trimethylsilyl groups. Where work has been published with angstroms as the unit of distance this has been retained in the thesis. Otherwise, picometers are used. Chapter 2 is concerned with the structure of 1,2-di-*tert*-butyltetrachlorodisilane, with a bulky group at each end of the molecule, in both the gas phase and the solid phase. Chapter 3 tackles the very unusual structure of 1,1,2-tri-*tert*-butyldisilane, where there are now two butyl groups at one end of the molecule, which can interact with each other as well as with the single group at the other end. Both GED data and vibrational data are presented and compared for this molecule. Chapter 4 examines the even more challenging structure of 1,1,2,2-tetra-*tert*-butyldisilane, which has two butyl groups at each end of the molecule. Chapter 5 looks at the structure of tris-*tert*-butylsulfurtriimide with its "Isle-of-Man" structure, comparing the gas and solid-phase structures. The structure of *tert*-butylbis(trichlorosilyl)phosphine is presented in Chapter 6. Chapter 7 compares the structures of the bis[bis(trimethylsilyl)-methyl]phosphinyl and arsinyl radicals with those of their dimeric parents. The energetics for the very unusual dissociation process from dimer to monomer have been investigated

using *ab initio* calculations in an attempt to unravel the source of the energy to break the P-P and As-As bonds. In Chapter 8, a comparison between molecular mechanical and semi-empirical methods as a tool for locating possible minima on the potential energy surface is presented. Finally, in Chapter 9, future work is discussed with the concept of complete structure determination for very large molecules. This new technique has been termed DYNAMITE, and the principals behind the method are outlined.

1.7 References

1. L. De Broglie, *Phil. Mag.*, 1924, **47**, 446.
2. P. P. Debye, *Phys. Z.*, 1939, **80**, 404; C. Finbak, *Avh. Norsk. Vidensk-Akad. Oslo*, 1937, 13.
3. S. Cradock, J. Koprowski and D. W. H. Rankin, *J. Mol Struct.*, 1981, **77**, 113.
4. J. R. Lewis, P. T. Brain and D. W. H. Rankin, *Spectrum*, 1997, **15**, 7.
5. A. H. Clark, B. Beagley and D. W. J. Cruickshank, *J. Chem. Soc. A*, 1970, 872.
6. Molecular Structure by Diffraction Methods – Volume 1, Specialist Periodical Reports, The Chemical Society, 1973, pp 21-23.
7. Y. Morino and T. Iijima, *Bull. Chem. Soc. Japan*, 1962, **35**, 1661; O. Bastiansen and M. Traetteberg, *Acta Cryst.*, 1960, **13**, 1108.
8. C. Møller and M. S. Plesset, *Phys. Rev.*, 1934, **46**, 618.
9. W. J. Hehre, R. Ditchfield and J. A. Pople, *J. Chem. Phys.*, 1972, **56**, 2257.
10. P. C. Hariharan and J. A. Pople, *Theor. Chim. Acta*, 1973, **28**, 213.
11. M. S. Gordon, *Chem. Phys. Lett.*, 1980, **76**, 163.
12. J. B. Foresman and Æ. Frisch, "Exploring Chemistry with Electronic Structure Methods", 2nd Edition, Gaussian Inc., 1996, pp 4-6, 98.
13. T. H. Dunning Jr. and P. J. Hay, "Modern Theoretical Chemistry", Vol. 3, Ed. H. F. Schaefer III, Plenum, 1976, p1.
14. D. E. Woon and T. H. Dunning Jr., *J. Chem. Phys.*, 1993, **98**, 1358.
15. R. A. Kendall, T. H. Dunning Jr. and R. J. Harrison, *J. Chem. Phys.*, 1992, **96**, 6796.
16. T. H. Dunning Jr., *J. Chem. Phys.*, 1989, **90**, 1007.
17. K. A. Peterson, D. E. Woon and T. H. Dunning Jr., *J. Chem. Phys.*, 1994, **100**, 7410.
18. A. D. Becke, *J. Chem. Phys.*, 1993, **98**, 5648.
19. C. Lee, W. Yang and R. G. Parr, *Phys. Rev. B*, 1988, **37**, 785.
20. B. Miehlich, A. Savin, H. Stoll and H. Preuss, *Chem. Phys. Lett.*, 1989, **157**, 200.

21. M. J. S. Dewar, E. G. Zoebisch and E. F. Healy, *J. Am. Chem. Soc.*, 1985, **107**, 3902.

22. M. Dewar and W. Thiel, *J. Am. Chem. Soc.*, 1977, **99**, 4499.

23. L. P. Davis, R. M. Guidry, J. R. Williams, M. J. S. Dewar, H. S. Rzepa, *J. Comp. Chem.*, 1981, **2**, 433.

24. M. J. S. Dewar, M. L. McKee and H. S. Rzepa, *J. Am. Chem. Soc.*, 1978, **100**, 3607.

25. M. S. Dewar and C. H. Reynolds, *J. Comp. Chem.*, 1986, **2**, 140.

26. M. J. S. Dewar and W. Thiel, *J. Am. Chem. Soc.*, 1977, **99**, 4899.

27. M. J. S. Dewar and H. S. Rzepa, *J. Am. Chem. Soc.*, 1978, **100**, 777.

28. M. J. S. Dewar and M. L. McKee, *J. Comp. Chem.*, 1983, **4**, 84.

29. M. J. S. Dewar and E. F. Healy, *J. Comp. Chem.*, 1983, **4**, 542.

30. M. J. S. Dewar, G. L. Grady and J. J. P. Stewart, *J. Am. Chem. Soc.*, 1984, **106**, 6771.

31. M. J. S. Dewar, G. L. Grady, K. M. Merz, J. J. P. Stewart, *Organometallics*, 1985, **4**, 1964.

32. J. J. P. Stewart, *J. Comp. Chem.*, 1989, **10**, 209.

33. J. J. P. Stewart, *J. Comp. Chem.*, 1989, **10**, 221.

34. A. K. Tappe, C. J. Caséwit, K. S. Colwell, W. A. Goddard III and W. M. Skiff, *J. Am. Chem. Soc.*, 1992, **114**, 10024

35. A. J. Blake, P. T. Brain, H. McNab, J. Miller, C. A. Morrison, S. Parsons, D.W. H. Rankin, H. E. Robertson and B. A. Smart, *J. Phys. Chem.*, 1996, **100**, 12280; P. T. Brain, C.A. Morrison, S. Parsons and D. W. H. Rankin, *J. Chem. Soc., Dalton Trans.*, 1996, 4589.

Chapter 2

Molecular Structure of $Bu^tCl_2SiSiCl_2Bu^t$ by Gas phase Electron Diffraction, *Ab Initio* Calculations, Vibrational Spectroscopy and X-Ray Crystallography. Molecular Structures of $Bu^tBr_2SiSiBr_2Bu^t$ and $Bu^tI_2SiSiI_2Bu^t$ by *Ab initio* Calculations and X-Ray Crystallography.

2.1 Introduction

Silicon is the second most abundent element by weight in the earths surface and gives rise to some remarkable chemistry. The use of various forms of silicon has exploded in the last twenty years, with applications in polymer chemistry, semiconductors and lubricants, as well as more traditional uses such as ceramics and abrasives.[1] Silicon has a smaller energy gap between the occupied and unoccupied orbitals than the analogous diamond structure, making it easier to promote the less tightly held outer electrons from the valence band to the empty conduction band.[2] Its semiconductor properties can be enhanced by seeding with small amounts of impurity like phosphorus or aluminium. Silicone polymers are extremely stable and form the basis of many oils, rubbers and resins.[3] Silicone is formed when the terminal O^- groups in silicates are replaced by R groups like $-CH_3$ as shown in Figure 1.

Figure 1 From silicate to single chain silicone

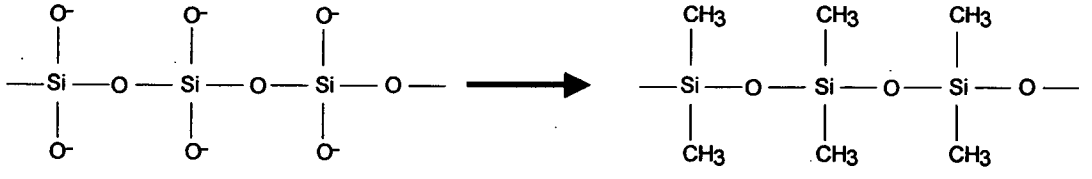

Silicate Silicone

Due to the larger size of silicon in comparison to carbon, there are major differences in the observed reactivity. Silicon will normally only form Si=Si double bonds at very low presures and high temperatures.[4] However, a new route to a disilene involving the use of a bulky 2,6-dimethylphenyl ligand was reported in 1982, which was found to promote a very clean reaction with no side products.[5] The disilene was, unsurprisingly, very sensitive to air and moisture but, nontheless, could be characterised by electron impact mass spectroscopy and proton NMR spectroscopy. Thus the idea of using of bulky alkyl ligands to control chemical reactions was able to yield this highly reactive molecule.

Our interest is in disilanes rather in disilenes, but the principles are the same. All the disilanes studied in the course of this PhD have a common theme, that of bulky alkyl ligands and steric strain. The structures of some disilanes partially substituted with larger bromine and iodine atoms, including 1,1,2,2-tetrabromodisilane,[6] 1,2-diiododisilane[7] and 1,1,2,2-tetraiododisilane,[7] have recently been studied in the gas phase. In all of these examples, the favoured conformations are staggered about the Si-Si bonds.

However, systems containing the more sterically demanding *tert*-butyl groups are of greater structural interest, because the effect of the bulky alkyl ligands on the conformation of the groups around the silicon-silicon bond can lead to surprising results. In two compounds with just two *tert*-butyl groups, 1,2-di-*tert*-butyldisilane[8] and 1,2-di-*tert*-butyltetrafluorodisilane,[9] the *transiod* conformation was preferred, as expected, although for 1,2-di-*tert*-butyltetrafluorodisilane the data are consistent with a single conformer with a large-amplitude motion over a torsional range of around 140-220°.[9] In contrast, the most stable conformation of the even more sterically crowded 1,1,2-tri-*tert*-butyldisilane, the structure of which has recently been elucidated (see Chapter 3) is the most unusual eclipsed arrangement, in which each butyl group eclipses a hydrogen atom at the opposite end of the molecule. This was found to be far more energetically favourable than either of the two possible staggered structures, which brought the butyl groups into closer contact.

In view of the interesting and unusual conformational behaviour of the di- and tri-*tert*-butyl substituted disilanes, a structural structural study on the series of compounds $Bu^tX_2SiSiX_2Bu^t$, where X = Cl, Br and I has been undertaken. In these cases, the steric demands of the butyl groups must be accommodated in conjunction with the increasingly large halogen atoms. The gas-phase structure of 1,2-di-*tert*-butyltetrachlorodisilane has been determined, whilst the crystal structures have been obtained for all three molecules. Vibrational spectra have been recorded, and *ab initio* calculations have provided geometrical and vibrational information.

2.2 Experimental

2.2.1 Synthesis

A sample of $Bu^tCl_2SiSiCl_2Bu^t$ was prepared by K. Hassler and R. Zink according to the literature method[10] and provided for use on the Edinburgh diffraction apparatus.

2.2.2 *Ab initio* calculations

All calculations at the HF level were performed on a Dec Alpha 1000 4/200 workstation using the Gaussian 94[11] and Gaussian 98[12] programs. An extensive search of the torsional potential of all the compounds was undertaken at the HF/3-21G*[13-15] level in order to locate all minima. For 1,2-di-*tert*-butyltetrachlorodisilane three non-equivalent conformers were found with ϕ(CSiSiC) 56, 94 and 169° and for 1,2-di-*tert*-butyltetrabromodisilane two non-equivalent conformers were found with ϕ(CSiSiC) 116° (C_2) and 180° (C_{2h}). For 1,2-di-*tert*-butyltetraiododisilane, one conformer with ϕ(CSiSiC) 170° (C_1 symmetry) was located. Further geometry optimisations were undertaken at the HF and MP2 levels using the standard 6-31G*[16-18] basis set. MP2 calculations for 1,2-di-*tert*-butyltetrabromodislane and 1,2-di-*tert*-butyltetraiododisilane were carried out using resources of the U.K. Computational Chemistry Facility, on a DEC 8400 superscalar cluster equipped with 10 fast processors, 6 GB of memory and 150 GB disk. For 1,2-di-*tert*-butyltetraiododisilane, the LanL2DZ[19] basis set employing the Los Alamos effective core potential plus DZ on iodine, was used at all levels.

Vibrational frequencies, calculated from analytic second derivatives at the HF/3-21G* and HF/6-31G* levels to determine the nature of stationary points. They also provided estimates of amplitudes of vibration (u) for use in the gas electron diffraction (GED) refinements and comparison with experimentally determined frequencies for 1,2-di-*tert*-butyltetrachlorodisilane.

2.2.3 X-Ray Crystallography

(With R. A. Coxall and S. Parsons, Edinburgh, Scotland)

Crystal data for 1,2-di-*tert*-butyltetrachlorodisilane (See Table 1): $Si_2C_8H_{18}Cl_4$, M = 312.20, triclinic, space group $P\bar{1}$, a = 6.718(2), b = 7.529(2), c = 8.789(2) Å, α = 94.93(4), β = 107.60(3), γ = 112.43(4)°, V = 381.35(16) Å^3, Z = 1, D_c = 1.359 Mgm^{-3}, F(000) 162, μ(Mo-Kα) 0.901 mm^{-1}, λ 0.71073 Å, T = 150 K, data were collected on an APEX SMART CCD diffractometer. 2182 reflections were collected (1420 unique, R_{int} 0.0245). The structure was solved by direct methods and refined against F^2 (SHELXTL),[20] yielding R_1 = 0.0380, for 1155 independent reflections with $F >$ 4$\delta(F)$, wR_2 = 0.0933. All non-H atoms were refined with anisotropic thermal parameters, with H-atoms placed in calculated positions.

Crystal structures for 1,2-di-*tert*-butlytetrabromodisilane and 1,2-di-*tert*-butyltetraiododisilane were provided by *K. Hassler, Graz*, and used for comparison with the structures obtained *ab initio*.

2.2.3.1 Structure solution and refinement

See Table 1(*c*). The weighting scheme adopted was $w^{-1} = [\sigma^2(F_o^2) + (0.0490P)^2 + 0.0000P]$ where $P = [1/3 (F_o^2 + 2F_c^2)]$ for 1,2-di-*tert*-butyltetrachlorodisilane.

2.2.4 Infrared and Raman spectra

(Conducted by K. Hassler and R. Zink, Graz, Austria)

Infrared spectra in the range 3200-250 cm^{-1} were measured with a Perkin-Elmer 883 spectrometer using a film of pure liquid between CsBr plates. The Raman spectra were recorded with a Jobin Yvon T64000 triple monochromator employing a charge-coupled device (CCD) camera and the 514.5 nm line of an argon-ion laser as the source of excitation. Variable-temperature Raman spectra were obtained by mounting a capillary containing the sample on a copper block equipped with a heater and a thermocouple. Liquid nitrogen was used for cooling the sample.

Table 1. X-Ray crystal structure, (a) crystal data, (b) data collection and processing, (c) structure solution and refinement.

	$Bu^tCl_2SiSiCl_2Bu^t$
(a) Crystal Data	
Empirical formula	$C_8H_{18}Cl_4Si_2$
M	312.2
Wavelength	0.71073 Å
Temperature	150(2) K
Crystal system	Triclinic
Space group	$P\bar{1}$
Unit cell dimensions	a = 6.7183(17) Å α = 94.93(4)°
	b = 7.5290(19) Å β = 107.60(3)°
	c = 8.789(2) Å γ =112.43(4)°
Volume	381.35(16) $Å^3$
Number of reflections for cell	1828 ($5 < \theta < 52°$)
Z	1
Density (calculated)	1.359 Mg/m^3
Absorption coefficient	0.901 mm^{-1}
F(000)	162
(b) Data Collection	
Crystal description	colourless cylinder
Crystal size	0.40 x 0.17 x 0.17 mm
θ range	2.50 to 26.36°
Index ranges	$-7 \le h \le 8$, $-9 \le k \le 8$, $-10 \le l \le 10$
Reflections collected	2182
Independent reflections	1420 [R_{int} = 0. 0245]
Scan type	φ and ω scans
Absorption correction	Empirical (T_{min}=0.533, T_{max}=0.962)
(c) Solution and Refinement	
Solution	direct [SHELXS-97 (Sheldrick, 1990)]
Refinement type	Full-matrix least-squares on F^2
Program used for refinement	SHELXL-97
Hydrogen atom placement	geom
Hydrogen atom treatment	riding, rotation groups Me
Data / restraints / parameters	1420/0/67
Goodness-of-fit on F^2	0.944
Conventional R [$F \ge 4\sigma(F)$]	R_1 = 0.0380 [1155 data]
Weighted R (F^2 and all data)	wR_2 = 0.0933
Final maximum δ/σ	0
Largest diff. Peak and hole	0.688 and -0.321 $e.Å^{-3}$

2.2.5 Electron diffraction

Electron scattering intensities were recorded on Kodak Electron Image plates using the Edinburgh gas diffraction apparatus operating at *ca.* 44.5 kV (electron wavelength *ca.* 5.6 pm).[21] Nozzle-to-plate distances for the metal inlet nozzle were *ca.* 94 and 259 mm yielding data in the s range 20-356 nm^{-1}. The sample and nozzle temperatures were maintained at *ca.* 455 K during the exposure periods.

The scattering patterns of benzene were also recorded for the purpose of calibration; these were analysed in exactly the same way as those for $Bu^tCl_2SiSiCl_2Bu^t$ so as to minimise systematic errors in the wavelengths and camera distances. Nozzle-to-plate distances, weighting functions used to set up the off-diagonal weight matrix, correlation parameters, final scale factors and electron wavelengths for the measurements are collected in Table 2.

The electron-scattering patterns were converted into digital form using a PDS densitometer at the Institute of Astronomy in Cambridge with a scanning program described elsewhere.[22] The programs used for data reduction[23] and least-squares refinement[24] have been described previously; the complex scattering factors were those listed by Ross *et al.*[25]

Table 2. Nozzle-to-plate distances (mm), weighting functions (nm^{-1}), correlation parameters, scale factors and electron wavelengths (pm) used in the electron diffraction study.

Nozzle-to-plate distance[a]	Δs	s_{min}	sw_1	sw_2	s_{max}	Correlation parameter	Scale factor[b]	Electron wavelength
93.34	4	100	120	270	300	-0.0777	0.556(23)	5.655
258.02	2	20	40	144	168	0.1907	0.831(21)	5.654

[a] Determined by reference to the scattering pattern of benzene vapour.

[b] Values in parentheses are the estimated standard deviations.

2.2.6 Gas Electron Diffraction Model

On the basis of the *ab initio* calculations described above, electron diffraction refinements were carried out using a model of the *transiod* conformation (C_2 symmetry) of 1,2-di-*tert*-butyltetrachlorodisilane to describe the vapour. The large number of geometric parameters needed to define the model made it necessary to make a number of assumptions, including local C_{3v} symmetry for all methyl groups and local C_3 symmetry for the *tert*-butyl groups. These assumptions are justified by the *ab initio* results. Initially, some of the differences between similar bond lengths and bond angles were restrained using the SARACEN[26] method. However, since many of these difference parameters proved to be uncorrelated with other refining parameters, and returned values and e.s.d.'s which were close to the restraints, they were fixed in the final refinement. We can therefore be confident that the refined parameters, and their e.s.d.'s, are not affected significantly by the assumptions applied to the molecular model.

The structure of $Bu^tCl_2SiSiCl_2Bu^t$ was finally defined in terms of seventeen independent geometric parameters, comprising five bond lengths, five bond angles and seven torsion and tilt parameters, and four dependent parameters comprising four bond angles [Table 3; atom numbering shown in Figure 2].

Figure 2 Molecular structure of 1,2-di-*tert*-butyltetrachlorodisilane

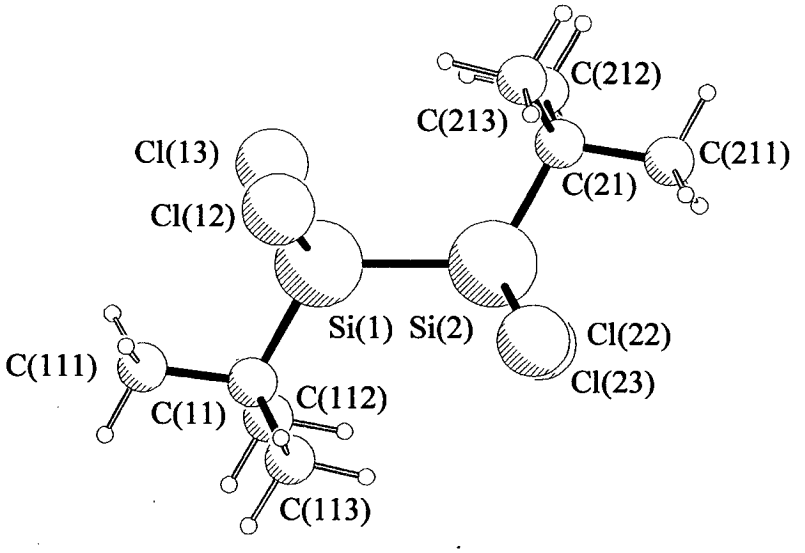

Table 3 Refined and calculated geometric parameters for 1,2-di-*tert*-butyltetrachlorodisilane (distances in pm, angles in deg.) from the GED study.[a]

No.	Parameter	GED (r_a)	MP2/6-31G* (r_e)
Independent Parameters			
p_1	C-H (mean)	114.2(4)	109.5
p_2	C-C (mean)	154.3(2)	153.6
p_3	Si-Si	238.0(7)	235.8
p_4	Si-C	187.2(7)	188.9
p_5	Si-Cl (mean)	207.1(1)	207.2
p_6	C-C-H	109.2(9)	110.9
p_7	C-C-C	109.1(3)	109.4
p_8	Si-Si-C	119.8(6)	117.6
p_9	Si-Si-Cl (mean)	105.2(3)	106.8
p_{10}	Si-Si-Cl (diff)	1.8(5)	2.8
p_{11}	Me twist	176.6(21)	178.3
p_{12}	Me tilt	2.5(19)	-
p_{13}	Bu^t twist	167.5(17)	171.1
p_{14}	Bu^t tilt	2.3(8)	-
p_{15}	Cl torsion (mean)[b]	124.4(5)	122.7
p_{16}	Cl torsion (diff)[c]	2.8(11)	2.1
p_{17}	CSiSiC	167.7(11)	167.9
Dependent Parameters			
p_{18}	Si-C-C(211)	109.3(4)	109.1
p_{19}	Si-C-C(212)	112.0(8)	110.0
p_{20}	Si-C-C(213)	108.2(7)	108.9
p_{21}	Cl-Si-Cl	105.5(8)	106.1

[a] Figures in parentheses are the estimated standard deviatioins of the last digits. See text for parameter definitions.

[b] Average of torsions C(21)-Si(2)-Si(1)-Cl(22) and C(21)-Si(2)-Si(1)-Cl(23).

[c] Difference C(21)-Si(2)-Si(1)-Cl(22) minus C(21)-Si(2)-Si(1)-Cl(23).

The independent parameters include the C-H and C-C bond lengths (p_1 and p_2), and average bond lengths for the Si-Si, Si-C and Si-Cl bonds (p_3-p_5), with small differences between non-equivalent bond lengths fixed at the *ab initio* values. All C-C-H bond angles (p_6) were assumed to be identical, as were all C-C-C bond angles (p_7). The Si-Si-C angle was also included (p_8). The Si-Si-Cl angles were defined in terms of the average (p_9) of Si(2)-Si(1)-Cl(12) and Si(2)-Si(1)-Cl(13) and the difference (p_{10}) between the two angles.

Of the remaining seven parameters, two represent the torsion and tilt of the *tert*-butyl groups. These groups were generated initially by placing a methyl group carbon atom at the origin, with its three H atoms arranged with local C_{3v} symmetry about the x-axis and one H in the xy plane in the positive x and y directions. The methyl torsion and tilt parameters (p_{11}-p_{12}) are rotations about the local x and y axes respectively. The methyl group is then translated along the positive x axis by the C-C bond length and the central carbon of the *tert*-butyl group is placed at the origin. The correct C-C-C bond angles are generated by rotating the methyl group about the z axis, moving the methyl carbon atom in the positive y direction, and then generating the other methyl groups by rotation of the first group about the x axis by 120° or -120°, respectively. The *tert*-butyl torsion angle is a rotation of the group about the x axis (p_{13}).

The tilt parameter is a rotation of the whole butyl group about the y axis (p_{14}). A positive tilt would move the butyl group with C(21) at the centre away from that with C(11) at the centre in the local y direction of the butyl groups.

Having generated the *tert*-butyl groups in their local coordinate systems, they need to be rotated about the x axis to put them in the correct position relative to the silicon atoms. The *tert*-butyl group and the two chlorines attached to Si(1) were initially placed in the xy plane, and the chlorine atoms were then rotated about the x axis. These rotations are defined in terms of the average of the torsion angles C(11)-Si(1)-Si(2)-Cl(12) and C(11)-Si(1)-Si(2)-Cl(13) (p_{15}) and the difference between these two angles.

Finally, the dihedral angle C(21)-Si(2)-Si(1)-C(13) (p_{17}) described the overall conformation about the Si-Si bond, with a value of zero indicating the conformation in which the two central carbon atoms of the *tert*-butyl groups were eclipsing one another.

Four dependent parameters were also used, describing the SiCC angles to the methyl carbon atoms and the ClSiCl angle.

2.3 Results

2.3.1 *Ab initio* calculations

Extensive searches of the torsional potential of all three molecules led to the location of three minima each for 1,2-di-*tert*-butyltetrachlorodisilane and 1,2-di-*tert*-butyltetrabromodisilane, and one minimum for 1,2-di-*tert*-butyltetraiododisilane. Vibrational frequency calculations at the HF/6-31G* level confirm that all the forms represent local minima on the potential energy surface. The three tetrachloro conformers with ϕ(CSiSiC) 163.8, 94.6 and 56.4° had relative energies of 0, 8.84 and 8.35 kJ mol^{-1}. This equates to a mixture containing 93.8% of the *transiod* conformer, and 3.4% and 2.8% of the 94° and 56° conformers, respectively, at room temperature. The two tetrabromo conformers with ϕ(CSiSiC) 180.0 and 116.3° had relative energies of 0 and 0.42 kJ mol^{-1}. This would equate to a mixture containing 50.1% of the *transiod* conformer, and 49.9% of the 116.3° conformer at room temperature. Only one *transiod* conformer with ϕ(CSiSiC) 168.1° was found for 1,2-di-*tert*-butyltetraiododisilane.

As the *transiod* conformer is dominant in most cases, discussion will focus on these structures with addition of the gauche structure found for 1,2-di-*tert*-butyltetrabromodisilane. The molecular geometries of these conformers at the MP2/6-31G* level are presented in Table 4; those calculated at the HF/3-21G* and HF/6-31G* levels of theory are presented in Appendix 1 [Table 1]. The molecular geometries of the highest level calculations for the other conformations of 1,2-di-*tert*-butyltetrachlorodisilane

are presented in Appendix 1 [Table 2]. As expected, since these systems contain no multiple bonds or lone pairs of electrons, the molecular geometry of the conformers proved to be relatively insensitive to changes in the theoretical method. For this reason, only the highest level results (MP2/6-31G*) will be discussed and presented in the order 1,2-di-*tert*-butyltetrachlorodisilane, 1,2-di-*tert*-butyltetrabromodisilane (with the gauche conformation in brackets) and 1,2-di-*tert*-butyltetraiododisilane where multiple results are discussed.

The molecular geometries appear to be dictated predominately by steric and, to a lesser extent, electronic interactions, as evident in the predicted values of the Si(1)-Si(2)-C(21) angle. This angle was predicted to be 117.6°, 119.2° (118.0°) and 118.5° compared to 109.5° for an ideal tetrahedral geometry around the silicon atom. In contrast, the X(22)-Si(2)-X(23) angles were predicted to be 107.4°, 108.6° (107.9°) and 107.3°, possibly indicating that the bulk of the *tert*-butyl groups is forcing the halogen atoms closer together. This could also be attributed to an electronic effect of the electron-withdrawing halogen atoms. The Si-Si-C angles are similar to those calculated for 1,2-di-*tert*-butyltetrafluorodisilane[9] (117.6°) and 1,2-di-*tert*-butyldisilane[8] (114.4°). The internal C-C-C angles [109.6°, 109.8° (109.9°) and 109.4°] indicate that the tert-butyl groups are hardly distorted from local C_3 symmetry in all the molecules studied.

Bond length predictions are generally within the expected ranges based on the results obtained previously for disilanes with *tert*-butyl or halogen groups. For example, the Si-Si bond length was predicted to be 235.7 pm for 1,2-di-*tert*-butyltetrachlorodisilane, and 234.6 pm (238.0 pm) for the bromo analogue as compared to 234.9 pm in 1,2-di-*tert*-butyltetrafluorodisilane[9] and 236.8 pm in 1,2-di-*tert*-butyldisilane.[8] All the predicted C-C bond lengths were similar [153.5 pm, 153.5 pm (153.5 pm) and 153.6 pm], as were the Si-C bond lengths [188.9 pm, 189.4 pm 189.2 pm) and 191.5 pm]. This falls within a range of Si-C bonds previously observed, for example 188.2(1) pm and 188.6(1) pm for 1,4-disilabutane and 1,5-disilapentane,[27] and 191.9 pm in 1,2-di-*tert*-butyldisilane.[8]

Table 4 Theoretical geometrical parameters at the MP2/6-31G* level for the *transiod* conformers of 1,2-di-*tert*-butyltetrachlorodisilane (C_2), 1,2-di-*tert*-butyltetrabromodisilane (C_{2h} and C_2) and at the MP2/DZP level[a] for 1,2-di-*tert*-butyltetraiododisilane (C_1).[b,c]

	$Bu^tCl_2SiSiCl_2Bu^t$	$Bu^tBr_2SiSiBr_2Bu^t$		$Bu^tI_2SiSiI_2Bu^t$
	C_2	C_{2h}	C_2	C_1
Parameter	Value	Value	Value	Value
Si(1)-Si(2)	235.7	234.6	238.0	238.5
Si(2)-C(21)	188.9	189.4	189.2	191.5
C(21)-C(211)	153.4	153.6	153.5	153.5
C(21)-C(212)	153.6	153.5	153.5	153.6
C(21)-C(213)	153.6	153.5	153.5	153.6
Si(2)-X(22)	207.1	223.3	222.0	250.8
Si(2)-X(23)	207.3	223.3	224.1	250.8
C-H[d]	109.5	109.5	109.5	109.5
Si(1)-Si(2)-C(21)	117.6	119.2	118.0	118.5
Si(2)-C(21)-C(211)	109.1	108.5	109.1	109.5
Si(2)-C(21)-C(212)	110.0	109.5	108.8	110.6
Si(2)-C(21)-C(213)	108.9	109.5	109.3	108.7
Si(1)-Si(2)-X(22)	105.4	105.8	106.5	105.0
Si(1)-Si(2)-X(23)	108.2	105.8	107.8	108.8
C-C-H[d]	110.9	110.8	110.8	110.8
C(21)-Si(2)-Si(1)-C(11)	167.8	180.0	116.3	168.1

[a] 6-31G* on C, Si, H and LanL2DZ on I. See text for details.

[b] All distances in pm, all angles in degrees. See Figure 2 for atom numbering.

[c] Absolute energies of conformers: 1,2-di-*tert*-butyltetrachlorodisilane = -2731.1717, 1,2-di-*tert*-butyltetrabromodisilane (C_{2h} = -11172.7815, C_2 = -11172.7814) and 1,2-di-*tert*-butyltetraiododisilane = -937.5001.

[d] Average value.

The Si-Cl bond lengths were predicted to be 207.0 and 207.3 pm, which compare well to that found experimentally in 1,2-dichlorotetramethyldisilane[28] [207.7(2) pm] but are sigificantly longer than in 1,1,2,2-tetrachlorodisilane[29] [203.9(2) pm (average value)]. The Si-Br bond length was predicted to be 223.3 pm (222.0 and 224.1 pm) which are all longer than that found experimentally in 1,1,2,2-tetrabromodisilane[6] [220.5(5) pm].

The Si-I bond lengths were all predicted to be 250.8 pm which are much longer than those found experimentally in 1,2-diiododisilane[30] (242.9(13) pm) and 1,1,2,2-tetraiododisilane[30] [244.0(9) pm]. The Si-Si bond length was also predicted to be longer than those observed previously (238.5 pm). The most likely explaination for this is the fact that effective core potentials (ECP's) were used on the iodine atoms. The LanL2DZ ECP was used, replacing the core and some valence electrons. Given that there are two iodine atoms attached to each silicon atom, it is more than likely that there are not enough electrons involved in the bonding; this will elongate the calculated Si-I and Si-Si distances.

2.3.2 Gas-phase electron diffraction (GED) refinement of 1,2-di-*tert*-butyl-tetrachlorodisilane

The starting parameters for the r_a refinement were taken from the theoretical geometry optimised at the MP2/6-31G* level. The r_α structure was not determined because the rectilinear vibrational corrections (i.e. parallel and perpendicular correction terms) are known to be unreliable for a molecule of this size, with many low-lying vibrational modes. Theoretical (HF/6-31G*) Cartesian force fields were obtained and converted into force fields described by a set of symmetry coordinates using the ASYM40 program.[32] All geometric parameters were then refined.

In total seventeen geometric parameters and thirty groups of vibrational amplitudes were refined. Eight geometric and twenty-four amplitude flexible restraints were employed using the SARACEN method.[26] These are listed in Appendix 1 [Tables 3 and 4].

The success of the final refinement, for which $R_G = 0.075$ ($R_D = 0.065$), can be assessed on the basis of the molecular scattering intensity curves (Figure 3) and the radial distribution

curve (Figure 4). Final refined parameters are listed in Table 3, interatomic distances and the corresponding amplitudes of vibration in Table 5, with the least-squares correlation matrix shown in Appendix 1 [Table 5] and the experimental coordinates from the GED analysis in Appendix 1 [Table 6]. In the SARACEN[26] analysis, all correlation between refining parameters is allowed for in the error estimates by the use of flexible restraints. We therefore quote the estimated standard deviations, σ, and believe that these are realistic estimates of the uncertainties of the parameters.

Figure 2 shows a perspective view of the *transiod* conformer of $Bu^tCl_2SiSiCl_2Bu^t$ in the optimum refinement of the GED data.

Figure 3 Experimental and final weighted difference (experimental - theoretical) molecular-scattering intensities for 1,2-di-*tert*-butyltetrachlorodisilane.

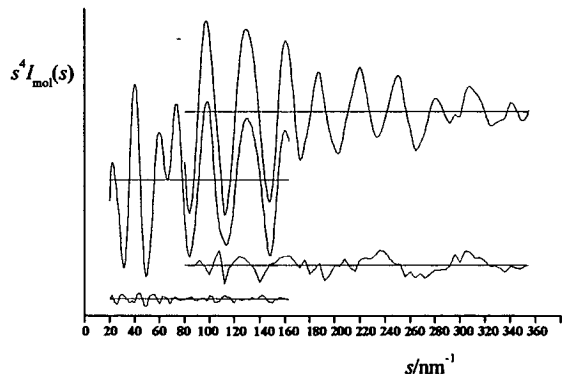

Figure 4 Experimental and difference (experimental - theoretical) radial distribution curves, $P(r)/r$, for $Bu^tCl_2SiSiCl_2Bu^t$. Before Fourier inversion the data were multiplied by $s.\exp(-0.00002s^2)/(Z_{Si} - f_{Si})/(Z_{Cl} - f_{Cl})$.

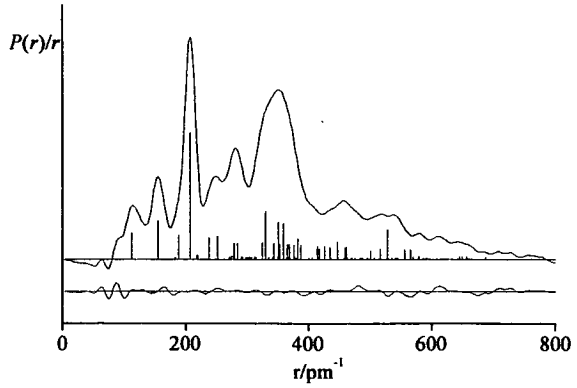

Table 5 Selected interatomic distances and mean amplitudes of vibration for 1,2-di-*tert*-butyltetrachlorodisilane from the GED study.[a]

No.	Atom pair	r_a/pm	u/pm
u_1	Si(1)-Si(2)	238.0(7)	6.5(6)
u_2	Si(2)-C(21)	187.2(7)	7.1(7)
u_3	Si(2)-Cl(22)	206.9(1)	5.6(3)
u_4	C-C	154.3(2)	6.9(4)
u_5	C-H	114.2(4)	8.7(5)
u_6	Cl(22)...Cl(23)	329.8(17)	12.5(9)
u_7	C(211)...C(212)	251.4(6)	7.1(7)
u_8	Si(1)...C(21)	368.8(14)	10.8(10)
u_9	Si(1)...C(211)	499.5(11)	9.7(20)
u_{10}	Si(1)...C(212)	420.7(28)	22.7(21)
u_{11}	Si(2)...C(211)	279.2(4)	9.1(5)
u_{12}	C(11)...C(21)	533.1(21)	14.2 (fixed)
u_{13}	Si(1)...Cl(22)	349.6(13)	13.0(12)
u_{14}	Si(1)...Cl(23)	358.3(15)	12.5(10)
u_{15}	C(21)...Cl(22)	323.5(32)	10.6(10)
u_{16}	C(21)...Cl(23)	323.1(34)	10.5(tied to u_{15})

[a] See Figure 2 for atom numbering. (Other amplitudes were used in the refinement but are not shown here.) A full list of the heavy atom distances and amplitudes of vibration is given in Appendix 1 [Table 11].

2.3.3 Crystal structure determination

All three solid structures were found to possess $P\bar{1}$ symmetry. Most of the common parameters associated with the structures agree to within 1-2 pm or 1-2°. For example, the Si-Si bond lengths were found to be 236.9, 235.5 and 236.6 pm for the chloro, bromo and iodo analogues respectively, whilst the mean C-C distances were 154.3, 153.7 and 154.0 pm. A gradual lengthening of the Si-C bond was observed from the chloro to iodo compound (188.1, 189.7 and 190.4 pm). Si-Cl bond lengths were observed to be 206.6 and 206.1 pm, whilst Si-Br bond lengths were 221.8 and 223.2 pm and Si-I bond lengths were 246.1 and 246.8 pm.

The mean CCC angles within the butyl groups were found to agree extremely well, 109.5° in 1,2-di-*tert*-butyltetrachlorodisilane, 110.1° in 1,2-di-*tert*-butyltetrabromodisilane and 109.2° in 1,2-di-*tert*-butyltetraiododisilane. The SiSiC angles were found to increase slightly from chlorine to bromine to iodine (118.2 to 119.2 to 120.0°). SiSiX angles were found to be 107.2 and 106.4° for 1,2-di-*tert*-butyltetrachlorodisilane, 106.1 and 106.5° for 1,2-di-*tert*-butyltetrabromodisilane and 106.7 and 105.4° for 1,2-di-*tert*-butyltetraiododisilane, whilst the XSiX angles were 106.9, 107.6 and 108.1° respectively. Geometrical parameters obtained for all three compounds by x-ray crystallography are presented in Appendix 1 [Table 7]. Atomic coordinates and equivalent isotropic displacement parameters for 1,2-di-*tert*-butyltetrachlorodisilane are presented in Appendix 1 [Table 12] and anisotropic displacement parameters are presented in Appendix 1 [Table 13]. The crystal structure of 1,2-di-*tert*-butyltetrachlorodisilane is shown in Figure 5.

Figure 5 X-ray crystallographic structure of 1,2-di-*tert*-butlytetrachlorodisilane

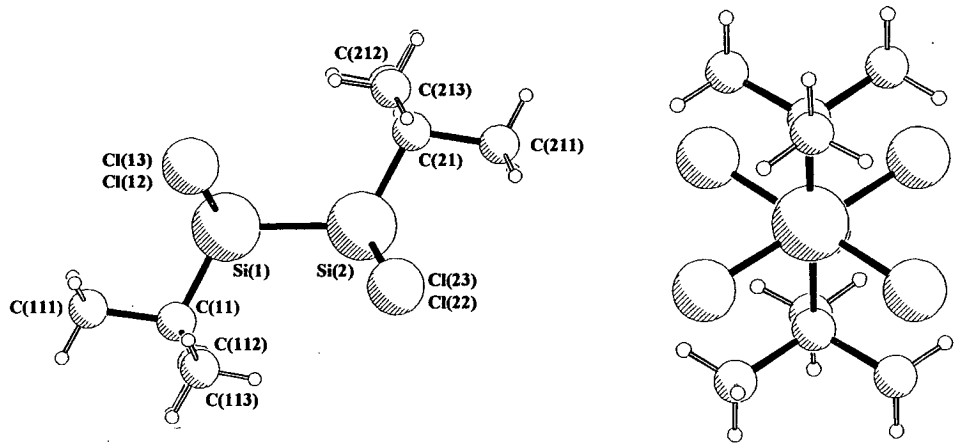

2.3.4 Vibrational spectra and normal coordinate analyses

(*Experiments conducted and assignments made by K. Hassler and R. Zink, Graz, Austria*)

The molecules $Bu^tX_2SiSiX_2Bu^t$ (where X = Cl, Br or I) have 90 fundamental modes which distribute in the following way between the symmetry species of the hypothetical perfectly staggered *anti* structure (point group C_{2h}) and the *gauche* structure (point group C_2):

anti (C_{2h}): Γ_{vib} = 25 a_g (Raman) + 20 b_g (Raman) + 21 a_u (IR) + 24 b_u (IR),

gauche (C_2): Γ_{vib} = 46 a (IR, Raman) + 44 b (IR, Raman).

The spectral positions of methyl stretching and deformation modes ($\nu_{sym}CH_3$, $\nu_{asym}CH_3$, $\delta_{sym}CH_3$ and $\delta_{asym}CH_3$) are of little interest. Exclusion of these modes from further discussion simplifies the vibrational problem to

anti (C_{2h}): Γ_{vib} = 15 a_g (Raman) + 12 b_g (Raman) + 13 a_u (IR) + 14 b_u (IR),

gauche (C_2): Γ_{vib} = 28 a (IR, Raman) + 26 b (IR, Raman).

To characterise the calculated vibrational modes, normal coordinate and potential energy distribution (PED) analyses have been carried out following the Wilson FG method[31] utilizing the calculated optimised structures and Cartesian force constants. The Cartesian Hessian matrices were thereby transformed into force fields defined in symmetry coordinates, which were linear combinations of redundant internal coordinates, resulting in a description of normal modes in terms of symmetry coordinates according to the PED values. The ASYM40[32] program was used for these computations. The chosen symmetry coordinates are listed in Table 6. The measured vibrational wavenumbers are collected in Table 7. Appendix 1 [Tables 8-10] summarise experimental wavenumbers, scaled theoretical wavenumbers and the tentative description of the modes by a single symmetry coordinate according to the PED values. For reasons of clarity and available space only calculated PED values for the transoid conformers have been listed. Moreover, the following discussion also focuses on the transoid species and uses the symmetry species of the hypothetical perfectly staggered structures.

Table 6 Symmetry coordinates for $Bu^tSiX_2SiX_2Bu^t$.[a]

Species[b]	No.	Description	Species[b]	No.	Description
a_g	S_1	ρ_1CH_3 (CH_3 rock)	b_g	S_{29}	ρ_1CH_3 (CH_3 rock)
	S_2	ρ_2CH_3 (CH_3 rock)		S_{30}	ρ_2CH_3 (CH_3 rock)
	S_3	ρ_3CH_3 (CH_3 rock)		S_{31}	ρ_3CH_3 (CH_3 rock)
	S_4	$\nu_{sym}CC_3$ (CC_3 sym stretch)		S_{32}	$\nu_{asym}CC_3$ (CC_3 asym stretch)
	S_5	$\nu_{asym}CC_3$ (CC_3 asym stretch)		S_{33}	$\delta_{asym}CC_3$ (CC_3 asym def)
	S_6	$\delta_{sym}CC_3$ (CC_3 sym def)		S_{34}	ρCC_3 (CC_3 rock)
	S_7	$\delta_{asym}CC_3$ (CC_3 asym def)		S_{35}	$\nu_{asym}SiX_2$ (SiX_2 asym stretch)
	S_8	ρCC_3 (CC_3 rock)		S_{36}	τSiX_2 (SiX_2 twist)
	S_9	νSiC (SiC stretch)		S_{37}	ρSiX_2 (SiX_2 rock)
	S_{10}	$\nu_{sym}SiX_2$ (SiX_2 sym stretch)		S_{38}	τ_1CC (CC torsion)
	S_{11}	νSiSi		S_{39}	τ_2CC (CC torsion)
	S_{12}	δSiSiC (SiSiC def)		S_{40}	τSiC (SiC torsion)
	S_{13}	δSiX_2 (SiX_2 scissoring)	b_u	S_{41}	ρ_1CH_3 (CH_3 rock)
	S_{14}	γSiX_2 (SiX_2 wag)		S_{42}	ρ_2CH_3 (CH_3 rock)
	S_{15}	τCC (CC torsion)		S_{43}	ρ_3CH_3 (CH_3 rock)
a_u	S_{16}	ρ_1CH_3 (CH_3 rock)		S_{44}	$\nu_{sym}CC_3$ (CC_3 sym stretch)
	S_{17}	ρ_2CH_3 (CH_3 rock)		S_{45}	$\nu_{asym}CC_3$ (CC_3 asym stretch)
	S_{18}	ρ_3CH_3 (CH_3 rock)		S_{46}	$\delta_{sym}CC_3$ (CC_3 sym def)
	S_{19}	$\nu_{asym}CC_3$ (CC_3 asym stretch)		S_{47}	$\delta_{asym}CC_3$ (CC_3 asym def)
	S_{20}	$\delta_{asym}CC_3$ (CC_3 asym def)		S_{48}	ρCC_3 (CC_3 rock)
	S_{21}	ρCC_3 (CC_3 rock)		S_{49}	νSiC (SiC stretch)
	S_{22}	$\nu_{asym}SiX_2$ (SiX_2 asym stretch)		S_{50}	$\nu_{sym}SiX_2$ (SiX_2 sym stretch)
	S_{23}	τSiX_2 (SiX_2 twist)		S_{51}	δSiSiC (SiSiC def)
	S_{24}	ρSiX_2 (SiX_2 rock)		S_{52}	δSiX_2 (SiX_2 scissoring)
	S_{25}	τ_1CC (CC torsion)		S_{53}	γSiX_2 (SiX_2 wag)
	S_{26}	τ_2CC (CC torsion)		S_{54}	τCC (CC torsion)
	S_{27}	τSiC (SiC torsion)			
	S_{28}	τSiSi (SiSi torsion)			

[a] Symmetry coordinates for methyl stretching and deformation modes have been omitted.

[b] Symmetry species corresponding to the hypothetical planar (*anti*) structure of C_{2h} symmetry. The a_g and a_u blocks and the b_g and b_u blocks combine to a and b blocks, respectively, for the point group C_2 of transoid and twisted (*gauche*, *ortho*) conformers.

Table 7 Infrared and Raman spectra (< 1250 cm^{-1}) of $Bu^tX_2SiSiX_2Bu^t$ (X = Cl, Br and I).

$Bu^tCl_2SiSiCl_2Bu^t$		$Bu^tBr_2SiSiBr_2Bu^t$		$Bu^tI_2SiSiI_2Bu^t$	
IR(s)	Raman(s)	IR(s)	Raman(s)	IR(s)	Raman(s)
1204m	1227w,sh				
	1202s		1200sh		1182m
1185m	1188sh	1193ms	1186ms	1169m	1167sh
1006s	1006w	1004ms	1007m	1005m	1005w
940s	939w	939m	939m	937m	938w
815vs	814s	809s	810s	804ms	806m
					800sh
670vvw		620sh	622m		601mw
630sh	632s	601s			
616vs					
587m,sh	585w	561mw		584m	
562vvs	548w	534vw	537w	543w	
525vw		516mw		489w	502mw
483vs		474vs	470m	424vs	425m
443m	437vs	425sh	421sh	390sh	396m
396vs	391vw	407vs	410s	374vs	375m
352vs	383w	390sh	381m	355sh	
	307ms	342s		327vs	
279m	289w		284sh		276vw,b
	274w				239sh
	264w		244m		230w,b
	233ms		223vs		198vs
	186s		158w		
	158w		141vs		
	137vs		131s		
	130s		114s		118s
	110ms		96s		100vs
	49w		77vs		80s
	34w				55vs
					30w

s = strong, m = medium, w = weak, v = very, sh = shoulder, b = broad.

Inspection of the computed PED values shows that the description of normal modes by a single symmetry coordinate is highly approximate since several modes represent mixtures of two, three or even more dominant symmetry coordinates, and sometimes a symmetry coordinate is the most important contribution in two different modes [see Appendix 1 (Tables 8-10)].

2.3.5 Rotational isomerism

(*Experiments conducted and assignments made by K. Hassler and R. Zink*)

Variable temperature Raman spectroscopy is a useful tool for the investigation of conformational mixtures because Raman-active skeletal modes usually vary significantly with the backbone conformation. Previously the rotational isomers of the disilanes MeX_2SiSiX_2Me[33] and the trisilanes $SiMe_3SiMe_2SiMe_2X$[34] and $SiMe_3SiMe_2SiMeX_2$[35] have been detected by this technique. For example, in $MeBr_2SiSiBr_2Me$ the wavenumber of the strongly Raman-active symmetric SiBr stetching mode ($\nu_{sym}SiBr_2$) was found to differ by 20 cm^{-1} between *anti* and *gauche* conformers. Unexpectedly, the calculated vibrational frequencies of transoid and twisted (*gauche* and *ortho*) conformers of the disilanes $Bu^tX_2SiSiX_2Bu^t$ (X = Cl, Br and I) are predicted to differ very little from each other and there is little hope of identifying rotational isomers from vibrational spectra of the condensed phases. Indeed, Raman spectra of liquid $Bu^tCl_2SiSiCl_2Bu^t$, liquid $Bu^tBr_2SiSiBr_2Bu^t$ and of a solution of $Bu^tI_2SiSiI_2Bu^t$ in various organic solvents are not sensitive to temperature and thus do not reveal clues about the existence of rotational isomers. Moreover, the vibrational spectra of solid $Bu^tBr_2SiSiBr_2Bu^t$ and $Bu^tI_2SiSiI_2Bu^t$ strictly follow the rule of mutual exclusion and this strongly suggests that the planar *anti* rotamer (point group C_{2h}) is the only structure present in the solid state. However, this is not true for $Bu^tCl_2SiSiCl_2Bu^t$. For the transoid conformer, the modes $\delta_{sym}CC_3$ (a,a_g) and $\nu SiSi$ (a,a_g) are predicted to have fairly high intensities in the Raman whereas the intensities in the IR are very small. In the solid state these modes are tentatively assigned to the peaks at around 437 and 585 cm^{-1}. Surprisingly, the IR spectrum of solid $Bu^tCl_2SiSiCl_2Bu^t$ also shows two rather strong peaks at similar positions (443 and 587 cm^{-1}). This suggests that a substantial fraction of twisted conformers (*gauche* and/or *ortho*) is present in solid $Bu^tCl_2SiSiCl_2Bu^t$ as only the twisted structures are predicted to possess high IR intensities at these spectral positions. The calculated amount of twisted conformers present is ~10%. This agrees with that predicted in the gas-phase by *ab initio* calculations with 94% transiod and ~3% each of the other 2 conformers. As the solid was formed by sublimation, the presence of these bands can thus be

explained, although no other conformers were observed in the crystal structure of the solid.

2.4 Discussion

Theoretical and experimental studies show that 1,2-di-*tert*-butyltetrachlorodisilane exists as a single conformer in the gas phase, with a C-Si-Si-C dihedral angle of 168°. The final experimental structure is in satisfactory agreement with that calculated *ab initio* at the MP2/6-31G* level; computed bond lengths and angles generally fall within 1-2 pm or 1-2° of the GED values (Table 2). For example, the Si-Si bond length refined to 238.0(7) pm compared to the computed value of 235.7 pm. The mean C-C bond length refined to 154.3(2) pm compared to 153.6 pm (mean) from the calculations and the Si-C bond length was 187.2(7) pm compared to the calculated value of 188.9 pm. The experimental Si-Cl (mean) bond length (207.1 pm) compared very well with the calculated value of 207.2 pm. The Si-Si-C bond angle refined to 119.8(6)° compared with predicted value of 117.6° and the Cl-Si-Cl bond angle refined to 105.5(8)° compared to the calculated value of 107.4°. The torsion about the Si-Si axis, dihedral angle C(11)-Si(1)-Si(2)-C(21), which uniquely describes the position of the butyl groups about the Si-Si axis, agrees extremely well with the predicted value; 167.7(11)° *vs.* 167.9°.

Observed geometric parameters are generally consistent with those for a number of closely related compounds. For example, the Si-Si bond distance in 1,2-di-*tert*-butyltetrachlorodisilane [238.0(7) pm] is within the range of values found for other disilanes from GED refinements, including 1,2-diiododisilane[7] [238.0(34) pm] and 1,1,2,2-tetraiododisilane[7] [238.9(37) pm] and 1,1,2-tri-*tert*-butyldisilane (See Chapter 3) [236.3(8) pm]. It is somewhat longer than those in some other halogenated and/or bulky disilanes, including 1,2-di-*tert*-butyldisilane[8] [234.8(3) pm] and 1,1,2,2-tetrabromodisilane[6] [234.9(19) pm]. However, 1,1,2,2-tetrachlorodisilane[28] is reported as having a Si-Si bond length of only 231.0(8) pm. This gives an indication that the bulky alkyl ligands have a large steric effect on the bond lengths within the

molecule, as might be expected. Refined values of the C-Ċ [154.3(2) pm] and Si-Cl [207.1(1) pm] bond lengths are in excellent agreement with calculated values, but again, the Si-Cl bonds were found to be much longer in 1,2-di-*tert*-butyltetrachlorodisilane than in 1,1,2,2-tetrachlorodisilane[28] [203.9(2) pm]. This may be a steric effect of the bulky alkyl groups at each end of the molecule, but may also be influenced by the electron-releasing properties of these groups. Both types of effect must play significant roles in determining bond distances in disilanes.

The dramatic deviation of the Si-Si-C bond angle [119.8(6)°] from the "pure" sp^3 tetrahedral angle [109.5°] is a common feature of disilanes with butyl groups. For example, in 1,1,2-tri-*tert*-butyldisilane (See Chapter 3) Si-Si-C angles of up to 116.0(8)° are observed, whilst 1,2-di-*tert*-butyldisilane[8] [113.7(3)°] and 1,2-di-*tert*-butyltetrafluorodisilane[9] [114.6(7)°] also demonstrate widening of the Si-Si-C angle. This provides more evidence for significant steric interaction between the butyl groups at one end of the molecule and chlorine atoms at the other end in 1,2-di-*tert*-butyltetrachlorodisilane.

The structure of 1,1,2,2-tetrachlorodisilane has recently been reported.[28] Johansen and co-workers report that in the gas phase there is a mixture of two conformers, *anti* [ϕ(HSiSiH) = 180°] and *gauche* [ϕ(HSiSiH) $\approx$ 60°]. In this case, however, the *gauche* conformer was found to predominate in the gas phase mixture, existing in an 80:20% ratio with the *anti* conformer. This is in complete contrast to the di-*tert*-butyl substituted case, where the *anti* conformation was found to be dominant in the gas phase. This is yet more evidence for steric crowding amongst these bulky alkyl substituted disilanes.

The solid-state structure of 1,2-di-*tert*-butyltetrachlorodisilane has also been determined. The space group $P\bar{1}$ indicates that the molecule has an inversion centre, and thus the C-Si-Si-C dihedral angle is 180.0° as opposed to the C_2 structure [ϕ(CSiSiC) = 167.7(11)°] found in the gas phase. Thermal parameters associated with the solid structure were investigated to ascertain whether there was much

disorder within the crystal, given the change in the C-Si-Si-C torsion angle between the solid and gaseous structures indicating that there are intermolecular forces acting on the solid. There was found to be a slight distortion of the carbon and chlorine atoms in the *y* direction, but no significant distortion was detected.

Bond lengths and angles agree in the solid and gaseous structures very well. For example, the Si-C bond length was found to be 188.1(3) pm in the solid compared to 187.2(7) in the gas. The mean C-C distances also agree extremely well [solid 154.3(4) pm; gas 154.3(2) pm] as do the mean Si-Cl distances [solid 206.3(1) pm; gas 207.1(1) pm]. There is a slight discrepancy between the experimental Si-Si distances, 236.9(1) pm in the solid, 238.0(7) pm in the gas. However, this is not a major difference when one considers the uncertainties associated with both distances.

Angles were also found to agree well between the solid and gaseous phases, with the Si-Si-C angle found to be 118.2(9)° in the solid phase compared to 119.8(6)° in the gas phase. The Cl-Si-Cl angle refined to 106.9(5)° in the crystal compared to 105.5(8)° in the GED refinement. The mean C-C-C angles, 109.4(2) and 109.1(3)° in the solid and gas phases, also agree well.

The crystal structures of the bromo and iodo analogues were also determined. Unfortunately, they are not volatile enough to collect GED data, but we can compare the crystal structures with each other, and with those calculated *ab initio*. Both structures were found to behave very similarly to the chloro analogue in the solid phase, i.e. possessing $P\bar{1}$ symmetry with an inversion centre at the centre of the Si-Si bond. Si-Si bond lengths in 1,2-di-*tert*-butyltetrabromodisilane and 1,2-di-*tert*-butyltetraiododisilane were found to be very similar to each other and to that found in 1,2-di-*tert*-butyltetrachlorodisilane; 235.4 pm in 1,2-di-*tert*-butyltetrabromodisilane and 236.6 pm in 1,2-di-*tert*-butyltetraiododisilane compared to 236.9 pm in 1,2-di-*tert*-butyltetrachlorodisilane. A slight variation in the Si-C bond lengths was found, with 189.7 pm in 1,2-di-*tert*-butyltetrabromodisilane and 190.4 pm in 1,2-di-*tert*-butyltetraiododisilane compared to 188.1 pm in 1,2-di-*tert*-butyltetrachlorodisilane.

The mean C-C bond lengths were all consistent with each other; 153.8 pm in 1,2-di-*tert*-butyltetrabromodisilane and 154.0 pm in 1,2-di-*tert*-butyltetraiododisilane compared to 154.3 pm in 1,2-di-*tert*-butyltetrachlorodisilane.

The C-C-C angles were also found to be very consistent [1,2-di-*tert*-butyltetrachlorodisilane 109.4, 1,2-di-*tert*-butyltetrabromodisilane 110.1 and 1,2-di-*tert*-butyltetraiododisilane 109.2°], indicating very little steric strain within the butyl groups themselves. The Si-Si-C angles were found to increase from X = Cl to I (Cl 118.2°; Br 119.2°; I 120.0°), as did the X-Si-X angles (Cl 106.9°; Br 107.6°; I 108.1°). This is to be expected on steric and electronic grounds. Electronically, chlorine is more electron-withdrawing than bromine and iodine, thus ClSiCl is smaller than BrSiBr and ISiI. Sterically, as the halogen increases in size, the X-Si-X angle would be expected to increase, as would the Si-Si-C angle at the opposing end of the molecule. However, this increase is offset by steric constraints of the halogens at the same end of the molecule

2.5 References

1. "*Frontiers of Organisilicon Chemistry*", Eds. A. R. Bassindale and P. P. Gaspar, The Royal Society of Chemistry, 1991.
2. H. Rossotti, "*Diverse Atoms: Profiles of the Chemical Elements*", Oxford University Press, 1998, p. 149.
3. J. Emsley, "*The elements*", Clarendon Press, 1989, p. 172.
4. "*Organosilicon Chemistry III*", Eds. N. Auner and J. Weis, Wiley-VCH, 1998. P. 3.
5. S. Masamune, Y. Hanzawa, S. Murakami, T. Bally and J. F. Blount, *J. Am. Chem. Soc.*, 1982, **104**, 1150.
6. H. Thomassen, K. Hagen, R. Stølevik and K. Hassler, *J. Mol. Struct.*, 1986, **147**, 331.
7. E. Røhmen, K. Hagen, R. Stølevik, K. Hassler and M. Pöschl, *J. Mol. Struct.*, 1991, **244**, 41.
8. D. Hnyk, R. S. Fender, H. E. Robertson, D. W. H. Rankin, M. Bühl, K. Hassler and K. Schenzel, *J. Mol. Struct.*, 1995, **346**, 215.
9. B. A. Smart, H. E. Robertson, N. W. Mitzel, D. W. H. Rankin, R. Zink and K. Hassler, *J. Chem. Soc., Dalton Trans.*, 1997, 2475.
10. B. Reiter and K. J. Hassler, *J. Organomet. Chem.* 1994, **467**, 21.
11. Gaussian 94 (Revision C.2), M. J. Frisch, G. W. Trucks, H. B. Schlegel, P. M. W. Gill, B. G. Johnson, M. A. Robb, J. R. Cheesman, T. A. Keith, G. A. Petersson, J. A. Montgomery, K. Raghavachari, M. A. Al-Laham, V. G. Zakrzewski, J. V. Ortiz, J. B. Foresman, J. Cioslowski, B. B. Stefanov, A. Nanayakkara, M. Challacombe, C. Y. Peng, P. Y. Ayala, W. Chen, M. W. Wong, J. L. Andres, E. S. Replogle, R. Gomperts, R. L. Martin, D. J. Fox, J. S. Binkley, D. J. Defrees, J. Baker, J. P. Stewart, M. Head-Gordon, C. Gonzalez and J. A. Pople, Gaussian Inc., Pittsburgh, PA, 1995.
12. Gaussian 98, Revision A.7, M. J. Frisch, G. W. Trucks, H. B. Schlegel, G. E. Scuseria, M. A. Robb, J. R. Cheeseman, V. G. Zakrzewski, J. A. Montgomery, R. E. Stratmann Jr, J. C. Burant, S. Dapprich, J. M. Millam, A. D. Daniels, K. N. Kudin, M. C. Strain, O. Farkas, J. Tomasi, V. Barone, M. Cossi, R. Cammi, B. Mennucci, C. Pomelli, C. Adamo, S. Clifford, J. Ochterski, G. A. Petersson, P. Y.

Ayala, Q. Cui, K. Morokuma, D. K. Malick, A. D. Rabuck, K. Raghavachari, J. B. Foresman, J. Cioslowski, J. V. Ortiz, A. G. Baboul, B. B. Stefanov, G. Liu, A. Liashenko, P. Piskorz, I. Komaromi, R. Gomperts, R. L. Martin, D. J. Fox, T. Keith, M. A. Al-Laham, C. Y. Peng, A. Nanayakkara, C. Gonzalez, M. Challacombe, P. M. W. Gill, B. Johnson, W. Chen, M. W. Wong, J. L. Andres, C. Gonzalez, M. Head-Gordon, E. S. Replogle and J. A. Pople, Gaussian, Inc., Pittsburgh PA, 1998.

13. J. S. Binkley, J. A. Pople and W. J. Hehre, *J. Am. Chem. Soc.*, 1980, **102**, 939.
14. M. S. Gordon, J. S. Binkley, J. A. Pople, W. J. Pietro and W. J. Hehre, *J. Am. Chem. Soc.*, 1982, **104**, 2797.
15. W. J. Pietro, M. M. Francl, W. J. Hehre, D. J. DeFrees, J. A. Pople and J. S. Binkley, *J. Am. Chem. Soc.*, 1982, **104**, 5039.
16. W. J. Hehre, R. Ditchfield and J. A. Pople, *J. Chem. Phys.*, 1972, **56**, 2257.
17. P. C. Hariharan and J. A. Pople, *Theor. Chim. Acta*, 1973, **28**, 213.
18. M. S. Gordon, *Chem. Phys. Lett.*, 1980, **76**, 163.
19. T. H. Dunning Jr. and P. J. Hay, "Modern Theoretical Chemistry", Vol. 3, Ed. H. F. Schaefer III, Plenum, 1976, p. 1; P. J. Hay and W. R. Wadt, *J. Chem. Phys.*, 1985, **82**, pp. 270, 284 and 299.
20. G. M. Sheldrick, SHELXTL version 5.1, Bruker AXS., Madison, WI, USA, (1998).
21. C. M. Huntley, G. S. Laurenson and D. W. H. Rankin, *J. Chem. Soc., Dalton Trans.*, 1980, 954.
22. J. R. Lewis, P. T. Brain and D. W. H. Rankin, *Spectrum*, 1997, **15**, 7.
23. S. Cradock, J. Koprowski and D. W. H. Rankin, *J. Mol. Struct.*, 1981, **77**, 113.
24. A. S. F. Boyd, G. S. Laurenson and D. W. H. Rankin, *J. Mol. Struct.*, 1981, **71**, 217.
25. A. W. Ross, M. Fink and R. Hilderbrandt, in A. J. C. Wilson (Ed.), *International Tables for Crystallography*, Vol. C, Kluwer Academic Publishers, Dordrecht, 1992, p. 245.
26. A. J. Blake, P. T. Brain, H. McNab, J. Miller, C. A. Morrison, S. Parsons, D. W. H. Rankin, H. E. Robertson and B. A. Smart, *J. Phys. Chem.*, 1996, **100**, 12280;

P. T. Brain, C.A. Morrison, S. Parsons and D. W. H. Rankin, *J. Chem. Soc., Dalton Trans.*, 1996, 4589.

27. N. W. Mitzel, B. A. Smart, A. J. Blake, H. E. Robertson and D. W. H. Rankin, *J. Phys. Chem.*, 1996, **100**, 9339.
28. K. Kveseth, *Acta Chem. Scand.*, 1979, **A33**, 453.
29. T. H. Johansen, K. Hagen and R. Stølevik, *J. Mol. Struct.*, 1999, **485-486**, 121.
30. E. Røhmen, K. Hagen and R. Stølevik, *J. Mol. Struct.*, 1991, **244**, 41.
31. E. B. Wilson Jr., J. C. Decius and P. C. Cross, Molecular Vibrations, McGraw-Hill, New York, 1955.
32. L. Hedberg and I. M. Mills, *J. Mol. Spectrosc.*, 1993, **160**, 117.
33. R. Zink, K. Hassler and M. Ramek, *Vibrational Spectrosc.*, 1998, **18**, 123.
34. A. Jähn, K. Schenzel, R. Zink and K. Hassler, *J. Raman Spectrosc.*, 1998, **29**, 841.
35. A. Jähn, K. Schenzel, R. Zink and K. Hassler, *J. Raman Spectrosc.*, 1998, **29**, 1055.

Chapter 3

1,1,2-tri-*tert*-butyldisilane, $Bu^t_2HSiSiH_2Bu^t$: Vibrational Spectra and Molecular Structure in the Gas Phase by Electron Diffraction and *Ab Initio* Calculations.

3.1 Introduction

Compounds with Si-Si bonds are important, for example, in polymers. Spectroscopic properties are surprisingly sensitive to conformation[1] therefore studies of conformation of model compounds are important. The conformations will depend on both electronic and steric effects, so combinations of halogens and big (butyl) groups will be interesting. The structures of some simple disilanes including Si_2H_6 and Si_2Cl_6 have been determined previously,[2] as have the structures of some partially halogenated disilanes such as 1,1,2,2-tetrabromodisilane,[3] 1,2-diiododisilane[4] and 1,1,2,2-tetraiododisilane.[4] Recently, more sterically crowded systems containing *tert*-butyl groups were studied, including 1,2-di-*tert*-butyldisilane,[5] 1,2-di-*tert*-butyltetrafluorodisilane[6] and 1,2-di-*tert*-butyltetrachlorodisilane (Chapter 2). Several compounds have been investigated in the course of this project. In this chapter, a disilane with only butyl groups and relatively low symmetry will be described.

Ab initio computations have been performed on all of these compounds. For the disilanes with only halogens and no bulky groups, a mixture of *gauche* and *anti* structures was found in each case. However, for the compounds containing butyl groups, as might be expected on steric grounds, the *anti* conformation is favoured in all cases. The compound 1,2-di-*tert*-butyltetrachlorodisilane is predicted to exhibit three local minima on the potential energy surface at the MP2/6-31G* level, with C-Si-Si-C dihedral angles of 56°, 94° and 169°, the *anti* conformer being slightly distorted from the idealised (C_{2h}) structure. This distortion is due to the bulky butyl groups twisting by ~18° away from the Si-Si-C-C plane within the molecules. In contrast to 1,2-di-*tert*-butyltetrachlorodisilane, only two conformers were located for 1,2-di-*tert*-butyldisilane at the HF/6-31G* level, *anti* and *gauche* (C-Si-Si-C dihedral angles of 176.8° and 69.0° respectively). The energy minimum for the *gauche* structure of 1,2-di-*tert*-butyldisilane was estimated to lie 5.4 kJ mol^{-1} above that for the *anti* structure on the potential energy surface and therefore the *gauche* structure should not be observable by electron diffraction in the gas phase. It was not possible to determine from the GED data how much of the *gauche* conformer was present,

although it was certainly less than 20%. The lower limit for observation of another conformer by GED is typically 10-15%. For 1,2-di-*tert*-butyltetrafluorodisilane two conformers, *gauche* and *anti*, were predicted from calculations at the HF/6-31G* level, with vibrational frequency calculations indicating that both forms represent local minima. However, the barrier to interconversion between *gauche* and *anti* was predicted to lie just 0.25 kJ mol^{-1} above the *gauche* isomer, which may therefore represent a quasi-minimum on the potential energy surface rather than a distinct conformer. The experimental structure was modelled with two conformers, but as the C-Si-Si-C dihedral angles refined to 184(7)° and 152(3)°, the data are consistent with a single conformer with a large-amplitude motion over a torsional range of around 140-220° rather than with a mixture of two distinct conformers.

In view of the interesting conformational behaviour of di-*tert*-butyl-substituted disilanes, a further structural study on a disilane with three butyl groups, 1,1,2-tri-*tert*-butyldisilane, has been undertaken employing the techniques of vibrational spectroscopy (*carried out by K. Hassler and R. Zink, Graz*), gas-phase electron diffraction and *ab initio* calculations. This system is more crowded than the di-*tert*-butyl substituted disilanes and the structure would be expected to be dominated by steric interactions between these groups.

3.2 Experimental

3.2.1 Synthesis

A sample of $Bu^t_2HSiSiH_2Bu^t$ was prepared by K. Hassler and R. Zink according to the literature method[7] and provided for use on the Edinburgh diffraction apparatus.

3.2.2 *Ab initio* calculations

All calculations at the HF/3-21G*[8-10] and HF/6-31G*[11-13] levels were performed on a Dec Alpha 1000 4/200 workstation using the Gaussian 94 program.[14] Calculations at the MP2 level using the 6-31G* and D95*[15] basis sets were performed using resources of the U.K. Computational Chemistry Facility, on a DEC 8400 superscalar cluster equipped with 10

fast processors, 6 GB of memory and 150 GB disk. An extensive search of the torsional potential of 1,1,2-tri-*tert*-butyldisilane was undertaken at the HF/3-21G* level in order to locate all local minima. Three conformers, *syn*, *gauche* and *antiperiplanar*, were located and further geometry optimisations were undertaken at the HF/6-31G* level and at the MP2 level using the 6-31G* and D95* basis sets. The D95* basis set is a *double zeta* basis set that forms molecular orbitals from a linear combination of functions for each atomic orbital and gives a good orbital representation of the first and second row atoms in molecules. Vibrational frequencies were calculated from analytic second derivatives at the HF/3-21G* and HF/6-31G* levels to determine the nature of stationary points for comparison with experimentally determined frequencies, and the force field provided estimates of amplitudes of vibration (u) for use in the GED refinements.

3.2.3 Infrared and Raman spectra

(*Conducted by K. Hassler and R. Zink, Graz, Austria*)

Infrared spectra in the range 3200-300 cm^{-1} were measured with a Perkin-Elmer 883 spectrometer using a film of pure liquid between CsBr plates. The Raman spectra were recorded with a Jobin Yvon T64000 triple monochromator employing a charge-coupled device (CCD) camera and the 514.5 nm line of an argon-ion laser as the source of excitation. Variable-temperature Raman spectra were obtained by mounting a capillary containing the sample on a copper block equipped with a heater and a thermocouple. Liquid nitrogen was used for cooling the sample.

3.2.4 Electron diffraction

Electron scattering intensities were recorded on Kodak Electron Image plates using the Edinburgh gas diffraction apparatus operating at *ca.* 44.5 kV (electron wavelength *ca.* 5.6 pm).[16] Nozzle-to-plate distances for the metal inlet nozzle were *ca.* 94 and 259 mm yielding data in the s range 20-356 nm^{-1}; three plates were exposed at each camera distance. The sample and nozzle temperatures were maintained at *ca.* 411 K during the exposure periods.

The scattering patterns of benzene were also recorded for the purpose of calibration; these were analysed in exactly the same way as those for $Bu^t_2HSiSiH_2Bu^t$ so as to minimise systematic errors in the wavelengths and camera distances. Nozzle-to-plate distances, weighting functions used to set up the off-diagonal weight matrix, correlation parameters, final scale factors and electron wavelengths for the measurements are collected in Table 1.

The electron-scattering patterns were converted into digital form using a computer-controlled Joyce Loebl MDM6 microdensitometer with a scanning program described elsewhere.[17] The programs used for data reduction[17] and least-squares refinement[18] have been described previously; the complex scattering factors were those listed by Ross *et al.*[19]

Table 1 Nozzle-to-plate distances (mm), weighting functions (nm^{-1}), correlation parameters, scale factors and electron wavelengths (pm) used in the electron diffraction study.

Nozzle-to-plate distance[a]	Δs	s_{min}	sw_1	sw_2	s_{max}	Correlation parameter	Scale factor[b]	Electron wavelength
93.34	4	80	100	304	336	0.1658	0.575(15)	5.654
258.15	2	20	40	140	160	0.1779	0.807(14)	5.653

[a] Determined by reference to the scattering pattern of benzene vapour.

[b] Values in parentheses are the estimated standard deviations.

3.3 Results

3.3.1 Theoretical computations

A series of *ab initio* molecular-orbital calculations was undertaken to investigate the structure of 1,1,2-tri-*tert*-butyldisilane. An extensive search of the torsional potential led to the location of three minima, conformers *syn*, ϕ[C(21)-Si(2)-Si(1)-H(13)] = -4.2°, *gauche*, ϕ[C(21)-Si(2)-Si(1)-H(13)] = 63.4°, and *antiperiplanar*, ϕ[C(21)-Si(2)-Si(1)-H(13)] = 163.8° [Figure 1]. The nomenclature used to define the three conformers describes the positions of the hydrogen atom at the Bu^t_2HSi end of the molecule relative to

the lone butyl group at the Bu^tH_2Si end. The twist about the silicon-silicon bond is uniquely described by this torsion angle.

Figure 1 Graphical representation of the energy differences (MP2/D95* level) between the three comformers of 1,1,2-tri-*tert*-butyldisilane.

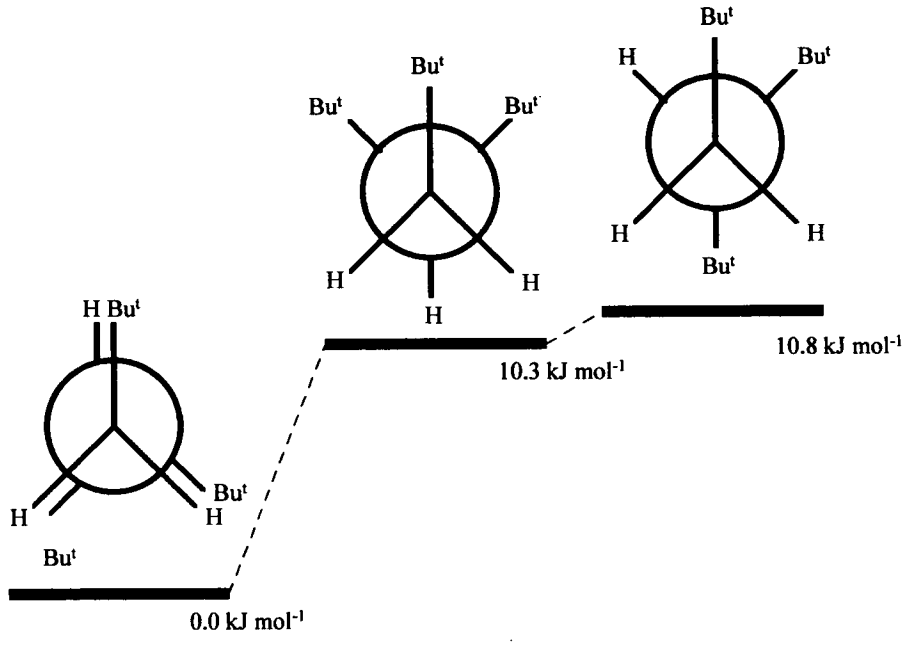

Vibrational frequency calculations at the HF/6-31G* level confirm that all three forms represent local minima on the potential energy surface. However, the *syn* structure was found to be 10.8 kJ mol^{-1} lower in energy than the *gauche* structure and 10.3 kJ mol^{-1} below the *antiperiplanar* structure, a very surprising result given that the *syn* structure is eclipsed. This would equate to a mixture containing 96.3% of the *syn* conformer and 2.3% and 1.4% of the *gauche* and *antiperiplanar* conformers, respectively, at room temperature. Attention will therefore be paid mainly to the *syn* structure. The relative energies of all 3 conformations are shown in Figure 1 and Table 2. The molecular geometry of the *syn* conformer for the MP2/D95* calculation is presented in Table 3; those calculated at the HF/3-21G*, HF/6-31G* and MP2/6-31G* levels of theory are presented in Appendix 2 [Table 1]. The molecular geometries of the *gauche* and *antiperiplanar* conformers calculated at the HF/3-21G*, HF/6-31G*, MP2/6-31G* and MP2/D95* levels are presented in Appendix 2 [Table 2].

As expected, since this system contains no multiple bonds or lone pairs of electrons, the molecular geometry of the conformer proved to be insensitive to changes in the theoretical method. For this reason, only the highest level results (MP2/D95*) will be discussed.

Table 2 Relative energies (kJ mol^{-1}) of the *syn*, *gauche* and *antiperiplanar* conformers of 1,1,2-tri-*tert*-butyldisilane.

Level/Basis Set	*syn*	*gauche*	*antiperiplanar*
HF/3-21G*	0	12.7	14.8
HF/6-31G*	0	11.1	12.1
MP2/6-31G*	0	10.1	10.2
MP2/D95*	0	10.8	10.3

Table 3 Theoretical geometrical parameters (MP2/D95* level) for the *syn* conformer of 1,1,2-tri-*tert*-butyldisilane.[a]

Parameter	Value	Parameter	Value
Si(1)-Si(2)	237.5	C(11)-Si(1)-C(12)	118.6
Si(1)-C(11)	192.3	Si(1)-Si(2)-C(21)	112.6
C(11)-C(111)	153.8	Si(2)-C(21)-C(211)	109.7
C(11)-C(112)	154.2	Si(2)-C(21)-C(212)	109.2
C(11)-C(113)	154.2	Si(2)-C(21)-C(213)	110.6
Si(1)-C(12)	192.4	Si(2)-Si(1)-C(11)	110.4
C(12)-C(121)	154.2	Si(1)-C(11)-C(111)	112.2
C(12)-C(122)	153.9	Si(1)-C(11)-C(112)	111.3
C(12)-C(123)	153.9	Si(1)-C(11)-C(113)	107.6
Si(2)-C(21)	191.5	Si(2)-Si(1)-C(12)	108.8
C(21)-C(211)	153.9	Si(1)-C(12)-C(121)	106.8
C(21)-C(212)	154.0	Si(1)-C(12)-C(122)	111.8
C(21)-C(213)	153.9	Si(1)-C(12)-C(123)	112.5
Si(1)-H(13)	150.5	Si(1)-Si(2)-H(22)	110.4
Si(2)-H(22)	149.8	Si(1)-Si(2)-H(23)	110.9
Si(2)-H(23)	149.9	Si(2)-Si(1)-H(13)	107.2
C-H[b]	110.1	C-C-H[b]	111.1
		C(21)-Si(2)-Si(1)-H(13)	-4.2

[a] All distances in pm, all angles in degrees. See Figure 2 for atom numbering.

[b] Average value.

The molecular geometry of the conformer appears to be dictated predominately by steric interactions, as evident in the calculated values for the C(11)-Si(1)-C(12) angle (See Figure 2 for atom numbering). In the *syn* conformer, the C(11)-Si(1)-C(12) angle is predicted to be 118.6° compared to 109.5° for an ideal tetrahedral geometry. Further evidence of steric repulsion is found in the value of the Si(1)-Si(2)-C(21) angle, 112.6°. On the other hand, the calculated Si(2)-Si(1)-C(11) angle shows very little deviation from the parent tetrahedral angle of 109.5° (110.4°), as does the Si(2)-Si(1)-C(12) angle (108.8°). The Si(1)-Si(2)-C(21) angle is similar to the Si-Si-C angles calculated for 1,2-di-*tert*-butyldisilane[5] (114.4°). These structural changes relative to the idealised tetrahedral angle of 109.5° serve to reduce the steric interactions in these systems. However, resultant nearest-neighbour H...H distances were still predicted to be 219 pm, as compared to 240 pm for the sum of the van der Waals' radii of two hydrogen atoms. Internal C-C-C angles indicate that the *tert*-butyl groups are not significantly distorted from local C_3 symmetry. Bond lengths are generally within the expected ranges based on the results obtained previously for disilanes with *tert*-butyl groups. For example, the Si-Si bond length was predicted to be 237.5 pm as compared to 236.8 pm in 1,2-di-*tert*-butyldisilane.[5] All the C-C bond lengths fell within the range 153.8-154.2 pm, and the Si-C distances are all in the range 191.5-192.4 pm. These Si-C bond lengths are longer than those of normal Si-C bonds, for example 188.2(1) pm and 188.6(1) pm for 1,4-disilabutane and 1,5-disilapentane,[20] but compare well with the calculated Si-C bond length in 1,2-di-*tert*-butyldisilane[5] (191.9 pm), which may be a further demonstration of steric interactions in these crowded disilanes, although it could be an electronic effect of the electron-releasing *tert*-butyl groups.

Figure 2 Molecular structure of 1,1,2-tri-*tert*-butyldisilane.

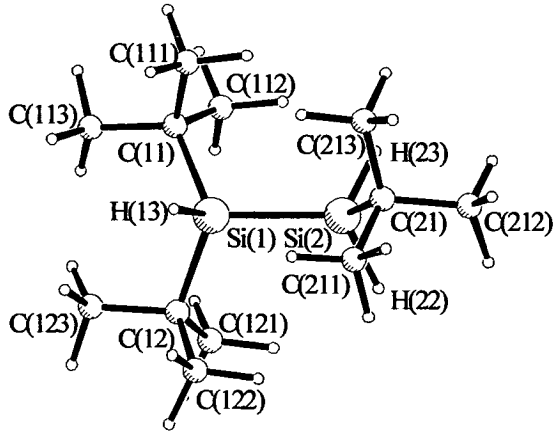

The molecular geometries of the *gauche* and *antiperiplanar* conformers also appear to be dictated predominately by steric interactions, as evident in the predicted values for the Si(1)-Si(2)-C(21) angles. In the *gauche* conformer, the Si(1)-Si(2)-C(21) angle is predicted to be 122.0° and, as might be expected, the same angle is predicted to be even wider in the *antiperiplanar* structure (124.7°), since all the *tert*-butyl groups are in closer proximity in this conformer. Further evidence of steric repulsion is found in the values of the C(11)-Si(1)-C(12) angles in the two conformers, predicted to be 115.8° in the *gauche* conformer but again, as expected, rather wider at 117.5° in the *antiperiplanar* conformer. The Si(2)-Si(1)-C(11) angles in both conformers show a much less dramatic deviation from the parent tetrahedral angle of 109.5° (*gauche* 107.2°, *antiperiplanar* 111.5°). The predicted Si(2)-Si(1)-C(12) angles show a larger deviation (*gauche* 113.4°, *antiperiplanar* 113.7°) and, again, these angles are similar to Si-Si-C angles calculated for 1,2-di-*tert*-butyldisilane[5] (114.4°). The Si-Si-C(12) angles are larger than those to C(11) as the butyl groups with C(12) at the centre are closer to the lone butyl at the other end of the molecule. Thus the C(12) butyl group moves away, creating a larger Si-Si-C angle. This however, brings it into closer contact with the C(11) butyl group at the same end of the molecule, which in turn moves reducing the Si-Si-C(11) angle. The Si-Si bond lengths were predicted to be 237.3 pm and 237.6 pm in the *gauche* and the *antiperiplanar* conformers respectively. These bond lengths are very similar to the predicted value for the *syn* conformer and agree well with those found for 1,2-di-*tert*-butyldisilane.[5] Views down the Si-Si bond for each of the 3 conformations of 1,1,2-tri-*tert*-butyldisilane are shown in Figure 3.

Figure 3 Views down the Si(1)-Si(2) bond of the three conformers of $Bu^t_2HSiSiH_2Bu^t$.

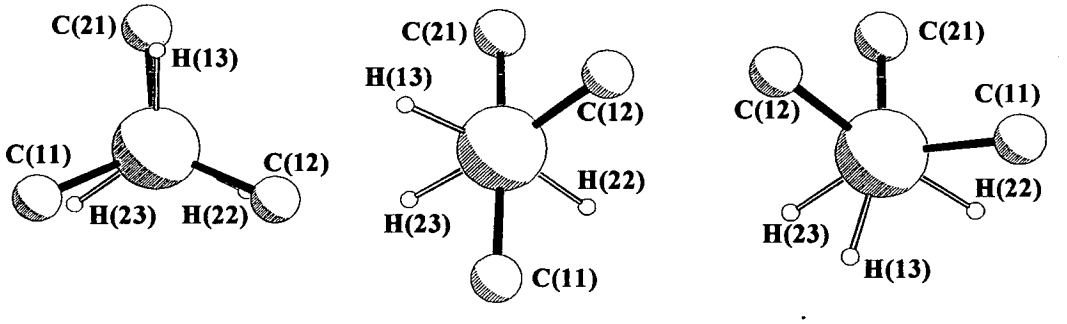

Syn ***Gauche*** ***Antiperiplanar***

3.3.2 Vibrational spectra and rotational isomerism

(Experiments conducted and assignments made by K. Hassler and R. Zink, Graz, Austria)

As mentioned previously, calculations predict the existence of three conformers, *syn*, *gauche* and *antiperiplanar*, on the potential energy surface of $Bu^t_2HSiSiH_2Bu^t$ with the high-energy conformations (*antiperiplanar* and *gauche*) lying 10.3 kJ mol^{-1} and 10.8 kJ mol^{-1} respectively above the *syn* structure. The GED data can be fitted with the single *syn* structure corresponding to the global minimum. Vibrational spectroscopy should be a slightly more sensitive tool for the detection of the less stable rotamers, whose presence in the conformational mixture should be very small according to their predicted energies. In particular, variable-temperature Raman spectroscopy has proven to be an extremely useful tool for conformational analyses, as Raman-active skeletal modes are usually very sensitive to the backbone conformation. For example, the energy difference between the *anti* and *gauche* rotamers of $MeCl_2SiSiCl_2Me$ has been determined recently from temperature-dependent Raman intensities.[21] In the present study the infrared spectrum of liquid $Bu^t_2HSiSiH_2Bu^t$, variable-temperature Raman spectra in the temperature range from 25°C to 150°C, and the Raman spectrum of the solid have been recorded. Selected vibrational spectra of liquid and solid $Bu^t_2HSiSiH_2Bu^t$ are summarised in Table 4. Calculated and observed vibrational wavenumbers are compared in Table 5.

Using the program ASYM40,[22] the calculated Cartesian Hessian matrices were converted into symmetry force fields, resulting in a description of normal modes in terms of symmetry coordinates according to the potential energy distributions. Most of the normal coordinates of the molecule $Bu^t_2HSiSiH_2Bu^t$ are dominated by more than just a single symmetry coordinate and the description given in Table 5 is highly approximate. Its primary use is to help with labelling rather than to permit an accurate visualisation of the vibrational motions.

For reasons of clarity and simplicity high-frequency vibrations involving the methyl groups ($\nu_{s,as}CH_3$ and $\delta_{s,as}CH_3$) are omitted from Table 5. These vibrations are well

known, not sensitive to the conformation around the SiSi bond and therefore unimportant from the viewpoint of rotational isomerism. The following discussion and characterisation of vibrational frequencies refers explicitly to the global minimum, the *syn* conformer, if not stated otherwise. The eighteen rocking vibrations of the methyl groups occur in three main spectral regions and have been summarised by their respective wavenumber ranges using the labels ρ_1CH_3, ρ_2CH_3 and ρ_3CH_3, respectively. Wavenumber ranges have also been used for the modes $\nu_{s,as}CC_3$, $\delta_{s,as}CC_3$, ρCC_3 and the torsional vibrations about the CC single bonds (τCC), because of the large number of each type of these vibrational modes. Further, calculations predict that the symmetry coordinates ρCC_3 and τCC are strongly mixed with each other, implying that the torsional vibrations around the CC bonds, which usually elude observation in the case of smaller molecules like Bu^tSiX_3,[23] gain intensity. Therefore, no attempt was made to describe normal modes dominated by both ρCC_3 and τCC by a single symmetry coordinate and only one wavenumber range for these vibrations has been given.

The shoulder at 740 cm^{-1} (IR) and the weak shoulder around 730 cm^{-1} in the Raman spectrum (intensity of the shoulder increasing with temperature) might be due to the mode δSiSiH of a high energy conformer, perhaps the *antiperiplanar* structure. Similarly, the shoulder at 770 cm^{-1} (IR) could also stem from another rotamer (possibly from the *gauche* structure). However, due to the high probability of the presence of strong combination bands or overtones in the IR spectrum of a molecule with 126 fundamental modes care must be taken when stating evidence for the presence of more than just a single rotamer.

A slightly stronger argument in favour of the presence of high energy rotamers in liquid $Bu^t_2HSiSiH_2Bu^t$ is provided by the appearance of several Raman peaks around 479 cm^{-1}. The peaks at 479 cm^{-1} and 502 cm^{-1} are assigned to νSiSi and ρSiH_2 of the *syn* conformation, respectively. However, the intensity of the weak shoulder at 460 cm^{-1} seems to increase slightly with temperature, as shown in Figure 4. This could be due to one or both of the modes νSiSi of the high-energy conformations, which are

predicted to differ by approximately 20 cm^{-1} from the value of the *syn* structure.

Figure 4 Portion of the Raman spectrum of liquid $Bu^t_2HSiSiH_2Bu^t$ at 25°C and 150°C.

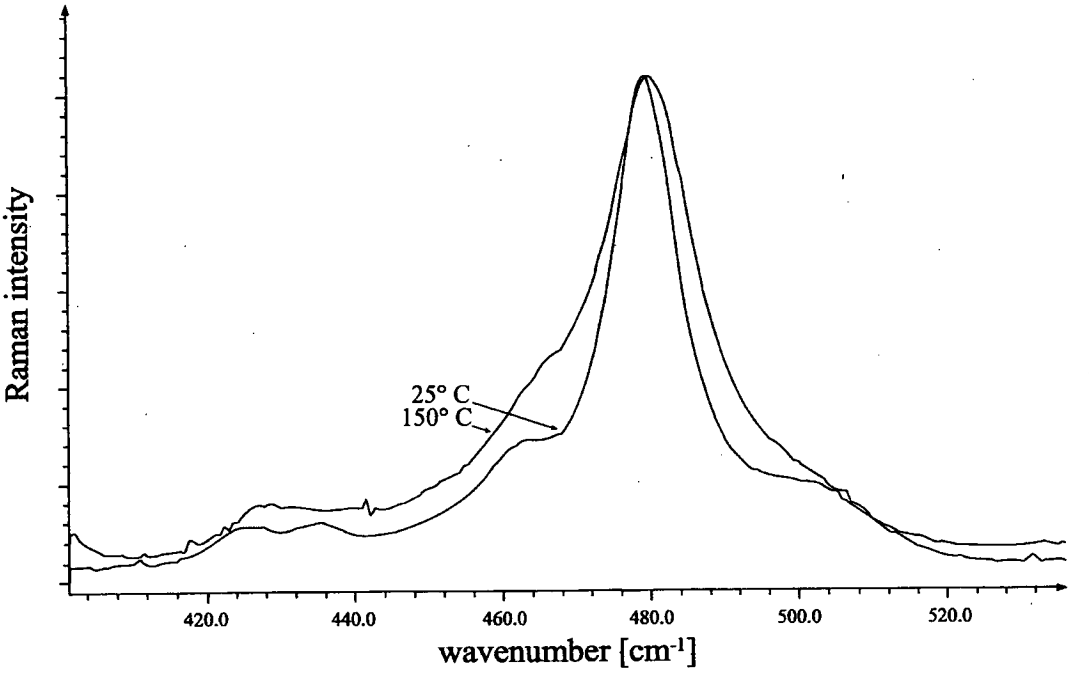

It can be summarised that the present study of the rotational isomerism of $Bu^t_2HSiSiH_2Bu^t$ employing IR spectroscopy at ambient temperature and variable temperature Raman spectroscopy is consistent with a single conformer, but with inconclusive evidence for one or more other conformers. This is in accordance with the calculations, which predict only 2.3% of the *gauche* and 1.4% of the *antiperiplanar* conformers at room temperature.

Table 4 Vibrational spectra of 1,1,2-tri-*tert*-butyldisilane (<2250 cm^{-1}).[a]

IR (l, 25°C)	Ra (l, 25°C)	Ra (s)	IR (l, 25°C)	Ra (l, 25°C)	Ra (s)
2104 vs	2104 vvs	2108 vvs	613 m	-	617 w
2080 vs	2080 s	2076 s	595 sh	593 vs	594 s
1210 sh	-	-	575 s	575 ms	575 m
1200 s	1201 s	1203 vs	501 s	502 sh	502 w
1188 s	1189 sh	1192 s	479 m	479 s	481 s
1163 ms	-	1178 sh	465 vw, sh	460 sh	461 w
1089 s	1090 vw	1089 vw	435 ms	434 w	434 w
1070 sh	-	-	-	424 w	423 vw
1035 ms	1034 vw	1035 vw	410 vw	408 vvw	407 vw
1012 vs	1014 w	1015 m	387 m	-	385 sh
-	1003 vw	1004 vw	-	382 m	382 m
935 sh	939 ms	940 s	370 m	372 sh	370 w
927 vs	928 sh	927 m	-	-	353 sh
890 sh, vw	888 vvw	890 vvw	349 s	348 w	348 w
-	862 vvw	860 vvw	-	305 w	314 w
840 sh	-	841 vw	-	272 w	281 mw, b
818 vs	824 s	825 vs	-	242 w	245 w
-	-	816 sh	-	219 s	220 ms
793 vs	794 w	792 w	-	-	206 s
770 sh	-	-	-	185 vw	187 vvw
740 sh	730 sh	-	-	-	165 sh
707 vs, b	710 m	711 mw	-	152 w	154 w
-	-	702 mw	-	134 ms	135 m
656 s	654 vw	654 vw	-	100 w	103 w

[a]SiH stretching vibrations are included.

Key: vvw = very very weak, vw = very weak, w = weak, mw = medium weak, m = medium, ms = medium strong, s = strong, vs = very strong, vvs = very very strong, sh = shoulder, b = broad.

Table 5 Calculated and observed wavenumbers for 1,1,2-tri-*tert*-butyldisilane.

	ab initio (unscaled)			*ab initio* (scaled by 0.92)			observed (IR,l,25°C)	observed (Raman,l,25°C)
approximate description	*syn*	*gauche*	*antiperiplanar*	*syn*	*gauche*	*antiperiplanar*	*syn*	*syn*
$\nu_s SiH_2$	2329.1	2335.7	2326.4	2143	2149	2140	2104	2104
$\nu_{as} SiH_2$	2320.1	2312.6	2319.3	2134	2128	2134	2104	2104
νSiH	2298.7	2300.8	2292.5	2115	2117	2109	2080	2080
$\rho_1 CH_3$	1348.9-1316.1	1347.9-1316.7	1348.4-1316.6	1241-1211	1240-1211	1241-1211	1210/1200/1188	1201/1189
$\rho_2 CH_3$	1136.7-1122.7	1136.8-1124.3	1136.4-1123.9	1046-1033	1046-1034	1045-1034	1012	1014/1003
$\rho_3 CH_3$	1052.5-1050.2	1051.6-1048.6	1051.8-1049.0	968-966	967-965	968-965	-	-
$\nu_{as} CC_3$	1028.3-1017.7	1030.0-1017.8	1030.0-1015.9	946-936	948-936	948-935	935/927	939/928
δSiH_2	1042.9	1027.8	1029.0	959	946	947	935 or 927	939 or 928
γSiH_2	923.3	926.3	903.0	849	852	831	840	-
$\nu_s CC_3$	889.0-883.5	889.8-883.5	889.1-883.9	818-813	819-813	818-813	818	824
ρSiC_2	878.8	874.0	880.9	808	804	810	793	794
$\delta SiSiH$	801.4	850.6	825.7	737	783	760	707	710
τSiH_2	782.3	772.9	799.2	720	711	735	707	710
$\nu_{as} SiC_2$	649.1	644.7	649.4	597	593	597	613	593
νSiC	628.7	631.1	634.2	578	581	583	595	593
$\nu_s SiC_2$	611.5	610.2	611.9	563	561	563	575	575
ρSiH_2	559.3	551.5	540.7	515	507	497	501	502

Table 5 continued

	ab initio (unscaled)			*ab initio* (scaled by 0.92)			observed (IR,l,25°C)	observed (Raman,l,25°C)
approximate description	*syn*	*gauche*	*antiperiplanar*	*syn*	*gauche*	*antiperiplanar*	*syn*	*syn*
νSiSi	518.3	499.3	500.4	477	459	460	479	479
ρSiH_2	559.3	551.5	540.7	515	507	497	501	502
νSiSi	518.3	499.3	500.4	477	459	460	479	479
$\delta_{s,as}CC_3$	472.7-372.4	459.2-368.6	459.7-360.2	435-343	422-339	423-331	435/387/370/349	434/382/372/348
ρCC_3, τCC	342.0-219.7	349.5-218.1	343.8-223.1	315-202	322-201	316-205	-	305/272/242/219/185
δSiC_2	159.9	153.1	145.7	147	141	134	-	152
γSiC_2	136.6	139.3	146.9	126	128	135	-	134
τSiC_2	140.4	128.7	129.5	129	118	119	-	134
δSiSiC	96.2	87.6	101.1	89	81	93	-	100
τSiC	62.6-29.5	100.5-44.0	76.5-48.8	58-27	92-40	70-45	-	-
τSiSi	48.2	32.5	26.9	44	30	25	-	-

3.3.3 Electron diffraction analysis

On the basis of the *ab initio* calculations described above, electron-diffraction refinements were carried out using a model of the *syn* conformation (C_1 symmetry) to describe the vapour. The conformer is in C_1 symmetry rather than C_s due to the twists of the butyl groups in the Bu^t_2Si fragment to avoid methyl...methyl interactions. A Bu^t_2Si group usually has approximately C_2 local symmetry as this minimises 1,3-methyl-methyl interactions within the group as shown in Figure 5. This has the effect of lowering the overall symmetry of the molecule. The large number of geometric parameters needed to define the model made it necessary to make a number of assumptions including local C_{3v} symmetry for all methyl groups and local C_3 symmetry for the *tert*-butyl groups. Initially, some of the differences between similar bond lengths and bond angles were restrained using the SARACEN[24] method. However, since many of these difference parameters proved to be uncorrelated with other refining parameters, and returned values and e.s.d.'s which were close to the restraints, they were fixed in the final refinement. We can therefore be confident that the refined parameters, and their e.s.d.'s, are not affected by the assumptions applied to the molecular model.

Figure 5 Butyl twists in Bu^t_2Si fragment

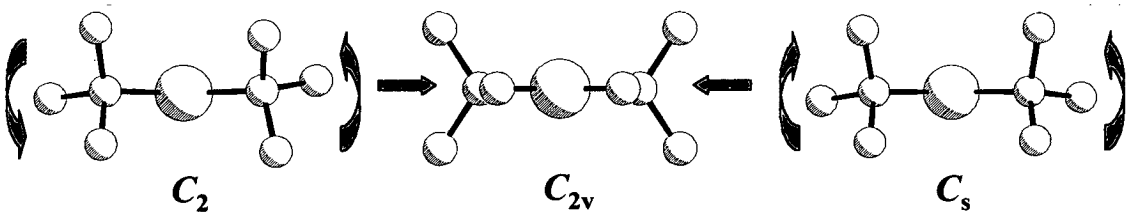

The structure of $Bu^t_2HSiSiH_2Bu^t$ was finally defined in terms of twenty-seven independent geometric parameters, comprising five bond lengths, six bond angles and sixteen torsion, rock and tilt parameters (Table 6; atom numbering shown in Figure 2). The independent parameters include the C-H and C-C bond lengths (p_1 and p_2). Average bond lengths were used for the Si-Si, Si-C and Si-H bond lengths (p_3-p_5), with small differences between non-equivalent bond lengths fixed at the *ab initio* values. All C-C-H bond angles (p_6) were assumed to be identical, as were all C-C-C bond angles (p_7). An average value was adopted for the three Si-Si-H angles (p_8), with the small differences

from the mean being set at the *ab initio* values. The Si-Si-C angles were defined in terms of the average (p_9) of Si(1)-Si(2)-C(21), Si(2)-Si(1)-C(11) and Si(2)-Si(1)-C(12), and two difference parameters, which were included in the refinement procedure since the predicted Si-Si-C angles spanned a wide range of values. The differences were described as Si(1)-Si(2)-C(21) minus Si(2)-Si(1)-C(11) (p_{10}) and Si(1)-Si(2)-C(21) minus Si(2)-Si(1)-C(12) (p_{11}).

Of the remaining sixteen parameters, nine represent the tilts, rocks and torsions of the three *tert*-butyl groups. These groups were generated by initially placing a methyl group carbon atom at the origin, with its three H atoms arranged with local C_{3v} symmetry about the *x*-axis and one H in the *xy* plane in the positive *x* and *y* directions. The methyl torsion, tilt and rock parameters, (p_{12}-p_{14}) are rotations of the group about the local *x*, *z*, and *y* axes respectively. The methyl group is then translated along the positive *x*-axis by the C-C bond length and the central carbon of the *tert*-butyl group is placed at the origin. The correct C-C-C bond angles are generated by rotating the methyl group about the *z*-axis, moving the methyl carbon atom in the positive *y* direction, and then generating the other methyl groups by rotation of the first group about the *x*-axis by 120° or -120°, respectively. The *tert*-butyl torsion angle is a rotation of the group about the *x*-axis. Parameters introduced here for the *tert*-butyl torsions include the average (p_{15}) of torsions C(211)-C(21)-Si(2)-Si(1), C(111)-C(11)-Si(1)-Si(2), and C(121)-C(12)-Si(1)-Si(2), and two differences. These were the difference between torsion C(211)-C(21)-Si(2)-Si(1) and torsion C(111)-C(11)-Si(1)-Si(2) or C(121)-C(12)-Si(1)-Si(2) (p_{16} and p_{17}).

The rock and tilt parameters are rotations of the whole butyl groups about the *y*-axis and the *z*-axis respectively. Three individual rocks (p_{18}-p_{20}) and three individual tilts (p_{21}-p_{23}) were introduced here for the *tert*-butyl groups with C(21), C(11) and C(12) as their central atoms. Positive values of the rock parameters would move the butyl group with C(21) at the centre away from that with C(12) at the centre, the butyl with C(11) at the centre towards C(12), and C(12) away from C(11), all in the local *y* direction of the butyl groups. Positive tilts would move the butyl groups at one end of the molecule towards the the other end of the molecule in the local *z* direction.

Having generated the *tert*-butyl groups in their local coordinate systems they all lie in the *xy* plane. They need to be rotated about the *x*-axis to put them in the correct positions. The two *tert*-butyl groups and the hydrogen attached to Si(1) were initially placed in the *xy* plane, and the *tert*-butyl groups were then rotated about the *x*-axis. These rotations are defined in terms of the average of C(11)-Si(1)-Si(2)-H(13) and C(12)-Si(1)-Si(2)-H(13) (p_{24}) and the difference between torsion angles C(11)-Si(1)-Si(2)-H(13) and C(12)-Si(1)-Si(2)-H(13) (p_{25}).

The *tert*-butyl group and H atoms attached directly to Si(2) were placed in the *xy* plane and the two hydrogen atoms were then rotated about the *x*-axis in opposite directions by torsion angles H(21)-Si(2)-Si(1)-C(21) and H(23)-Si(2)-Si(1)-C(21). The average of these two dihedral angles is (p_{26}) and the difference was set at the *ab initio* value.

Finally, the dihedral angle C(21)-Si(2)-Si(1)-H(13) (p_{27}) described the overall conformation about the Si-Si bond, with a value of zero indicating the conformation in which the hydrogen of the Bu^t_2HSi group and the carbon of the Bu^tH_2Si group were eclipsing one another.

The starting parameters for the r_a refinement were taken from the theoretical geometry optimised at the MP2/D95* level. The r_α structure was not refined because the rectilinear vibrational corrections (i.e. parallel and perpendicular correction terms) are known to be unreliable for a molecule this size with many low-lying vibrational modes. Theoretical (HF/6-31G*) Cartesian force fields were obtained and converted into force fields described by a set of symmetry coordinates using a version of the ASYM40 program[22] modified to work for molecules with more than forty atoms. Amplitudes were calculated from this and all geometric parameters were then refined.

In total twenty-seven geometric parameters and forty-three vibrational amplitudes were refined. Flexible restraints were employed during the refinement using the SARACEN method.[24] In total, twenty-one geometric and thirty-seven amplitude restraints were employed. Amplitude restraints were either absolute values of amplitudes, or restraints on

the ratios between pairs of amplitudes. These are listed in Appendix 2 [Tables 3 and 4]. The success of the final refinement, for which $R_G = 0.060$ ($R_D = 0.052$), can be assessed on the basis of the molecular scattering intensity curves (Figure 6) and the radial distribution curve (Figure 7).

Figure 6 Experimental and final weighted difference (experimental - theoretical) molecular-scattering intensities for 1,1,2-tri-*tert*-butyldisilane.

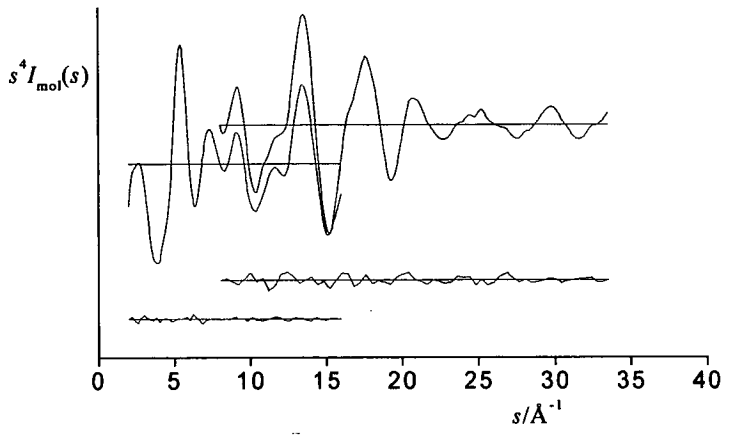

Figure 7 Experimental and difference (experimental - theoretical) radial-distribution curves, $P(r)/r$, for $Bu^t_2HSiSiH_2Bu^t$. Before Fourier inversion the data were multiplied by $s.\exp(-0.00005s^2)/(Z_{Si} - f_{Si})/(Z_C - f_C)$.

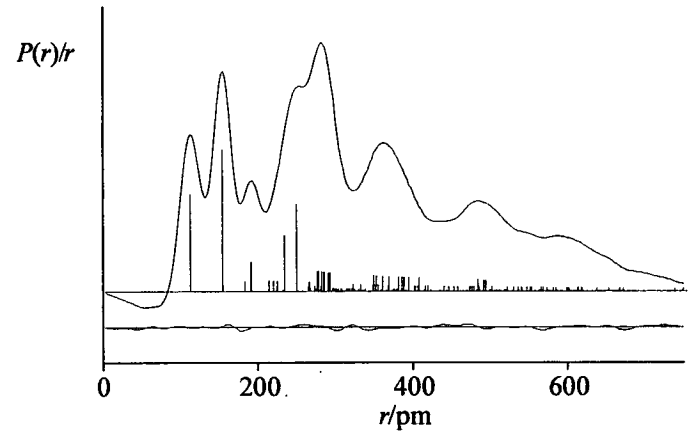

Final refined parameters are listed in Table 6, interatomic distances and the corresponding amplitudes of vibration in Table 7, with the least-squares correlation matrix shown in Appendix 2 [Table 5] and the experimental coordinates from the GED analysis in

Appendix 2 [Table 6]. In the SARACEN analysis, all correlation between refining parameters is included in the error estimates by the use of flexible restraints. Therefore the estimated standard deviations, σ, are quoted, and are believed to be realistic estimates of the uncertanties of the parameters.

Figure 2 shows a perspective view of the *syn* conformer of $Bu^t_2HSiSiH_2Bu^t$ in the optimum refinement of the GED data with a projection along the Si-Si bond vector shown in Figure 3.

Table 6 Refined and calculated geometric parameters for 1,1,2-tri-*tert*-butyldisilane (distances in pm, angles in deg.) from the GED study.[a]

No.	Parameter[b]	GED (r_a)	D95*/MP2 (r_e)
p_1	C-H	112.4(1)	110.1
p_2	C-C	154.5(1)	154
p_3	Si-Si	236.3(8)	237.5
p_4	Si-C (mean)	191.0(3)	192.1
p_5	Si-H (mean)	149.7(10)	150.1
p_6	CCH	110.1(6)	111.1
p_7	CCC	108.5(2)	108.7
p_8	SiSiH average	109.3(11)	109.5
p_9	SiSiC average	112.0(6)	110.6
p_{10}	SiSiC difference1	4.8(10)	2.2
p_{11}	SiSiC difference2	7.3(11)	3.8
p_{12}	Me twist	58.4(22)	61.4
p_{13}	Me tilt	-4.4(11)	-
p_{14}	Me rock	2.0(21)	-
p_{15}	Bu^t twist average	62.0(14)	61.5
p_{16}	Bu^t twist difference1	-12.3(20)	-8.7
p_{17}	Bu^t twist difference2	-0.3(16)	-1.3
p_{18}	Bu^t rock (gpA)	2.4(11)	-
p_{19}	Bu^t rock (gpB)	4.0(10)	-
p_{20}	Bu^t rock (gpC)	-4.7(9)	-
p_{21}	Bu^t tilt (gpA)	-3.0(10)	-
p_{22}	Bu^t tilt (gpB)	-2.0(9)	-
p_{23}	Bu^t tilt (gpC)	-2.4(10)	-
p_{24}	C twist average	112.1(7)	114.1
p_{25}	C twist difference	-0.3(11)	0.2
p_{26}	H twist average	122.0(11)	121.3
p_{27}	HsiSiC	-6.2(11)	-4.2

[a] Figures in parentheses are the estimated standard deviations of the last digits. See text for parameter definitions.

[b] gpA = *tert*-butyl group with C(21) at centre; gpB = *tert*-butyl group with C(11) at centre; gpC = *tert*-butyl group with C(12) at centre.

Table 7 Selected interatomic distances and mean amplitudes of vibration for 1,1,2-tri-*tert*-butyldisilane from the GED study.[a]

No.	Atom pair	r_a/pm	u/pm
1	Si(1)-Si(2)	236.3(8)	7.2(6)
2	Si(2)-C(21)	190.4(3)	6.1(7)
3	Si(1)-C(11)	191.7(3)	6.2(6)
4	Si(1)-C(12)	191.3(3)	6.2(6)
5	Si(2)-H(23)	149.3(10)	9.4(2)
6	Si(2)-H(22)	149.7(10)	9.4(tied to u_5)
7	Si(1)-H(13)	150.0(10)	9.4(tied to u_5)
8	C-C	154.5(1)	5.2(2)
9	C-H	112.4(1)	6.9(2)
10	C(21)...H(2111)	220.7(25)	9.7(12)
11	C(211)...C(212)	250.8(3)	7.3(5)
12	Si(1)...C(21)	362.7(14)	13.9(12)
13	Si(2)...C(211)	283.3(19)	10.7(5)
14	Si(2)...C(212)	278.6(17)	10.3(7)
15	Si(2)...C(213)	289.8(18)	10.9(7)
16	Si(2)...C(11)	354.1(19)	14.0(12)
17	Si(1)...C(111)	279.7(18)	10.3(7)
18	Si(1)...C(112)	292.4(16)	10.7(7)
19	Si(1)...C(113)	282.8(16)	10.8(7)
20	Si(2)...C(12)	348.5(18)	12.8(9)
21	Si(1)...C(121)	293.5(51)	10.4(7)
22	Si(1)...C(122)	279.4(53)	10.2(7)
23	Si(1)...C(123)	280.8(106)	10.0(7)
24	C(11)...C(12)	333.4(20)	10.0(11)

[a] See Figure 2 for atom numbering. (Other atom pairs were also used in the refinement but are not shown here.)

3.4 Discussion

Theoretical and experimental studies show that 1,1,2-tri-*tert*-butyldisilane exists essentially as a single *syn* conformer in the gas phase. The electron diffraction data for the compound were fitted well using the SARACEN[24] method on the basis of such a *syn* structure.

The vibrational spectra do not change significantly with changes in the temperature, indicating the probable presence of a single conformer. Spectroscopic studies are therefore consistent with the GED experiment and theory, but do not unambiguously prove that there is only one conformer present in the vapour.

The final experimental structure is in good agreement with that calculated *ab initio* at the MP2/D95* level; computed bond lengths and angles generally fall within 1-2 pm or 1-2° of the GED values (Table 5). For example, the Si-Si bond length refined to 236.3(8) pm as compared to the computed value of 237.5 pm. The mean C-C bond length refined to 154.5(1) pm compared to 154.0 pm (mean) from the calculations and the experimental range of Si-C bond lengths was 190.4-191.7 pm compared to the calculated range of 191.5-192.4 pm. However, the Si(1)-Si(2)-C(21) bond angle refined to 116.0(8)°, a lot wider than the predicted value of 112.6°, and the C(11)-Si(1)-C(12) bond angle refined to 121.1(11)° compared to the calculated value of 118.6°. All these observations of wide angles serve to highlight the significant steric interactions within the molecule. The torsion about the Si-Si axis, dihedral angle C(21)-Si(2)-Si(1)-H(13), which uniquely describes the position of all the groups about the Si-Si axis, agrees well with the predicted value; -6.2(11)° *vs.* -4.2°.

The values quoted here are the r_a values. As mentioned earlier the r_α structure was not refined because the rectilinear vibrational corrections are unreliable. Some parameters quoted for other reference molecules are r_a or r_g values. r_g values compare with r_a values as shown in Equation 3.1 below

$$r_g = r_a + \frac{u_2^2}{r} \qquad 3.1$$

where u is the amplitude of vibration and r is the distance. r_α compares to r_g according to Equation 3.2 below

$$r_\alpha = r_g - K \qquad 3.2$$

where K is the perpendicular amplitude of vibration shown in Figure 8.

Figure 8 Rectilinear vibration of CO_2

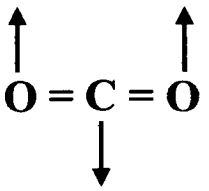

As can be seen from Figure 8, the oxygen atoms are assumed to move in straight lines and K **O**...**O** is zero, and K **C** = **O** is large and positive. Sipachev refers to r_α as r_{h0} and his curvilenear corrections[25] (instead of rectilinear K's) yield r_{h1}. This higher level correction takes the second derivative of the nuclear positions with respect to the amplitude of the internal coordinate as shown in Figure 9.

Figure 9 Curvilinear vibration of CO_2

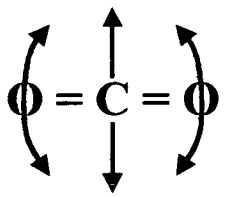

In this case, K' **O**...**O** is large and negative, and K' **C** = **O** is zero. Obviously it is advantageous to correct for curvilinear vibrational motion whenever possible. Sipachevs' method will provide more realistic values of the parallel amplitudes, u. However, neither of these corrections (to r_{h0} and r_{h1}) can be applied when there are

very low-lying vibrational frequencies corresponding to large torsional motions within the molecule. In these cases, it is better to use a dynamic model, where the motion is modelled explicitly by "snapshots" of the molecule at different positions.

Observed geometric parameters are generally consistent with those for a number of other closely related compounds. For example, the Si-Si bond distance in the *syn* conformer of 1,1,2-tri-*tert*-butyldisilane [236.3(8) pm (r_a)] is within the range of values found for other disilanes from GED refinements including 1,2-di-*tert*-butyldisilane[5] [234.8(3) pm (r_a)], 1,1,2,2-tetrabromodisilane[3] [234.9(19) pm (r_a)], 1,2-diiododisilane[4] [238.0(34) pm (r_g)] and 1,1,2,2-tetraiododisilane[4] [238.9(37) pm (r_g)], but a little longer as might be expected, either on steric or electronic grounds, with the butyl groups being electron-donating. The consistency of the calculated Si-Si distance in the three conformers suggests that steric effects are not very important in this case. Refined values of the C-C [154.5(1) pm] and Si-H [149.7-150.0 pm] bond lengths are in excellent agreement with calculated values and compare well with other previously reported bond lengths,[20] as would be expected.

The most striking feature of the structure is the deviation of the C(11)-Si(1)-C(12) bond angle from the "pure" sp^3 tetrahedral angle [109.5°] by 11.6°. This provides evidence of steric strain and the wide angle observed is probably caused by the close proximity of two of the *tert*-butyl groups at one end of the molecule. This could be proved by carrying out calculations on 1,1-di-*tert*-butyldisilane, or di-*tert*-butylsilane. It also reflects the easy deformation of angles at silicon, which allows the accommodation of several large substituents. Another structural feature of note is the value obtained for the Si(1)-Si(2)-C(21) bond angle [116.0(8)°]. This angle is similar to, but even larger than, those previously observed for 1,2-di-*tert*-butyldisilane[5] [113.7(3)°] and 1,2-di-*tert*-butyltetrafluorodisilane[6] [114.6(7)°] and provides evidence for significant steric interaction between butyl groups at opposite ends of the molecules.

In the early stages of this analysis, before the existence of the *syn* conformer had been recognised, the experimental data were also fitted with a mixture of the other two conformers, *gauche* {ϕ[C(21)-Si(2)-Si(1)-H(13)] = 63.4°} and *antiperiplanar* {ϕ[C(21)-Si(2)-Si(1)-H(13)] = 163.8°}, in equal amounts, as predicted *ab initio*. All geometric parameters were then refined before determining the relative weights of the two conformations. The final weight of the *gauche* conformer was thus determined to be 50.8% with a standard deviation of 3.2% according to the Hamilton test for this parameter.[26] From the final refinement, for which $R_G = 0.057$ ($R_D = 0.054$), it can be seen that this two-conformer model fits the experimental data as well as the single *syn* model. This demonstrates that caution must be exercised when initially exploring the potential energy surface to locate all structurally stable minima and to determine the differences in energy between them. The two-conformer model used forty-two independent geometric parameters comprising five bond lengths, nine bond angles and twenty-eight torsion, rock and tilt parameters. This large number of refinable parameters probably contributed to the overall goodness of fit of these two conformers compared to the single *syn* conformer. Mixtures of all three conformers will also fit the data well. However, we believe that the refinement based on the *syn* conformer alone is the most satisfactory result, in the light of all available information, both theoretical and experimental.

In Chapter 8, the use of molecular mechanics (MM) and semi-empirical methods to investigate the potential energy surface for a range of molecules is discussed. The unique torsion angle in 1,1,2-tri-*tert*-butyldisilane means that this molecule might have benefitted from this treatment before the experimental structural study was undertaken, to ensure that all possible minima had been located. However, the MM study in Chapter 8 showed that very low level calculations are not good at predicting these very crowded structures. More discussion of the MM/semi-empirical study carried out is given in Chapter 8.

3.5 References

1. R. D. Miller and J. Michl, *Chem. Rev.*, 1989, **89**, 1359.
2. V. S. Mastryukov, in *Stereochemical Applications of Gas-Phase Electron Diffraction,* Eds. I. Hargittai and M. Hargittai, VCH, Weinheim, Germany, 1990, vol. B, p.1.
3. H. Thomassen, K. Hagen, R. Stølevik and K. Hassler, *J. Mol Struct.*, 1986, **147**, 331.
4. E. Røhmen, K. Hagen, R. Stølevik, K. Hassler and M. Pöschl, *J. Mol Struct.*, 1991, **244**, 41.
5. D. Hnyk, R. S. Fender, H. E. Robertson, D. W. H. Rankin, M. Bühl, K. Hassler and K. Schenzel, *J. Mol. Struct.*, 1995, **346**, 215.
6. B. A. Smart, H. E. Robertson, N. W. Mitzel, D. W. H. Rankin, R. Zink and K. Hassler, *J. Chem. Soc., Dalton Trans.*, 1997, 2475.
7. B. Reiter and K. Hassler, *J. Organomet. Chem.*, 1994, **467**, 21
8. J. S. Binkley, J. A. Pople and W. J. Hehre, *J. Am. Chem Soc.*, 1980, **102**, 939.
9. M. S. Gordon, J. S. Binkley, J. A. Pople, W. J. Pietro and W. J. Hehre, *J. Am. Chem. Soc.*, 1982, **104**, 2797.
10. W. J. Pietro, M. M. Francl, W. J. Hehre, D. J. DeFrees, J. A. Pople and J. S. Binkley, *J. Am. Chem. Soc.*, 1982, **104**, 5039.
11. W. J. Hehre, R. Ditchfield and J. A. Pople, *J. Chem. Phys.*, 1972, **56**, 2257.
12. P. C. Hariharan and J. A. Pople, *Theor. Chim. Acta*, 1973, **28**, 213.
13. M. S. Gordon, *Chem. Phys. Lett.*, 1980, **76**, 163.
14. Gaussian 94 (Revision C.2), M. J. Frisch, G. W. Trucks, H. B. Schlegel, P. M. W. Gill, B. G. Johnson, M. A. Robb, J. R. Cheesman, T. A. Keith, G. A. Petersson, J. A. Montgomery, K. Raghavachari, M. A. Al-Laham, V. G. Zakrzewski, J. V. Ortiz, J. B.Foresman, J. Cioslowski, B. B. Stefanov, A. Nanayakkara, M. Challacombe, C. Y. Peng, P. Y. Ayala, W. Chen, M. W. Wong, J. L. Andres, E. S. Replogle, R. Gomperts, R. L. Martin, D. J. Fox, J. S. Binkley, D. J. Defrees, J. Baker, J. P. Stewart, M. Head-Gordon, C. Gonzalez and J. A. Pople, Gaussian Inc., Pittsburgh, PA, 1995.

15. T. H. Dunning, Jr. and P. J. Hay, in *Modern Theoretical Chemistry*, H. F. Schaefer III (Ed.), Plenum Press, New York, 1976, p.1.

16. C. M. Huntley, G. S. Laurenson and D. W. H. Rankin, *J. Chem. Soc., Dalton Trans.*, 1980, 954.

17. S. Cradock, J. Koprowski and D. W. H. Rankin, *J. Mol. Struct.*, 1981, **77**, 113.

18. A. S. F. Boyd, G. S. Laurenson and D. W. H. Rankin, *J. Mol. Struct.*, 1981, **71**, 217.

19. A. W. Ross, M. Fink and R. Hilderbrandt, in A. J. C. Wilson (Ed.), *International Tables for Crystallography*, Vol. C, Kluwer Academic Publishers, Dordrecht, 1992, p. 245.

20. N. W. Mitzel, B. A. Smart, A. J. Blake, H. E. Robertson and D. W. H. Rankin, *J. Phys. Chem.*, 1996, **100**, 9339.

21. For example, see M. Ernst, K. Schenzel, A. Jähn and K. Hassler, *J. Mol. Struct.*, 1997, **412**, 83.

22. L. Hedberg and I. M. Mills, *J. Mol. Spectrosc.*, 1993, **160**, 117.

23. R. Zink and K. Hassler, *Spectrochimica Acta Part A-Molecular and Bimolecular Spectroscopy*, 1999, **55**, 333.

24. A. J. Blake, P. T. Brain, H. McNab, J. Miller, C. A. Morrison, S. Parsons, D. W. H. Rankin, H. E. Robertson and B. A. Smart, *J. Phys. Chem.*, 1996, **100**, 12280 ; P. T. Brain, C.A. Morrison, S. Parsons and D. W. H. Rankin, *J. Chem. Soc., Dalton Trans.*, 1996, 4589.

25. V. A. Sipachev, *J. Mol. Struc. (Theochem)*, 1985, **121**, 143.

26. W. C. Hamilton, *Acta Cryst.*, 1965, **18**, 502.

Chapter 4

1,1,2,2-tetra-*tert*-butyldisilane, $Bu^t_2HSiSiHBu^t_2$: Molecular Structure in the Gas Phase by Electron Diffraction and *Ab Initio* Calculations. 1,1,2,2-tetra-*tert*-butyl-digermane and -distannane: Molecular Structures by *Ab Initio* Calculations.

4.1 Introduction

Having studied the di- and tri-*tert*-butyl substituted disilanes, the next logical step in the series was to examine the structure of 1,1,2,2-tetra-*tert*-butyldisilane. This molecule would present some interesting structural challenges, not least in examining the steric interactions between the four *tert*-butyl groups within the molecule.

1,2-di-*tert*-butyltetrachlorodisilane (see Chapter 2) presented very few structural surprises. The *transoid* conformation was located *ab initio* and the structure agreed well with that found from the electron diffraction data. However, some degree of steric crowding was observed in this molecule, which prompted the study of 1,1,2-tri-*tert*-butyldisilane (see Chapter 3). Initially, two conformers of approximately equal energy (*gauche* and *antiperiplanar*) were located on the potential energy surface, and the refinement was carried out assuming these two conformers. However, further calculations revealed that there was in fact a *syn* conformer that was 10 kJ mol^{-1} lower in energy that the two located originally. Initially, this seemed most unlikely. However, examination of the structure revealed that each hydrogen atom attached to silicon was eclipsing a *tert*-butyl group at the other end of the molecule. This served to reduce the steric crowding between the *tert*-butyl groups, as evident in the average Si-Si-C angles (*syn* = 110.6°, *gauche* = 114.2°, *antiperiplanar* = 116.6°). Although there is still some steric crowding present, it is much reduced in the *syn* conformation.

The question then arises as to what the structure of 1,1,2,2-tetra-*tert*-butyldisilane is most likely to be. Two possibilities (shown in Figure 1) can be predicted, based on what has been observed in the di- and tri-*tert*-butyl substituted cases.

Figure 1 Newman projections of possible structures for 1,1,2,2-tetra-*tert*-butyldisilane.

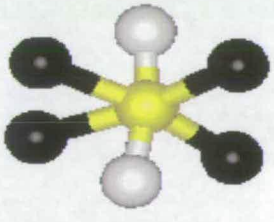

anti

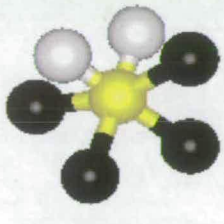

gauche

The *anti* structure, as observed for 1,2-di-*tert*-butyltetrachlorodisilane, would lead to interactions between the *tert*-butyl groups at opposite ends of the molecule. The *gauche* structure would compound these interactions between one pair of *tert*-butyl groups, whilst reducing it for the other pair (Figure 1). An interesting question with regard to this molecule is whether the methyl and *tert*-butyl groups are able to distort enough in the *anti* structure to make it the preferred form, or whether distortions around the silicon atom would be observed in the *gauche* structure, making it the more favoured conformation. If these groups can spread and tilt, unexpected results could ensue.

The molecular structures of 1,1,2,2-tetra-*tert*-butyldigermane and 1,1,2,2-tetra-*tert*-butyldistannane have also been investigated by *ab initio* calculations, to provide comparisons with the structure found for the disilane. The question arises as to whether these molecules will have a different conformation from the 1,1,2,2-tetra-*tert*-butyldisilane due to the elongated Y-Y and Y-C bonds (Y = Si, Ge, Sn). Although no experimental gas phase data are available for these molecules yet, we hope that they will be in the near future.

4.2 Experimental

4.2.1 Synthesis

A sample of 1,1,2,2-tetra-*tert*-butyldisilane was prepared according to literature methods[1] and provided for use in the Edinburgh electron diffraction apparatus by *K. Hassler, Graz, Austria* without modification.

4.2.2 *Ab initio* calculations

Calculations for all three molecules at the HF/3-21G*[2-4] and HF/6-31G*[5-7] levels were performed on a Dec Alpha 1000 4/200 workstation using the Gaussian 98 program.[8] Calculations at the MP2 level using the 6-31G* basis set were performed using resources of the U.K. Computational Chemistry Facility, on a DEC 8400 superscalar cluster equipped with 10 fast processors, 6 GB of memory and 150 GB disk. An extensive search of the torsional potential of all three molecules was undertaken at the

HF/3-21G* level in order to locate all local minima. For 1,1,2,2-tetra-*tert*-butyldisilane, one conformer with ϕ(H-Si-Si-H) = -102° was located and further geometry optimisations were undertaken at the HF/6-31G* and MP2/6-31G* levels. Vibrational frequencies were calculated from analytic second derivatives at the HF/3-21G* and HF/6-31G* levels to determine the nature of stationary points and for comparison with experimentally determined frequencies. The force field should also have provided estimates of amplitudes of vibration (*u*) for use in the GED refinements, but there was a problem associated with obtaining the force constants from the HF/6-31G* calculation, apparently due to an error in the Gaussian 98 program. The amplitudes of vibration appeared to be grossly overestimated at this level of theory. To obtain a usable force field from which amplitudes of vibration could be estimated, the MP2/6-31G* structure was optimised using the Universal Force Field[9] method of molecular mechanics. Force constants calculated at this level were used to generate the amplitudes of vibration, which appeared to be more reliable from this method.

Calculations performed on 1,1,2,2-tetra-*tert*-butyldigermane and 1,1,2,2-tetra-*tert*-butyldistannane revealed similar results to the disilane analogue, with just one conformer each being found from the search of the potential energy surface. For 1,1,2,2-tetra-*tert*-butyldigermane, one conformer with ϕ(H-Ge-Ge-H) = 98.9° was located, while for 1,1,2,2-tetra-*tert*-butyldistannane, one conformer with ϕ(H-Sn-Sn-H) = -88° was located. Further calculations were carried out on both molecules as for the disilane. For 1,1,2,2-tetra-*tert*-butyldistannane, the LanL2DZ[10] basis set employing the Los Alamos effective core potential plus DZ on tin was used at the HF/6-31G* and MP2/6-31G* levels.

4.2.3 Electron diffraction

Data were collected using the Edinburgh gas diffraction apparatus.[11] An accelerating voltage of *ca.* 40 kV (electron wavelength *ca.* 6.0 pm) was used, whilst maintaining the sample and nozzle temperatures at 393.5 and 461 K respectively. Scattering intensities were recorded at nozzle-to-plate distances of 86.9 and 256.1 mm on Kodak Electron Image plates. The weighting points for the off-diagonal weight matrices, correlation parameters and scale factors for the two camera distances are

given in Table 1, together with electron wavelengths, which were determined from the scattering patterns of benzene vapour. These were recorded immediately after the patterns of $Bu^t_2HSiSiHBu^t_2$ and analysed in exactly the same way, to minimise systematic errors in wavelengths and camera distances. The electron-scattering patterns were converted into digital form using a PDS densitometer at the Institute of Astronomy in Cambridge with a scanning program described elsewhere.[12] Data reduction and least-squares refinements were carried out using standard programs,[13,14] employing the scattering factors of Ross *et al.*[15]

Table 1 Nozzle-to-plate distances (mm), weighting functions (nm^{-1}), correlation parameters, scale factors and electron wavelengths (pm) used in the electron-diffraction study.

Nozzle-to-plate distance[a]	Δs	s_{min}	sw_1	sw_2	s_{max}	Correlation parameter	Scale factor[b]	Electron wavelength
256.1	2	40.0	60.0	134.0	156.0	0.4820	0.729(22)	6.016
86.9	4	120.0	140.0	256.0	300.0	0.4527	0.814(43)	6.016

[a] Determined by reference to the scattering pattern of benzene vapour.

[b] Values in parentheses are the estimated standard deviations.

4.3 Results

4.3.1 *Ab initio* calculations

A series of molecular orbital calculations was undertaken to investigate the structure of $Bu^t_2HSiSiHBu^t_2$. Preliminary investigations of the structure assuming C_{2h} symmetry returned imaginary frequencies at the HF/3-21G* level, as did a C_1 structure [ϕ(H-Si-Si-H) fixed at 180°] with the butyl groups twisting in opposite senses to each other at opposing ends of the molecule. Further investigation of the structure in C_2 symmetry revealed one minimum with ϕ(H-Si-Si-H) = -102°. Surprisingly, this observed *antiperiplanar* structure is different to the postulated *anti* and *gauche* structures (Figure 1) and is shown in Figure 2.

Figure 2 Postulated and observed structures for 1,1,2,2-tetra-*tert*-butyldisilane

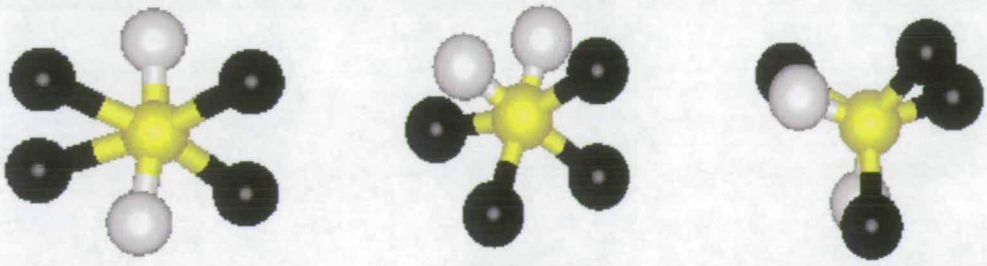

anti ***gauche*** ***antiperiplanar***

Further calculations at the MP2/6-31G* level were performed in C_2 symmetry, with little change in the ϕ(H-Si-Si-H) dihedral angle. The molecular geometry of $Bu^t_2HSiSiHBu^t_2$ from the MP2/6-31G* calculation is presented in Table 2, along with those calculated at the HF/3-21G* and HF/6-31G* levels of theory.

In general, the bond angles did not change by more than 1° upon the inclusion of electron correlation in the calculations. However, the bond lengths were observed to vary greatly upon going from the HF/6-31G* to the MP2/6-31G* level of thoery. For example, the Si-Si bond length shorted from 243.5 pm (HF) to 240.8 pm (MP2), and the Si-C(3/16) bond lengths shortened from 194.6 and 195.1 pm to 193.0 and 193.4 pm. The Si-H bond length was observed to lengthen upon the inclusion of electron correlation, from 148.5 pm to 150.1 pm. In general, the torsion angles did not vary by much more than 1°. For example, ϕ[C(4)-C(3)-Si(2)-Si(1)] was observed to change from 60.0° to 59.4°, and the important angle ϕ[H(30)-Si(1)-Si(2)-H(29)] changed from –101.4° to –102.5°.

The most important feature to arise from the calculations was the orientation of the butyl groups in relation to one another. Earlier, two possible structures, *anti* and *gauche*, were postulated for 1,1,2,2-tetra-*tert*-butyldisilane. The *ab initio* calculations revealed that the *antiperiplanar* structure is the global minimum on the potential energy surface, with the *anti* structure returning imaginary frequencies.

Table 2 Molecular geometry of the C_2 structure of $Bu^t_2HSiSiHBu^t_2$ at the HF/3-21G*, HF/6-31G* and MP2/6-31G* levels of theory.[a,b]

Parameter	HF/3-21G*	HF/6-31G*	MP2/6-31G*
Si(1)-Si(2)	241.3	243.5	240.8
Si(2)-C(3)	192.6	194.6	193.0
Si(2)-C(16)	193.1	195.1	193.4
Si(2)-H(29)	148.6	148.5	150.1
C-C (mean)	155.3	154.2	153.5
C-H (mean)	108.5	108.6	109.6
Si(1)-Si(2)-C(3)	108.1	108.6	107.7
Si(1)-Si(2)-C(16)	120.7	120.4	120.5
C(3)-Si(2)-C(16)	115.6	115.6	115.5
Si(2)-C(3)-C(4)	112.8	112.6	111.9
Si(2)-C(3)-C(5)	112.6	111.7	111.4
Si(2)-C(3)-C(6)	108.0	108.2	107.9
Si(2)-C(16)-C(17)	110.1	109.8	109.1
Si(2)-C(16)-C(18)	109.2	108.6	108.4
Si(2)-C(16)-C(19)	114.8	114.6	114.2
C(4)-C(3)-Si(2)-Si(1)	57.9	60.0	59.4
C(17)-C(16)-Si(2)-Si(1)	34.5	32.0	33.3
H(30)-Si(1)-Si(2)-H(29)	-98.7	-101.4	-102.5

[a] All bond lengths in pm; angles in degrees.

[b] See Figure 3 for atom numbering.

It is also very interesting to observe the calculated Si-Si-C angles in this molecule. The angle out to the eclipsed *tert*-butyl groups is calculated to be 120.5°, whereas the angle to the *tert*-butyl groups eclipsed by hydrogen atoms is calculated to be 107.7°, much less than the ideal tetrahedral angle of 109.5°. This distortion of angles around the Si atoms leads to a reduction in the overall steric strain of the molecule by pushing the *syn* butyl groups further apart from one another. The C-Si-C angle was calculated to be 115.5°, indicating that the adjacent *tert*-butyl groups need to spread apart from each other to reduce steric strain. In the *anti* structure, the molecule

cannot do both of these distortions. If the eclipsed *tert*-butyl groups push apart, the adjacent *tert*-butyl groups are forced closer together, increasing the steric strain at each end of the molecules. If the eclipsed *tert*-butyl groups do not push apart, then there are too many close-range H...H contacts between the methyl groups in the *tert*-butyl groups. This helps to explain why the initially more unlikely *antiperiplanar* structure is favoured for this molecule.

Figure 3 Computed (MP2/6-31G*) molecular structure of 1,1,2,2-tetra-*tert*-butyldisilane in the gas phase, with a perspective view down the Si-Si bond.

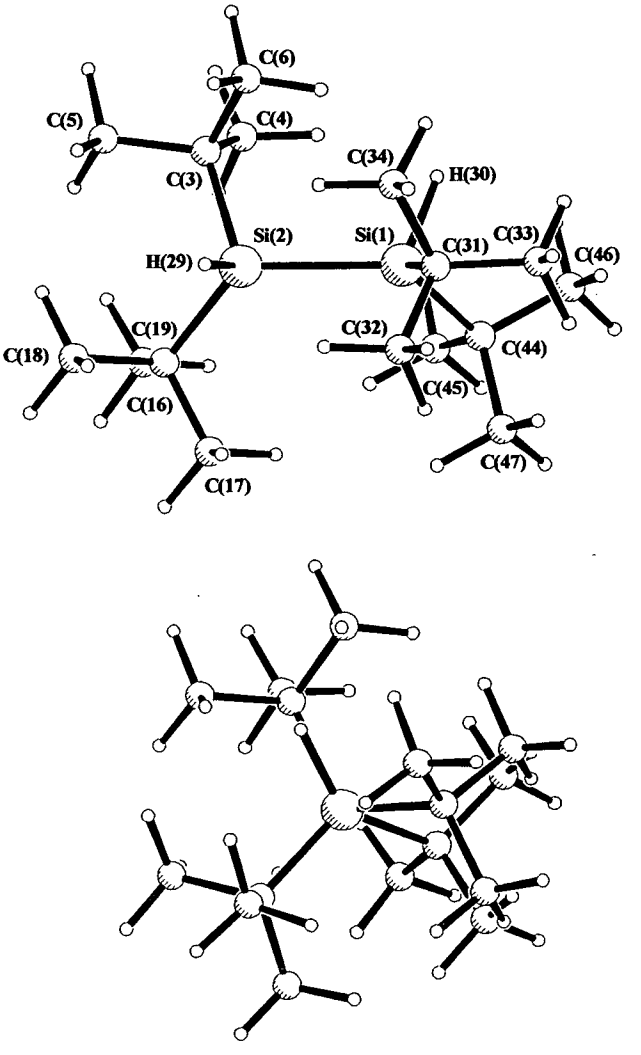

Another interesting feature of the calculations of the structure of this molecule is that, whether starting from a torsion angle of ϕ(H-Si-Si-H) = 0° or from ϕ(H-Si-Si-H)

= 180°, the same minimum is reached. From the torsion angle ϕ(H-Si-Si-H) = 180°, the *tert*-butyl groups which end up close to eclipsing actually pass each other on the way there. In other words, the fully eclipsed structure is lower in energy than the *anti* structure. This indicates that there must be a lot of flexibility around the silicon atoms but the question still lingers as to why this phenomenon occurs and why a minimum with ϕ(H-Si-Si-H) of ~130° is not observed from the ϕ(H-Si-Si-H) = 180° starting point.

The calculated structures of 1,1,2,2-tetra-*tert*-butyldigermane and, perhaps more surprisingly, 1,1,2,2-tetra-*tert*-butyldistannane both exhibit very similar structural motifs to the disilane, as shown in Figure 4. Calculated ϕ[H-Y-Y-H] torsion angles were 98.9° and –88.0° for Y = Ge and Sn respectively, compared to -102° calculated for 1,1,2,2-tetra-*tert*-butyldisilane. In 1,1,2,2-tetra-*tert*-butyldigermane, the Ge-Ge-C bond angles were predicted to be 119.8 and 107.0°, similar to the equivalent predictions for the disilane. The Ge-Ge and Ge-C(3/16) bond lengths were predicted to be 244.3 pm and 198.4 and 198.3 pm respectively. In 1,1,2,2-tetra-*tert*-butyldistannane, the Sn-Sn-C bond angles were predicted to be 115.7 and 108.5°. These differ by up to 5° from those predicted for the disilane, but this is to be expected due to the reduction in steric strain within the molecule due to the increased bond lengths. The Sn-Sn and Sn-C bond lengths were predicted to be 288.5 pm and 219.5 pm respectively. It is interesting to note from Figure 4 that as Y goes from Si → Ge → Sn, the observed conformation gradually approaches the expected *gauche* form. This suggests that the critical factor in obtaining the *antiperiplanar* structure for the disilane is end-to-end steric crowding.

Figure 4 Structural motifs of 1,1,2,2-tetra-*tert*-butyl-disilane, -digermane and -distannane.

$Bu^t_2HSiSiHBu^t_2$ $Bu^t_2HGeGeHBu^t_2$ $Bu^t_2HSnSnHBu^t_2$

The most surprising outcome from these predicted structures is that no *anti* structure is found for the 1,1,2,2-tetra-*tert*-butyldistannane. It could be envisaged that, with the general reduction of strain throughout the molecule due to longer bonds, an *anti* structure could exist. However, a rigorous search of the potential energy surface of the molecule revealed only one *syn* structure. The predicted C_2 structures of 1,1,2,2-tetra-*tert*-butyldigermane at the MP2/6-31G* level, and 1,1,2,2-tetra-*tert*-butyldistannane at the MP2/GEN level are presented in Table 3.

Table 3 Molecular geometries of the C_2 conformations of $Bu^t_2HGeGeHBu^t_2$ and $Bu^t_2HSnSnHBu^t_2$ at the MP2/6-31G* and MP2/GEN levels of theory.[a,b,c]

Parameter	$Bu^t_2HGeGeHBu^t_2$	$Bu^t_2HSnSnHBu^t_2$
Y(1)-Y(2)[d]	244.3	288.5
Y(2)-C(3)	198.3	219.5
Y(2)-C(16)	198.4	219.4
Y(2)-H(29)	162.0	175.0
C-C (mean)	152.9	153.0
C-H (mean)	109.6	109.8
Y(1)-Y(2)-C(3)	118.8	108.5
Y(1)-Y(2)-C(16)	107.0	115.7
C(3)-Y(2)-C(16)	119.8	115.4
Y(2)-C(3)-C(4)	113.1	110.6

Table 3 Continued

Parameter	$Bu^t_2HGeGeHBu^t_2$	$Bu^t_2HSnSnHBu^t_2$
Y(2)-C(3)-C(5)	109.5	110.6
Y(2)-C(3)-C(6)	105.2	107.1
Y(2)-C(16)-C(17)	105.2	108.6
Y(2)-C(16)-C(18)	111.0	108.8
Y(2)-C(16)-C(19)	110.9	111.2
C(4)-C(3)-Y(2)-Y(1)	69.6	52.5
C(17)-C(16)-Y(2)-Y(1)	63.5	45.5
H(30)-Y(1)-Y(2)-H(29)	98.9	-88.0

[a] All bond lengths in pm; angles in degrees.

[b] See Figure 3 for atom numbering.

[c] 6-31G* on C and H, LanL2DZ on Sn

[d] Y = Ge or Sn

4.3.2 Gas-phase electron diffraction refinement

On the basis of the *ab initio* calculations described above, electron-diffraction refinements were carried out using a model of C_2 symmetry to describe the vapour. The large number of geometric parameters needed to define the model made it necessary to make the assumption of local C_{3v} symmetry for the methyl groups, and C_s symmetry about the *tert*-butyl groups. The deviations from these local symmetries in the computed structure were small (less than 1°).

The structure of $Bu^t_2HSiSiHBu^t_2$ was finally defined in terms of twenty-two independent geometric parameters, comprising five bond lengths and differences, eight bond angles and differences and nine torsion parameters and differences [Table 4; atom numbering shown in Figure 3].

Table 4 Refined and calculated geometric parameters for $Bu^t_2HSiSiHBu^t_2$ (distances in pm, angles in °) from the GED study.[a]

No.	Parameter	GED (r_a)	MP2/6-31G*	Restraint
p_1	C-H	111.5(5)	109.9	110.0(10)
p_2	Si-Si	239.4(9)	240.7	240.7(10)
p_3	Si-C (mean)	193.6(3)	193.2	-
p_4	[C-C + Si-H] / 2	152.0(2)	151.8	151.8(20)
p_5	C-C – Si-H	3.4(3)	3.3	3.4(3)
p_6	Si-Si-H	104.3(11)	104.1	104.1(10)
p_7	C-C-H	108.0(7)	109.4	109.5(10)
p_8	{[Si-Si-C(3)] + [Si-Si-C(16)]} / 2	115.7(5)	114.1	-
p_9	[Si-Si-C(3)] – [Si-Si-C(16)]	10.6(4)	12.8	-
p_{10}	C-C-C mean	108.5(10)	108.4	107.9(10)
p_{11}	[C-C-C av (gp1)] – [C-C-C av (gp2)]	-0.2(11)	0.2	0.2(10)
p_{12}	Si-C-C mean	110.9(2)	110.5	-
p_{13}	[Si-C-C av (gp1)] – [Si-C-C av (gp2)]	-0.1(5)	-0.2	-0.2(5)
p_{14}	[Si(2)-C(3)-C(6)] – [Si(2)-C(3)-C(4/5)]	-2.8(9)	-3.8	-3.82(10)
p_{15}	[Si(2)-C(16)-C(19)] – [Si(2)-C(16)-C(17/18)]	5.5(9)	5.4	5.4(10)
p_{16}	Methyl torsion gp 1	-177.6(30)	-179.6	-178.9(30)
p_{17}	Butyl torsion gp1	58.9(20)	59.4	
p_{18}	Methyl torsion gp2	58.5(21)	52.5	58.0(20)
p_{19}	Butyl torsion gp2	-93.5(13)	-88.8	-
p_{20}	{ϕ[C(3)-Si(2)-Si(1)-H(29)] + ϕ[C(16)-Si(2)-Si(1)-H(29)]} / 2	112.1(5)	112.3	111.7(5)
p_{21}	ϕ[C(3)-Si(2)-Si(1)-H(29)] – ϕ[C(16)-Si(2)-Si(1)-H(29)]	2.9(11)	3.7	3.0(10)
p_{22}	ϕ[H(29)-Si(2)-Si(1)-H(30)]	-109.1(19)	-102.5	-

[a] Figures in parentheses are the estimated standard deviations of the last digits. See text for parameter definitions.

On the basis of the highest level *ab initio* calculations the independent distance parameters are the C-H and Si-Si bond lengths (p_1 and p_2) and the average Si-C distance (p_3). An average value was used for the C-C and Si-H distances (p_4), with a difference parameter (p_5). The Si-Si-H angle (p_6) was included, and all C-C-H bond angles (p_7) were assumed to be identical. An average (p_8) and a difference (p_9) were used to describe the Si-Si-C(3/16) angles. The C-C-C angles were defined in terms of the average (p_{10}) C-C-C angles of both *tert*-butyl groups, and a difference parameter (p_{11}), defined as the average C-C-C angle of the first *tert*-butyl group minus the average C-C-C angle of the second *tert*-butyl group.

The *tert*-butyl groups were calculated to have approximate C_s local symmetry, and the Si-C-C angles were defined in terms of an average (p_{12}) of all the Si-C-C angles and three difference parameters. The first of these differences is the average Si-C-C bond angle for the first *tert*-butyl group minus the average for the second group (p_{13}). The remaining two are differences within the individual *tert*-butyl groups, i.e. Si(2)-C(3)-C(6) minus Si(2)-C(3)-C(4/5) (p_{14}) and Si(2)-C(16)-C(19) minus Si(2)-C(16)-C(17/18) (p_{15}).

Of the remaining seven parameters, four represent the torsions of the *tert*-butyl and methyl groups. These groups were generated by initially placing a methyl group carbon atom at the origin, with its three H atoms arranged with local C_{3v} symmetry about the *x*-axis and one H in the *xy* plane in the positive *x* and *y* directions. The methyl torsion parameter (p_{16}) is a rotation of the group about the local *x*-axis. The methyl group is then translated along the positive *x*-axis by the C-C bond length and the central carbon of the *tert*-butyl group is placed at the origin. The correct Si-C-C bond angles are generated by rotating the methyl group about the *z*-axis, moving the methyl carbon atom in the positive *y* direction, and then generating the other methyl groups by positive and negative rotation of the first group about the *x*-axis. The *tert*-butyl torsion angle is a rotation of the group about the *x*-axis. The first *tert*-butyl torsion parameter is introduced here (p_{17}), described as C(4)-C(3)-Si(2)-Si(1). The second *tert*-butyl group was generated in exactly the same was as the first, but with different methyl torsion (p_{18}) and *tert*-butyl torsion (p_{19}) [ϕ = C(17)-C(16)-Si(2)-Si(1)] parameters.

Having generated the *tert*-butyl groups in their local coordinate systems they all lie in the *xy* plane. They need to be rotated about the *x*-axis to put them in the correct positions. The two *tert*-butyl groups and the hydrogen attached to Si(2) were initially placed in the *xy* plane, and the *tert*-butyl groups were then rotated about the *x*-axis. These rotations are defined in terms of the average of C(3)-Si(2)-Si(1)-H(29) and C(16)-Si(2)-Si(1)-H(29) (p_{20}) and the difference between torsion angles C(3)-Si(2)-Si(1)-H(29) and C(16)-Si(2)-Si(1)-H(29) (p_{21}).

Translating the first half of the molecule along the *x*-axis by (p_2)/2 and performing a C_2 rotation about the z-axis generated the second half of the molecule. Finally, the dihedral angle H(29)-Si(2)-Si(1)-H(30) (p_{22}) described the overall conformation about the Si-Si bond, with a value of zero indicating the conformation in which the two hydrogen atoms were eclipsing one another.

The starting parameters for the r_a refinement were taken from the theoretical geometry optimised at the MP2/6-31G* level. The r_α structure was not refined because the rectilinear vibrational corrections (i.e. parallel and perpendicular correction terms) are known to be unreliable for a molecule this size with many low-lying vibrational modes. Theoretical (UFF) Cartesian force fields were obtained and converted into force fields described by a set of symmetry coordinates using a version of the ASYM40 program[16] modified to work for molecules with more than 40 atoms. All geometric parameters were then refined.

In total all twenty-two geometric parameters and twelve groups of vibrational amplitudes were refined. Flexible restraints were employed during the refinement using the SARACEN method.[17] Altogether, fifteen geometric and four amplitude restraints were employed. These are listed in Tables 4 and 5.

The success of the final refinement, for which $R_G = 0.167$ ($R_D = 0.127$), can be assessed on the basis of the radial distribution curve (Figure 5) and the molecular scattering intensity curves (Figure 6). Final refined parameters are listed in Table 4, interatomic distances and the corresponding amplitudes of vibration in Table 5 with the least-

squares correlation matrix shown in Table 6. Experimental coordinates from the GED analysis are given in Appendix 3 [Table 1]. In the SARACEN analysis, because all parameters are refining, the error estimates are realistic. We therefore quote the estimated standard deviations, σ, and do not need to add any further allowance for correlation with fixed parameters. Figure 3 shows a perspective view of $Bu^t_2HSiSiHBu^t_2$ in the optimum refinement of the GED data, as well as a view down the Si-Si bond.

Table 5 Interatomic distances (r/pm) and amplitudes of vibration (u/pm) for the restrained GED structure of $Bu^t_2HSiSiHBu^t_2$.[a]

No.	Atom Pair	r_a/pm	u/pm[b]	Restraint
u_1	C(4)-C(3)	153.7(2)	3.4(5)	-
u_2	H(7)-C(4)	111.5(5)	6.2(7)	4.8(7)
u_3	C(3)-Si(2)	193.6(4)	3.1(6)	-
u_4	C(17)...Si(2)	283.9(8)	8.2(6)	-
u_5	C(4)...Si(2)	288.4(8)	7.7(tied to u_4)	-
u_6	H(7)...C(3)	215.9(9)	11.8(16)	-
u_7	Si(2)-Si(1)	239.4(9)	5.7(5)	5.0(5)
u_8	C(6)...Si(2)	283.6(12)	7.6(tied to u_4)	-
u_9	C(19)...C(17)	248.1(12)	6.4(6)	-
u_{10}	C(6)...C(4)	248.6(12)	6.3 (tied to u_9)	-
u_{11}	C(19)...Si(2)	293.0(12)	7.9 (tied to u_4)	-
u_{12}	C(3)...Si(1)	344.9(16)	8.2(7)	7.8(7)
u_{13}	C(6)...Si(1)	365.2(34)	10.6 (tied to u_{12})	-
u_{14}	C(16)...Si(1)	386.9(12)	8.4 (tied to u_{12})	-
u_{15}	C(4)...Si(1)	372.8(33)	14.7 (fixed)	-
u_{16}	C(17)...Si(1)	401.0(18)	11.6 (tied to u_{12})	-
u_{17}	C(19)...Si(1)	461.4(26)	14.8(14)	14.3(14)
u_{18}	C(5)...Si(1)	487.5(13)	8.1 (tied to u_{17})	-
u_{19}	C(18)...Si(1)	506.9(12)	9.8 (tied to u_{17})	-
u_{20}	C(18)...C(17)	249.7(18)	6.2 (tied to u_9)	-
u_{21}	C(5)...C(4)	249.4(18)	6.3 (tied to u_9)	-

Table 5 Continued

No.	Atom Pair	r_a/pm	u/pm[b]	Restraint
u_{22}	C(16)...C(3)	324.3(16)	5.3(24)	-
u_{23}	C(16)...C(5)	347.7(29)	6.9 (tied to u_{22})	-
u_{24}	C(18)...C(5)	342.5(41)	9.6 (tied to u_{22})	-
u_{25}	H(8)...H(7)	183.6(11)	12.7 (fixed)	-
u_{26}	C(19)...C(3)	359.5(23)	7.2 (tied to u_{22})	-
u_{27}	C(19)...C(5)	367.2(46)	8.2 (tied to u_{22})	-
u_{28}	C(19)...C(4)	370.3(52)	14.5 (fixed)	-
u_{29}	H(21)...Si(2)	296.1(25)	10.1 (fixed)	-
u_{30}	C(18)...C(3)	377.4(24)	7.0 (tied to u_{22})	-
u_{31}	H(20)...Si(2)	299.1(23)	4.2(35)	-
u_{32}	H(29)-Si(2)	150.3(3)	6.7 (tied to u_1)	-
u_{33}	H(9)...Si(2)	305.6(33)	2.7 (tied to u_{31})	-
u_{34}	H(7)...Si(2)	301.1(31)	4.1 (tied to u_{31})	-
u_{35}	C(16)...C(4)	390.7(36)	10.7(22)	-
u_{36}	C(45)...C(19)	435.1(52)	26.1 (tied to u_{35})	-
u_{37}	C(32)...C(17)	431.2(51)	18.5 (tied to u_{35})	-
u_{38}	C(44)...C(17)	445.1(42)	14.2 (tied to u_{35})	-
u_{39}	C(16)...C(6)	451.6(15)	8.2 (tied to u_{35})	-
u_{40}	C(17)...C(3)	454.2(12)	8.1 (tied to u_{35})	-
u_{41}	C(31)...C(6)	432.3(48)	16.1 (tied to u_{35})	-
u_{42}	C(32)...C(16)	474.7(37)	18.3 (tied to u_{35})	-
u_{43}	C(31)...C(17)	486.3(35)	14.6 (tied to u_{35})	-

[a] Estimated standard deviations, obtained in the least-squares refinement, are given in parentheses.

[b] Amplitudes not refined were fixed at the values obtained using the UFF force field.

Table 6 Least-squares correlation matrix (× 100) for $Bu^t_2HSiSiHBu^t_2$.[a]

	p_3	p_5	p_{21}	p_{19}	u_9	u_{31}	k_2
p_2					56		
p_4		-63					
p_{12}	-52						
p_{20}				-50			
p_{22}			-54				
u_1							73
u_2							53
u_4						60	

[a] Only elements with absolute values ≥50% are shown; k_2 is a scale factor.

Figure 5 Experimental and difference (experimental - theoretical) radial-distribution curve, $P(r)/r$, for $Bu^t_2HSiSiHBu^t_2$. Before Fourier inversion the data were multiplied by $s.\exp(-0.00002s^2)/(Z_{Si}-f_{Si})/(Z_C-f_C)$.

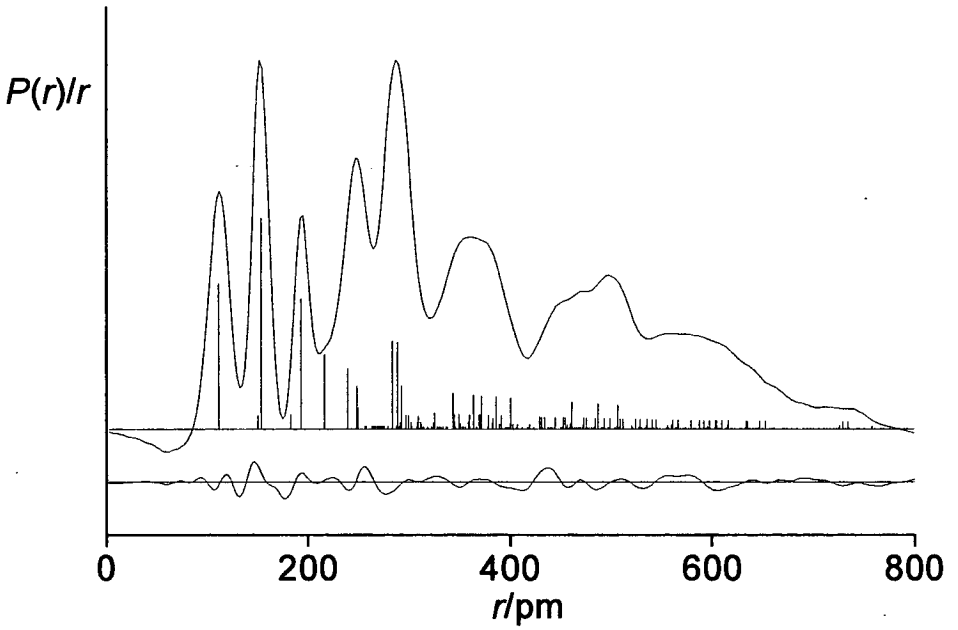

Figure 6 Experimental and final weighted difference (experimental - theoretical) molecular-scattering intensities for $Bu^t_2HSiSiHBu^t_2$.

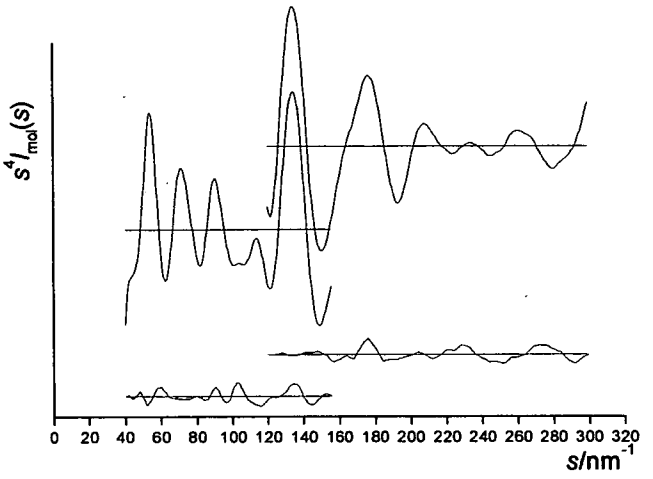

As the model used did not appear to fit the experimental data very well, as reflected by the poor R_G factor, a refinement with the torsion angle ϕ(H-Si-Si-H) $\approx$ 180° was also attempted. The molecular model to define the structure was exactly the same as before, with the starting torsion angle (p_{22}) set at 180°. A theoretical Cartesian force field could not be used to convert to a force field using symmetry coordinates as imaginary frequencies were obtained when these calculations are performed. Thus a program (DistList)[18] was used to generate a distance list with an empirical starting set of amplitudes for this molecule.

In total eighteen geometric parameters and ten groups of vibrational amplitudes were refined. Flexible restraints were employed during the refinement using the SARACEN method.[17] In total, twelve geometric and six amplitude restraints were employed. These are listed in Tables 7 and 9. The quality of the final refinement, for which R_G = 0.197 (R_D = 0.143), can be assessed on the basis of the radial distribution curve (Figure 7) and the molecular scattering intensity curves (Figure 8). This refinement appears to be significantly poorer than the original refinement. Final refined parameters are listed in Table 7, the least-squares correlation matrix is shown in Table 8 and interatomic distances and the corresponding amplitudes of vibration in Table 9. Experimental coordinates from the GED analysis are shown in Appendix 3 [Table 2]. Figure 9 shows a perspective view of this conformer of $Bu^t_2HSiSiHBu^t_2$ in the optimum refinement of the GED data, as well as the view down the Si-Si bond.

Table 7 Refined and calculated geometric parameters for the second refinement of $Bu^t_2HSiSiHBu^t_2$ (distances in pm, angles in °) in the GED study.[a]

No.	Parameter	GED (r_a)	Restraint
p_1	C-H	112.5(4)	110.0(10)
p_2	Si-Si	241.4(9)	240.8(10)
p_3	Si-C (mean)	195.0(5)	-
p_4	[C-C + Si-H] / 2	152.9(3)	151.8(20)
p_5	C-C – Si-H	3.4(3)	3.4(3)
p_6	Si-Si-H	110.0(11)	110.0(10)
p_7	C-C-H	109.7(7)	109.5(10)
p_8	{[Si-Si-C(3)] + [Si-Si-C(16)]} / 2	118.0(6)	-
p_9	[Si-Si-C(3)] – [Si-Si-C(16)]	0.0 (fixed)	-
p_{10}	C-C-C mean	108.5(10)	107.9(10)
p_{11}	[C-C-C av (gp1)] – [C-C-C av (gp2)]	0.0 (fixed)	-
p_{12}	Si-C-C mean	110.3(10)	-
p_{13}	[Si-C-C av (gp1)] – [Si-C-C av (gp2)]	0.0 (fixed)	-
p_{14}	[Si(2)-C(3)-C(6)] – [Si(2)-C(3)-C(4/5)]	-6.1(9)	-3.8(10)
p_{15}	[Si(2)-C(16)-C(19)] – [Si(2)-C(16)-C(17/18)]	6.3(9)	5.4(10)
p_{16}	Methyl torsion gp 1	10.6(31)	10.0(30)
p_{17}	Butyl torsion gp1	-1.5(26)	-
p_{18}	Methyl torsion gp2	-28.9(31)	-30.0(30)
p_{19}	Butyl torsion gp2	95.9(17)	-
p_{20}	{ϕ[C(3)-Si(2)-Si(1)-H(29)] + ϕ[C(16)-Si(2)-Si(1)-H(29)]} / 2	111.6(5)	111.7(5)
p_{21}	ϕ[C(3)-Si(2)-Si(1)-H(29)] – ϕ[C(16)-Si(2)-Si(1)-H(29)]	0.0 (fixed)	-
p_{22}	ϕ[H(29)-Si(2)-Si(1)-H(30)]	189.8(25)	-

[a] Figures in parentheses are the estimated standard deviations of the last digits. See text for parameter definitions.

Table 8 Least-squares correlation matrix (× 100) for the second refinement of $Bu^t_2HSiSiHBu^t_2$.[a]

	p_5	p_{12}	u_1	u_{11}	k_2
p_2				52	
p_3		-65			
p_4	-52				
p_8					50
u_9			50		

[a] Only elements with absolute values ≥50% are shown; k_2 is a scale factor.

Table 9 Interatomic distances (r/pm) and amplitudes of vibration (u/pm) in the second attempted GED structure of $Bu^t_2HSiSiHBu^t_2$.[a]

No.	Atom Pair	r_a/pm	u/pm[b]	Restraint
1	C(4)-C(3)	154.6(2)	4.6(4)	4.7(5)
2	H(7)-C(4)	112.5(4)	6.2(8)	-
3	C(3)-Si(2)	195.0(5)	4.7(5)	5.0(5)
4	C(17)...Si(2)	284.3(6)	7.9(6)	7.0(7)
5	C(4)...Si(2)	291.3(6)	7.9 (tied to u_4)	-
6	H(7)...C(3)	219.7(8)	6.5(10)	-
7	C(3)...Si(1)	374.8(11)	9.9(7)	8.0(8)
8	C(17)...Si(1)	500.7(13)	17.2(21)	-
9	Si(2)-Si(1)	241.3(9)	5.1(5)	5.0(5)
10	C(4)...Si(1)	480.6(25)	17.2 (tied to u_8)	-
11	C(6)...Si(2)	280.8(13)	7.9(9)	-
12	C(5)...C(4)	250.9(17)	7.9 (tied to u_{11})	-
13	C(19)...C(17)	251.1(10)	7.9 (tied to u_{11})	-
14	C(6)...C(4)	251.1(11)	7.9 (tied to u_{11})	-
15	C(19)...Si(2)	294.9(12)	7.9 (tied to u_{11})	-
16	C(6)...Si(1)	357.7(24)	13.0 (fixed)	-
17	C(19)...Si(1)	444.9(21)	13.0 (fixed)	-
18	C(31)...C(17)	650.7(15)	16.2(13)	13.8(14)

4.5 Further Work

Having eliminated the possibility of the *anti* conformer existing within the gas-phase mixture, there is still some work to be done on remodelling the existing *antiperiplanar* structure before we resort to collecting more experimental data. It seems that the steric crowding within this molecule is a very important factor in determining the overall conformation, and therefore the details of the structures of the *tert*-butyl and methyl groups are extremely important. We have assumed C_s symmetry within the *tert*-butyl groups for our model, so re-evaluation with C_1 symmetry for those groups would seem prudent. However, it is possible that we need even more sophisticated methods to model the hydrogen and methyl group positions accurately, to take account of local distortions at the sites of greatest steric strain. A proposed method to do this is outlined in Chapter 9 of this thesis, and will be developed and applied to $Bu^t_2HSiSiHBu^t_2$ over the next three years.

It is possible that we need to obtain better quality short camera distance data, as there appears to be a bad fit to the present set with large peaks in the difference curve (See Figure 6). *K. Hassler, Graz, Austria*, hopes to obtain infrared and Raman spectroscopic data for this molecule in the very near future, as well as an X-ray crystallographic structure for comparison with that determined in the gas phase. By studying the disorder of the solid structure, we can further analyse the interactions of the *tert*-butyl groups on the same side of the molecule, and across the molecule.

4.6 References

1. B. Reiter and K. Hassler, *J. Organomet. Chem.*, 1994, **467**, 21.
2. J. S. Binkley, J. A. Pople and W. J. Hehre, *J. Am. Chem Soc.*, 1980, **102**, 939.
3. M. S. Gordon, J. S. Binkley, J. A. Pople, W. J. Pietro and W. J. Hehre, *J. Am. Chem. Soc.*, 1982, **104**, 2797.
4. W. J. Pietro, M. M. Francl, W. J. Hehre, D. J. DeFrees, J. A. Pople and J. S. Binkley, *J. Am. Chem. Soc.*, 1982, **104**, 5039.
5. W. J. Hehre, R. Ditchfield and J. A. Pople, *J. Chem. Phys.*, 1972, **56**, 2257.
6. P. C. Hariharan and J. A. Pople, *Theor. Chim. Acta*, 1973, **28**, 213.
7. M. S. Gordon, *Chem. Phys. Lett.*, 1980, **76**, 163.
8. Gaussian 98, Revision A.7, M. J. Frisch, G. W. Trucks, H. B. Schlegel, G. E. Scuseria, M. A. Robb, J. R. Cheeseman, V. G. Zakrzewski, J. A. Montgomery, R. E. Stratmann Jr, J. C. Burant, S. Dapprich, J. M. Millam, A. D. Daniels, K. N. Kudin, M. C. Strain, O. Farkas, J. Tomasi, V. Barone, M. Cossi, R. Cammi, B. Mennucci, C. Pomelli, C. Adamo, S. Clifford, J. Ochterski, G. A. Petersson, P. Y. Ayala, Q. Cui, K. Morokuma, D. K. Malick, A. D. Rabuck, K. Raghavachari, J. B. Foresman, J. Cioslowski, J. V. Ortiz, A. G. Baboul, B. B. Stefanov, G. Liu, A. Liashenko, P. Piskorz, I. Komaromi, R. Gomperts, R. L. Martin, D. J. Fox, T. Keith, M. A. Al-Laham, C. Y. Peng, A. Nanayakkara, C. Gonzalez, M. Challacombe, P. M. W. Gill, B. Johnson, W. Chen, M. W. Wong, J. L. Andres, C. Gonzalez, M. Head-Gordon, E. S. Replogle and J. A. Pople, Gaussian, Inc., Pittsburgh PA, 1998.
9. A. K. Tappe, C. J. Caséwit, K. S. Colwell, W. A. Goddard III and W. M. Skiff, *J. Am. Chem. Soc.*, 1992, **114**, 10024.
10. T. H. Dunning Jr. and P. J. Hay, "Modern Theoretical Chemistry", Vol. 3, Ed. H. F. Schaefer III, Plenum, 1976, p. 1; P. J. Hay and W. R. Wadt, *J. Chem. Phys.*, 1985, **82**, pp. 270, 284 and 299.
11. C. M. Huntley, G. S. Laurenson and D. W. H. Rankin, *J. Chem. Soc., Dalton Trans.*, **1980**, 954.
12. J. R. Lewis, P. T. Brain and D. W. H. Rankin, *Spectrum*, 1997, **15**, 7.
13. S. Cradock, J. Koprowski and D. W. H. Rankin, *J. Mol. Struct.*, 1981, **77**, 113.

14. A. S. F. Boyd, G. S. Laurenson and D. W. H. Rankin, *J. Mol. Struct.*, **1981**, *71*, 217.

15. A. W. Ross, M. Fink and R. Hilderbrandt, *International Tables for Crystallography*, Ed. A. J. C. Wilson, Kluwer Academic Publishers, Dordrecht, Boston and London, 1992; Vol. C, p. 245.

16. L. Hedberg and I. M. Mills, *ASYM 40, Program for Force Constants and Coordinate Analysis,* Version 3.0; see also L. Hedberg and I. M. Mills, *J. Mol. Spectrosc.* **1993**, *160*, 117.

17. N. W. Mitzel, B. A. Smart, A. J. Blake, H. E. Robertson and D. W. H. Rankin, *J. Phys. Chem.* **1996**, *100*, 9339; A. J. Blake, P. T. Brain, H. McNab, J. Miller, C. A. Morrison, S. Parsons, D. W. H. Rankin, H. E. Robertson and B. A. Smart, *J. Phys. Chem.* **1996**, *100*, 12280.

18. B. F. Johnston, University of Edinburgh, Personal communication.

19. D. Hnyk, R. S. Fender, H. E. Robertson, D. W. H. Rankin, M. Bühl, K. Hassler and K. Schenzel, *J. Mol. Struct.*, 1995, **346**, 215.

Chapter 5

Tris(*tert*-butyl)sulfurtriimide, $S(NBu^t)_3$: Molecular Structure by Gas-Phase Electron Diffraction, X-ray Crystallography and *Ab Initio* Calculations.

5.1 Introduction

The first stable three-coordinate sulfur (VI) nitrogen species were isolated more than 20 years ago, although very little is known about their chemistry.[1] One of the first stable sulfur triimides reported was $S(NSiMe_3)_3$, formed by the reaction of NSF_3 and $LiN(SiMe_3)_2$ in yields of up to 23%.[2] Other routes to sulfur triimides include the reaction of sulfur tetrafluoride oxide, $O{=}SF_4$ with the bissilylated alkali sodium amide $NaN(SiMe_3)_2$,[3] the trans-imination of sulfur tris(*tert*-butylimide) and sulfur tris(trimethylsilyl-imide).[4,5] It is worth noting that the stability of the triimides formed varies greatly with the steric bulk of the substituent attached. $(Me_3CN{=})_2S{=}NCF_3$ was found to decompose within a day whereas $(Me_3CN{=})_2S{=}NSF_5$ was found to be almost as stable as $S(NSiMe_3)_3$. In the $(Me_3CN{=})_2S{=}NSF_5$ example, S(VI) is also found to exist in its highest and lowest possible coordination numbers of 6 and 3 respectively.

The isolation and characterisation of the more bulky sulfur triimides has been of interest since the first were synthesised. The triimide $S(NBu^t)_3$ was first isolated in 1977 by Glemser and co-workers,[6] with further characterisation being carried out in 1979.[7] The great interest at this time was as to whether the "Y" framework of the triimide was actually planar, or whether the sulfur was at the apex of a trigonal based pyrimid.[1] Initial crystallographic studies at the time were inconclusive as to whether the molecule was planar or bent, although large thermal ellipsoids were observed perpendicular to the SN_3 plane, perhaps indicating that the observed planar structure is an average of a more disordered, slightly pyramidal structure.

Our interest in this sterically crowded molecule was sparked by the remarkable lack of structural investigation carried out since these initial studies. Structural investigations using gas phase electron diffraction, X-ray crystallography (*carried out by D. Stalke, Germany*) and *ab initio* calculations have been carried out with comparisons drawn between the structures obtained from each technique.

5.2 Experimental

5.2.1 Synthesis

A sample of $S(NBu^t)_3$ was provided by *D. Stalke, Germany*, and used in the electron diffraction experiment without further purification.

5.2.2 Theoretical Methods

All calculations were performed on a Dec Alpha 1000 4/200 workstation using the Gaussian 98 program.[8] An extensive search of the torsional potential of $S(NBu^t)_3$ was undertaken at the HF/3-21G*[9-11] level in order to locate all minima. One conformer of C_{3h} symmetry was located and further geometry optimizations were undertaken at the HF and MP2 levels using the standard 6-31G*[12-14] basis set. Vibrational frequencies, calculated from analytic second derivatives at the HF/3-21G* and HF/6-31G* levels to determine the nature of stationary points, provided estimates of amplitudes of vibration (u) for use in the gas electron diffraction (GED) refinements and comparison with experimentally determined frequencies. The structure of $S(NBu^t)_3$ with the atom numbering scheme is shown in Figure 1.

Figure 1 Molecular structure of $S(NBu^t)_3$ in the gas phase.

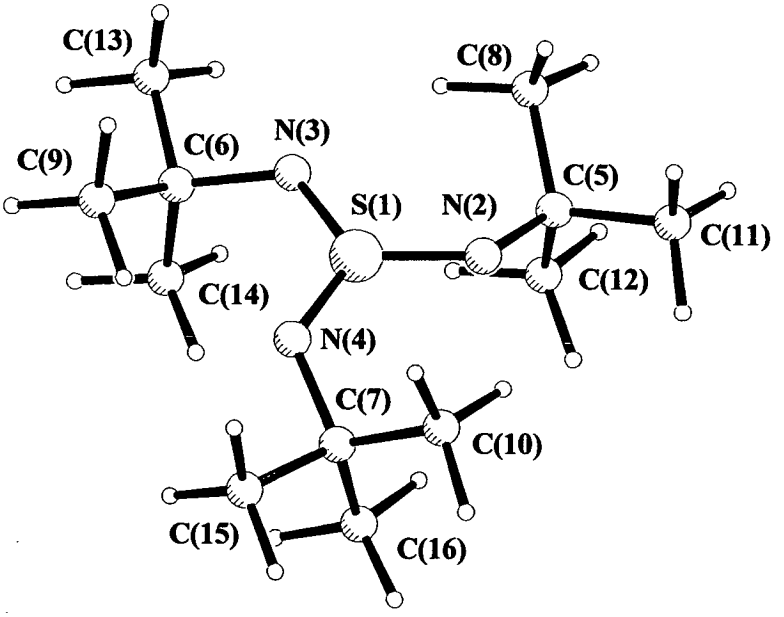

The optimisation procedure for $S(NBu^t)_3$ did not lead to a convergence of the S=N bond length, and so further calculations on the parent $S(NH)_3$ were undertaken at much higher levels of theory and with larger basis sets by *M. Bühl (Germany)*. For $S(NH)_3$, a series of geometry optimisations was also performed at the MP2 level employing Dunning's correlation-consistent basis sets,[15] namely cc-pVDZ, cc-pVTZ, cc-pVQZ' (*i.e.* cc-pVQZ on S and N, cc-pVTZ on H), and cc-pV5Z' (*i.e.* cc-pV5Z on S and N, cc-pVQZ on H). Optimised S=N bond lengths are collected in Table 1.

Table 1 Optimised and extrapolated S=N bond length (pm) for $S(NH)_3$

Level/Basis Set	*r*(S=N)	Level/Basis Set	*r*(S=N)
HF/6-31G*	149.3	MP2/cc-pV5Z'	151.3
MP2/6-31G*	154.1	MP2 extrapol. $[e^{-x}]$[a]	151.2
MP2/cc-pVDZ	155.7	MP2 extrapol. $[x^{-2}]$[b]	150.6
MP2/cc-pVTZ	153.0	B3LYP/GEN[c]	153.5
MP2/cc-pVQZ'	152.0		

[a] Extrapolated using inverse exponential fit.

[b] Extrapolated using inverse quadratic fit.

[c] 6-311+G* on S and N, 6-31G* on H.

Inverse exponential functions were subsequently fitted to a plot of the MP2/cc-pV*x*Z S=N bond length, which proved to be very sensitive to changes in the basis set, and extrapolated to the basis-set limit (*i.e.* to $x = \infty$). It turned out that inverse quadratic functions can be fitted equally well to the data in the range from $x = 2$ to 5. Such functions converge much more slowly, affording significantly smaller extrapolated values. It was therefore decided to regard the corresponding extrapolated distances as upper and lower limits (thereby marking "theoretical error bars") and to take their mean value as the final MP2 estimate which is thus 150.9(3) pm.

In the case of S(NH)2, CCSD(T)/cc-pVTZ' calculations gave S=N bond lengths 0.6 – 0.7 pm shorter than at the MP2/cc-pVTZ level, so we estimate the distance at CCSD(T)/extrapolated basis set to be 150.2(3) pm.

Using these results, the final S=N bond-length estimate was made for the Bu^t derivative according to the following incremental procedure:

$(Bu^t,estim.) = r(H,MP2\ estim.) + \{-0.7\ pm\ [from\ S(NH)_2\ calculation]\} + [r(tBu,MP2) - r(H,MP2)]$

where r(H,MP2 estim.) is an extrapolated value from Table 1 and the values r(R,level) in square brackets are distances optimised using a basis of 6-31G* quality. S=N bond lengths in $S(NH)_3$ are 2.4 pm shorter than the average length in $S(NH)_2$. Therefore, we expect the S=N bond length to be 152.8 pm in $S(NBu^t)_3$. DFT calculations were also carried out on the parent $S(NH)_3$ compound, using the B3LYP level of theory with the 6-311+G* basis set on S and N and 6-31G* on H.

5.2.3 Gas-Phase Electron Diffraction

Data were collected using the Edinburgh gas diffraction apparatus.[16] An accelerating voltage of *ca.* 40 kV (electron wavelength *ca.* 6.0 pm) was used, whilst maintaining the sample and nozzle temperatures at 383 K. Scattering intensities were recorded at nozzle-to-plate distances of 93 and 258 mm on Kodak Electron Image plates. The weighting points for the off-diagonal weight matrices, correlation parameters and scale factors for the two camera distances are given in Table 2, together with electron wavelengths which were determined from the scattering patterns of benzene vapour, recorded immediately after the patterns of $S(NBu^t)_3$ and analysed in exactly the same way, to minimise systematic errors in wavelengths and camera distances. A Joyce-Loebl MDM6 microdensitometer[17] was used to convert the intensity patterns into digital form. Data reduction and least-squares refinements were carried out using standard programs,[17,18] employing the scattering factors of Ross *et al.*[19]

Table 2 Nozzle-to-plate distances (mm), weighting functions (nm^{-1}), correlation parameters, scale factors and electron wavelengths (pm) used in the electron-diffraction study.

Compound	$S(NBu^t)_3$	
Nozzle-to-plate distance[a]	92.5	258.05
Δs	4	2
s_{min}	92	20
sw_1	112	40
sw_2	256	128
s_{max}	300	150
Correlation parameter	0.400	0.325
Scale factor[b]	0.684(17)	0.945(7)
Electron wavelength	6.016	6.016

[a] Determined by reference to the scattering pattern of benzene vapour.

[b] Values in parentheses are the estimated standard deviations.

5.3 Results

5.3.1 *Ab initio* Calculations

A series of molecular orbital calculations was undertaken to investigate the structure of $S(NBu^t)_3$. One conformer, with C_{3h} symmetry, was located and a vibrational frequency calculation at the HF/6-31G* level confirms that this structure is a minimum on the potential energy surface. As no other conformers were located, this structure is the global minimum.

Most parameters remained insensitive to changes in basis set and level of theory used. However, a large jump in S=N bond length from HF/6-31G* to MP2/6-31G* levels was observed and can be attributed to the effects of electron correlation. Further geometry optimisations at higher levels were not undertaken due to the size of the molecule.

However, in view of the large variation in the predicted values of the S=N bond length in $S(NBu^t)_3$, a series of computations was carried out for the parent, $S(NH)_3$, in an attempt to quantify how further improvements in the calculations might affect the bond length in $S(NBu^t)_3$. These involved larger basis sets and higher theoretical levels than are currently possible for the butyl derivative. From the results in Table 1 it is clear that the optimised S=N bond length in $S(NH)_3$ is very sensitive to the basis set employed. At the MP2 level, a very large basis is required for convergence of the results. For instance, between MP2/cc-pVQZ' and MP2/cc-pV5Z', the S=N bonds vary by as much as 0.7 pm. The series of correlation-consistent basis sets employed has been specifically designed for extrapolation to the basis-set limit. According to our extrapolation scheme (see Section 5.2.2), the MP2/6-31G* distances are larger than the final MP2 estimates by about 3 pm. By applying the higher-level corrections obtained for $S(NH)_3$ to the Bu^t derivative (see Theoretical Methods) one arrives at the final extrapolated theoretical estimates of 152.8 pm for the S=N bond, compared to the MP2/6-31G* estimate of 155.5 pm.

Density Functional Theory calculations were also carried out on the parent $S(NH)_3$ compound using Becke's 3 parameter hybrid functional[20] with a 6-311+G* basis set on S and N and 6-31G* on H. This estimates the S=N bond length to be 153.5 pm, which compares extremely well with the experimentally determined S=N bond length of 153.5(3) pm.

The molecular geometry of $S(NBu^t)_3$ for the MP2/6-31G* calculation is presented in Table 3; Those calculated at the HF/3-21G* and HF/6-31G* levels of theory are presented in Appendix 4 [Table 1].

5.3.2 Gas Electron Diffraction Study

On the basis of the *ab initio* calculations described above, electron-diffraction refinements were carried out using a model of C_3 symmetry to describe the vapour. The large number of geometric parameters needed to define the model made it necessary to make some assumptions, including local C_{3v} symmetry for all methyl groups.

The structure of $S(NBu^t)_3$ was finally defined in terms of twelve independent geometric parameters, comprising four bond lengths, five bond angles and three torsion parameters [Table 3; atom numbering shown in Figure 1].

Table 3 Refined and calculated geometric parameters for $S(NBu^t)_3$ (distances in pm, angles in °) from the GED study.[a]

No.	Parameter	GED (r_a)	MP2/6-31G*	Restraint
p_1	C-H	112.9(3)	109.4	-
p_2	(S=N + C-C + 0.4N-C)/2.4	151.3(1)	153.2	153.2(10)
p_3	S=N – [C-C + C-N)/2]	4.9(5)	4.6	4.6(5)
p_4	C-C – C-N	2.7(4)	4.1	4.1(5)
p_5	C-C-H	107.1(5)	108.8	108.8(10)
p_6	N-C-C average	108.4(3)	108.4	-
p_7	N-C-C difference	10.5(5)	7.4	-
p_8	C-C-C difference	0.5(7)	1.3	1.3(8)
p_9	S=N-C	122.9(4)	123.2	-
p_{10}	N=S=N-C	173.0(5)	180.0	-
p_{11}	Methyl twist	53.4(23)	54.9	54.9(30)
p_{12}	Butyl twist	188.5(7)	180.0	180.0(100)

[a] Figures in parentheses are the estimated standard deviations of the last digits. See text for parameter definitions.

The independent distance parameters are the C-H bond length (p_1) and the weighted average of the C-C, S=N and 0.4 × C-N distances (p_2), with two differences, [(S=N + C-C)/2 – C-N] (p_3) and [S=N – C-C] (p_4). All C-C-H bond angles (p_5) were assumed to be identical, but the calculated large asymmetry in the butyl groups was allowed for by introducing an average N-C-C bond angle (p_6) (which therefore defines the mean C-C-C angle), with difference angles p_7 [N-C-C(4) – N-C-C(5/6)] and p_8 [C(5)-C(3)-C(6) – C(4)-C(3)-C(5/6)]. These three together define the six angles at the central carbon atom with local C_s symmetry as calculated *ab initio*. The S=N-C angle was also included (p_9), as was the N=S=N-C dihedral angle (p_{10}), to allow for possible deviation from the C_{3h} plane.

The remaining two parameters represent the torsions of the methyl and butyl groups. These groups were generated initially by placing a methyl group carbon atom at the origin, with its three H atoms arranged with local C_{3v} symmetry about the *x*-axis and one H in the *xy* plane in the positive *x* and *y* directions. The methyl torsion parameter (p_{11}) is a rotation about the local *x* axis. The methyl group is then translated along the positive *x* axis by the C-C bond length and the central carbon of the *tert*-butyl group is placed at the origin. The correct C-C-C bond angles are generated by rotating the methyl group about the *z* axis, moving the methyl carbon atom in the positive *y* direction, and then generating the other methyl groups by rotation of the first group about the local *x* axis. The *tert*-butyl torsion angle is a rotation of the group about the local *x* axis (p_{12}).

The *tert*-butyl group is then translated along the positive *x* axis by the N-C bond length and the butyl group rotated into position by the S=N-C angle. The other NBu^t groups are then generated by 120° and 240° rotations of the first group about the *z* axis of the central S atom. Finally, the N=S=N-C torsion angle describes the deviation of the NBu^t groups from the C_{3h} axis of the molecule.

The starting parameters for the r_a refinement were taken from the theoretical geometry optimised at the MP2/6-31G* level. The r_α structure was not refined because the rectilinear vibrational corrections (i.e. parallel and perpendicular correction terms) are known to be unreliable for a molecule this size with many low-lying vibrational modes. Theoretical (HF/6-31G*) Cartesian force fields were obtained and converted into force fields described by a set of symmetry coordinates using a version of the ASYM40 program[21] modified to work for molecules with more than 40 atoms. All geometric parameters were then refined.

In total twelve geometric parameters and eighteen groups of vibrational amplitudes were refined. Flexible restraints were employed during the refinement using the SARACEN method.[22] In total, seven geometric and five amplitude restraints were employed. These are listed in Tables 3 and 5.

The success of the final refinement, for which $R_G = 0.039$ ($R_D = 0.030$), can be assessed on the basis of the radial distribution curve (Figure 2) and the molecular scattering intensity curves (Figure 3). Final refined parameters are listed in Table 3, the least-squares correlation matrix is shown in Table 4 with interatomic distances and the corresponding amplitudes of vibration in Table 5. Experimental coordinated from the GED analysis are shown in Appendix 4 [Table 2]. In the SARACEN analysis, because all parameters are refining, the error estimates are realistic. We therefore quote the estimated standard deviations, σ, and do not need to add any further allowance for fixed parameters. Figure 1 shows a perspective view of $S(NBu^t)_3$ in the optimum refinement of the GED data.

Figure 2 Experimental and difference (experimental - theoretical) radial-distribution curve, $P(r)/r$, for $S(NBu^t)_3$. Before Fourier-inversion the data were multiplied by $s.\exp(-0.00002s^2)/(Z_N - f_N)/(Z_C - f_C)$.

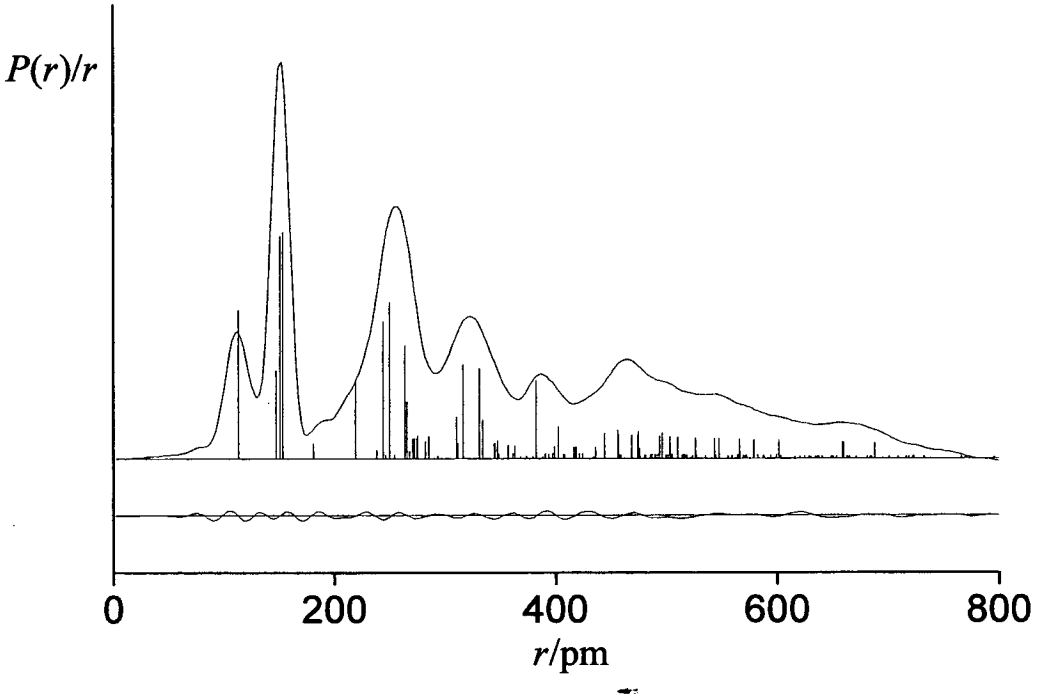

Figure 3 Experimental and final weighted difference (experimental - theoretical) molecular-scattering intensities for $S(NBu^t)_3$.

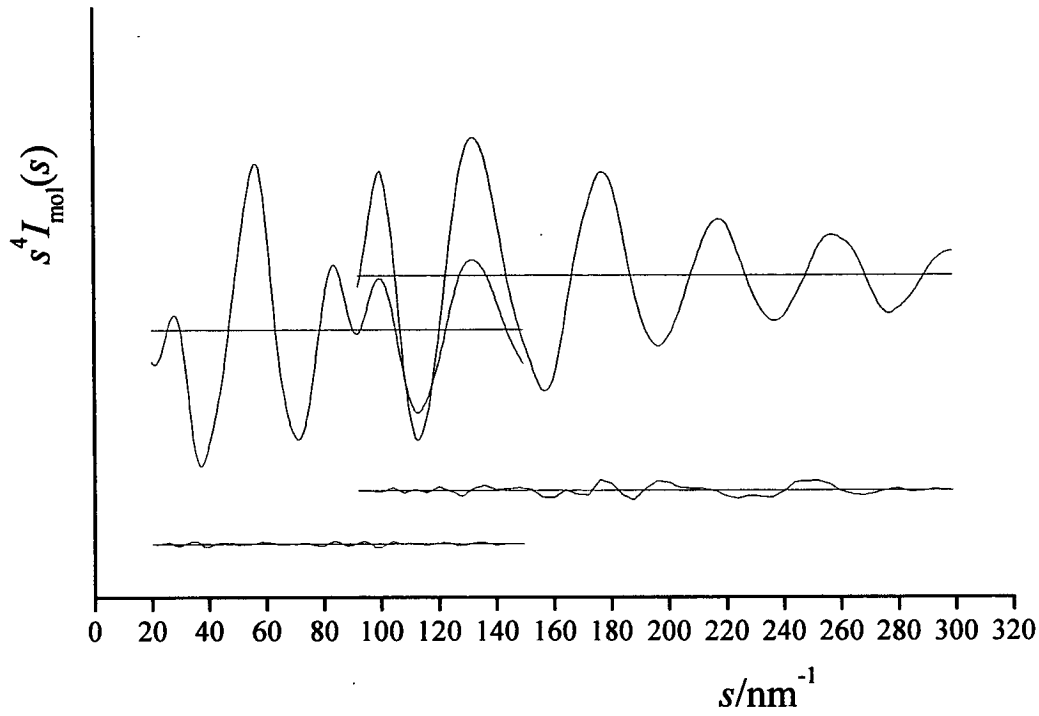

Table 4 Least-squares correlation matrix (× 100) for $S(NBu^t)_3$.[a]

	p_7	p_8	p_{10}	u_6	u_7	u_{12}	u_{25}	k_2
p_4	-50	-70	54					
p_7		63	-54					
p_8			-70					
p_{12}					-79			
u_1								63
u_4				66		62		
u_5				51			56	
u_6						80		

[a] Only elements with absolute values ≥50% are shown; k_2 is a scale factor.

Table 5 Interatomic distances (r/pm) and amplitudes of vibration (u/pm) for the restrained GED structure of $S(NBu^t)_3$.[a]

No.	Atom Pair	r_a/pm	u/pm[b]	Restraint[c]
u_1	C(5)-C(8)	150.8(2)	5.0(2)	-
u_2	S(1)-N(2)	153.5(3)	3.8 (tied to u_1)	-
u_3	N(2)-C(5)	147.2(4)	5.0 (tied to u_1)	-
u_4	N(2)...C(8)	250.0(5)	7.4(4)	-
u_5	C(8)-H(17)	112.9(3)	8.4(3)	-
u_6	S(1)...C(5)	264.2(4)	8.6(8)	-
u_7	S(1)...C(8)	331.0(8)	9.6(5)	-
u_8	S(1)...C(11)	382.3(4)	7.6(6)	-
u_9	S(1)...C(12)	316.6(7)	9.6 (tied to u_7)	-
u_{10}	S(1)...H(19)	311.9(24)	20.0 (fixed)	-
u_{11}	S(1)...H(29)	282.7(27)	20.0 (fixed)	-
u_{12}	N(2)...N(3)	265.8(5)	4.8(5)	-
u_{13}	N(2)...H(17)	275.8(22)	16.3 (fixed)	-
u_{14}	N(2)...H(18)	347.7(7)	9.9 (fixed)	-
u_{15}	N(2)...H(19)	285.8(21)	16.2 (fixed)	-
u_{16}	N(3)...C(5)	310.8(7)	8.9 (tied to u_7)	-
u_{17}	N(3)...C(8)	334.2(15)	14.7 (tied to u_7)	-
u_{18}	N(3)...C(11)	456.4(7)	10.3 (tied to u_{21})	-
u_{19}	N(3)...C(12)	316.7(12)	14.7 (tied to u_7)	-
u_{20}	N(4)...C(5)	402.3(4)	6.5 (fixed)	-
u_{21}	N(4)...C(8)	474.5(8)	13.0(6)	-
u_{22}	N(4)...C(11)	496.0(7)	12.3(8)	9.3(9)
u_{23}	N(4)...C(12)	456.6(9)	13.0 (tied to u_{21})	-
u_{24}	C(5)...C(6)	456.9(7)	12.2 (tied to u_{21})	-
u_{25}	C(5)...H(17)	219.3(6)	12.7(10)	-
u_{26}	C(6)...C(8)	474.3(16)	23.3 (tied to u_{21})	-
u_{27}	C(6)...C(11)	601.7(7)	10.1 (fixed)	-
u_{28}	C(6)...C(12)	444.5(13)	23.3 (tied to u_{21})	-
u_{29}	C(7)...C(8)	547.7(8)	9.6 (tied to u_{32})	-

Table 5 Continued

No.	Atom Pair	r_a/pm	u/pm[b]	Restraint[c]
u_{30}	C(7)...C(11)	510.3(7)	16.4 (fixed)	-
u_{31}	C(7)...C(12)	526.7(12)	13.4 (fixed)	-
u_{32}	C(8)...C(9)	543.6(16)	24.1(22)	33.6(34)
u_{33}	C(8)...C(11)	244.1(7)	11.1(6)	-
u_{34}	C(9)...C(11)	688.2(9)	24.4(17)	19.6(20)
u_{35}	C(9)...C(12)	566.4(13)	12.6 (tied to u_{32})	-
u_{36}	C(10)...C(11)	503.3(22)	40.5 (tied to u_{22})	-
u_{37}	C(10)...C(12)	579.2(18)	15.8 (tied to u_{32})	-
u_{38}	C(11)...C(13)	660.0(8)	20.4 (tied to u_{34})	-
u_{39}	C(11)...C(14)	659.2(12)	24.4 (tied to u_{34})	-
u_{40}	C(11)...H(17)	272.6(24)	16.4 (fixed)	-
u_{41}	C(11)...H(18)	270.8(22)	16.5 (fixed)	-
u_{42}	C(12)...C(13)	468.8(21)	25.7 (fixed)	-
u_{43}	C(12)...C(14)	493.7(21)	44.5 (tied to u_{22})	-
u_{44}	C(12)...H(18)	271.5(25)	16.7 (fixed)	-
u_{45}	C(12)...H(19)	274.5(27)	16.2 (fixed)	-

[a] Estimated standard deviations, obtained in the least-squares refinement, are given in parentheses.

[b] Amplitudes not refined were fixed at the values obtained using the HF/6-31G* force field.

[c] Restraints were also applied to the ratios of u_4/u_{33} [0.661(33)] and u_6/u_{12} [1.817(91)]. Uncertainties are 5% of the amplitude ratios.

5.3.3 Crystal Structure Determination

(Conducted by D. Stalke, Germany; results provided for comparison)

Table 6 gives a comparison of the solid, gas and theoretical structures of $S(NBu^t)_3$. As can be seen, the solid structure agrees reasonably well with that calculated *ab initio*, possessing approximately C_{3h} molecular symmetry. The gaseous structure possesses C_3 symmetry. The dihedral angle ϕ(NSNC) was found to be 179.4°, whilst the SNC angle was found to be 126.0°. This compares with 173.0° for ϕ(NSNC) and

122.9° for the SNC angle in the gas-phase structure. There are also differences in the observed S=N and mean C-C bond distances. In the solid structure these were observed to be 151.3 and 153.1 pm whilst in the gas structure they were observed to be 153.5 and 150.8 pm. The final structure from the X-ray crystallographic study, showing the atom numbering used, is shown in Figure 4.

Figure 4 Final X-ray crystallographic structure of $S(NBu^t)_3$ showing ~C_{3h} mirror plane.

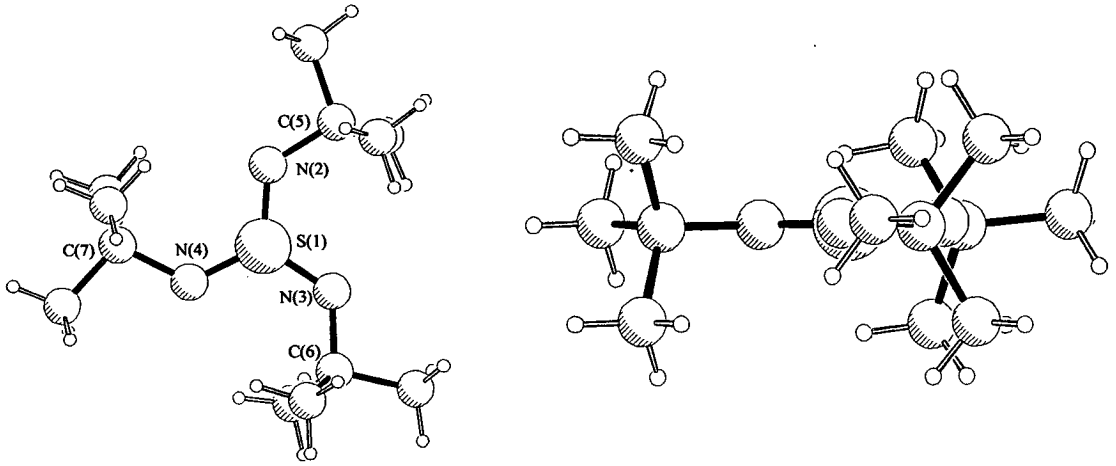

Table 6 Comparison of geometrical parameters for $S(NBu^t)_3$ from the experimental and theoretical structures.[a]

Geometrical parameter	X-ray	GED	*Ab initio* (MP2/6-31G*)
S(1)=N(2)	151.3	153.5(3)	152.8[b]
N(2)-C(5)	148.7	147.3(5)	148.7
C-C (mean)	153.1	150.8(2)	152.8
C-H (mean)	98.0	112.9(3)	109.3
S(1)-N(2)-C(5)	126.0	122.9(4)	123.2
C-C-C (mean)	110.0	109.9(3)	110.4
H-C-H (mean)	109.5	107.1(5)	108.8
N(2)=S(1)=N(3)-C(5)	179.4	173.0(5)	180.0

[a] See Figure 1 for atom numbering.

[b] Extrapolated value (see Theoretical Methods).

5.4 Discussion

The structural properties of $S(NBu^t)_3$ have been investigated in the gas phase by GED, in the solid state by low temperature X-ray crystallography, and by *ab initio* calculations.

The solid structure was found to possess ~C_{3h} symmetry. The S=N distance [151.3 pm] is in good agreement with that found for $S(NSiMe_3)_2$[23] from an X-ray crystallographic study [151.9(1) pm] and in the normal range found for SN double bonds in a range of solid-state structures including $S\{NP(S)Bu^t_2\}_2$[24] and $Me_3SiNSNSC_6H_4$-4-NO_2.[25]

In the gas phase, all three $=S(NBu^t)_2$ fragments are *E/Z* with a third NBu^t group attached. This is very similar to that adopted by the $S(NBu^t)_2$ molecule.[26] This is the only possible conformation for the triimide that avoids the steric crowding associated with the *Z/Z* conformation. GED studies were undertaken assuming the presence of this one conformation. On the basis of this assumption an excellent fit to the experimental data was obtained [R_G = 0.039].

Furthermore, impressive agreement between the theoretical and experimental structures was achieved. For example, the S=N bond length refined to 153.5(3) pm, compared to the extrapolated theoretical estimates of 152.9 pm (MP2) and 153.5 pm (DFT). Similarly, the C-N bond distance refined to 147.2(4) pm, compared to 148.7 pm at the MP2/6-31G* level. Bond angles also agreed well with the S=N-C angle refined to 122.9(4)° compared to 123.2°(MP2/6-31G*). As the molecule has C_3 symmetry, there is just one S=N-C angle, slightly wider than the average of the *Z* and *E* angles observed in $S(NBu^t)_2$.[26]

$S(NBu^t)_3$ was calculated to have C_{3h} symmetry. However, the observed GED structure has C_3 symmetry, with the butyl groups twisted out of the plane by ~7° [ϕ(NSNC): MP2/6-31G* 180.0°, experimental 173.0(5)°]. An r_a refinement was carried out rather than r_α, because the calculation of perpendicular amplitudes is

known to be unreliable for molecules of this size with many low-frequency torsional vibrations. Therefore there are shrinkage effects leading to the apparent non-planarity of the refined structure of the molecule.

The main difference between the solid and gaseous structures occurs in the NSNC torsion angle. Other parameters generally agree well, although there are differences between the structures, for example, the mean C-C distance refined to 150.8(2) pm in the GED study, whereas it was observed to be 153.1 pm in the crystal. Another significant difference is in the S=N-C bond angles, 122.9(4)° in the gas structure, 126.0° in the solid structure. This could be an effect of the packing constraints imposed on the solid structure. The bulky butyl groups are not able to deviate from the C_{3h} plane, so instead the S=N-C angles increase to accommodate the butyl groups. The internal CCC angles are consistent with each other and with calculated values, and deviate very little from 109.5°. This indicates that there is very little distortion actually within the butyl groups themselves, and the widening of the S=N-C angles provides all release of steric strain.

The refined structure of $S(NBu^t)_3$ appears to be slightly different to that calculated for $S(NMe)_3$ at the B3PW91/cc-pVDZ level.[20,27-31] The calculated S=N and N-C bond lengths were 155.2 and 146.0 pm compared to 153.5(3) and 147.3(5) pm for the experimental structure of $S(NBu^t)_3$. The difference in the S=N bond lengths cannot be analysed quantitatively because of the uncertainties in the calculated S=N bond lengths. However, the lengthening of the N-C bond length in $S(NBu^t)_3$ can be attributed to the inductive effect of the butyl groups. Another observation is the marked widening of the S=N-C angle to 122.9(4)° in $S(NBu^t)_3$. This widening may be attributed to the bulk of the butyl groups.

5.5 References

1. R. Mews, P. G. Watson and E. Lork, *Coordination Chemistry Reviews*, 1997, **158**, 233.
2. O. Glemser and J. Wegener, *Agnew. Chem. Int. Ed. Engl.*, 1970, **9**, 309.
3. W. Lidy, W. Sundermeyer and W. Verbeek, *Z. Anorg. Allg. Chem.*, 1974, **406**, 208.
4. F.-M. Tesky and R. Mews, *Chem. Ber.*, 1980, **113**, 2183.
5. F.-M. Tesky and R. Mews, *J. Fluorine Chem.*, 1988, **38**, 399.
6. O. Glemser, S. Pohl, F.-M. Tesky and R. Mews, *Agnew. Chem. Int. Ed. Engl.*, 1977, **16**, 789.
7. S. Pohl, B. Krebs, U. Seyer and G. Henkel, *Chem. Ber.*, 1979, **112**, 1751.
8. Gaussian 98, Revision A.7, M. J. Frisch, G. W. Trucks, H. B. Schlegel, G. E. Scuseria, M. A. Robb, J. R. Cheeseman, V. G. Zakrzewski, J. A. Montgomery, R. E. Stratmann Jr, J. C. Burant, S. Dapprich, J. M. Millam, A. D. Daniels, K. N. Kudin, M. C. Strain, O. Farkas, J. Tomasi, V. Barone, M. Cossi, R. Cammi, B. Mennucci, C. Pomelli, C. Adamo, S. Clifford, J. Ochterski, G. A. Petersson, P. Y. Ayala, Q. Cui, K. Morokuma, D. K. Malick, A. D. Rabuck, K. Raghavachari, J. B. Foresman, J. Cioslowski, J. V. Ortiz, A. G. Baboul, B. B. Stefanov, G. Liu, A. Liashenko, P. Piskorz, I. Komaromi, R. Gomperts, R. L. Martin, D. J. Fox, T. Keith, M. A. Al-Laham, C. Y. Peng, A. Nanayakkara, C. Gonzalez, M. Challacombe, P. M. W. Gill, B. Johnson, W. Chen, M. W. Wong, J. L. Andres, C. Gonzalez, M. Head-Gordon, E. S. Replogle and J. A. Pople, Gaussian, Inc., Pittsburgh PA, 1998.
9. J. S. Binkley, J. A. Pople and W. J. Hehre, *J. Am. Chem Soc.*, 1980, **102**, 939.
10. M. S. Gordon, J. S. Binkley, J. A. Pople, W. J. Pietro and W. J. Hehre, *J. Am. Chem. Soc.*, 1982, **104**, 2797.
11. W. J. Pietro, M. M. Francl, W. J. Hehre, D. J. DeFrees, J. A. Pople and J. S. Binkley, *J. Am. Chem. Soc.*, 1982, **104**, 5039.
12. W. J. Hehre, R. Ditchfield and J. A. Pople, *J. Chem. Phys.*, 1972, **56**, 2257.
13. P. C. Hariharan and J. A. Pople, *Theor. Chim. Acta*, 1973, **28**, 213.
14. M. S. Gordon, *Chem. Phys. Lett.*, 1980, **76**, 163.

15. (a) T. H. Dunning, *J. Chem. Phys.*, **1989**, *90*, 1007; (b) D. E. Woon and T. H. Dunning, *J. Chem. Phys.*, **1993**, *98*, 1358.

16. C. M. Huntley, G. S. Laurenson, D. W. H. Rankin, *J. Chem. Soc., Dalton Trans.*, **1980**, 954.

17. S. Cradock, J. Koprowski, D. W. H. Rankin, *J. Mol. Struct.*, **1981**, *77*, 133.

18. A. S. F. Boyd, G. S. Laurenson, D. W. H. Rankin, *J. Mol. Struct.*, **1981**, *71*, 217.

19. A. W. Ross, M. Fink, R. Hilderbrandt, *International Tables for Crystallography*, Ed. A. J. C. Wilson, Kluwer Academic Publishers, Dordrecht, Boston and London, 1992; Vol. C, p 245.

20. A. D. Becke, "Density-functional thermochemistry. III. The role of exact exchange." *J. Chem. Phys.* 1993, **98**, 5648.

21. L. Hedberg, I. M. Mills, *ASYM 40, Program for Force Constants and Coordinate Analysis,* Version 3.0; see also L. Hedberg, I. M. Mills, *J. Mol. Spectrosc.* **1993**, *160*, 117.

22. N. W. Mitzel, B. A. Smart, A. J. Blake, H. E. Robertson, D. W. H. Rankin, *J. Phys. Chem.* **1996**, *100*, 9339; A. J. Blake, P. T. Brain, H. McNab, J. Miller, C. A. Morrison, S. Parsons, D. W. H. Rankin, H. E. Robertson, B. A. Smart, *J. Phys. Chem.* **1996**, *100*, 12280.

23. M. Herberhold, S. Gerstmann, S. Wrackmann, H. Boomann, *J. Chem. Soc., Dalton Trans.* **1994**, 633.

24. M. Herberhold, W. Ehrenreich, A. Gieren, H. Betz, T. Hübner, *Chem. Ber.* **1985**, *118*, 1476.

25. R. Jones, D. J. Williams, P. T. Wood, J. D. Woollins, *Polyhedron* **1989**, *8*, 91.

26. S. Freitag, D. Stalke, M. Bühl, W. Thiel, P. Trickey, P. T. Brain, H. E. Robertson, B. A. Smart, S. J. Obrey, D. W. H. Rankin, A. R. Barron, *Manuscript in Preperation.*

27. K. Burke, J. P. Perdew and Y. Wang, in *Electronic Density Functional Theory: Recent Progress and New Directions*, Ed. J. F. Dobson, G. Vignale and M. P. Das (Plenum, 1998).

28. J. P Perdew, in *Electronic Structure of Solids'91*, Ed. P. Ziesche and H. Eschrig (Akademie Verlag, Berlin, 1991) 11.

29. J. P. Perdew, J. A. Chevary, S. H. Vosko, K. A. Jackson, M. R, Pederson, D. J. Singh and C. Fiolhais, *Phys. Rev. B*, 1992, **46**.

30. J. P. Perdew, J. A. Chevary, S. H. Vosko, K. A. Jackson, M. R. Pederson, D. J. Singh and C. Fiolhais, *Phys. Rev*, 1993, **48**.

31. J. P. Perdew, K. Burke and Y. Wang, *Phys. Rev. B*, 1996, **54**, 16533.

Chapter 6

Bis(trichlorosilyl)*tert*-butylphosphine, $P(SiCl_3)_2Bu^t$: Molecular Structure by Gas-Phase Electron Diffraction and *Ab Initio* Calculations.

6.1 Introduction

In the previous chapter, the structure of the tri-coordinated $S(NBu^t)_3$, with a planar configuration at the sulfur atom, has been explored. In contrast, Group 15 phosphines can demonstrate acute pyramidal coordination at phosphorus. For example, angles of 96.5(5)° and 95.4° are observed in $P(SiH_3)_3$[1] and $P(GeH_3)_3$[2] respectively. By widening the angles at the phosphorus atom it should be possible to accommodate more bulky ligands such as $SiMe_3$ and *tert*-butyl groups. This is demonstrated in the studies of $P(SiMe_3)_3$,[3] and $PClBu^t_2$,[4] with the Si-P-Si and C-P-C angles found to be 105.1(2)° and 108.9(13)° respectively. A study of PBu^t_3[5] returned C-P-C angles of 109.9(1)° and the authors noted that "the steric interactions between two *tert*-butyl groups were very similar to the steric interactions between a *tert*-butyl group and the lone electron pair".[5] In PBu^t_3O and PBu^t_3NH, the C-P-C angles were observed to be 112.9(5)° and 109.4(7)°,[6] indicating that replacement of the lone pair on the phosphorus by a bonded group allows even more flexibility around the phosphorus.

The structure of $PBu^t_2(SiCl_3)$ has recently been elucidated.[7] The C-P-C angle in this case was found to be 110.6(13)°. However, the C-P-Si angles were found to be much smaller [103.4(8)° and 102.8(6)°]. This can be attributed to the steric effects of the bulky *tert*-butyl groups repelling each other towards the $SiCl_3$ group, and also the electron-withdrawing effect of the $SiCl_3$ group itself. Examination of the observed tilt parameters in this molecule reveal that all the groups are tilted in an axial sense ~6° towards the lone pair on the phosphorus. There are also small components of the tilts of these groups in the equatorial belt of the molecule. Rather surprisingly, the *tert*-butyl groups are actually tilted towards each other by ~2°, an indication that any residual interactions between the two groups after widening of the C-P-C angle are less than those between the *tert*-butyl groups and the $SiCl_3$ group.[7]

Although these groups of molecules have fewer atoms than some in the case studies in this thesis, they are still interesting from the point of view of steric interactions between the groups themselves and with the lone pair of electrons present on the

phosphorus atom. Having studied $PBu^t_2SiCl_3$ and determined the behaviour of the groups, it was decided to study the analogous $PBu^t(SiCl_3)_2$ molecule. The presence of two electron withdrawing groups and the lone pair is likely to give rise to some interesting behaviour of the ligands, both in the bond lengths and angles, and in the twists and tilts of the groups in relation to each other and the lone pair.

6.2 Experimental

6.2.1 Synthesis

A sample of $P(SiCl_3)_2Bu^t$ was provided by *Professor Wolf-W. du Mont, Braunschweig, Germany*, for use in the electron diffraction experiment without further purification.

6.2.2 Theoretical Methods

All calculations were performed on a Dec Alpha 1000 4/200 workstation using the Gaussian 98 program.[8] An extensive search of the torsional potential of $P(SiCl_3)_2Bu^t$ was undertaken at the HF/3-21G*[9-11] level in order to locate all minima. One conformer of C_1 symmetry was located and further geometry optimizations were undertaken at the HF and MP2 levels using the standard 6-31G*[12-14] basis set. Vibrational frequencies, calculated from analytic second derivatives at the HF/3-21G* and HF/6-31G* levels to determine the nature of stationary points, provided estimates of amplitudes of vibration (u) for use in the gas electron diffraction (GED) refinements and comparison with experimentally determined frequencies. The structure of $P(SiCl_3)_2Bu^t$ with the atom numbering scheme is shown in Figure 1.

6.2.3 Gas-Phase Electron Diffraction

Data were collected using the Edinburgh gas diffraction apparatus.[15] An accelerating voltage of *ca.* 40 kV (electron wavelength *ca.* 6.0 pm) was used, whilst maintaining the sample and nozzle temperatures at 408 and 435 K. Scattering intensities were recorded at nozzle-to-plate distances of 90 and 257 mm on Kodak Electron Image plates. Four plates were collected at the short distance and five at the long distance. The weighting points for the off-diagonal weight matrices, correlation parameters

and scale factors for the two camera distances are given in Table 1, together with electron wavelengths which were determined from the scattering patterns of benzene vapour, recorded immediately after the patterns of $P(SiCl_3)_2Bu^t$ and analysed in exactly the same way, to minimise systematic errors in wavelengths and camera distances. The electron-scattering patterns were converted into digital form using a PDS densitometer at the Institute of Astronomy in Cambridge with a scanning program described elsewhere.[16] Data reduction and least-squares refinements were carried out using standard programs,[17,18] employing the scattering factors of Ross *et al.*[19]

Figure 1 Molecular structure of $P(SiCl_3)_2Bu^t$ in the gas phase with perspective down P-C bond.

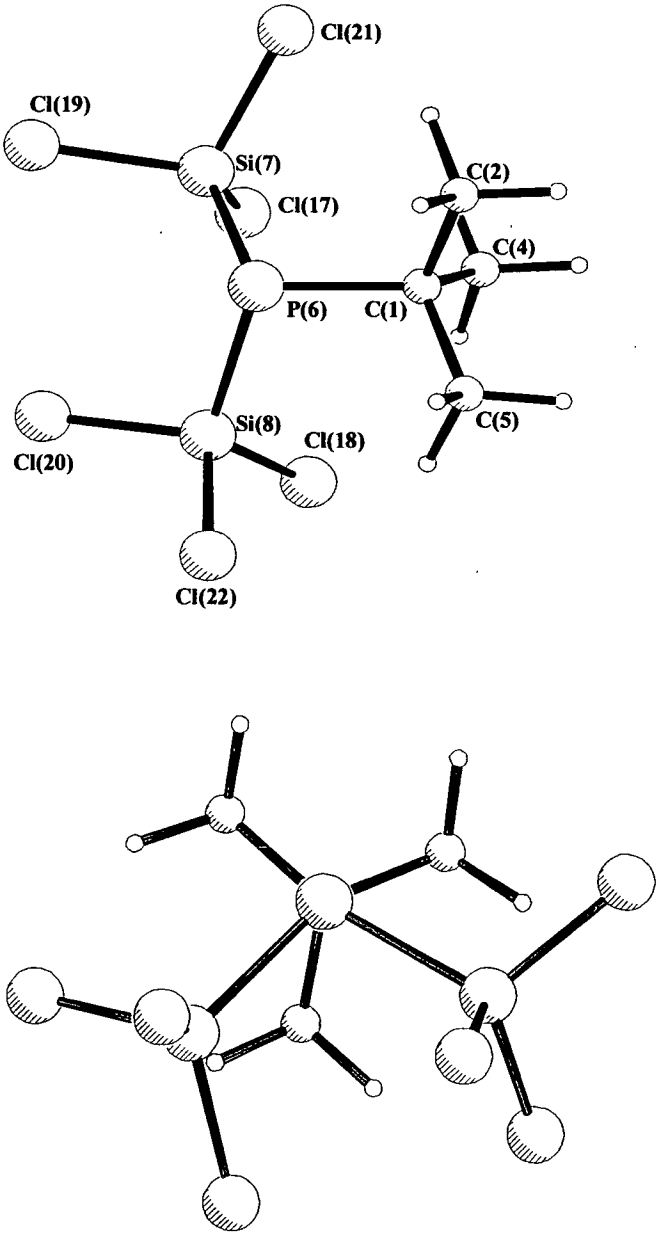

Table 1 Nozzle-to-plate distances (mm), weighting functions (nm^{-1}), correlation parameters, scale factors and electron wavelengths (pm) used in the electron-diffraction study.

Compound	$P(SiCl_3)_2Bu^t$	
Nozzle-to-plate distance[a]	89.56	256.76
Δs	4	2
s_{min}	84	26
sw_1	104	46
sw_2	260	130
s_{max}	340	152
Correlation parameter	0.2702	0.4781
Scale factor[b]	0.523(14)	0.808(8)
Electron wavelength	6.016	6.016

[a] Determined by reference to the scattering pattern of benzene vapour.

[b] Values in parentheses are the estimated standard deviations.

6.3 Results

6.3.1 *Ab initio* Calculations

A series of molecular orbital calculations was undertaken to investigate the structure of $P(SiCl_3)_2Bu^t$. Preliminary investigations of the structure assuming C_s symmetry returned two imaginary frequencies ($256i$ cm^{-1} and $30i$ cm^{-1}) at the HF/6-31G* level, indicating that the C_s structure is a transition state on the potential energy surface. Further investigation of the structure in C_1 symmetry revealed two equivalent minima. Thus the C_s structure can be thought of as a transition state connecting the two equivalent C_1 minima. The C_1 structure can be thought of as being derived from the fully staggered C_s structure with the *tert*-butyl and $SiCl_3$ groups twisted in the same sense by 15 - 20° reducing the molecular energy by 26.7 kJ mol^{-1} at the HF/6-31G* level.

Further calculations at the MP2/6-31G* level were performed in C_1 symmetry. The molecular geometry of $P(SiCl_3)_2Bu^t$ for the MP2/6-31G* calculation is presented in

Table 2; Those calculated at the HF/6-31G* level of theory for the C_1 and C_s structures are presented in Appendix 5 [Table 1]. As the molecule does not contain any significant double-bond character but has electronegative atoms, including the effects of electron correlation with the higher level of theory is important. Generally the bond lengths and angles did not change more than 1 pm or 1° upon going from HF/6-31G* to the MP2/6-31G* level of theory. For example, the P-C bond length is predicted to be 191.9 and 190.8 pm at the HF and MP2 levels, respectively. However, the P-Si(7/8) distances were observed to shorten from 226.0 and 225.8 pm at the HF level to 224.2 and 223.9 pm at the MP2 level. The C-P-Si(7/8) angles were also observed to change appreciably, from 109.5 and 108.7° at the HF level to 107.9 and 106.9° at the MP2 level. The Si-P-Si angle was also observed to change significantly from 104.2° (HF) to 101.5° (MP2). However, very little change was observed to the P-Si-Cl angles, for example, the predicted P-Si(7)-Cl(17) angle hardly changed from the HF (116.4°) to the MP2 (116.5°) level.

6.3.2 Gas Electron Diffraction Study

On the basis of the *ab initio* calculations described above, electron-diffraction refinements were carried out using a model of C_1 symmetry to describe the vapour. The large number of geometric parameters needed to define the model made it necessary to make the assumption of local C_{3v} symmetry for the methyl groups.

The structure of $P(SiCl_3)_2Bu^t$ was finally defined in terms of twenty eight independent geometric parameters, comprising five bond lengths, twelve bond angles and eleven torsion parameters [Table 2; atom numbering shown in Figure 1].

Table 2 Refined and calculated geometric parameters for $P(SiCl_3)_2Bu^t$ (distances in pm, angles in °) from the GED study.[a]

No.	Parameter	GED (r_a)	MP2/6-31G*	Restraint
p_1	C-H	112.9(15)	109.5	109.0(30)
p_2	P-C	190.6(6)	190.8	190.1(10)
p_3	C-C (mean)	156.5(6)	153.2	154.0(10)
p_4	P-Si (mean)	221.0(5)	224.0	-
p_5	Si-Cl (mean)	203.2(1)	204.4	-
p_6	C-C-H	111.8(5)	112.0	111.9(5)
p_7	P-C-C mean	109.7(6)	109.3	-
p_8	[P-C-C(2)] – [P-C-C(4)]	-9.2(9)	-9.5	-9.5(10)
p_9	[P-C-C(2)] – [P-C-C(5)]	-2.1(10)	-1.7	-1.8(10)
p_{10}	P-Si-Cl mean	111.1(2)	111.2	111.2(5)
p_{11}	[P-Si-Cl av (gp1)] – [P-Si-Cl av (gp2)]	-0.04(2)	-0.04	-0.04(2)
p_{12}	[P-Si(7)-Cl(17)] – [P-Si(7)-Cl(19)]	8.8(10)	8.6	8.6(10)
p_{13}	[P-Si(7)-Cl(17)] – [P-Si(7)-Cl(21)]	6.9(9)	7.5	7.5(10)
p_{14}	[P-Si(8)-Cl(18)] – [P-Si(8)-Cl(20)]	8.1(9)	8.7	8.7(10)
p_{15}	[P-Si(8)-Cl(18)] – [P-Si(8)-Cl(22)]	10.6(9)	9.8	9.8(10)
p_{16}	C-P-Si mean	104.7(7)	107.4	-
p_{17}	[C-P-Si(7)] – [C-P-Si(8)] / 2	0.5(2)	0.5	0.5(2)
p_{18}	$SiCl_3$ dip av {ϕ[C(2)-C(1)-P(6)-Si(7)] + ϕ[C(2)-C(1)-P(6)-Si(8)]} / 2	127.6(4)	125.8	-
p_{19}	$SiCl_3$ dip diff ϕ[C(2)-C(1)-P(6)-Si(7)] – ϕ[C(2)-C(1)-P(6)-Si(8)]	40.6(17)	38.6	38.6(20)
p_{20}	Methyl Torsion Angle	-63.6(20)	-64.2	-64.2(20)
p_{21}	{ϕ[C(2)-C(1)-P(6)-C(4)] + ϕ[C(2)-C(1)-P(6)-C(5)]} / 2	118.4(10)	118.4	118.4(10)
p_{22}	ϕ[C(2)-C(1)-P(6)-C(4)] – ϕ[C(2)-C(1)-P(6)-C(5)]	2.9(10)	2.8	2.8(10)
p_{23}	{ϕ[Cl(17)-Si(7)-P(6)-Cl(19)] + ϕ[Cl(17)-Si(7)-P(6)-Cl(21)]} / 2	122.3(10)	122.0	122.0(10)

Table 2 Continued

No.	Parameter	GED (r_a)	MP2/6-31G*	Restraint
p_{24}	ϕ[Cl(17)-Si(7)-P(6)-Cl(19)] – ϕ[Cl(17)-Si(7)-P(6)-Cl(21)]	0.04(5)	0.1	0.1(5)
p_{25}	{ϕ[Cl(18)-Si(8)-P(6)-Cl(20)] + ϕ[Cl(18)-Si(8)-P(6)-Cl(22)]} / 2	121.4(10)	121.7	121.7(10)
p_{26}	ϕ[Cl(18)-Si(8)-P(6)-Cl(20)] – ϕ[Cl(18)-Si(8)-P(6)-Cl(22)]	1.0(1)	1.0	1.0(1)
p_{27}	$SiCl_3$ ϕ av {ϕ[Cl(17)-Si(7)-P(6)-C(1)] + ϕ[Cl(18)-Si(8)-P(6)-C(1)]} / 2	52.9(12)	55.4	-
p_{28}	$SiCl_3$ ϕ diff ϕ[Cl(17)-Si(7)-P(6)-C(1)] – ϕ[Cl(18)-Si(8)-P(6)-C(1)] / 2	15.4(10)	17.5	-

[a] Figures in parentheses are the estimated standard deviations of the last digits. See text for parameter definitions.

On the basis of the highest level *ab initio* calculations, all similar types of bond lengths were assumed to be equal, with any small differences fixed at zero. The independent distance parameters are the C-H and P-C bond lengths (p_1 and p_2) and the average C-C, P-Si and Si-Cl distances (p_3 - p_5). All C-C-H bond angles (p_6) were assumed to be identical. The P-C-C angles were defined in terms of the average (p_7) of P(6)-C(1)-C(2), P(6)-C(1)-C(4) and P(6)-C(1)-C(5), and two difference parameters, which were included in the refinement procedure since the butyl group was predicted to have C_1 local symmetry. The differences were described as P(6)-C(1)-C(2) minus P(6)-C(1)-C(4) (p_8) and P(6)-C(1)-C(2) minus P(6)-C(1)-C(5) (p_9).

The trichlorosilyl groups were calculated to have C_1 local symmetry, and the P-Si-Cl angles were defined in terms of an average (p_{10}) of all the P-Si-Cl angles, and five difference parameters. The first of these differences is the average P-Si-Cl bond angle for the first $SiCl_3$ group minus the average P-Si-Cl bond angle for the second group (p_{11}). The remaining four are internal differences within the individual $SiCl_3$ groups i.e. P(6)-Si(7)-Cl(17) minus P(6)-Si(7)-Cl(19) (p_{12}), P(6)-Si(7)-Cl(17) minus P(6)-Si(7)-

Cl(21) (p_{13}), P(6)-Si(8)-Cl(18) minus P(6)-Si(8)-Cl(20) (p_{14}) and P(6)-Si(8)-Cl(18) minus P(6)-Si(8)-Cl(22) (p_{15}).

There are three angles to be defined at the central phosphorus atom. An average (p_{16}) and a difference (p_{17}) C-P-Si angle were introduced, as were two dip angles (p_{18} and p_{19}) relating the central Si atoms of each $SiCl_3$ group to C(2) of the *tert*-butyl group. These two parameters define the Si-P-Si angle and the torsion angle of the butyl group i.e. around the C-P bond axis.

The remaining eleven parameters represent the torsion angles of the methyl, butyl and trichlorosilyl groups. The methyl groups were generated initially by placing a methyl group carbon atom at the origin, with its three H atoms arranged with local C_{3v} symmetry about the x-axis and one H in the xy plane in the positive x and y directions. The methyl torsion parameter (p_{20}) is a rotation about the local x axis. The methyl group is then translated along the positive x axis by the C-C bond length and the central carbon of the *tert*-butyl group is placed at the origin. The correct C-C-C bond angles are generated by rotating the methyl group about the z axis, moving the methyl carbon atom in the positive y direction, and then generating the other methyl groups by rotation of the first group about the local x axis by two different torsion angles (p_{21} and $-p_{22}$). The *tert*-butyl group is then translated along the positive x axis by the P-C bond length.

The $SiCl_3$ groups are generated in a similar way to the methyl groups in the negative x axis direction. The first chlorine is placed in the xy plane, in the negative x and positive y directions. The remaining two chlorine atoms of each group are placed adjacent to the initial chlorine, each with its correct P-Si-Cl angle, and then rotated about the z axis by the correct torsion angles ($p_{23} - p_{26}$) to generate the two $SiCl_3$ groups. The $SiCl_3$ torsion angle parameters (p_{27} and p_{28}) are rotations of the groups about the local x axis.

The starting parameters for the r_a refinement were taken from the theoretical geometry optimised at the MP2/6-31G* level. The r_α structure was not refined because the rectilinear vibrational corrections (i.e. parallel and perpendicular correction terms) are known to be unreliable for a molecule this size with many low-lying vibrational modes.

Theoretical (SCF/6-31G*) Cartesian force fields were obtained and converted into force fields described by a set of symmetry coordinates using a version of the ASYM40 program[20] modified to work for molecules with more than 40 atoms. All geometric parameters were then refined.

In total twenty-eight geometric parameters and fourteen groups of vibrational amplitudes were refined. Flexible restraints were employed during the refinement using the SARACEN method.[21] In total, twenty-one geometric and five amplitude restraints were employed. These are listed in Tables 2 and 4.

The success of the final refinement, for which $R_G = 0.080$ ($R_D = 0.048$), can be assessed on the basis of the radial distribution curve (Figure 2) and the molecular scattering intensity curves (Figure 3). Final refined parameters are listed in Table 2, the least-squares correlation matrix is shown in Table 3 with interatomic distances and the corresponding amplitudes of vibration in Table 4. Experimental coordinates from the GED analysis are shown in Appendix 5 [Table 2]. In the SARACEN analysis, because all parameters are refining, the error estimates are realistic. We therefore quote the estimated standard deviations, σ, and do not need to add any further allowance for fixed parameters. Figure 1 shows a perspective view of $P(SiCl_3)_2Bu^t$ in the optimum refinement of the GED data as well as the view down the P-C bond.

Table 3 Least-squares correlation matrix (× 100) for $P(SiCl_3)_2Bu^t$.[a]

	p_3	p_4	p_{10}	p_{12}	p_{28}	u_1	u_9
p_7	-51						
p_{10}					72		
p_{20}		64	-56		-58		
u_{12}				-71			
u_{17}							-57
k_2						72	

[a] Only elements with absolute values ≥50% are shown; k_2 is a scale factor.

Figure 2 Experimental and difference (experimental - theoretical) radial-distribution curve, $P(r)/r$, for $P(SiCl_3)_2Bu^t$. Before Fourier inversion the data were multiplied by $s.\exp(-0.00002s^2)/(Z_{Cl}-f_{Cl})/(Z_C-f_C)$.

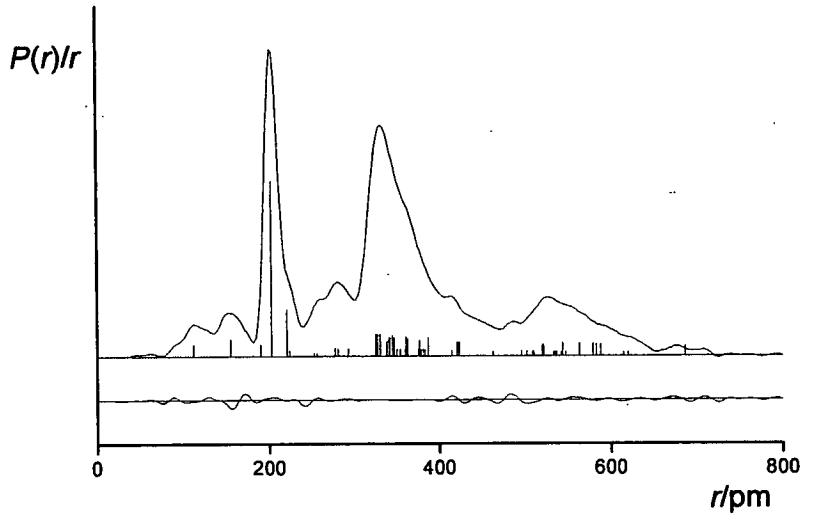

Figure 3 Experimental and final weighted difference (experimental - theoretical) molecular-scattering intensities for $P(SiCl_3)_2Bu^t$.

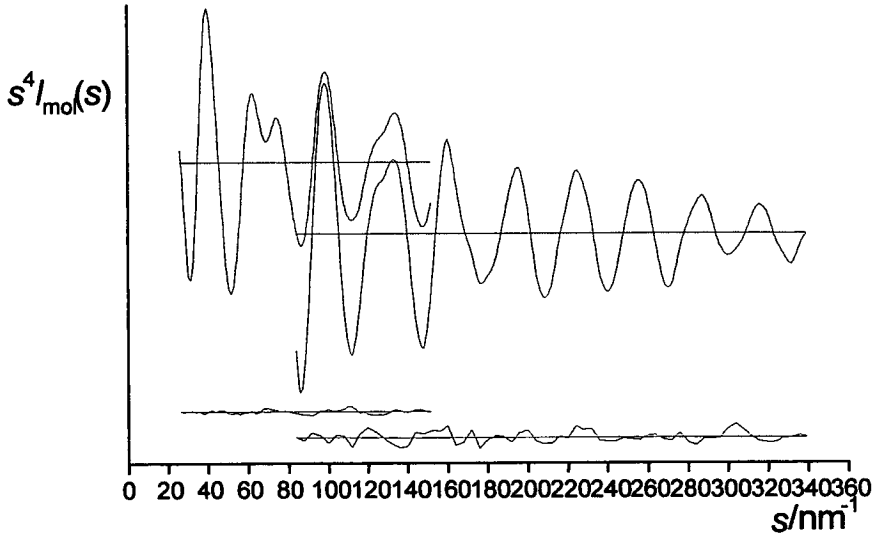

Table 4 Interatomic distances (r/pm) and amplitudes of vibration (u/pm) for the restrained GED structure of $P(SiCl_3)_2Bu^t$.[a]

No.	Atom Pair	r_a/pm	u/pm[b]	Restraint
u_1	Cl(17)-Si(7)	203.2(1)	3.8(2)	-
u_2	Si(7)-P(6)	221.0(5)	6.2(5)	-
u_3	Cl(20)...Cl(18)	327.3(20)	9.5(4)	-
u_4	Cl(21)...Cl(19)	325.8(36)	9.3(tied to u_3)	-
u_5	Cl(21)...Cl(17)	328.1(21)	9.5(tied to u_3)	-
u_6	Cl(22)...Cl(18)	327.2(19)	9.5(tied to u_3)	-
u_7	Cl(22)...Cl(20)	330.0(36)	9.4(tied to u_3)	-
u_8	Cl(19)...Cl(17)	330.5(21)	9.5(tied to u_3)	-
u_9	Cl(20)...Cl(19)	344.4(14)	5.2(15)	-
u_{10}	Cl(18)...Cl(17)	360.3(24)	7.2(tied to u_9)	-
u_{11}	Cl(20)...Cl(17)	387.1(75)	41.0(fixed)	-
u_{12}	Cl(20)...P(6)	340.7(15)	21.4(38)	-
u_{13}	Cl(19)...P(6)	342.4(18)	21.2(tied to u_{12})	-
u_{14}	Cl(22)...P(6)	346.1(14)	20.6(tied to u_{12})	-
u_{15}	Cl(21)...P(6)	346.4(15)	20.9(tied to u_{12})	-
u_{16}	C(2)-C(1)	156.5(6)	5.9(5)	5.1(5)
u_{17}	Cl(17)...P(6)	360.5(11)	13.2(22)	-
u_{18}	Cl(18)...P(6)	362.6(12)	13.1(tied to u_{17})	-
u_{19}	Cl(20)...Si(7)	362.3(34)	20.5(19)	19.9(19)
u_{20}	Cl(17)...Si(8)	376.4(28)	23.8(tied to u_{19})	-
u_{21}	Si(8)...Si(7)	338.5(13)	10.6(10)	10.5(10)
u_{22}	Cl(19)...Si(8)	420.4(16)	16.0(15)	-
u_{23}	Cl(18)...Si(7)	422.7(16)	18.7(tied to u_{22})	-
u_{24}	Cl(19)...Cl(18)	544.1(33)	25.7(26)	27.7(27)
u_{25}	Cl(21)...Cl(20)	563.9(32)	17.5(tied to u_{24})	-
u_{26}	H(3)-C(2)	112.9(14)	7.6(7)	7.4(7)
u_{27}	Cl(22)...Cl(19)	582.7(32)	23.2(17)	-
u_{28}	Cl(22)...Cl(17)	578.8(26)	22.5(tied to u_{27})	-
u_{29}	Cl(21)...Cl(18)	588.0(32)	24.2(tied to u_{27})	-

Table 4 Continued

No.	Atom Pair	r_a/pm	u/pm[b]	Restraint
u_{30}	P(6)-C(1)	190.6(9)	9.3(tied to u_1)	-
u_{31}	Cl(21)...Si(8)	519.8(13)	13.2(14)	-
u_{32}	Cl(22)...Si(7)	521.5(14)	13.5(tied to u_{31})	-
u_{33}	Cl(22)...Cl(21)	686.7(14)	13.6(fixed)	-
u_{34}	P(6)...C(2)	277.8(13)	5.3(17)	-
u_{35}	P(6)...C(5)	281.4(13)	5.4(tied to u_{34})	-
u_{36}	P(6)...C(4)	293.4(16)	5.1(tied to u_{34})	-

[a] Estimated standard deviations, obtained in the least-squares refinement, are given in parentheses.

[b] Amplitudes not refined were fixed at the values obtained using the HF/6-31G* force field.

6.4 Discussion

The structural properties of $P(SiCl_3)_2Bu^t$ have been investigated in the gas phase by gas-phase electron diffraction and theoretical calculations. The perfectly staggered C_s structure was found to be a transition state on the potential energy surface of $P(SiCl_3)_2Bu^t$, with the C_1 structure where all the groups are twisted by 15 - 20° found to be the preferred structure. This has been observed for other similar molecules, for example, the $P(SiCl_3)Bu^t_2$ analogue also exhibited this behaviour.[7]

Overall, there is reasonable agreement between the experimental and theoretical structures. Theoretical bond lengths were generally found to be within 1 – 2 pm of the experimental values, the exceptions being the C-H and P-Si bond lengths. The P-Si bond length was calculated to be 224.0 pm, compared to the experimental value of 221.0 pm. Clearly there is a shortening of the P-Si bond, possibly due to the electron withdrawing effect of the adjacent $SiCl_3$ groups. Theoretical bond angles also tended to be within 1 – 2° of those found experimentally, although the angles around the phosphorus atom tended to be overestimated. For example, the C-P-Si(7/8) angles were predicted to be 107.9 and 106.9° as compared to 105.0 and 104.5° found

experimentally. Consequently the Si-P-Si angle was also overestimated theoretically, 101.5° compared to 99.9° found experimentally. This decrease in the angles around the phosphorus atom can be attributed to lone pair – bond pair repulsion between the phosphorus lone pair and the P-C and P-Si bonds.

The two $SiCl_3$ groups and the *tert*-butyl group were observed to have approximate local 3-fold symmetry. However, the local axes do not coincide with either the P-Si or the P-C bonds. The magnitude of the tilt of the groups away from the bonds can be represented by one parameter for each group. For example, if we consider the $Si(7)Cl_3$ group, the centroid of the triangle created by the 3 Cl atoms [Cl(17), Cl(19) and Cl(21)] can be represented by V and the angle created by the V-Si and the Si-P bonds is the tilt parameter. If we consider the other $SiCl_3$ group and the *tert*-butyl group in the same manner, with W representing the centroid of the Cl(18)...Cl(20)...Cl(22) triangle, and X the centroid of the C(2)...C(4)...C(5) triangle, tilt parameters for each group can be defined. Centroids V, W and X are shown graphically in Figure 4. The tilt angles were found to be 5.8° for the $Si(7)Cl_3$ group, 5.6° for the $Si(8)Cl_3$ group and 6.8° for the $C(1)C_3$ group.

The direction of the tilt of each group is determined by initially introducing a point Y along the P-C(1) vector at a distance equivalent to the P-Si distance, then defining Z as the centroid of the Y...Si(7)...Si(8) triangle. This is shown in Figure 5. The *tert*-butyl group torsion angle ϕ[X-C(1)-P(6)-Z] is -174°, indicating that the *tert*-butyl group is tilted more or less up towards the lone pair on the phosphorus atom. The $Si(7)Cl_3$ and $Si(8)Cl_3$ groups returned corresponding torsion angles of ϕ[V-Si(7)-P(6)-Z] = -133° and ϕ[W-Si(8)-P(6)-Z] = -147°. The tilts can then each be resolved into two components. For the $Si(7)Cl_3$ group, there is a 4.0° component towards the phosphorus lone pair, and a 4.3° component around the equatorial belt, away from the $Si(8)Cl_3$ group and towards the *tert*-butyl group. For the $Si(8)Cl_3$ group, there is a 4.7° axial tilt and a 3.0° equatorial tilt, the latter being towards the $Si(7)Cl_3$ group and away from the *tert*-butyl group.

Figure 4 Diagrammatic representation of (a) V for the $Si(7)Cl_3$ group, (b) W for the $Si(8)Cl_3$ group and (c) X for the $C(1)C_3$ group.

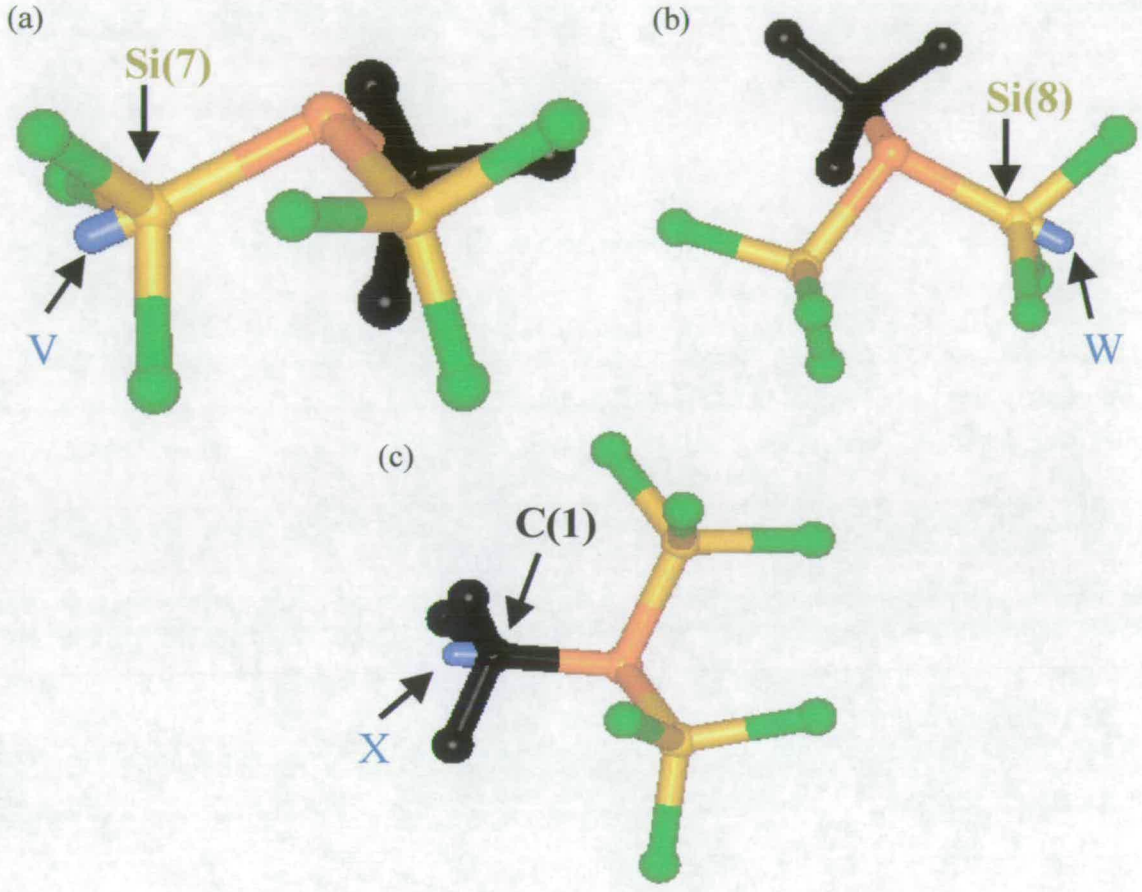

Figure 1 shows a view down the P-C bond of $PBu^t(SiCl_3)_2$, and the butyl group torsion can clearly be seen to bring one of the methyl groups in to closer contact with the $Si(8)Cl_3$ group. Hence the equatorial tilt component of the group is away from the *tert*-butyl group, and the equivalent tilt of the $Si(7)Cl_3$ group is towards the *tert*-butyl group.

In the $PBu^t_2SiCl_3$ analogue, the overall tilts are very similar to those in $PBu^t(SiCl_3)_2$. The equatorial components of the tilts in the present example are associated with the $SiCl_3$ groups, whereas in the di-*tert*-butyl case they are associated with the two butyl groups. These groups are tilted away from each other and towards the lone $SiCl_3$ group, which has virtually no equatorial tilt component.

The observed angles at the phosphorus atom are much smaller than tetrahedral due to the lone pair - bond pair repulsion. Tilting the ligand groups rather than expanding the angles at the central atom accommodates longer-range interactions within the molecule. The flexibility of these ligands, which allows this tilting, is a recurring theme throughout this thesis, and is very important in the accommodation of steric strain in these bulky molecules.

Figure 5 (a) Point Y equivalent to P-Si distance and (b) centroid Z of the Y...Si(7)...Si(8) triangle.

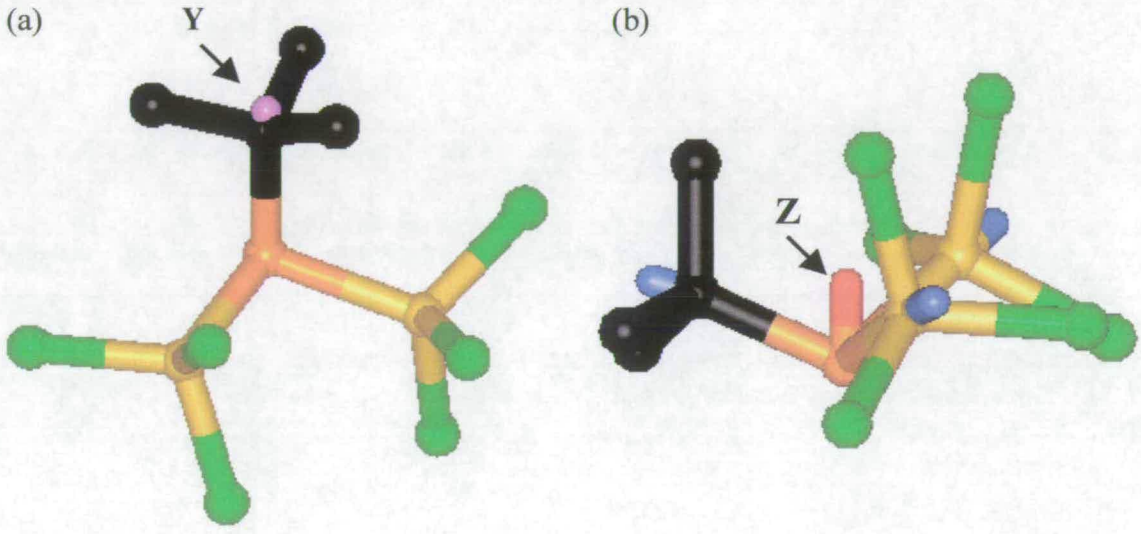

6.5 References

1. B. Beagley, A. G. Robiette and G. M. Sheldrick, *J. Chem. Soc. (A)*, 1968, 3002.
2. D. W. H. Rankin, A. G. Robiette, G. M. Sheldrick, B. Beagley, and T. G. Hewitt, *J. Inorg. Nuclear Chem.*, 1969, **31**, 2351.
3. G. A. Forsyth, H. E. Robertson and D. W. H. Rankin, *J. Mol. Struc.*, 1990, **239**, 209.
4. V. A. Naumov and O. Kataeva, *Zh. Strukt. Khim.*, 1983, **24**(5), 96.
5. H. Oberhammer, R. Schmutzler and O. Stelzer, *Inorg. Chem.*, 1978, **17**(5), 1254.
6. R. Seip, H. Schmidbaur, G. Blaschke, H. E. Robertson and D. W. H. Rankin, *J. Chem. Soc. Dalton Trans.*, 1985, 827.
7. W-W. du Mont, L. Müller, R. Martens, P. M. Papathomas, B. A. Smart, H. E. Robertson and D. W. H. Rankin, *Eur. J. Inorg. Chem.*, 1999, 1381.
8. Gaussian 98, Revision A.7, M. J. Frisch, G. W. Trucks, H. B. Schlegel, G. E. Scuseria, M. A. Robb, J. R. Cheeseman, V. G. Zakrzewski, J. A. Montgomery, R. E. Stratmann Jr, J. C. Burant, S. Dapprich, J. M. Millam, A. D. Daniels, K. N. Kudin, M. C. Strain, O. Farkas, J. Tomasi, V. Barone, M. Cossi, R. Cammi, B. Mennucci, C. Pomelli, C. Adamo, S. Clifford, J. Ochterski, G. A. Petersson, P. Y. Ayala, Q. Cui, K. Morokuma, D. K. Malick, A. D. Rabuck, K. Raghavachari, J. B. Foresman, J. Cioslowski, J. V. Ortiz, A. G. Baboul, B. B. Stefanov, G. Liu, A. Liashenko, P. Piskorz, I. Komaromi, R. Gomperts, R. L. Martin, D. J. Fox, T. Keith, M. A. Al-Laham, C. Y. Peng, A. Nanayakkara, C. Gonzalez, M. Challacombe, P. M. W. Gill, B. Johnson, W. Chen, M. W. Wong, J. L. Andres, C. Gonzalez, M. Head-Gordon, E. S. Replogle and J. A. Pople, Gaussian, Inc., Pittsburgh PA, 1998.
9. J. S. Binkley, J. A. Pople and W. J. Hehre, *J. Am. Chem Soc.*, 1980, **102**, 939.
10. M. S. Gordon, J. S. Binkley, J. A. Pople, W. J. Pietro and W. J. Hehre, *J. Am. Chem. Soc.*, 1982, **104**, 2797.
11. W. J. Pietro, M. M. Francl, W. J. Hehre, D. J. DeFrees, J. A. Pople and J. S. Binkley, *J. Am. Chem. Soc.*, 1982, **104**, 5039.
12. W. J. Hehre, R. Ditchfield and J. A. Pople, *J. Chem. Phys.*, 1972, **56**, 2257.
13. P. C. Hariharan and J. A. Pople, *Theor. Chim. Acta*, 1973, **28**, 213.

14. M. S. Gordon, *Chem. Phys. Lett.*, 1980, **76**, 163.

15. C. M. Huntley, G. S. Laurenson, D. W. H. Rankin, *J. Chem. Soc., Dalton Trans.*, **1980**, 954.

16. J. R. Lewis, P. T. Brain and D. W. H. Rankin, *Spectrum*, 1997, **15**, 7.

17. S. Cradock, J. Koprowski and D. W. H. Rankin, *J. Mol. Struct.*, 1981, **77**, 113.

18. A. S. F. Boyd, G. S. Laurenson, D. W. H. Rankin, *J. Mol. Struct.*, **1981**, *71*, 217.

19. A. W. Ross, M. Fink, R. Hilderbrandt, *International Tables for Crystallography*, Ed. A. J. C. Wilson, Kluwer Academic Publishers, Dordrecht, Boston and London, 1992; Vol. C, p 245.

20. L. Hedberg, I. M. Mills, *ASYM 40, Program for Force Constants and Coordinate Analysis,* Version 3.0; see also L. Hedberg, I. M. Mills, *J. Mol. Spectrosc.* **1993**, *160*, 117.

21. N. W. Mitzel, B. A. Smart, A. J. Blake, H. E. Robertson, D. W. H. Rankin, *J. Phys. Chem.* **1996**, *100*, 9339; A. J. Blake, P. T. Brain, H. McNab, J. Miller, C. A. Morrison, S. Parsons, D. W. H. Rankin, H. E. Robertson, B. A. Smart, *J. Phys. Chem.* **1996**, *100*, 12280.

Chapter 7

Spontaneous Generation of Stable Radicals from Dipnictines: A Solid-state, Gas-phase and Theoretical Investigation of the Nature of Steric Stabilization.

7.1 Introduction

The use of bulky substituents to stabilize compounds that are otherwise too reactive to be isolated is one of the major developments in modern chemistry. By means of such stabilization (kinetic and thermodynamic), it has proved possible to isolate, characterize, and study a number of intriguing species that includes coordinatively unsaturated cations and radicals as well as a host of multiply-bonded derivatives. Surprisingly, despite the importance and ubiquity of sterically demanding substituents, there have been few studies regarding the nature and details of the stabilization afforded by bulky ligands. Recently, we disclosed our preliminary findings[1] concerning a system that is particularly well suited for this purpose, and herein we report the results and insights gained from a considerably more comprehensive experimental and theoretical study.

In considering the homolytic cleavage of the Z-Z single bonds of molecules of the general type $R'_nZZR'_n$, the formation of the corresponding R'_nZ radicals or neutral molecules is expected to be favored by increased steric bulk of the substituents, R'. The conventional view is that such increases of steric strain would be manifested primarily in elongation of the Z-Z bond and that beyond a critical point of steric loading this bond would rupture. We have communicated the X-ray crystal structure of the sterically encumbered diphosphine, $(PR_2)_2$ (**1**) [R = $CH(SiMe_3)_2$], and the gas-phase electron diffraction (GED) structure of the corresponding homolysis product, $^{\bullet}PR_2$ (**2**), the exclusive species found in both solution and in the gas phase.[2] In conjunction with *ab initio* calculations on **2**, comparisons of the structural features of the radical with those of the cognate dimer **1** demonstrated that the conventional view is incorrect and furnished some new insights into the origins of the stabilization of the free radical **2**. However, in order to provide a broader, more reliable basis for the foregoing conclusions, we considered it important to extend the study to include the heavier congeneric arsenic derivatives $(AsR_2)_2$ (**3**) and $^{\bullet}AsR_2$ (**4**).

7.2 Experimental

7.2.1 Synthesis

(Carried out by Alan Cowley and Charles MacDonald, Austin, Texas)

Samples of $\{P[CH(SiMe_3)_2]_2\}_2$ and $\{As[CH(SiMe_3)_2]_2\}_2$ were obtained either by methods described previously[2] or by slight variations thereof.

7.2.2 *Ab Initio* Calculations

All calculations at the UHF/3-21G*,[3-5] UHF/6-31G*,[6-8] UHF/DZP and UB3LYP/DZP levels were performed on a Dec Alpha 1000 4/200 workstation using the Gaussian 94 program.[9] The energy calculations were performed using the resources of the U.K. Computational Chemistry Facility, on a DEC 8400 superscalar cluster equipped with 10 fast processors, 6 GB of memory and 150 GB disk.

Graded series of geometry optimizations were undertaken for both radicals, $P[CH(SiMe_3)_2]_2$ **(2)** and $As[CH(SiMe_3)_2]_2$ **(4)**, from which the effect of increasing the quality of the basis set and the level of theory could be observed. Geometry optimizations were undertaken at the UHF level using the standard 3-21G* and 6-31G* basis sets. Further calculations were then carried out to investigate the effect of adding diffuse functions onto the phosphorus and arsenic atoms at the UHF and UB3LYP[10] levels, using a 6-311G*[11-12] basis set for the phosphorus and arsenic atoms and 6-31G* for the carbon, silicon and hydrogen atoms.

Vibrational frequencies were calculated from analytic second derivatives at the UHF/3-21G* level to determine the nature of stationary points, to provide estimates of amplitudes of vibration (u) for use in the GED refinements and for comparison with experimentally determined frequencies. The C_2 symmetry structures were confirmed as local minima for both molecules and the force constants obtained were used in the construction of force fields using a version of the ASYM40 program[13] modified for molecules with more than 40 atoms.

7.2.3 Energy calculations

Ab initio single point energy calculations were carried out to determine the approximate energy differences associated with the structural distortions between the dimer **(1)** (solid phase) and the monomer **(2)** (gas phase) for the phosphorus compound. For the dimer, the experimental heavy atom coordinates were taken from the crystal structure determination and used without further modification. The hydrogen atom coordinates were added at fixed positions based on previous experience, because their positions were poorly defined in the crystal structure. A single point energy calculation was then performed on the dimer at the B3LYP/DZP level. The same coordinates were then used to carry out single point energy calculations on the two halves of the dimer separately at the UB3LYP/DZP level. The difference between the sum of these energies and the energy of the dimer can be seen as a representation of what the dissociation energy of the P-P bond would be if no relaxation of the radical fragments occured. The hydrogen atom positions were then allowed to optimize fully at the UB3LYP/DZP level, whilst the heavy atom coordinates were fixed. The whole structure was then allowed to optimize at the UB3LYP/DZP level, to give the fully optimized structure for that conformation. Finally, the gaseous C_2 structure was optimized, to give the lowest energy conformation. This gives an indication of the energy required to undergo the conformational change, and of the energy released by the change. For all the UB3LYP/DZP single point energy calculations, a general basis set was used, specifying a 6-311G*[11-12] level of theory for the phosphorus and arsenic atoms, and a 6-31G* level of theory for the carbon, silicon and hydrogen atoms. These calculations thus give an indication of how energy is provided by relaxation of steric strain to allow dissociation of the P-P bond.

7.2.4 X-Ray Crystallography

(Carried out by Alan Cowley and Charles MacDonald, Austin, Texas)

7.2.4.1 Crystallization. Crystalline samples of chlorophosphine **(5)** and chloroarsine **(6)** suitable for X-ray diffraction study were obtained by slow cooling (253 K) of concentrated CH_2Cl_2 solutions. Crystals of diphosphine **1** in admixture with those of the starting chlorophosphine **(5)** were obtained by slow cooling (279 K) of the red solution obtained from the sodium metal reduction of **(5)** in hexanes. The yellow

crystals of **(1)** and colorless crystals of **(5)** were separated manually with the aid of a microscope.

Diarsine **(3)** was prepared by treatment of a toluene solution of R_2AsI (obtained via the reaction of iodotrimethylsilane with **6**) with lithium metal. Following removal of the solvent and volatiles, the orange residue was extracted with hexanes. Yellow crystals of **(3)** suitable for study by X-ray diffraction study were obtained by slow cooling (-20 °C) of the hexane solution. A summary of the crystallographic data for **(1)**, **(3)**, **(5)** and **(6)** is presented in Table 1.

7.2.4.2 Data Collection. Suitable crystals of tetra(disyl)diphosphine **(1)**, bis(disyl)chlorophosphine **(5)** and bis(disyl)chloroarsine **(6)** were coated in poly(perfluoroether), mounted and rapidly placed into the 193 K nitrogen stream of a Siemens P4 diffractometer using Mo Kα radiation (λ = 0.71073 Å). For bis(disyl)chlorophosphine, the unit cell was determined by the accurate recentering of 25 reflections; a total of 6906 reflections were collected in the range $4.00° < 2\theta < 55.96°$. Lorentz, polarization and absorption corrections were applied to the data. For tetra(disyl)diphosphine, the unit cell was determined by the accurate recentering of 25 reflections; a total of 9263 reflections were collected in the range $2.38° < 2\theta < 50.12°$. Lorentz, polarization and absorption (integration) corrections were applied to the data. For bis(disyl)chloroarsine the unit cell was determined by the accurate recentering of 25 reflections; a total of 8258 reflections were collected in the range $2.74° < 2\theta < 60.0°$. Lorentz and polarization corrections were applied to the data. In each case, the location of heavy atoms was accomplished by direct methods and subsequent difference Fourier syntheses and the structure was refined using full-matrix least-squares on F^2. Hydrogen atoms were placed in calculated positions and each was assigned an isotropic displacement factor equal to 1.5 times U(eq) of the carbon atom to which it is attached. A summary of the crystallographic data for **(1)**, **(3)**, **(5)** and **(6)** is presented in Table 1. Tables of atomic coordinates, and anisotropic displacement parameters are given in Appendix 6 [Tables 1-9].

Table 1 Summary of crystallographic data for tetra(disyl)diphosphine **(1)**, tetra(disyl)diarsine **(3)**, bis(disyl)chlorophosphine **(5)** and bis(disyl)chloroarsine **(6)**.

Compound	**1**	**3**	**5**	**6**
Empirical formula	$C_{28}H_{76}P_2Si_8$	$C_{28}H_{76}As_2Si_8$	$C_{14}H_{38}ClPSi_4$	$C_{14}H_{38}AsClSi_4$
Formula weight	699.54	784.44	385.22	429.17
Temperature (K)	183(2)	153(2)	183(2)	183(2)
Wavelength (Å)	0.71073	0.71073	0.71073	0.71073
Crystal system	Monoclinic	Triclinic	Monoclinic	Monoclinic
Space group	$P2_1/c$	$P\bar{1}$	$P2_1/n$	$P2_1/n$
Unit cell dimensions:				
a (Å)	18.341(2)	20.348(4)	9.319(1)	11.5626(11)
b (Å)	13.4240(10)	26.342(5)	12.406(2)	12.3944(10)
c (Å)	19.033(2)	37.012(7)	20.453(2)	17.542(2)
α (°)	90	102.11(3)	90	90
β (°)	110.650(10)	104.54(3)	95.08(1)	108.276(9)
γ (°)	90	102.35(3)	90	90
Volume ($Å^3$)	4385.0(7)	18015(6)	2355.3(5)	2387.2(4)
Z	4	16	4	4
Density (calculated) (g cm^{-3})	1.060	1.161	1.086	1.194
Absorption coefficient (cm^{-1})	3.35	17.13	4.27	17.30
F(000)	1544	6752	840	912
θ range for data collection (°)	1.19 to 25.06	2.92 to 27.47	2.00 to 27.49	1.87 to 30.00
Limiting indices	$-20 < h < 21$, $-2 < k < 15$, $-22 < l < 21$	$-6 < h < 6$, $-34 < k < 9$, $-42 < l < 48$	$-1 < h < 12$, $-1 < k < 16$, $-26 < l < 26$	$-1 < h < 16$, $-1 < k < 17$, $-24 < l < 23$
Reflections collected	9263	100000	6906	8258
Independent reflections	7709	27687	5392	6795
R_{int}	0.0173	0.0614	0.0214	0.0905

Table 1 continued

Compound	**1**	**3**	**5**	**6**
Absorption correction	Integration	None	SHELXA	None
Data / restraints / parameters	7702 / 0 / 360	27654 / 0 / 2737	5387 / 0 / 195	6793 / 0 / 182
Goodness-of-fit on F^2	1.705	1.511	1.018	1.043
Final R indices [$I>2\sigma(I)$]	$R1$ = 0.0375, $wR2$ = 0.1159	$R1$ = 0.0531, $wR2$ = 0.1213	$R1$ = 0.0395, $wR2$ = 0.0806	$R1$ = 0.0582, $wR2$ = 0.1377
R indices (all data)	$R1$ = 0.0451, $wR2$ = 0.1203	$R1$ = 0.0913, $wR2$ = 0.1344	$R1$ = 0.0657, $wR2$ = 0.0915	$R1$ = 0.0897, $wR2$ = 0.1567
Largest diff. peak and hole (e $Å^{-3}$)	0.295 and -0.312	0.536 and -0.522	0.307 and -0.243	1.831 and -0.879

7.2.5 Gas-phase Electron Diffraction (GED) Studies of the Bis(disyl)phosphinyl and arsinyl Radicals

7.2.5.1 Data Collection. Electron scattering intensities of the bis(disyl)phosphinyl and arsinyl radicals were recorded on Kodak Electron Image plates using the Balzers' gas electron diffraction apparatus in Oslo[14] operating at *ca.* 41.5 kV (electron wavelength *ca.* 0.058 Å). Nozzle-to-plate distances for the metal inlet nozzle were *ca.* 248 and 498 mm, yielding data in the *s* range 1.5-29 $Å^{-1}$. For the phosphinyl radical, three plates were exposed at the long distance and five at the short distance, while for the arsinyl radical, the numbers of plates were three and four respectively. The sample and nozzle temperatures were maintained at 420 K for the phosphorus radical and 425 K for the arsenic radical during the exposure periods.

The scattering patterns of benzene were used for the purpose of calibration of the electron wavelength. Nozzle-to-plate distances, weighting functions used to set up the off-diagonal weight matrices, correlation parameters, final scale factors and electron wavelengths for the measurements are collected in Appendix 6 [Table 10].

The electron-scattering patterns were converted into digital form using a Joyce Loebl microdensitometer.[15] The programs used for data reduction[15,16] and least-squares refinement[17] have been described previously; the complex scattering factors were those listed by Ross *et al.*[18]

7.2.5.2 Structural Models. The structures of $P\{CH[Si(CH_3)_3]_2\}_2$ and $As\{CH[Si(CH_3)_3]_2\}_2$ were defined in exactly the same way. On the basis of the *ab initio* calculations described above, electron diffraction refinements were carried out using models in C_2 symmetry. The large number of geometric parameters needed to define the models made it necessary to make the assumption that all the methyl groups are equivalent and have local C_{3v} symmetry. Initially, some of the differences between correlated bond lengths and bond angles were restrained using the SARACEN[19] method. However, since many proved to be uncorrelated with other parameters and returned values and e.s.d.'s which were close to the restraints. In these cases parameters were fixed in the final

refinement. The atom numbering for $P\{CH[Si(CH_3)_3]_2\}_2$ and $As\{CH[Si(CH_3)_3]_2\}_2$ is shown in Figures 1(a) and 1(b). The independent geometric parameters are listed in Table 2.

Figure 1 Experimentally determined molecular structures of (a) $P[CH(SiMe_3)_2]_2$ **(2)** and (b) $As[CH(SiMe_3)_2]_2$ **(4)** in the gas phase.

(a)

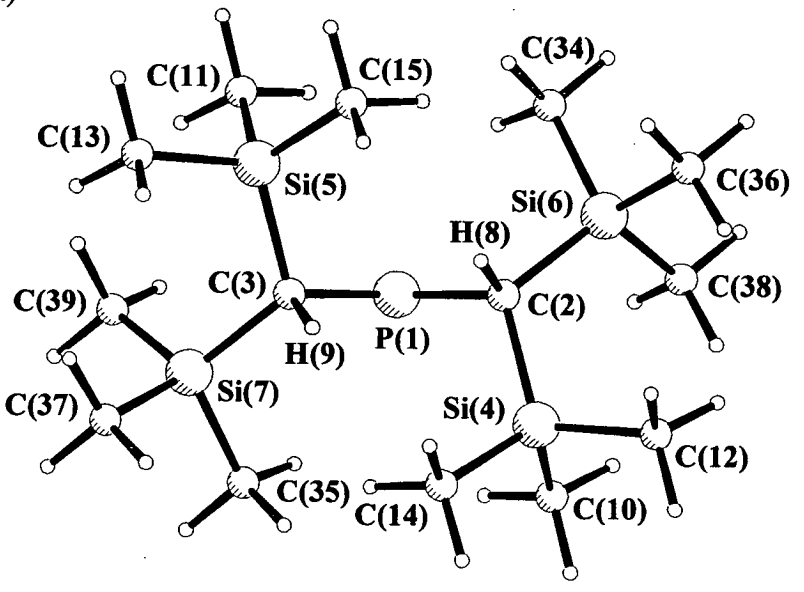

(b)

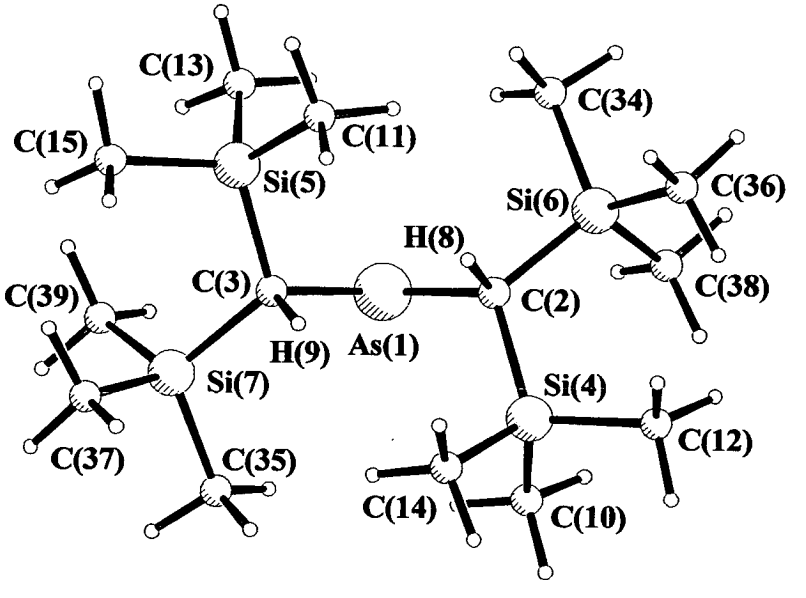

Table 2 Theoretical geometrical parameters at the UB3LYP/DZP level for bis[bis(trimethylsilyl)methyl]phosphinyl **(2)** and bis[bis(trimethylsilyl)methyl]arsinyl[a] **(4)** (distances in Å, angles in °).

Parameter	$P[CH(SiMe_3)_2]_2$	$As[CH(SiMe_3)_2]_2$
Z(1)-C(2)[b]	1.876	2.016
C(2)-Si(4)	1.926	1.917
C(2)-Si(6)	1.926	1.919
Si(4)-C(10)	1.894	1.896
Si(4)-C(12)	1.900	1.901
Si(4)-C(14)	1.900	1.900
Si(6)-C(34)	1.898	1.899
Si(6)-C(36)	1.899	1.899
Si(6)-C(38)	1.896	1.897
C(2)-H(8)	1.101	1.100
C-H[c]	1.096	1.097
C(2)-Z(1)-C(3)[b]	104.8	101.8
Z(1)-C(2)-Si(4)[b]	111.6	111.2
Z(1)-C(2)-Si(6)[b]	109.9	110.7
Z(1)-C(2)-H(8)[b]	108.6	106.0
Si(4)-C(2)-Si(6)	116.1	116.8
C(2)-Si(4)-C(10)	111.9	111.9
C(2)-Si(4)-C(12)	112.0	112.1
C(2)-Si(4)-C(14)	109.5	109.5
C(2)-Si(6)-C(34)	110.9	111.8
C(2)-Si(6)-C(36)	110.0	109.6
C(2)-Si(6)-C(38)	111.7	111.7
Si-C-H[c]	111.3	111.3
H(8)-C(2)-Z(1)-C(3)[b]	-26.6	-24.3
Z(1)-C(2)-Si(4)-C(10)[b]	48.5	42.0
Z(1)-C(2)-Si(6)-C(34)[b]	40.6	39.0

[a] See Figure 1 for atom numbering. [b] Z = P or As. [c] Average value.

The structure of $P\{CH[Si(CH_3)_3]_2\}_2$ was defined in terms of 27 independent geometric parameters comprising four bond lengths, eleven bond angles and twelve torsion, rock and tilt parameters. The independent parameters include the average C-H bond length (p_1) for the methyl groups with a difference from this value for the C(2)-H(8) distance (p_2). An average Si-C bond length (p_3) was used, with small differences between non-equivalent bond distances fixed at the *ab initio* values and the difference between the mean Si-C and the C-P distances as a refinable parameter (p_4). The P-C-H (p_5) and C-P-C (p_6) bond angles were included and all the Si-C-H bond angles in the methyl groups (p_7) were assumed to be identical. The internal C-Si-C bond angles for the $SiMe_3$ groups were defined in terms of the average (p_8) of C(10)-Si(4)-C(12), C(10)-Si(4)-C(14), C(12)-Si(4)-C(14), C(34)-Si(6)-C(36), C(34)-Si(6)-C(38) and C(36)-Si(6)-C(38), and five difference parameters (p_9 - p_{13}), all of which were included in the refinement procedure because the predicted angles spanned a wide range of values. The differences were the average internal C-Si-C bond angle for the first $SiMe_3$ group minus the average angle for the second $SiMe_3$ group (p_9), the differences between C(10)-Si(4)-C(12) and C(10)-Si(4)-C(14) or C(12)-Si(4)-C(14) (p_{10} or p_{11}), and the differences between C(34)-Si(6)-C(36) and C(34)-Si(6)-C(38) or C(36)-Si(6)-C(38) (p_{12} or p_{13}). The P-C-Si angles were described by the average of angles P(1)-C(2)-Si(4) and P(1)-C(2)-Si(6) (p_{14}), and the difference between these two angles (p_{15}).

Of the remaining twelve parameters, three represent the twist, tilt and rock of the methyl groups. The other nine parameters are twist motions associated with various fragments of the disyl groups. The $SiMe_3$ groups were generated initially by placing a methyl group carbon at the origin, with its three H atoms arranged with local C_{3v} symmetry about the *x*-axis and one H in the *xy* plane in the positive *x* and *y* directions. The methyl torsion, tilt and rock parameters, (p_{16} - p_{18}) are rotations about the *x*, *z*, and *y* axes respectively. The methyl group is then translated along the positive *x*-axis by its associated Si-C bond length and the central silicon of the $SiMe_3$ group is placed at the origin. The correct internal C-Si-C bond angles are generated by rotating the methyl groups about the *z* axis, moving the methyl carbon in the positive *y* direction, and then generating the other methyl groups by rotation of the first group about the *x* axis by $p_{19} + p_{20}/2$ and the other by $-(p_{19} - p_{20}/2)$,

respectively. The $SiMe_3$ torsion angle is a rotation of the whole group about the x axis (p_{21}). C(2) was then placed at the origin and the $SiMe_3$ group translated in the positive x direction by the Si-C bond length. The second $SiMe_3$ group was then generated in exactly the same manner as the first, twisting the methyl groups into position about the x-axis by $p_{22} + p_{23}/2$ and $-(p_{22} - p_{23}/2)$ and twisting the $SiMe_3$ group about the x axis by p_{24}.

Having generated the $SiMe_3$ groups in their local coordinate systems, they needed to be rotated to put them in the correct positions relative to the phosphorus atom. The two $SiMe_3$ groups attached directly to C(2) were initially rotated in the xy plane by [(180° - <(P-C-Si)] and then rotated about the x axis. These rotations were defined in terms of an average and a difference of torsion angles [ϕC(3)-P(1)-C(2)-Si(4)] and [ϕC(3)-P(1)-C(2)-Si(6)] (p_{25} and p_{26}). The central atom P(1) was then placed at the origin by translation of the $CH(SiMe_3)_2$ fragment in the positive x direction by the P-C bond length. Then the torsion angle of the $CH(SiMe_3)_2$ fragment [ϕC(3)-P(1)-C(2)-H(8)] was introduced (p_{27}). Finally, the $CH(SiMe_3)_2$ group was rotated about the y axis by half the C(3)-P(1)-C(2) angle (p_6) and a C_2 rotation about the z axis through P(1) generated the full C(3)-P(1)-C(2) angle and the second half of the molecule.

The starting parameters for the r_a refinement were taken from the theoretical geometry optimized at the UB3LYP/DZP level. The r_α structure was not refined because the rectilinear vibrational corrections (i.e. parallel and perpendicular correction terms) are known to be unreliable for a molecule of this size with many low-lying vibrational modes. Theoretical (UHF/3-21G*) Cartesian force fields were obtained for the local minima and converted into force fields described by a set of symmetry coordinates using a modified version of the ASYM40 program[13] for molecules with more than 40 atoms. In total 27 geometric parameters and 46 groups of vibrational amplitudes were refined for $P\{CH[Si(CH_3)_3]_2\}_2$, and 27 geometric parameters and 27 groups of vibrational amplitudes were refined for $As\{CH[Si(CH_3)_3]_2\}_2$. Flexible restraints were employed during the refinement using the SARACEN method.[19] In total, 25 geometric and 43 amplitude restraints were employed for $P\{CH[Si(CH_3)_3]_2\}_2$ and 22 geometric and 24 amplitude

restraints were employed for $As\{CH[Si(CH_3)_3]_2\}_2$. These are listed in Appendix 6 [Tables 11 and 12].

The success of the final refinements, for which R_G = 6.9 (R_D = 5.7) and 6.8 (5.4) for $P\{CH[Si(CH_3)_3]_2\}_2$ and $As\{CH[Si(CH_3)_3]_2\}_2$ respectively, can be assessed on the basis of the radial distribution curves [Figures 2(a) and 2(b)] and the molecular scattering intensity curves [Figures 3(a) and 3(b)]. Final refined parameters are listed in Table 3, interatomic distances and the corresponding amplitudes of vibration in Table 4, the least-squares correlation matrices are shown in Appendix 6 [Tables 13 and 14] and the experimental coordinates from the GED analysis in Appendix 6 [Table 15].

Table 3 Geometric parameters for bis(disyl)phosphinyl **(2)** and bis(disyl)arsinyl **(4)**.[a]

		$P[CH(SiMe_3)_2]_2$		$As[CH(SiMe_3)_2]_2$	
No.	Parameter	GED (r_a)	UB3LYP/DZP (r_e)	GED (r_a)	UB3LYP/DZP (r_e)
p_1	C-H av	1.110(3)	1.096	1.106(4)	1.097
p_2	C-H diff	0.002(1)	0.005	0.003(12)	0.004
p_3	Si-C av	1.877(2)	1.905	1.876(2)	1.904
p_4	C-Z diff	-0.021(11)	-0.029	0.107(9)	0.112
p_5	ZCH	108.1(13)	108.6	106.4(12)	106
p_6	CZC	103.9(10)	104.8	100.6(10)	101.8
p_7	SiCH	111.1(6)	111.3	110.4(6)	111.3
p_8	CSiC av	111.7(3)	107.9	111.2(3)	111.1
p_9	av1 minus av2	0.2(1)	-0.3	0.1(1)	0.1
p_{10}	diff1 group1	0.5(1)	-0.5	-3.0(9)	-2.4
p_{11}	diff2 group1	2.5(1)	2.2	-0.6(9)	-2.6
p_{12}	diff1 group2	2.1(1)	-0.9	1.5(9)	2.2
p_{13}	diff2 group2	-0.7(1)	-3.2	0.1(1)	0.1
p_{14}	ZCSi av	109.4(4)	110.7	113.3(6)	110.9
p_{15}	ZCSi diff	0.7(9)	1.7	0.6(11)	0.5

Table 3 Continued

		$P[CH(SiMe_3)_2]_2$		$As[CH(SiMe_3)_2]_2$	
No.	Parameter	GED (r_a)	UB3LYP/DZP (r_e)	GED (r_a)	UB3LYP/DZP (r_e)
p_{16}	Me twist	16.8(13)	-	183.5(12)	-
p_{17}	Me tilt	0.7(12)	-	-4.2(11)	-
p_{18}	Me rock	1.2(13)	-	4.2(11)	-
p_{19}	C twist av group1	121.5(6)	121.3	120.2(6)	119.2
p_{20}	C twist diff1 group1	1.9(11)	1.1	2.3(11)	3.6
p_{21}	SiMe3 twist group1	37.3(11)	48.5	-72.9(19)	-72
p_{22}	C twist av group2	119.4(6)	118.9	119.6(6)	119.1
p_{23}	C twist diff1 group2	-2.4(11)	-2.2	-1.2(11)	-2.2
p_{24}	SiMe3 twist group2	50.9(12)	40.6	41.5(17)	39
p_{25}	Si twist av	115.0(5)	114.8	113.2(6)	114.2
p_{26}	Si twist diff1	0.4(1)	0.2	0.04(1)	0.03
p_{27}	H twist	-26.4(8)	-26.6	-25.3(9)	-24.3

[a] Distances in Å, angles in degrees; see text for parameter definitions; figures in parentheses are the estimated standard deviations of the last digits. Z = P or As.

Table 4 Selected interatomic distances and mean amplitudes of vibration for $P[CH(SiMe_3)_2]_2$ **(2)** and $As[CH(SiMe_3)_2]_2$ **(4)** from the GED study.[a]

		$P[CH(SiMe_3)_2]_2$ **(2)**		$As[CH(SiMe_3)_2]_2$ **(4)**	
No.	Atom pair	r_a/Å	u/Å	r_a/Å	u/Å
1	Z(1)-C(2)	1.856(9)	0.057(7)	1.982(8)	0.042(6)
2	C(2)-Si(6)	1.902(2)	0.050(6)	1.890(2)	0.052(6)
3	C(2)-Si(4)	1.905(2)	0.050 (tied to u_2)	1.891(2)	0.052 (tied to u_2)
4	C(2)-H(8)	1.113(4)	0.078(10)	1.109(12)	0.078 (fixed)
5	Si(4)-C(10)	1.878(2)	0.063(4)	1.871(2)	0.053 (tied to u_{10})
6	Si(4)-C(12)	1.878(2)	0.063 (tied to u_5)	1.871(2)	0.053 (tied to u_{10})
7	Si(4)-C(14)	1.876(2)	0.063 (tied to u_5)	1.869(2)	0.053(6)
8	Si(6)-C(34)	1.880(2)	0.063 (tied to u_5)	1.868(2)	0.053 (tied to u_{10})
9	Si(6)-C(36)	1.879(2)	0.063 (tied to u_5)	1.872(2)	0.053 (tied to u_{10})
10	Si(6)-C(38)	1.875(2)	0.063 (tied to u_5)	1.874(2)	0.053(5)
11	C(10)-H(16)	1.110(4)	0.073(5)	1.106(4)	0.060(7)
12	Z(1)...Si(6)	3.075(13)	0.111(8)	3.240(13)	0.120(9)
13	Z(1)...Si(4)	3.064(13)	0.111 (tied to u_{12})	3.230(15)	0.120(9)
14	Si(4)...Si(6)	3.255(9)	0.087(8)	3.192(16)	0.095(9)
15	C(2)...C(10)	3.098(6)	0.116 (tied to u_{19})	3.085(13)	0.093 (fixed)

Table 4 Continued

		$P[CH(SiMe_3)_2]_2$ **(2)**		$As[CH(SiMe_3)_2]_2$ **(4)**	
No.	Atom pair	r_a/Å	u/Å	r_a/Å	u/Å
16	C(2)...C(12)	3.138(6)	0.120 (tied to u_{19})	3.114(8)	0.096 (fixed)
17	C(2)...C(14)	3.149(6)	0.119 (tied to u_{19})	3.109(8)	0.096 (fixed)
18	C(2)...C(34)	3.104(6)	0.115 (tied to u_{19})	3.135(12)	0.092 (fixed)
19	C(2)...C(36)	3.140(6)	0.125(11)	3.082(11)	0.101 (fixed)
20	C(2)...C(38)	3.146(6)	0.122 (tied to u_{19})	3.094(13)	0.099 (fixed)
21	Si(4)...C(34)	4.844(9)	0.114 (tied to u_{26})	4.848(13)	0.095 (fixed)
22	Si(4)...C(36)	4.130(22)	0.150(17)	3.764(39)	0.172(99)
23	Si(4)...C(38)	3.721(21)	0.158 (fixed)	3.762(33)	0.162(20)
24	Si(6)...C(10)	3.992(28)	0.152 (tied to u_{22})	4.148(30)	0.157(18)
25	Si(6)...C(12)	3.730(18)	0.146 (fixed)	3.483(30)	0.131(18)
26	Si(6)...C(14)	4.880(7)	0.120(11)	4.741(17)	0.099(12)

[a] See Fig. 1 for atom numbering. (Other atom pairs were also used in the refinement, but are not shown here.)

Figure 2 Experimental and difference (experimental - theoretical) radial-distribution curves, $P(r)/r$, for (a) $P[CH(SiMe_3)_2]_2$ **(2)** and (b) $As[CH(SiMe_3)_2]_2$ **(4)**. Before Fourier inversion the data were multiplied by $s.\exp(-0.002s^2)/(Z_P - f_P)/(Z_{Si} - f_{Si})$ for $P[CH(SiMe_3)_2]_2$ and by $s.\exp(-0.002s^2)/(Z_{As} - f_{As})/(Z_{Si} - f_{Si})$ for $As[CH(SiMe_3)_2]_2$.

(a)

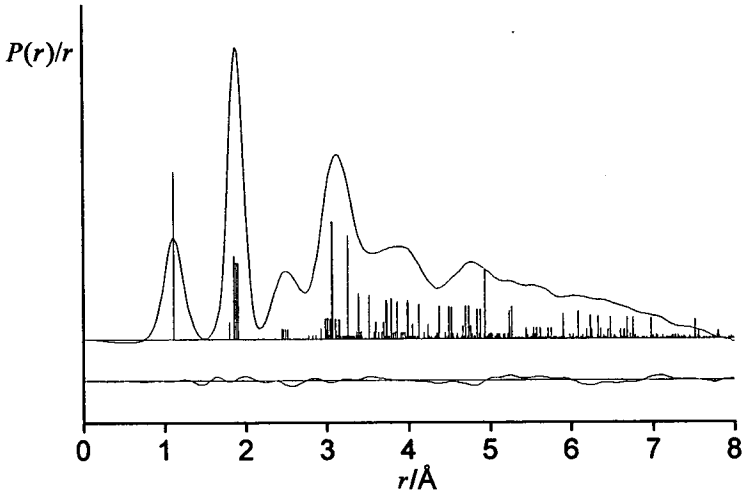

(b)

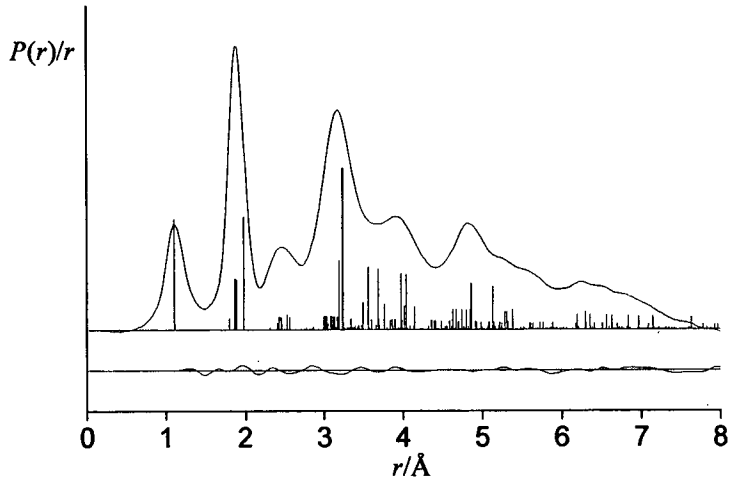

Figure 3 Experimental and final weighted difference (experimental - theoretical) molecular-scattering intensities for (a) $P[CH(SiMe_3)_2]_2$ **(2)** and (b) $As[CH(SiMe_3)_2]_2$ **(4)**.

(a)

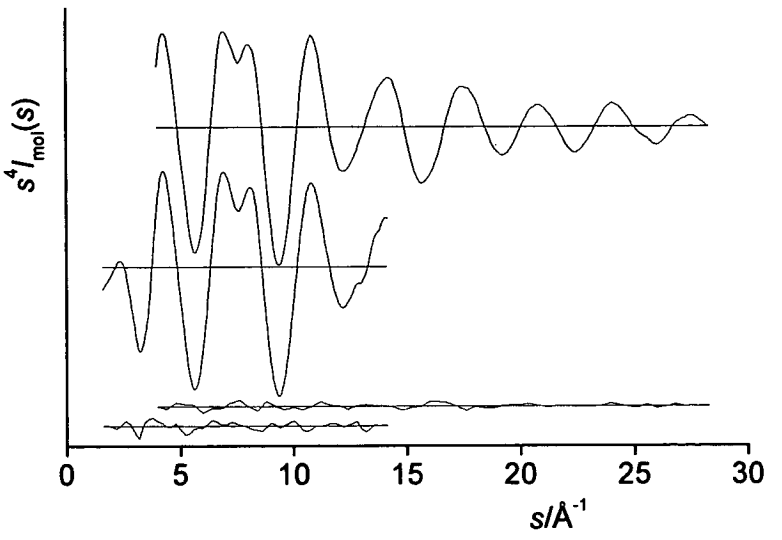

(b)

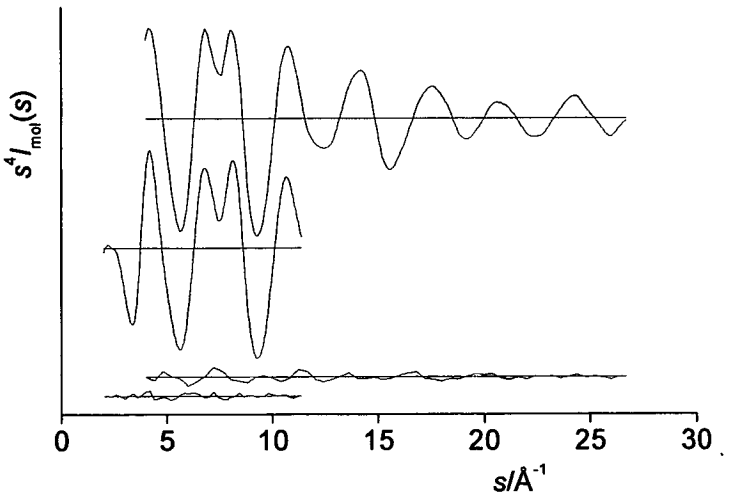

7.3 Results and Discussion

7.3.1 *Ab Initio* Calculations

Two graded series of molecular-orbital calculations were undertaken, one excluding and one including diffuse functions on the heavy atom skeleton, for each of the bis(disyl)phosphinyl and arsenyl radicals [Figures 1(a) and 1(b)].

A search of the potential energy surface led to the location of one minimum, with C_2 symmetry, for each molecule. Vibrational frequency calculations at the UHF/3-21G* level confirm that these structures represent local minima on the potential energy surface. The molecular geometries of the molecules for the UB3LYP/DZP calculation are presented in Table 3; those calculated at the UHF/6-31G* and UHF/DZP levels of theory are presented in Appendix 6 [Table 16].

Although each of these systems contains an unpaired electron, the molecular geometries proved to be relatively insensitive to changes in the theoretical method. For this reason, only the highest level results (UB3LYP/DZP) will be discussed.

The V-shaped molecular geometry of the C_2 conformation approximates to *syn,syn* with respect to the (Z)C-H bonds, with the torsion angle [ϕC(3)-Z(1)-C(2)-H(8)] calculated to be 26.6° for Z = P and 24.3° for Z = As. These angles are negative in Table 3, where their signs relative to other torsion angles are significant. The C-P-C bond angle was 104.8° with the P-C bond length 1.876 Å, while the C-As-C bond angle was 101.8° with As-C 2.016 Å. The predicted P(1)-C(2)-Si(4/6) angles show a slight distortion from regular tetrahedral geometry, 111.6° and 109.9° respectively, as do the As(1)-C(2)-Si(4/6) angles, 111.2° and 110.7°. However, there is evidence of significant steric crowding between the trimethylsilyl groups in these molecules, with the Si(4)-C(2)-Si(6) angle predicted to be 116.1° in the bis(disyl)phosphinyl radical and 116.8° in the bis(disyl)arsinyl radical, compared to 109.5° for an ideal tetrahedral geometry around carbon. These structural changes serve to reduce the steric interactions in this system. Resultant nearest neighbour H...H distances were calculated to be 2.39 and 2.34 Å for the phosphorus and the arsenic

radicals respectively, as compared to 2.40 Å for the sum of the van der Waals radii of two hydrogen atoms, indicating that most of the strain has been relieved within the fully optimized system. Internal C-Si-C angles in the trimethylsilyl groups indicate that they are only slightly distorted from local C_3 symmetry in both molecules; for example, the three internal C-Si-C angles around Si(6) are 105.1°, 107.8° and 108.2° in the phosphinyl radical whilst in the arsinyl radical they are 106.4°, 107.7° and 108.2°.

In both radicals the bond lengths are generally within the expected ranges based on the results obtained previously for related molecules. The inner Si(4/6)-C distances were computed to be 1.926 Å for the phosphorus radical and 1.917/1.919 Å for the arsenic radical. These Si-C bond lengths are longer than those of normal Si-C bonds, for example 1.882(1) Å and 1.886(1) Å for 1,4-disilabutane and 1,5-disilapentane,[20] but compare well with the calculated Si-C bond length in 1,2-di-*tert*-butyldisilane[21] (1.919 Å) and the ranges of Si-C bond lengths calculated for 1,1,2-tri-*tert*-butyldisilane[22] (1.915-1.924 Å). These long bonds may be a demonstration of steric interactions in these crowded molecules, although the lengthening could be an electronic effect of the electron-releasing trimethylsilyl groups. The ranges of the outer Si-C distances were calculated to be slightly shorter, 1.894-1.900 Å and 1.896-1.902 Å for bis(disyl)phosphinyl and arsinyl respectively. These compare well with those found in bis(disyl)germanium and tin: 1.881(3) - 1.897(3) Å.[23] The fact that the inner Si-C bonds lengthen more than the outer bonds in both radicals may be an example of an intra-ligand strain-relieving effect, as observed by experiment in the bis(disyl)germanium and tin cases.[23] But overall, the picture that emerges of the radicals is of systems which, though crowded, are not severly strained. The bulky groups have been accommodated by the adoption of the only conformation which avoids strong inter-ligand interactions.

7.3.2 GED Refinements

Theoretical and experimental studies show that both bis[bis(trimethylsilyl)methyl]-phosphinyl and arsinyl radicals exist as single C_2 conformers in the gas phase. The electron diffraction data for each compound were fitted using the SARACEN method[19] on the basis of such C_2 structures.

For each radical, the final experimental structure is in reasonable agreement with that calculated *ab initio* at the UB3LYP/DZP level. Computed bond lengths are generally 0.01-0.02 Å longer than the experimental values, even though the calculated equilibrium distances must be slightly shorter than vibrationally averaged r_a distances; calculated angles generally fall within 1-2° of the GED values (Table 2). For example, in bis[bis(trimethylsilyl)methyl]phosphinyl, the P-C bond length refined to 1.856(11) Å, compared to the computed value of 1.876 Å, and the experimental range of Si-C bond lengths was 1.875-1.905 Å, compared to the calculated range of 1.894-1.926 Å. The C-P-C angle refined to 103.9(10)° in comparison to the calculated angle of 104.8°. The angle differences are similar for bis[bis(trimethylsilyl)methyl]arsinyl, with a C-As-C bond angle of 101.2(10)° being obtained experimentally compared to a calculated value of 101.8°. There is rather more of a discrepancy between the observed and calculated As-C bond lengths, 1.981(8) Å *vs.* 2.016 Å, but in general calculated bond lengths appear to be *ca.* 0.02 Å longer than the experimentally obtained values.

The torison angle [ϕC(3)-P(1)-C(2)-H(8)], which uniquely describes the orientation of the disyl groups around the carbon-phosphorus bond, agrees very well with the predicted value; 26.4(8)° compared to 26.6°. A similar torsion angle of 25.3(9)° was observed experimentally for the arsenic structure, compared to the calculated value of 24.3°.

Observed geometric parameters are generally consistent with those for a number of closely related compounds. For example, the experimental ranges of Si-C bond lengths in the bis(disyl)phosphinyl radical (1.875-1.905 Å) and the bis(disyl)arsinyl radical (1.869-1.893 Å) are close to the ranges of values found in GED refinements for other bis(disyl) compounds, including bis(disyl)germanium (1.881-1.896 Å)[23] and bis(disyl)tin (1.882-1.897 Å).[23] The refined values of the P-C [1.856(11) Å] and As-C [1.986(8) Å] bond lengths are rather longer than the corresponding bonds in less crowded molecules, e.g. PMe_3 [1.847(3) Å][24] and $AsMe_3$ [1.968(3) Å].[25]

7.3.3 Structural Differences Between the Gas-phase Phosphorus and Arsenic Structures

The gas-phase structures of the bis(disyl)phosphinyl and arsinyl radicals are very similar, with the main differences between the two associated with the central phosphorus and arsenic atoms. The experimental structures of bis(disyl)germanium and tin differ mainly in the Y-C distances and the C-Y-C angles. The Y-C bond length increased from 2.038(15) to 2.220(2) Å as Y changed from Ge to Sn whilst the C-Y-C bond angle decreased from 107.0(2)° to 97.0(2)°.[23] These trends are also observed in the experimental structures of the phosphinyl and arsinyl radicals but the magnitudes of the effects are much smaller, reflecting the similarity of the covalent radii of P and As (1.10 and 1.21 Å). Observed parameters included bond lengths of P-C 1.856(11) Å and As-C 1.986(8) Å, and bond angles C-P-C 103.9(10)° and C-As-C 101.2(10)°. The differences between the angle at the germanium and the arsenic atoms is an example of the valence shell electron pair repulsion theory (VSEPR). The only difference between the two systems is an electron on the arsenic atom. Thus there is lone-pair lone-pair and lone-pair bond-pair repulsion which is greater than the bond-pair bond-pair repulsion so in turn reduces the C-As-C angle at the arsenic. The Si(4)-C(2)-Si(6) angles in the two radicals are very similar and hugely distorted from the ideal tetrahedral angle around carbon of 109.5°; 117.5(5)° for the phosphorus radical and 117.3(8)° for the arsenic radical. The torsion angles [ϕC(3)-E(1)-C(2)-H(8)] are also very similar in the two radicals [26.4(8)° and 25.3(9)°], giving an approximate *syn,syn* structure with both methine hydrogens pointing towards the middle of the V-shaped conformation. This, along with the substantially increased Si-C-Si angle, serves to maximize the interligand distances within the radicals and thus reduce the strain associated with these bulky disyl ligands. There is very little residual strain associated with the fully optimized phosphorus and arsenic structures, as can be seen from the internal C-Si-C angles in the trimethylsilyl groups. In each case there are only small distortions away from the ideal tetrahedral angle of 109.5° [see Appendix 6 (Table 17)]. In the phosphorus radical, the P-C-Si angles are near tetrahedral at 109.1° for P(1)-C(2)-Si(4) and 109.8° for P(1)-C(2)-Si(6), whilst in the arsenic radical the As-C-Si(4/6) angles are slightly more distorted at 111.8 and 112.1°

respectively. The C-Si distances are slightly longer in the phosphorus radical compared to the arsenic radical. This suggests a greater strain which is most likely due to the shorter P-C bond length compared to the As-C bond length. This in turn would bring the trimethylsilyl groups closer together, and so lead to longer C-Si bond lengths in compensation.

7.3.4 Crystal Structure Data Analysis

(Carried out by Alan Cowley and Charles MacDonald, Austin, Texas)

Single-crystal X-ray diffraction experiments were performed on the dipnictines **1** and **3** in order to assess the structural changes that occur upon dimerization of the corresponding radicals **2** and **4**, bearing in mind, of course, that the dimerization also involves a change from the vapor to the solid state. It was also considered useful to determine the X-ray crystal structures of the chloropnictine starting materials in order to provide comparative metrical parameters for R_2Z fragments attached to much smaller substituents (Cl vs. R_2Z).

The molecular structures of tetra(disyl)diphosphine **(1)** and tetra(disyl)diarsine **(3)**, omitting the hydrogen atoms for clarity, bis(disyl)chlorophosphine **(5)** and bis(disyl)chloroarsine **(6)** are presented in Figures 4, 5 and 6(a) and 6(b) respectively and geometrical parameters for each are listed in Tables 5, 6, and 7.

Table 5 Bond lengths (Å) and angles (°) for tetra(disyl)diphosphine **(1)**.

Parameter	Value	Parameter	Value	Parameter	Value
P(1)-C(1)	1.892(2)	C(1)-P(1)-C(2)	103.57(9)	C(20)-Si(6)-C(21)	103.9(2)
P(1)-C(2)	1.896(2)	C(1)-P(1)-P(2)	107.92(7)	C(22)-Si(6)-C(21)	108.47(12)
P(1)-P(2)	2.3103(7)	C(2)-P(1)-P(2)	104.83(6)	C(20)-Si(6)-C(3)	115.17(11)
P(2)-C(4)	1.892(2)	C(4)-P(2)-C(3)	103.00(9)	C(22)-Si(6)-C(3)	106.35(12)
P(2)-C(3)	1.893(2)	C(4)-P(2)-P(1)	106.98(6)	C(21)-Si(6)-C(3)	115.85(12)
Si(1)-C(5)	1.854(2)	C(3)-P(2)-P(1)	105.27(7)	C(25)-Si(7)-C(24)	106.71(13)
Si(1)-C(6)	1.866(2)	C(5)-Si(1)-C(6)	104.46(13)	C(25)-Si(7)-C(23)	102.9(2)
Si(1)-C(7)	1.882(2)	C(5)-Si(1)-C(7)	110.77(12)	C(24)-Si(7)-C(23)	110.06(12)
Si(1)-C(1)	1.905(2)	C(6)-Si(1)-C(7)	103.91(12)	C(25)-Si(7)-C(4)	112.57(12)
Si(2)-C(10)	1.864(3)	C(5)-Si(1)-C(1)	109.96(10)	C(24)-Si(7)-C(4)	111.28(10)
Si(2)-C(9)	1.871(3)	C(6)-Si(1)-C(1)	111.37(11)	C(23)-Si(7)-C(4)	112.86(10)
Si(2)-C(8)	1.875(3)	C(7)-Si(1)-C(1)	115.66(10)	C(28)-Si(8)-C(27)	104.8(2)
Si(2)-C(1)	1.915(2)	C(10)-Si(2)-C(9)	107.69(12)	C(28)-Si(8)-C(26)	108.17(13)
Si(3)-C(11)	1.861(2)	C(10)-Si(2)-C(8)	103.52(13)	C(27)-Si(8)-C(26)	103.52(13)
Si(3)-C(12)	1.870(2)	C(9)-Si(2)-C(8)	107.72(13)	C(28)-Si(8)-C(4)	111.01(10)
Si(3)-C(13)	1.875(2)	C(10)-Si(2)-C(1)	114.27(10)	C(27)-Si(8)-C(4)	110.73(13)
Si(3)-C(2)	1.918(2)	C(9)-Si(2)-C(1)	112.17(10)	C(26)-Si(8)-C(4)	117.66(10)
Si(4)-C(16)	1.860(3)	C(8)-Si(2)-C(1)	110.93(11)	P(1)-C(1)-Si(1)	123.33(11)
Si(4)-C(14)	1.864(2)	C(11)-Si(3)-C(12)	107.07(11)	P(1)-C(1)-Si(2)	111.88(10)
Si(4)-C(15)	1.877(3)	C(11)-Si(3)-C(13)	104.77(12)	Si(1)-C(1)-Si(2)	112.94(10)
Si(4)-C(2)	1.894(2)	C(12)-Si(3)-C(13)	107.65(12)	Si(4)-C(2)-P(1)	125.19(11)
Si(5)-C(18)	1.856(3)	C(11)-Si(3)-C(2)	113.69(9)	Si(4)-C(2)-Si(3)	111.21(10)
Si(5)-C(17)	1.864(3)	C(12)-Si(3)-C(2)	107.18(10)	P(1)-C(2)-Si(3)	112.35(10)
Si(5)-C(19)	1.886(3)	C(13)-Si(3)-C(2)	116.04(10)	Si(5)-C(3)-P(2)	125.07(11)
Si(5)-C(3)	1.892(2)	C(16)-Si(4)-C(14)	107.41(12)	Si(5)-C(3)-Si(6)	110.17(10)
Si(6)-C(20)	1.853(3)	C(16)-Si(4)-C(15)	109.17(14)	P(2)-C(3)-Si(6)	112.83(11)

Table 5 Continued

Parameter	Value	Parameter	Value	Parameter	Value
Si(6)-C(22)	1.875(3)	C(14)-Si(4)-C(15)	103.26(13)	P(2)-C(4)-Si(8)	123.83(11)
Si(6)-C(21)	1.876(3)	C(16)-Si(4)-C(2)	111.55(11)	P(2)-C(4)-Si(7)	110.88(10)
Si(6)-C(3)	1.926(2)	C(14)-Si(4)-C(2)	116.85(10)	Si(8)-C(4)-Si(7)	112.91(10)
Si(7)-C(25)	1.864(3)	C(15)-Si(4)-C(2)	108.11(11)		
Si(7)-C(24)	1.868(2)	C(18)-Si(5)-C(17)	108.10(14)		
Si(7)-C(23)	1.870(3)	C(18)-Si(5)-C(19)	108.95(13)		
Si(7)-C(4)	1.921(2)	C(17)-Si(5)-C(19)	102.89(14)		
Si(8)-C(28)	1.857(3)	C(18)-Si(5)-C(3)	112.30(12)		
Si(8)-C(27)	1.864(3)	C(17)-Si(5)-C(3)	115.37(11)		
Si(8)-C(26)	1.872(2)	C(19)-Si(5)-C(3)	108.70(12)		
Si(8)-C(4)	1.896(2)	C(20)-Si(6)-C(22)	106.6(2)		

Table 6 Bond lengths (Å) and angles (°) for bis(disyl)chlorophosphine **(5)**.

Parameter	Value	Parameter	Value
P(1)-C(1)	1.838(2)	C(1)-P(1)-C(2)	105.93(9)
P(1)-C(2)	1.849(2)	C(1)-P(1)-Cl(1)	105.04(7)
P(1)-Cl(1)	2.1161(8)	C(2)-P(1)-Cl(1)	97.87(7)
C(1)-Si(1)	1.910(2)	P(1)-C(1)-Si(1)	113.55(11)
C(1)-Si(2)	1.917(2)	P(1)-C(1)-Si(2)	108.32(10)
C(2)-Si(3)	1.898(2)	Si(1)-C(1)-Si(2)	112.74(10)
C(2)-Si(4)	1.907(2)	P(1)-C(2)-Si(3)	122.07(11)
Si(1)-C(11)	1.864(3)	P(1)-C(2)-Si(4)	107.58(10)
Si(1)-C(13)	1.865(3)	Si(3)-C(2)-Si(4)	115.39(10)
Si(1)-C(12)	1.869(2)	C(11)-Si(1)-C(13)	110.61(14)
Si(2)-C(22)	1.863(2)	C(11)-Si(1)-C(12)	104.17(13)
Si(2)-C(23)	1.864(3)	C(13)-Si(1)-C(12)	108.84(12)
Si(2)-C(21)	1.874(3)	C(11)-Si(1)-C(1)	111.26(11)
Si(3)-C(32)	1.861(3)	C(13)-Si(1)-C(1)	109.20(11)
Si(3)-C(33)	1.863(2)	C(12)-Si(1)-C(1)	112.66(11)
Si(3)-C(31)	1.872(3)	C(22)-Si(2)-C(23)	111.28(12)
Si(4)-C(41)	1.861(3)	C(22)-Si(2)-C(21)	105.33(13)
Si(4)-C(43)	1.865(3)	C(23)-Si(2)-C(21)	105.72(13)
Si(4)-C(42)	1.871(3)	C(22)-Si(2)-C(1)	112.77(11)
		C(23)-Si(2)-C(1)	108.48(11)
		C(21)-Si(2)-C(1)	113.05(10)
		C(32)-Si(3)-C(33)	105.33(12)
		C(32)-Si(3)-C(31)	106.30(14)
		C(33)-Si(3)-C(31)	109.48(13)
		C(32)-Si(3)-C(2)	115.76(10)
		C(33)-Si(3)-C(2)	112.69(10)
		C(31)-Si(3)-C(2)	107.02(11)
		C(41)-Si(4)-C(43)	108.9(2)
		C(41)-Si(4)-C(42)	110.4(2)
		C(43)-Si(4)-C(42)	105.66(12)
		C(41)-Si(4)-C(2)	111.41(11)
		C(43)-Si(4)-C(2)	110.30(11)
		C(42)-Si(4)-C(2)	110.01(12)

Table 7 Bond lengths (Å) and angles (°) for bis(disyl)chloroarsine **(6)**.

Parameter	Value	Parameter	Value
As(1)-C(1)	1.980(3)	C(1)-As(1)-C(2)	103.14(13)
As(1)-C(2)	1.981(3)	C(1)-As(1)-Cl(1)	103.15(10)
As(1)-Cl(1)	2.2311(11)	C(2)-As(1)-Cl(1)	97.28(10)
Si(4)-C(42)	1.870(4)	C(42)-Si(4)-C(43)	105.1(2)
Si(4)-C(43)	1.871(4)	C(42)-Si(4)-C(41)	110.3(2)
Si(4)-C(41)	1.871(4)	C(43)-Si(4)-C(41)	106.9(2)
Si(4)-C(2)	1.890(4)	C(42)-Si(4)-C(2)	106.9(2)
Si(2)-C(21)	1.865(5)	C(43)-Si(4)-C(2)	115.2(2)
Si(2)-C(23)	1.869(4)	C(41)-Si(4)-C(2)	112.3(2)
Si(2)-C(22)	1.871(4)	C(21)-Si(2)-C(23)	103.9(2)
Si(2)-C(1)	1.896(3)	C(21)-Si(2)-C(22)	110.0(2)
Si(1)-C(13)	1.859(4)	C(23)-Si(2)-C(22)	108.7(2)
Si(1)-C(12)	1.865(5)	C(21)-Si(2)-C(1)	111.3(2)
Si(1)-C(11)	1.866(5)	C(23)-Si(2)-C(1)	112.6(2)
Si(1)-C(1)	1.908(3)	C(22)-Si(2)-C(1)	110.1(2)
Si(3)-C(33)	1.859(5)	C(13)-Si(1)-C(12)	106.4(3)
Si(3)-C(32)	1.868(5)	C(13)-Si(1)-C(11)	111.1(2)
Si(3)-C(31)	1.870(5)	C(12)-Si(1)-C(11)	105.9(3)
Si(3)-C(2)	1.903(3)	C(13)-Si(1)-C(1)	112.0(2)
		C(12)-Si(1)-C(1)	112.7(2)
		C(11)-Si(1)-C(1)	108.5(2)
		C(33)-Si(3)-C(32)	106.0(3)
		C(33)-Si(3)-C(31)	108.6(3)
		C(32)-Si(3)-C(31)	109.4(3)
		C(33)-Si(3)-C(2)	109.8(2)
		C(32)-Si(3)-C(2)	111.3(2)
		C(31)-Si(3)-C(2)	111.5(2)
		Si(2)-C(1)-Si(1)	114.0(2)
		Si(2)-C(1)-As(1)	113.3(2)
		Si(1)-C(1)-As(1)	107.4(2)
		Si(4)-C(2)-Si(3)	115.3(2)
		Si(4)-C(2)-As(1)	122.0(2)
		Si(3)-C(2)-As(1)	106.3(2)

Figure 4 Crystal structure of $\{P[CH(SiMe_3)_2]_2\}_2$ **(1)** omitting the hydrogen atoms.

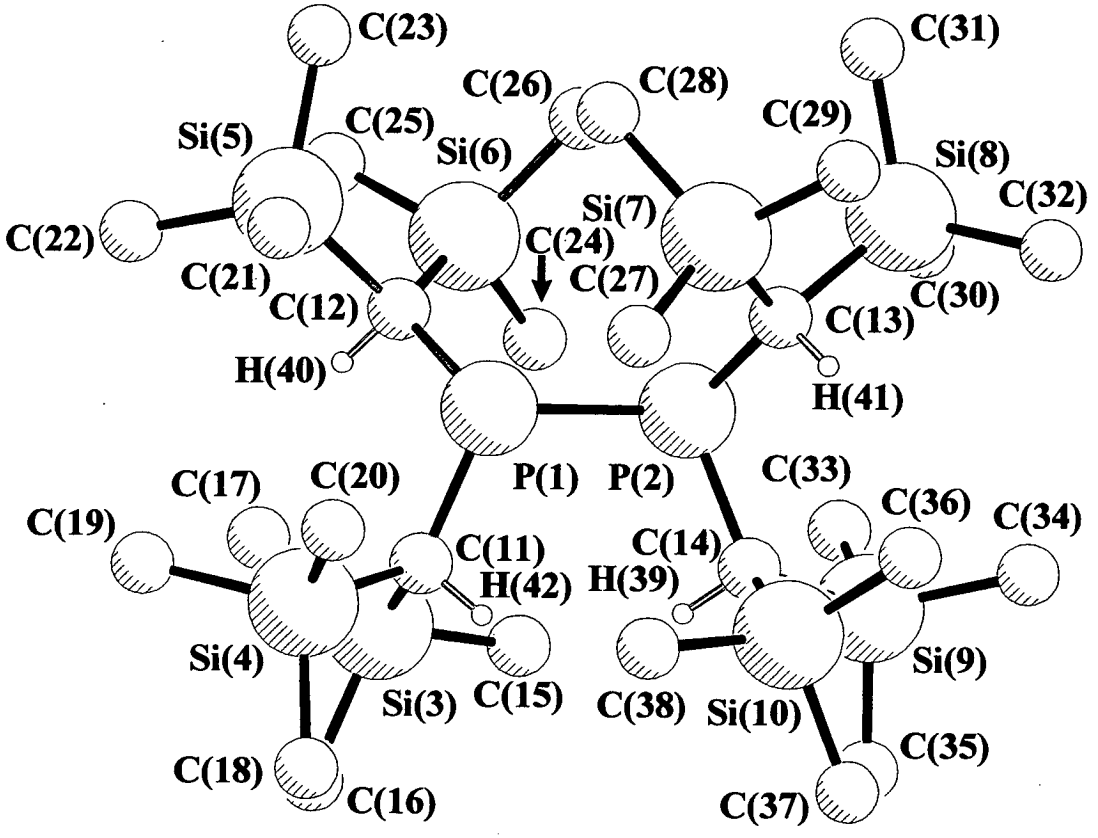

Figure 5 Crystal structure of $\{As[CH(SiMe_3)_2]_2\}_2$ **(3).**

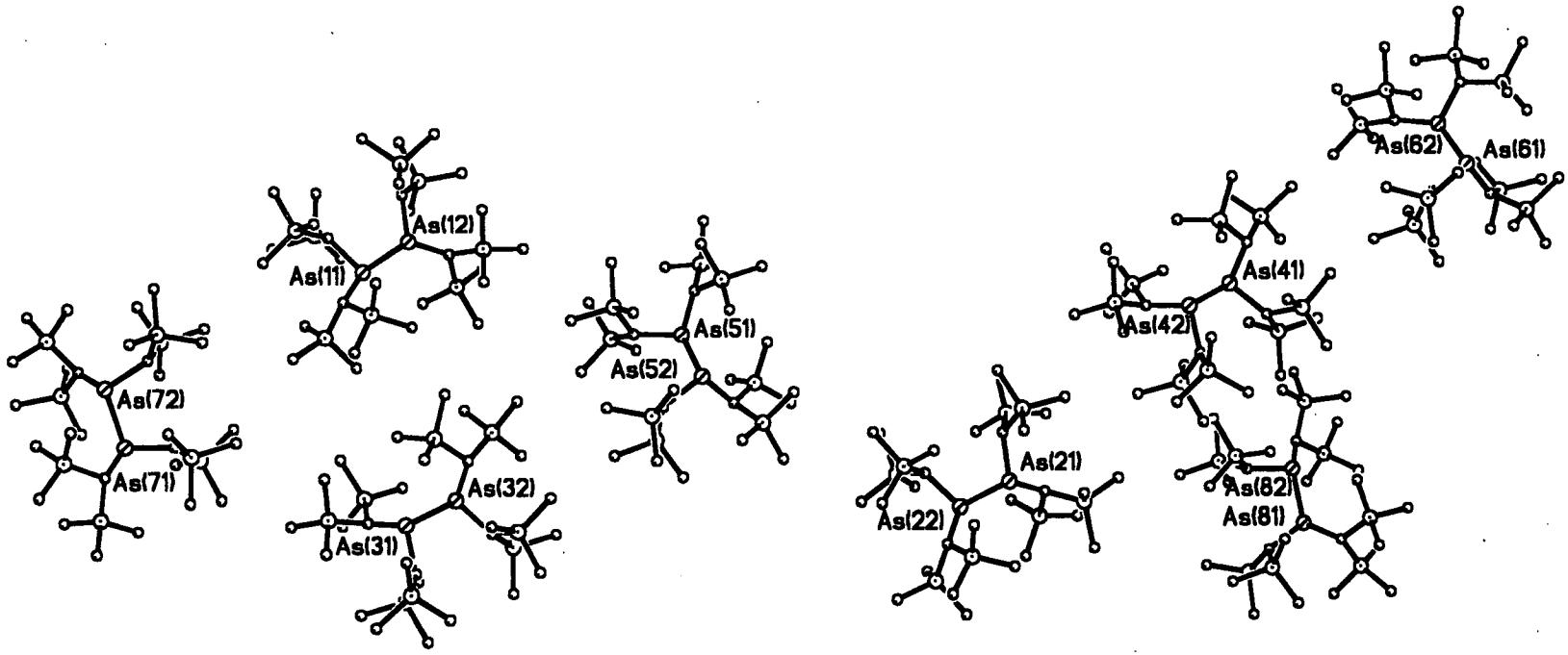

Figure 6 Crystal structures of (a) $PCl[CH(SiMe_3)_2]_2$ **(5)** and (b) $AsCl[CH(SiMe_3)_2]_2$ **(6)**.

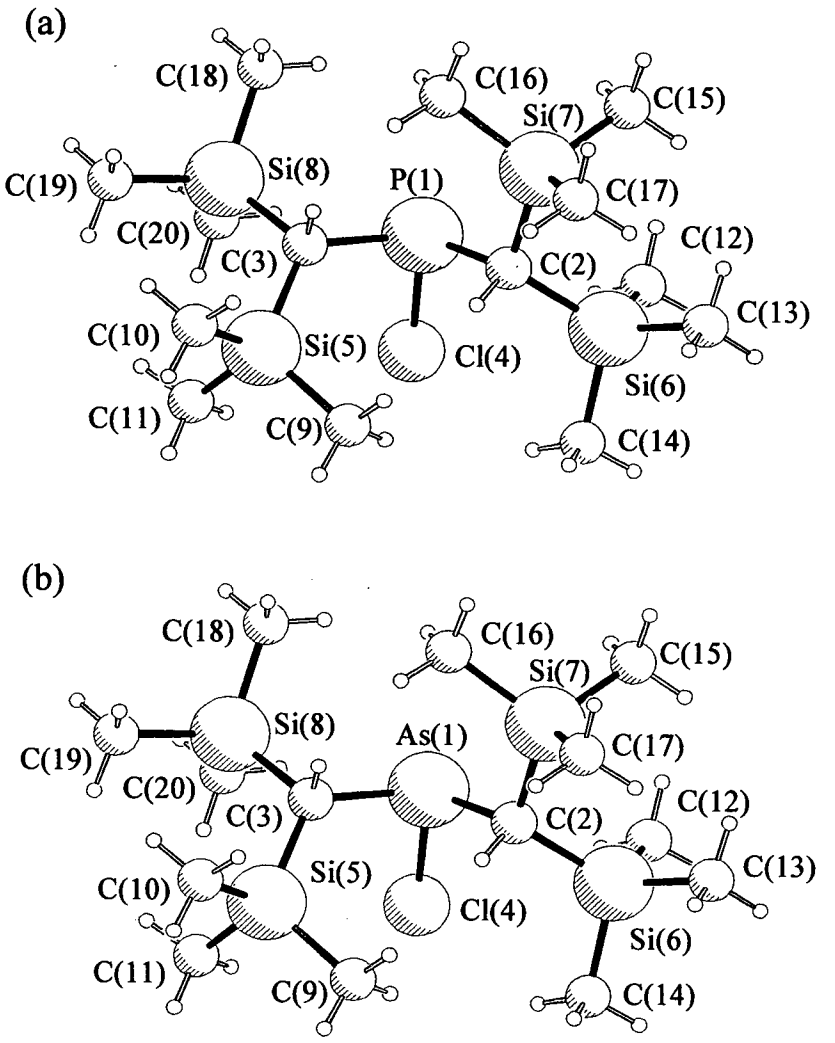

7.3.5 Discussion of the Chloropnictine Structures

The molecular structures of the bis(disyl)chloropnictines **(5)** and **(6)** are isotypical, each possessing the expected pyramidal geometry at Z; the sums of angles at Z are 308.8° for **(5)** and 303.6° for **(6)**. In each bis(disyl)chloropnictine, one disyl group is orientated in a way very similar to that adopted by both groups in the radicals, but the second group is twisted nearly an extra 30°, to reduce contact with the chlorine atom (see Figure 6). No significant intermolecular interactions are observed in either structure and the geometrical parameters in each are predictable. Incredibly, bis(disyl)chlorophosphine and

bis(disyl)chloroarsine represent the first examples of uncomplexed dialkylchloropnictines that have been characterized by X-ray crystallography, as confirmed by a search of the Cambridge Structural Database.[26] The structural features of bis(disyl)chlorophosphine are most appropriately compared to those found in the two other structurally characterized compounds containing the $P(disyl)_2$ fragment, $\{RhCl(cod)[PCl(disyl)_2]\}$[27] and $[PLi(disyl)_2]_2$,[28] both of which also feature *syn,syn* orientation of the two disyl ligands. The P-C distances in **(5)** [1.838(2) and 1.849(2) Å] are indistinguishable from those found in the rhodium complex [1.838(4) Å] and are, as expected, somewhat shorter than those of the phosphinyl radical [1.887(7) to 1.898(5) Å]. In fact, the P-C bond lengths are typical of those observed in a variety of P-disyl compounds such as $[P(disyl)]_3$ [1.856(9) to 1.869(9) Å][29] or even the coordinated diphosphene $\{Cr(CO)_5[P(disyl)]_2\}$ [1.824(6) and 1.836(6) Å].[30] Likewise the C-P-C angle in bis(disyl)chlorophosphine [105.9(9)°] falls within the range bounded by $[PLi(disyl)_2]_2$ [105.2(2)°] and $\{RhCl(cod)[PCl(disyl)_2]\}$ [111.8(2)°] and the P-Cl bond length [2.116(8) Å] is not unusual {*c.f.* $Cl_3Ga(PClPr^i_2)$: 2.01(2) Å;[31] Mes*Fl*(H)PCl: 2.098(2) Å;[32] $[PBu^t_2(GeCl_3)AgBr_2Ag(PBu^t_2Cl)]_2$: 2.070(4) Å;[33] $\{RhCl(cod)[PCl(disyl)_2]\}$: 2.090(2) Å;[27] $[(\mu_3\text{-}Bu^tC)_2(PCl)_3]$: 2.078(2) Å[34]}.

There are no other structures of compounds containing the $As(disyl)_2$ fragment in the literature, and so comparisons are best made with other analogues. The majority of compounds containing As-disyl bonds are in phospha-arsenes (disylAs=PR),[35] diarsenes (disylAs=AsR)[36] or transition metal complexes thereof.[37] The As-C(disyl) bond lengths in these compounds range from 1.937(7)[37(c)] to 1.995(5) Å[35(a)], and are comparable to the distances of 1.980(3) and 1.981(3) Å found in bis(disyl)chloroarsine **(6)**. A significantly longer As-disyl bond [2.022(4) Å] is found in $[(Ph_3Si)disylAsGaBu^t_2]$,[38] the only other formally As(III)-disyl compound. The C-As-C angle of 103.1(13)° in bis(disyl)chloroarsine is best compared to that of Ph_2AsCl[39] [105(2)°]. The As-Cl bond length of 2.231(11) Å in bis(disyl)chloroarsine compares well with those of Ph_2AsCl [2.26(2) Å] and cyclic diarylchloroarsines such as 10-phenoxarsine chloride[40] [2.255(5) Å], 10-chloro-5,10-dihydrophenarsazine[41] [2.301(4) Å], and 10-chlorophenothiarsenin[42] [2.241(1) Å].

7.3.6 Discussion of the Dimeric Phosphorus Structure

In contrast to the bis(disyl)chloropnictines, the geometrical parameters for tetra(disyl)diphosphine **(1)** are exceptional. The most interesting structural feature is the length of the P-P bond [2.310(7) Å]. This is the longest P-P bond yet reported for a diphosphine, but it is no where near long enough to cause the dimer to fall apart. The observed dissociation must therefore also reflect release of strain in other parts of the diphosphine. Previously reported distances for uncoordinated diphosphines include 2.260(1) Å for $[Mes_2P]_2$,[43] 2.215(3) Å for $[Cy_2P]_2$,[44] 2.211(2) and 2.206(2) Å for $\{[Bu^t(O)C]PhP\}_2$,[45] and 2.212(1) Å for $[Me_2P]_2$.[46] The P-P bond length in tetramethyldiphosphine does not change drastically upon complexation to boranes; these complexes feature slightly shortened P-P distances of 2.208(5) Å for $[Me_2P\text{-}BH_3]_2$,[47] 2.189(5) Å for $[Me_2P\text{-}BBrH_2]_2$ and 2.190(1) Å for $[(\mu_2\text{-}H_2B)Me_2P\text{-}PMe_2]_2$.[48] The partially eclipsed *anti* arrangement of the disyl ligands in the diphosphine is similar to the geometries observed in the other diphosphines with sterically demanding substituents such as $[Mes_2P]_2$,[43] $[Cy_2P]_2$[44] and $\{[Bu^t(O)C]PhP\}_2$.[45] The extent of eclipsing, as demonstrated by the C(1)-P(1)-P(2)-C(4) dihedral angle of 32.0°, falls between those of $[Cy_2P]_2$ (5.5°) and $[Mes_2P]_2$ (50.8°). As expected, the C(2)-P(1)-P(2)-C(3) dihedral angle of 109.0° also lies between the values of the corresponding angles in $[Cy_2P]_2$ (137.6°) and $[Mes_2P]_2$ (94.4°). Tetramethyldiphosphine, with much less bulky substitiuents, exhibits a symmetric *trans* geometry, which suggests that the twisting from the ideal arrangement is controlled by the packing requirements of the substituents. The C-P-C angles in tetra(disyl)diphosphine **(1)** [103.6(9)° and 103.0(9)°] are indistinguishable from those of $[Cy_2P]_2$ [103.1(3)° and 103.8(4)°] and $[Mes_2P]_2$ [103.5(2)°].

A most interesting feature of the molecular structure of the diphosphine is the *syn,anti* orientation of the disyl ligands on each $P(disyl)_2$ fragment (see above). Such an arrangement allows for more efficient packing of the ligands in the dimer than does the *syn,syn* orientation which is found in the radical monomer. However, the price of this packing is that there is substantial steric strain, (a) within each disyl group, i.e. between the two trimethylsilyl groups, (b) between the two disyl groups attached to each phosphorus atom, and (c) between the disyl groups on the two halves of the

molecule. That the strain is much greater in the diphosphine (dimer) than in the radical (monomer) can be easily seen by considering the angular distortions at the silicon atoms and the central carbon atoms in the two species. Tables 5 and Appendix 6 [Table 17] include all the individual angles, but the effects are shown simply by the root-mean-square variance from their means of the angles at carbon and silicon. In the gaseous radical these are 3.88 and 2.55° respectively, whereas in the dimer they are no less than 17.96 and 4.06°. There are also increases in some, but not all, bond lengths in the dimer, so the whole structure is a store of energy, much of which can be released when it dissociates. The magnitude of this effect has been explored in calculations which are discussed below. It is noteworthy that the other diphosphines with sterically demanding substituents such as $[Cy_2P]_2$, $[Mes_2P]_2$, $[Bu^t_2P]_2$[49] and $[(CF_3)_2P]_2$[50] maintain the P-P bonding in solution and the gas phase.

7.3.7 Comparison of the Chlorinated Solid and Radical Gaseous Phosphorus and Arsenic Structures

The structures of bis(disyl)chlorophosphine and bis(disyl)chloroarsine in the crystalline phase are quite different from those of the radicals in the gas phase. This is most probably due to the presence of the large electron-withdrawing chlorine atom attached to the central atom. In the solid arsenic structure **(6)**, the As-C bond length is shorter than in the computed structure of **(4)** by *ca.* 0.03 Å whilst the C(2)-As(1)-C(3) bond angle is wider by 2°. The torsion angles [ϕ(C-As-C-H)] differ dramatically, both being *ca.* 25° in the gas phase radical (C_2 symmetry), whereas there are two different angles of 26.2° and 51.7° in the solid phase bis(disyl)chloroarsine. Similar differences are observed for the phosphorus analogues with the P-C bond length shorter by *ca.* 0.02 Å and the C(2)-P(1)-C(3) bond angle wider by 2° in bis(disyl)chlorophosphine. The torsion angles [ϕ(C-P-C-H)] again show a marked change from 26° in the gas to 30.3° and 53.5° in the solid.

These structural changes provide evidence for both steric and electronic effects of the chlorine atom on the structures. The changes of up to 30° for both bis(disyl)chlorophosphine and arsine [ϕC(3)-Z(1)-C(2)-H(8)] torsion angles can be

attributed to the bulky alkyl ligands being forced to rotate away from the large chlorine atom situated between them. In turn, the Si(4)-C(2)-Si(6) bond angles are observed to decrease to 114.1°(av.) in bis(disyl)chlorophosphine and 114.6°(av.) in bis(disyl)chloroarsine from 117.5(5)° and 117.3(8)° in the radicals. The trimethylsilyl groups are thus being forced closer together by the presence of the chlorine atom. The general decreases in bond length and increases in bond angle around the atom with the chlorine attached to it can be attributed to the electron-withdrawing effect of the chlorine atom. This is a standard effect; as the electron-withdrawing atom reduces the electron density in the Z-C bonds, they get shorter. Valence-shell electron-pair repulsion theory can then explain the wider C-Z-C angle that occurs with the electron-withdrawing group present.

7.3.8 Comparison of the Solid Dimer and Gaseous Monomer (Radical) Structures of Bis(disyl)phosphorus

The main difference between the dimeric and monomeric phosphorus structures is in the orientation of the bulky alkyl ligands around the central phosphorus atom. As can be seen from Figure 4, the conformation of each PR_2 moiety in P_2R_4 approximates to *syn,anti* [ϕC(3)-P(1)-C(2)-H(8)= -4°, ϕC(2)-P(1)-C(3)-H(9)= 123°] and the four ligands R are orientated around the central P-P bond in such a way that the outside of the molecule is a ball of hydrogen atoms. In the gaseous structure [Figure 1(a)], the V-shaped C_2 conformation approximates to *syn,syn*, [ϕC(3)-P(1)-C(2)-H(8) = 26°], with the methine hydrogens pointing inside the V and the alkyl groups pointing outwards to minimize the steric strain associated with these bulky ligands.

Thus a lot of structural rearrangement occurs upon dissociation of the dimer to the monomer, with very large changes in the bond lengths and angles within the ligands. The most dramatic change to bond lengths occurs in the P-C distance, which shortens by almost 0.04 Å from the solid (1.892 - 1.896 Å) to the gaseous structure [1.856(11) Å]. This is a very good indicator of the inter-ligand strain that is associated with the dimeric system, with the disyl groups positioning themselves as far apart as possible. The C-P-C angle increases insignificantly upon dissociation to

103.9(10)° as opposed to 103.6(9) and 103.0(9)° in the solid structure. In the dimer, the C-P-C angle is dictated by the effects of the four disyl ligands pushing against one another. In the gaseous structure, the ligands are still close to one another, but the structure is no longer strained and so the C-P-C angle only increases slightly upon dissociation.

However, the Si-C-Si angles increase dramatically from a range of 110.2 - 112.9° in the dimer to 117.5(5)° in the radical. Thus, because of the conformational changes, the two trimethylsilyl groups in one disyl group are free to move away from each other and so reduce the intra-ligand strain which is a feature of the dimer. There is a slight shortening of some of the inner Si-C bonds observed in the radical, whilst the outer Si-C bonds show a much smaller range of values in the monomer than in the dimer (gas = 1.875 - 1.880 Å, solid = 1.853 - 1.905 Å). This is to be expected; as the Si-C-Si angles widen on dissociation, the Si-C bonds shorten slightly while the trimethylsilyl groups move further apart and so reduce the strain within the disyl ligand itself.

7.3.9 Analysis of As_2R_4 crystal structure

The determination of the crystal structure of tetrakis[bis(trimethylsilyl)-methyl]diarsine proved to be a mammoth task in itself with no less than eight molecules being found in the asymmetric unit. However, each molecule adopts a *syn,anti* conformation which is similar to that observed for diphosphine **(1)**. Specifically, each arsinyl moiety has one $CH(SiMe_3)_2$ group twisted by ~ 15° in one direction while the other is twisted by ~ 130° in the other. The significance of this observations is that it demonstrates that the *syn,anti* arrangement is still necessary despite the larger size of arsenic, thus supporting our preliminary conclusions regarding the role of the $CH(SiMe_3)_2$ ligands in the phosphinyl/diphosphine system (see above). The presence of a relatively large number of crystallographically independent molecules (determined under identical experimental conditions) also afforded a rare opportunity to analyze the effects of crystal packing by scrutiny of the

variations in dihedral angles, bond angles and bond distances among the eight individual molecules.

Of the eight molecules chosen to represent the asymmetric unit, three are of the opposite hand to the other five. With overall $P\bar{1}$ symmetry, there is, of course, an exactly opposite group of molecules where five are of the opposite hand to the other three. However, when all molecules of the same hand are chosen, they are scattered over a large area, so the mixture was taken as the best representation of the asymmetric unit. All eight molecules were found to have approximate C_2 molecular symmetry, with molecule #2 of eight being very close to this symmetry. The rest deviate primarily in the torsion angles about the C(2)-Si(4) and related C(3)-Si(6) bonds, but are almost identical to one another (See Figure 7 for atom numbering). In each molecule, one group is twisted ~30° in one direction and one is twisted ~30° in the other direction. This deviation allows the two trimethylsilyl groups at opposite ends of the molecule, but close in space, to mesh together. Figure 8 shows the structures of molecule #1 (~C_2 symmetry) and molecule #2 (C_2 symmetry).

As molecule #2 of eight was found to be different from the other seven it was omitted from the overall analysis. The seven single molecules were taken and the averages of dihedral angles, bond angles and bond distances for equivalent parts of the molecules were determined. Extreme care was taken that corresponding atoms in different molecules were used.

The results for the analysis of the dihedral angles, bond angles and bond distances, as well as average values and root-mean-square deviations for each geometric parameter, are shown in Tables 9-11.

Figure 7 Generic numbering system for all molecules of As_2R_4.

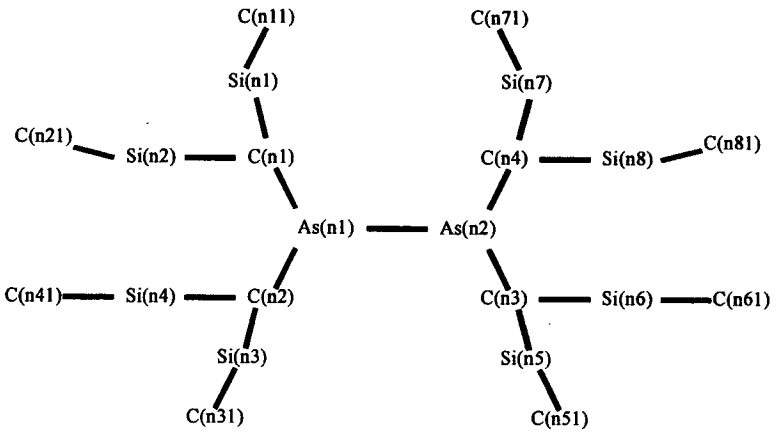

Figure 8 Structures of molecules #1 and #2 in As_2R_4.

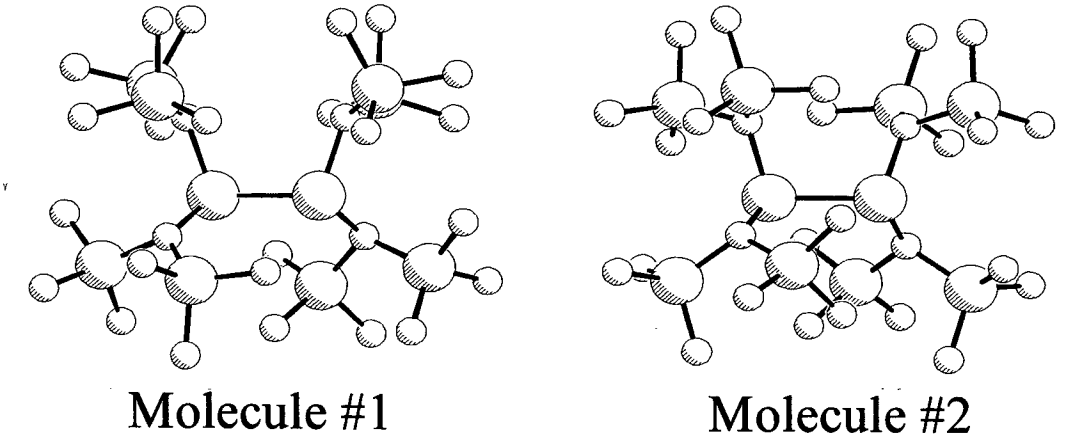

As can be seen from Table 9, the root-mean-square deviations for the sets of dihedral angles average 1.5°. The deviations for the individual parameters are consistently close to the mean value. This compares to a typical e.s.d of 0.5° for a crystallographic dihedral angle. There is therefore remarkably little variation in dihedral angles throughout all seven molecules, about 1.0° on each dihedral angle can be attributed to packing effects. This indicates that there is no significant torsional freedom within the molecules. Not even one of the eight trimethylsilyl groups can rotate freely, a situation which is most unusual and highlights the control of ligand close-packing on the solid state structure.

Table 10 shows the mean of root-mean-square differences of the sets of angles to be 0.7°, compared to a typical e.s.d of 0.5° for measured angles. On average therefore, only 0.2° of the distortion of any one angle can be attributed to packing. Thus the observed differences between angles at any given atom are due to *molecular* structure effects and not to *crystal* packing. Looking at the average As-C-Si angles in related halves of the molecules is a very good illustration of this. For example the As(n1)-C(n1)-Si(n1) mean is 120.8° whereas As(n1)-C(n1)-Si(n2) averages 113.8°. These values agree well with the related halves of the molecules [As(n2)-C(n4)-Si(n8/n7) = 121.0 and 113.9° respectively]. These angles are all in the upper, less crowded, half of the molecule shown in Figure 8. However, in the lower half of the molecules, As(n1)-C(n2)-Si(n3/n4) were observed to average 105.2(5) and 130.7(7)° compared to As(n2)-C(n3)-Si(n5/n6) [106.4(6) and 117.7(11)°]. Not only is the range of the angles around C(n2) staggering (24-27° difference in all seven molecules), but it can also be seen that it is the angles to Si(n4) that are the most distorted.

When looking at the $C_{methine}$-Si-C_{methyl} angles, the greatest distortion was observed around Si(n4), with a range of angles being 105.9 – 118.2° compared to just 109.2 – 113.5° about the related Si(n6). Analysis of the C_{methyl}-Si-C_{methyl} angles yields another surprising result. This time it is the range about Si(n6) that is greater (103.9 – 111.0°) than that about Si(n4) (104.8 – 107.4°). All the other related ranges for left and right halves of the molecules were found to be very consistent with one another.

Table 11 shows an average root-mean-square difference of 0.013 Å for the sets of distances compared to a typical e.s.d of 0.008 Å. As can be seen from the table, all the inner Si-C bond lengths are longer than the outer ones, and there is slight evidence that C(n1)-Si(n2) and C(n4)-Si(n7) are longer than the rest, but this is not very significant. There is no significant variation in the outer Si-C bond lengths at all.

It can be concluded from the analysis of the seven molecules that packing causes, on average, a change of 0.005 Å in all bond lengths, 0.2° in bond angles and (1.0°) in torsion angles. The small conformational effects are an unusual feature of this

fascinating molecule, given that small torsional force constants would normally allow relatively free twisting of the various groups. In contrast, there are huge distortions common to all seven molecules (and largely related in the eighth molecule). These distortions, most markedly of angles at C(n2), Si(n4) and Si(n6), allow the trimethylsilyl groups to mesh together within the overall framework of the molecule.

Molecule #2 shows that there is not only one possible conformation. Figure 8 shows that the major difference, the orientation of the groups containing Si(24) and Si(26), has ramifications throughout the whole molecule. Comparison of the parameters in the top and bottom halves of the dihedral angles in Table 12 show that the molecule is very close to having C_2 symmetry.

In the crystal structure of the analogous diphosphine, there is just one molecule in the asymmetric unit, with C_2 symmetry. The parameters in this molecule are remarkably similar to those observed for molecule #2 of the diarsine. Key parameters for the diphosphine are also listed in Table 12. If C_2 molecules can pack perfectly well in the crystal of the diphosphine, why is it necessary for seven out of every eight of them to adopt a different structure in the diarsine crystals?

Table 9 Geometric parameters, mean values and root-mean-square deviations for dihedral angles in molecules #1,#3-#8 of tetrakis[bis(trimethylsilyl)methyl]diarsine. Angles in degrees.

Parameter	#1	#3	#4	#5	#6	#7	#8	Mean	rms deviation	typical e.s.d
C(n1)-As(n1)-As(n2)-C(n3)	-133.5	-132.8	-134.4	-134.8	-137.9	-130.8	-132.6	-133.8	2.1	0.3
Si(n1)-C(n1)-As(n1)-As(n2)	-83.8	-84.8	-87.1	-85.6	-83.5	-85.6	-85.3	-85.1	1.1	0.5
Si(n2)-C(n1)-As(n1)-As(n2)	128.8	130.6	128.8	130.2	130.6	128.8	128.8	129.5	0.8	0.4
Si(n3)-C(n2)-As(n1)-As(n2)	-154.7	-152.7	-154.6	-150.7	-152.9	-153.3	-152.0	-153.0	1.3	0.4
Si(n4)-C(n2)-As(n1)-As(n2)	-13.4	-15.2	-16.8	-10.8	-13.3	-13.6	-14.1	-13.9	1.7	0.5
C(n11)-Si(n1)-C(n1)-As(n1)	46.3	46.7	49.4	50.3	48.5	48.7	48.9	48.4	1.3	0.6
C(n21)-Si(n2)-C(n1)-As(n1)	116.6	113.9	114.8	112.1	116.5	114.4	113.4	114.5	1.5	0.5
C(n31)-Si(n3)-C(n2)-As(n1)	-48.1	-51.8	-46.7	-52.3	-51.2	-50.2	-50.7	-50.1	1.9	0.6
C(n41)-Si(n4)-C(n2)-As(n1)	139.8	142.0	138.0	140.2	137.0	140.4	140.8	139.7	1.6	0.5
Si(n8)-C(n4)-As(n2)-As(n1)	-87.6	-84.3	-88.6	-83.4	-86.3	-85.1	-82.8	-85.4	2.0	0.5
Si(n7)-C(n4)-As(n2)-As(n1)	128.8	129.6	127.9	131.5	130.5	128.6	128.2	129.3	1.2	0.4
Si(n5)-C(n3)-As(n2)-As(n1)	-153.4	-158.0	-156.1	-157.4	-156.6	-155.7	-157.5	-156.4	1.4	0.3
Si(n6)-C(n3)-As(n2)-As(n1)	-25.8	-30.8	-28.3	-29.1	-27.5	-28.1	-30.9	-28.6	1.7	0.5
C(n81)-Si(n8)-C(n4)-As(n2)	50.5	46.7	50.0	48.2	51.3	47.4	45.3	48.5	2.0	0.7
C(n71)-Si(n7)-C(n4)-As(n2)	112.7	113.0	111.7	114.8	113.8	111.7	113.1	113.0	1.0	0.5
C(n51)-Si(n5)-C(n3)-As(n2)	-39.5	-43.7	-38.3	-42.1	-39.5	-41.2	-39.8	-40.6	1.7	0.5
C(n61)-Si(n6)-C(n3)-As(n2)	80.6	83.9	82.4	80.5	80.0	82.9	85.0	82.2	1.8	0.7
								mean	1.5	0.5

Table 10 Geometric parameters, mean values and root-mean-square deviations for bond angles in molecules #1,#3-#8 of tetrakis[bis(trimethylsilyl)methyl]diarsine. Angles in degrees.

Parameter	#1	#3	#4	#5	#6	#7	#8	Mean	rms deviation	typical e.s.d
C(n1)-As(n1)-C(n2)	102.3	102.9	102.4	101.7	101.7	102.3	101.6	102.1	0.5	0.3
As(n2)-As(n1)-C(n1)	103.6	103.1	102.9	104.2	102.5	103.7	103.9	103.4	0.6	0.2
As(n2)-As(n1)-C(n2)	104.6	105.7	105.6	104.6	106.0	105.5	105.8	105.4	0.5	0.2
As(n1)-C(n1)-Si(n1)	120.3	120.9	121.3	121.1	121.0	120.5	120.3	120.8	0.3	0.4
As(n1)-C(n1)-Si(n2)	113.6	114.6	114.0	113.7	113.6	113.6	113.6	113.8	0.3	0.3
Si(n1)-C(n1)-Si(n2)	117.7	115.0	114.9	115.4	116.4	116.7	116.9	116.1	1.0	0.3
As(n1)-C(n2)-Si(n3)	104.5	105.6	104.9	104.9	105.9	105.3	105.6	105.2	0.5	0.4
As(n1)-C(n2)-Si(n4)	132.0	129.9	130.7	130.8	131.0	130.4	129.7	130.6	0.7	0.3
Si(n3)-C(n2)-Si(n4)	113.2	111.8	112.1	113.1	111.9	112.9	112.2	112.5	0.6	0.5
C(n1)-Si(n1)-C(n11)	110.3	110.0	109.3	110.7	110.5	110.6	111.8	110.4	0.7	0.3
C(n1)-Si(n1)-C(n12)	116.5	116.2	117.4	117.1	116.5	116.4	116.7	116.7	0.4	0.3
C(n1)-Si(n1)-C(n13)	108.3	108.6	109.7	108.7	109.3	107.8	107.7	108.7	0.6	0.3
C(n11)-Si(n1)-C(n12)	106.0	108.7	109.0	108.6	108.8	107.7	108.0	108.1	1.0	0.4
C(n11)-Si(n1)-C(n13)	107.8	107.8	106.9	106.3	106.7	105.4	106.9	106.8	0.8	0.4
C(n12)-Si(n1)-C(n13)	107.7	105.2	104.1	104.8	104.4	108.4	105.1	105.7	1.6	0.4
C(n1)-Si(n2)-C(n21)	113.2	114.6	115.2	115.0	113.9	112.7	114.1	114.1	0.8	0.3
C(n1)-Si(n2)-C(n22)	114.3	112.3	112.9	114.3	114.6	114.4	114.2	113.9	0.8	0.3
C(n1)-Si(n2)-C(n23)	107.8	108.4	107.5	106.6	107.1	107.9	108.8	107.7	0.7	0.3
C(n21)-Si(n2)-C(n22)	108.5	109.4	108.7	105.7	108.3	108.5	106.8	108.0	1.2	0.4
C(n21)-Si(n2)-C(n23)	105.1	104.5	105.3	106.8	106.0	106.1	105.2	105.6	0.7	0.4
C(n22)-Si(n2)-C(n23)	107.4	107.1	106.7	107.9	106.4	106.9	107.1	107.0	0.4	0.4
C(n2)-Si(n3)-C(n31)	112.8	111.6	112.0	109.3	111.1	112.3	111.4	111.5	1.1	0.3
C(n2)-Si(n3)-C(n32)	111.3	111.3	111.2	111.7	111.6	111.6	111.8	111.5	0.2	0.3
C(n2)-Si(n3)-C(n33)	112.5	113.1	113.3	115.2	113.1	112.2	112.4	113.1	0.9	0.3

Table 10 Continued

Parameter	#1	#3	#4	#5	#6	#7	#8	Mean	rms deviation	typical e.s.d
C(n31)-Si(n3)-C(n32)	104.0	104.8	104.2	104.6	104.5	104.7	103.5	104.3	0.4	0.4
C(n31)-Si(n3)-C(n33)	106.4	107.5	105.6	107.1	107.0	106.6	108.0	106.9	0.7	0.4
C(n32)-Si(n3)-C(n33)	109.3	108.1	110.0	108.4	109.2	109.1	109.4	109.1	0.6	0.4
C(n2)-Si(n4)-C(n41)	106.5	106.2	106.2	104.9	105.2	106.3	105.9	105.9	0.6	0.3
C(n2)-Si(n4)-C(n42)	114.1	114.5	114.5	114.1	115.9	114.1	114.6	114.5	0.6	0.3
C(n2)-Si(n4)-C(n43)	118.0	117.6	117.8	120.0	118.2	117.9	118.2	118.2	0.7	0.3
C(n41)-Si(n4)-C(n42)	108.0	107.1	106.3	108.7	107.6	106.9	107.5	107.4	0.7	0.4
C(n41)-Si(n4)-C(n43)	105.5	104.9	105.5	104.0	105.7	105.1	105.9	105.2	0.6	0.4
C(n42)-Si(n4)-C(n43)	104.2	105.8	105.7	104.5	103.6	105.8	104.2	104.8	0.9	0.4
C(n3)-As(n2)-C(n4)	103.4	104.2	103.9	104.3	103.5	104.5	103.8	103.9	0.4	0.3
As(n1)-As(n2)-C(n4)	103.9	103.6	103.1	102.8	102.9	104.3	104.2	103.5	0.6	0.2
As(n1)-As(n2)-C(n3)	103.6	102.3	102.8	102.8	102.4	103.5	105.5	103.3	1.0	0.2
As(n2)-C(n4)-Si(n8)	121.0	120.7	121.5	120.6	120.7	120.9	121.5	121.0	0.4	0.4
As(n2)-C(n4)-Si(n7)	112.2	114.6	113.6	114.1	114.1	114.3	114.4	113.9	0.8	0.3
Si(n8)-C(n4)-Si(n7)	116.4	115.9	114.8	115.9	114.9	116.1	116.7	115.8	0.7	0.3
As(n2)-C(n3)-Si(n5)	106.6	105.7	106.4	105.7	106.4	107.1	107.2	106.4	0.6	0.4
As(n2)-C(n3)-Si(n6)	116.2	117.7	118.3	119.0	119.2	116.7	116.6	117.7	1.1	0.3
Si(n5)-C(n3)-Si(n6)	113.5	113.0	112.6	113.0	112.9	112.9	112.1	112.8	0.4	0.5
C(n4)-Si(n8)-C(n81)	111.4	110.5	111.1	110.2	110.7	111.5	112.1	111.1	0.6	0.3
C(n4)-Si(n8)-C(n82)	114.9	116.0	114.5	115.0	116.5	114.0	113.3	114.9	1.0	0.3
C(n4)-Si(n8)-C(n83)	108.6	109.0	108.4	109.1	108.3	108.5	108.9	108.7	0.3	0.3
C(n81)-Si(n8)-C(n82)	108.4	107.7	108.1	110.1	109.3	108.5	107.7	108.5	0.8	0.4
C(n81)-Si(n8)-C(n83)	106.5	106.9	106.5	107.1	105.6	106.5	106.6	106.5	0.4	0.4
C(n82)-Si(n8)-C(n83)	106.8	106.3	107.8	105.0	105.9	107.5	108.0	106.8	1.0	0.4
C(n4)-Si(n7)-C(n71)	114.1	114.9	115.3	114.4	115.3	115.0	114.9	114.9	0.3	0.3
C(n4)-Si(n7)-C(n72)	113.8	113.2	113.5	114.1	114.5	112.2	112.2	113.4	0.8	0.3

Table 10 Continued

Parameter	#1	#3	#4	#5	#6	#7	#8	Mean	rms deviation	typical e.s.d
C(n1)-Si(n7)-C(n73)	107.4	107.5	107.5	107.8	106.4	109.2	108.9	107.8	0.9	0.3
C(n71)-Si(n7)-C(n72)	107.8	106.6	105.9	108.1	106.0	106.4	107.0	106.8	0.8	0.4
C(n71)-Si(n7)-C(n73)	105.9	106.4	106.5	104.6	106.3	105.9	106.4	106.0	0.6	0.4
C(n72)-Si(n7)-C(n73)	107.4	107.8	107.8	107.1	107.9	107.9	106.9	107.5	0.4	0.4
C(n3)-Si(n5)-C(n51)	113.1	112.1	112.9	113.3	111.0	113.4	114.0	112.8	0.9	0.3
C(n3)-Si(n5)-C(n52)	110.7	110.7	110.0	110.2	112.1	111.0	112.2	111.0	0.8	0.3
C(n3)-Si(n5)-C(n53)	112.2	111.8	112.8	111.0	113.2	111.7	111.4	112.0	0.7	0.3
C(n51)-Si(n5)-C(n52)	105.2	105.8	106.1	107.1	105.0	105.5	104.5	105.6	0.8	0.4
C(n53)-Si(n5)-C(n53)	106.2	106.3	105.8	104.8	106.4	105.2	105.0	105.7	0.6	0.4
C(n52)-Si(n5)-C(n53)	109.2	109.9	109.0	110.3	108.7	109.7	109.4	109.5	0.5	0.4
C(n3)-Si(n6)-C(n61)	114.7	112.3	112.3	114.3	115.0	113.2	112.4	113.5	1.1	0.3
C(n3)-Si(n6)-C(n62)	110.4	113.5	112.6	115.1	111.7	112.9	113.9	112.9	1.4	0.3
C(n3)-Si(n6)-C(n63)	110.1	109.1	110.2	108.3	109.1	109.0	108.9	109.2	0.6	0.3
C(n61)-Si(n6)-C(n62)	103.8	104.8	104.4	103.6	103.5	103.5	103.6	103.9	0.5	0.4
C(n61)-Si(n6)-C(n63)	111.3	111.4	111.2	109.8	110.6	111.5	111.3	111.0	0.6	0.4
C(n62)-Si(n6)-C(n63)	106.0	105.6	105.8	105.3	106.7	106.6	106.6	106.1	0.5	0.4
								mean	0.7	

Table 11 Geometric parameters, mean values and root-mean-square deviations for bond distances in molecules #1,#3-#8 of tetrakis[bis(trimethylsilyl)methyl]diarsine. Distances in Å.

Parameter	#1	#3	#4	#5	#6	#7	#8	Mean	rms deviation	typical e.s.d
As(n1)-C(n1)	2.059	2.013	2.011	2.032	2.037	2.051	2.060	2.038	0.019	0.006
As(n1)-C(n2)	2.047	2.047	2.043	2.039	2.023	2.056	2.046	2.043	0.009	0.009
C(n1)-Si(n1)	1.885	1.901	1.898	1.892	1.875	1.893	1.864	1.887	0.012	0.006
C(n1)-Si(n2)	1.901	1.916	1.921	1.906	1.908	1.906	1.894	1.907	0.008	0.005
C(n2)-Si(n3)	1.880	1.901	1.911	1.911	1.915	1.888	1.897	1.900	0.012	0.006
C(n2)-Si(n4)	1.911	1.902	1.901	1.876	1.904	1.874	1.914	1.897	0.015	0.009
Si(n1)-C(n11)	1.867	1.871	1.873	1.868	1.873	1.851	1.866	1.867	0.007	0.008
Si(n1)-C(n12)	1.865	1.882	1.886	1.878	1.877	1.870	1.882	1.877	0.007	0.008
Si(n1)-C(n13)	1.852	1.888	1.899	1.859	1.887	1.872	1.877	1.876	0.015	0.008
Si(n2)-C(n21)	1.858	1.888	1.873	1.891	1.874	1.859	1.876	1.874	0.012	0.008
Si(n2)-C(n22)	1.887	1.906	1.882	1.859	1.869	1.858	1.883	1.878	0.016	0.008
Si(n2)-C(n23)	1.877	1.871	1.872	1.876	1.864	1.866	1.880	1.872	0.005	0.008
Si(n3)-C(n31)	1.858	1.874	1.832	1.867	1.852	1.890	1.873	1.865	0.017	0.008
Si(n3)-C(n32)	1.874	1.880	1.848	1.862	1.892	1.873	1.892	1.874	0.015	0.008
Si(n3)-C(n33)	1.852	1.860	1.882	1.868	1.883	1.866	1.900	1.873	0.015	0.008
Si(n4)-C(n41)	1.860	1.864	1.864	1.856	1.878	1.877	1.890	1.870	0.011	0.008
Si(n4)-C(n42)	1.887	1.876	1.837	1.817	1.882	1.889	1.883	1.867	0.026	0.008
Si(n4)-C(n43)	1.844	1.863	1.858	1.887	1.868	1.886	1.879	1.869	0.015	0.008
As(n2)-C(n4)	2.042	2.026	2.028	2.022	2.026	2.016	2.011	2.024	0.009	0.008
As(n2)-C(n3)	2.060	2.028	2.038	2.033	2.020	2.031	2.025	2.034	0.012	0.008
C(n4)-Si(n8)	1.881	1.888	1.897	1.876	1.896	1.907	1.893	1.891	0.010	0.008
C(n4)-Si(n7)	1.905	1.916	1.909	1.909	1.914	1.888	1.889	1.904	0.011	0.008
C(n3)-Si(n5)	1.883	1.894	1.898	1.916	1.880	1.894	1.896	1.894	0.011	0.008
C(n3)-Si(n6)	1.881	1.890	1.892	1.863	1.917	1.884	1.897	1.889	0.015	0.008

Table 11 Continued

Parameter	#1	#3	#4	#5	#6	#7	#8	Mean	rms deviation	typical e.s.d
Si(n8)-C(n81)	1.862	1.860	1.857	1.884	1.865	1.869	1.877	1.868	0.009	0.008
Si(n8)-C(n82)	1.884	1.877	1.887	1.884	1.878	1.906	1.903	1.888	0.011	0.008
Si(n8)-C(n83)	1.877	1.873	1.864	1.872	1.868	1.866	1.894	1.873	0.009	0.008
Si(n7)-C(n71)	1.879	1.865	1.852	1.864	1.881	1.867	1.867	1.868	0.009	0.008
Si(n7)-C(n72)	1.861	1.866	1.880	1.849	1.859	1.886	1.873	1.868	0.012	0.008
Si(n7)-C(n73)	1.874	1.882	1.867	1.887	1.865	1.883	1.881	1.877	0.008	0.008
Si(n5)-C(n51)	1.873	1.861	1.875	1.859	1.884	1.875	1.867	1.871	0.008	0.008
Si(n5)-C(n52)	1.868	1.892	1.876	1.880	1.851	1.891	1.880	1.877	0.013	0.008
Si(n5)-C(n53)	1.858	1.873	1.885	1.886	1.854	1.873	1.895	1.875	0.014	0.008
Si(n6)-C(n61)	1.890	1.886	1.873	1.846	1.907	1.858	1.881	1.877	0.019	0.008
Si(n6)-C(n62)	1.865	1.862	1.854	1.847	1.869	1.829	1.908	1.862	0.023	0.008
Si(n6)-C(n63)	1.864	1.872	1.885	1.845	1.859	1.857	1.856	1.863	0.012	0.008
								Mean	0.013	

Table 12 Key parameters for molecule #2 of tetrakis[bis(trimethylsilyl)methyl]-diarsine and tetrakis[bis(trimethylsilyl)methyl]diphosphine with mean values and the root-mean-square deviations for molecules #1,#3-#8. Angles in degrees.

Parameter	Mean	rms deviation	#2 As_2R_4	P_2R_4
C(n1)-Z(n1)-Z(n2)-C(n3)	-133.8	2.1	-140.0	-141.9
Si(n1)-C(n1)-Z(n1)-Z(n2)	-85.1	1.1	-70.6	-69.7
Si(n2)-C(n1)-Z(n1)-Z(n2)	129.5	0.8	149.0	151.1
Si(n3)-C(n2)-Z(n1)-Z(n2)	-153.0	1.3	-141.8	-141.0
Si(n4)-C(n2)-Z(n1)-Z(n2)	-13.9	1.7	-3.6	-2.1
C(n11)-Si(n1)-C(n1)-Z(n1)	48.4	1.3	-65.9	-61.1
C(n21)-Si(n2)-C(n1)-Z(n1)	114.5	1.5	92.8	93.9
C(n31)-Si(n3)-C(n2)-Z(n1)	-50.1	1.9	-10.6	-9.6
C(n41)-Si(n4)-C(n2)-Z(n1)	139.7	1.6	175.7	173.9
Si(n8)-C(n4)-Z(n2)-Z(n1)	-85.4	2.0	-74.9	-70.1
Si(n7)-C(n4)-Z(n2)-Z(n1)	129.3	1.2	148.3	149.8
Si(n5)-C(n3)-Z(n2)-Z(n1)	-156.4	1.4	-139.4	-138.3
Si(n6)-C(n3)-Z(n2)-Z(n1)	-28.6	1.7	-3.4	1.9
C(n81)-Si(n8)-C(n4)-Z(n2)	48.5	2.0	64.7	65.5
C(n71)-Si(n7)-C(n4)-Z(n2)	113.0	1.0	94.0	93.3
C(n51)-Si(n5)-C(n3)-Z(n2)	-40.6	1.7	-15.8	-5.8
C(n61)-Si(n6)-C(n3)-Z(n2)	82.2	1.8	181.2	173.4
Z(n1)-C(n1)-Si(n1)	120.8	0.3	121.8	123.8
Z(n1)-C(n1)-Si(n2)	113.8	0.3	109.7	110.9
Z(n1)-C(n2)-Si(n3)	105.2	0.5	110.2	112.8
Z(n1)-C(n2)-Si(n4)	130.6	0.7	125.1	125.1
Z(n2)-C(n4)-Si(n8)	121.0	0.4	123.2	123.3
Z(n2)-C(n4)-Si(n7)	113.9	0.8	109.0	111.9
Z(n2)-C(n3)-Si(n5)	106.4	0.6	110.0	112.4
Z(n2)-C(n3)-Si(n6)	117.7	1.1	123.4	125.2

7.4 Quantification of the Dissociation Process, $Z_2R_4 \rightarrow 2 \cdot ZR_2$

The experimental evidence presented above suggests that the ligand structures of the dipnictines **1** and **3** represent an energy storage reservoir, analogous to a collection of compressed springs, which, upon dissolution, melting or evaporation, are used to effect cleavage of the Z-Z bonds. In sharp contrast, other dipnictines R'_4Z_2 with sterically demanding substituents retain their Z-Z bonding in both solution and the gas phase. To obtain a more quantitative understanding of this system, a series of density functional theory (DFT) calculations were performed with a view to quantifying the energy changes associated with the dissociation and the structural rearrangement between the solid and gaseous structures.

Because of the virtually identical behavior of the phosphorus and arsenic analogues, the calculations were only performed for the smaller R_4P_2 system. An energy diagram summarizing the results of these investigations is given in Figure 9. Single-point calculations on **1** (using the crystallographically determined geometry with C-H bond lengths fixed at 1.08 Å) and the two fragments formed by breaking the P-P bond, $\mathbf{1A_1}$ and $\mathbf{1A_2}$, predict a P-P homolysis energy of 95 kJ mol^{-1}. The hydrogen atom positions in $\mathbf{1A_2}$ were then allowed to optimize to give $\mathbf{1B_2}$ ($\mathbf{1A_2}$ and $\mathbf{1B_2}$ are more distorted than $\mathbf{1A_1}$ and $\mathbf{1B_1}$). However, a similar optimization for the whole diphosphine was beyond our current computational resources. This energy change, which reflects the correction for the difference between the crystallographically (X-ray diffraction) and theoretically (which is more akin to neutron diffraction) determined hydrogen atom positions in the moiety, was 239 kJ mol^{-1}, and it was assumed to be the same for the other monomer (and presumably approximately twice this value for **1**). The heavy atom and hydrogen atom positions for $\mathbf{1B_2}$ were then allowed to relax, to give the optimized structure of the phosphinyl radical with the *syn,anti* conformation ($\mathbf{1C_2}$). This optimization releases 52 kJ mol^{-1}, corresponding to an estimate of 17 kJ mol^{-1} for $\mathbf{1B_1}$ (Figure 9), since $\mathbf{1C_1}$ and $\mathbf{1C_2}$ must be identical by definition. Finally, rotation of one of the R ligands of the monomer around the P-C bond to form the optimized *syn,syn* conformation (**2**), analogous to that observed experimentally, releases a

further 33 kJ mol^{-1} per radical. Thus, while the initial step in the homolysis reaction is endothermic, the relaxation and rotation of the R ligands releases at least 135 kJ mol^{-1}, which is more than sufficient to render the overall process exothermic. Note that although the contribution from H-atom relaxation cannot yet be assessed explicitly, it is likely that the energy of relaxation in diphosphine **1** will roughly cancel out the energies of relaxation of the individual moieties and can be safely neglected.

Figure 9 Dissociation Process $Z_2R_4 \rightarrow 2 \cdot ZR_2$

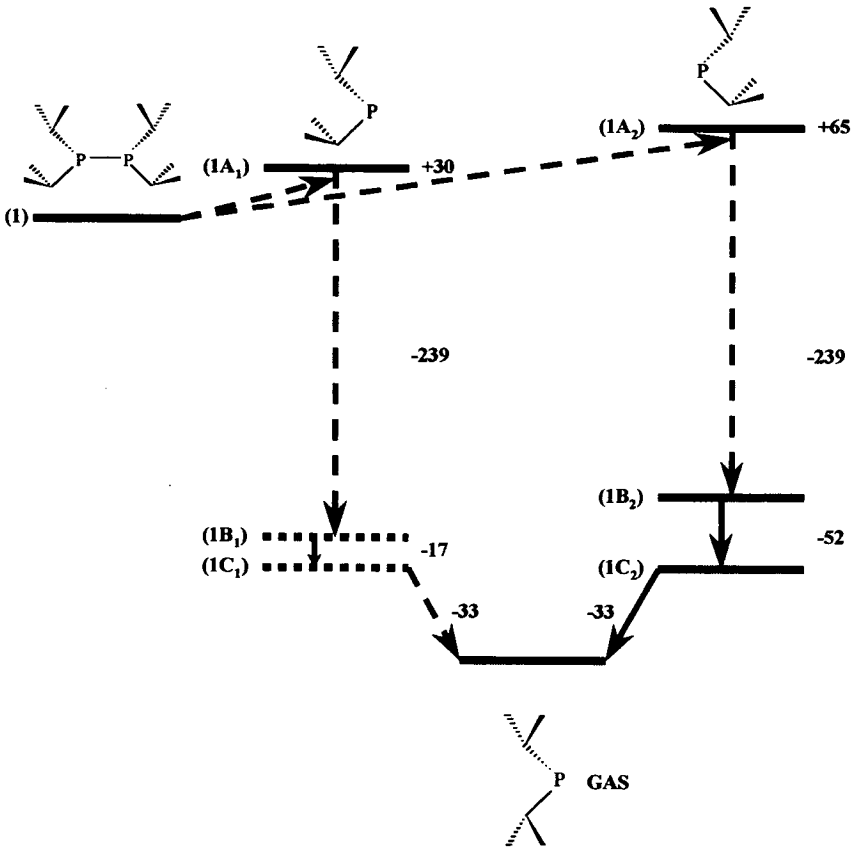

Overall, these calculations show that simple P-P bond dissociation of the diphosphine is thermodynamically unfavorable. Furthermore, the steric strain potential energy is stored by the deformation of the flexible and asymmetric $CH(SiMe_3)_2$ ligands and is released in solution or the gas phase to effect the dissociation. In fact, the release of energy is sufficient to render the pair of radicals more *thermodynamically* stable than the diphosphine in less condensed media.

7.5 References

1. S. L. Hinchley, C. A. Morrison, D. W. H. Rankin, C. L. B. Macdonald, R. J. Wiacek, A. H. Cowley, M. F. Lappert, G. Gundersen, J. A. C. Cyburne, P. P. Power, *Chem. Commun.* **2000**, 2045.
2. (a) M. J. S. Gynane, A. Hudson, M. F. Lappert, P. P. Power and H. Goldwhite, *J. Chem. Soc., Chem. Commun.*, **1976**, 623; (b) M. J. S. Gynane, A. Hudson, M. F. Lappert, P. P. Power and H. Goldwhite, *J. Chem. Soc., Dalton Trans.*, **1980**, 2428.
3. J. S. Binkley, J. A. Pople, W. J. Hehre, *J. Am. Chem Soc.* **1980**, *102*, 939.
4. M. S. Gordon, J. S. Binkley, J. A, Pople, W. J. Pietro, W. J. Hehre, *J. Am. Chem. Soc.* **1982**, *104*, 2797.
5. W. J. Pietro, M. M. Francl, W. J. Hehre, D. J. Defrees, J. A. Pople, J. S. Binkley, *J. Am. Chem. Soc.* **1982**, *104*, 5039.
6. W. J. Hehre, R. Ditchfield, J. A. Pople, *J. Chem. Phys.* **1972**, *56*, 2257.
7. P. C. Hariharan, J. A. Pople, *Theor. Chim. Acta* **1973**, *28*, 213.
8. M. S. Gordon, *Chem. Phys. Lett.* **1980**, *76*, 163.
9. Gaussian 94 (Revision C.2), M. J. Frisch, G. W. Trucks, H. B. Schlegel, P. M. W. Gill, B. G. Johnson, M. A. Robb, J. R. Cheesman, T. A. Keith, G. A. Petersson, J. A. Montgomery, K. Raghavachari, M. A. Al-Laham, V. G. Zakrzewski, J. V. Ortiz, J. B. Foresman, J. Cioslowski, B. B. Stefanov, A. Nanayakkara, M. Challacombe, C. Y. Peng, P. Y. Ayala, W. Chen, M. W. Wong, J. L. Andres, E. S. Replogle, R. Gomperts, R. L. Martin, D. J. Fox, J. S. Binkley, D. J. Defrees, J. Baker, J. P. Stewart, M. Head-Gordon, C. Gonzalez, J. A. Pople, Gaussian Inc., Pittsburgh, PA, 1995.
10. A. D. Becke, "Density-functional thermochemistry. III. The role of exact exchange." *J. Chem. Phys.* 1993, **98**, 5648.
11. A. D. McLean, G. S. Chandler, *J. Chem. Phys.* **1980**, *72*, 5639.
12. R. Krishnan, J. S. Binkley, R. Seeger, J. A. Pople, *J. Chem. Phys.* **1980**, *72*, 650.
13. L. Hedberg, I. M. Mills, *J. Mol. Spectrosc.* **1993**, *160*, 117.
14. W. Zeil, J. Haase, L. Z. Wegmann, *Instrumentk.* **1966**, *74*, 84.
15. O. E. Kjeldseth Moe, T. G. Strand, *J. Mol. Struct.* **1985**, *128*, 13.

16. S. Cradock, J. Koprowski, D. W. H. Rankin, *J. Mol. Struct.*, **1981**, *77*, 113.

17. C. M. Huntley, G. S. Laurenson, D. W. H. Rankin, *J. Chem. Soc., Dalton Trans.* **1980**, 954.

18. A. M. Ross, M. Fink, R. Hilderbrandt, in *International tables for Crystallography,* ed. A. J. C. Wilson, Vol. C, Kluwer Academic Publishers, Dortrecht, 1992, p. 245.

19. A. J. Blake, P. T. Brain, H. McNab, J. Miller, C. A. Morrison, S. Parsons, D. W. H. Rankin, H. E. Robertson, B. A. Smart, *J. Phys. Chem.* **1996**, *100*, 12280: P. T. Brain, C. A. Morrison, S. Parsons, D. W. H. Rankin, *J. Chem. Soc., Dalton Trans.* **1996**, 4589.

20. See, for example, N. W. Mitzel, B. A. Smart, A. J. Blake, H. E. Robertson, D. W. H. Rankin, *J. Phys. Chem.* **1996**, *100*, 9339.

21. D. Hnyk, R. S. Fender, H. E. Robertson, D. W. H. Rankin, M. Bühl, K. Hassler, K. Schenzel, *J. Mol. Struct.* **1995**, *346*, 215.

22. S. L. Hinchley, B. A. Smart, C. A. Morrison, H. E. Robertson, D. W. H. Rankin, R. Zink, K. Hassler, *J. Chem. Soc., Dalton Trans.* **1999**, 2303.

23. T. Fjeldberg, A. Haaland, B. Schilling, M. F. Lappert, A. J. Thorne, *J. Chem. Soc., Dalton Trans.* **1986**, 1551.

24. A. McAdam, B. Beagley, T. G. Hewitt, *Transactions of Faraday Society* **1970**, *66*, 2732.

25. A. J. Downs, N. I. Hunt, G. S. McGrady, D. W. H. Rankin, H. E. Robertson, *J. Molecular Structure* **1991**, *248*, 393.

26. F. H. Allen, O. Kennard, *Chemical Design and Automation News* **1993**, *8*, 131.

27. B. D. Murray, H. Hope, J. Hvoslef, P. P. Power, *Organometallics* **1984**, *3*, 657.

28. P. B. Hitchcock, M. F. Lappert, P. P. Power, S. J. Smith, *J. Chem. Soc., Chem. Commun.* **1984**, 1669.

29. A. Baldy, J. Estienne, *Acta Cryst.* **1988**, *C44*, 747.

30. K. M. Flynn, H. Hope, M. M. Olmstead, P. P. Power, *J. Am. Chem. Soc.* **1983**, *105*, 7750.

31. N. Burford, T. S. Cameron, D. J. LeBlanc, P. Losier, S. Sereda, G. Wu, *Organometallics* **1997**, *16*, 4712.

32. A. Decken, C. J. Carmalt, J. A. C. Clyburne, A. H. Cowley, *Inorg. Chem.* **1997**, *36*, 3741.

33. W. W. Du Mont, M. Karnop, J. Mahnke, R. Martens, C. Druckenbrodt, J. Jeske, P. G. Jones, *Chem. Ber. Recueil* **1997**, *130*, 1619.

34. P. Binger, T. Wettling, R. Schneider, F. Zurmühlen, U. Bergsträsser, J. Hoffmann, G. Maas, M. Regitz, *Angew. Chem. Int. Ed. Engl.* **1991**, *30*, 207.

35. (a) A. H. Cowley, J. G. Lasch, N. C. Norman, M. Pakulski, B. R. Whittlesey, *J. Chem. Soc., Chem. Commun.* **1983**, 881. (b) A. H. Cowley, J. E. Kilduff, J. G. Lasch, S. K. Mehrotra, N. C. Norman, M. Pakulski, B. R. Whittlesey, J. L. Atwood, W. E. Hunter, *Inorg. Chem.* **1984**, *23*, 2582.

36. (a) A. H. Cowley, J. G. Lasch, N. C. Norman, M. Pakulski, *J. Am. Chem. Soc.* **1983**, *105*, 5506. (b) Reference 32(b)

37. (a) A. H. Cowley, J. G. Lasch, N. C. Norman, M. Pakulski, *Angew. Chem. Int. Ed. Engl.* **1983**, *22*, 978. (b) A. H. Cowley, J. E. Kilduff, J. G. Lasch, N. C. Norman, M. Pakulski, F. Ando, T. C. Wright, *Organometallics* **1984**, *3*, 1044. (c) H. Lang, G. Huttner, B. Sigwarth, U. Weber, L. Zsolnai, I. Jibril, O. Orama, *Z. Naturforsch.* **1986**, *41b*, 191.

38. M. A. Petrie, P. P. Power, *J. Chem. Soc., Dalton Trans.* **1993**, 1737.

39. J. Trotter, *Can. J. Chem.* **1962**, *40*, 1590.

40. J. E. Stuckey, A. W. Cordes, L. B. Handy, R. W. Perry, C. K. Fair, *Inorg. Chem.* **1972**, *11*, 1846.

41. A. Camerman, J. Trotter, *J. Chem. Soc.* **1965**, 730.

42. W. T. Pennington, A. W. Cordes, J. C. Graham, Y. W. Jung, *Acta Cryst.* **1983**, *C39*, 1010.

43. S. G. Baxter, A. H. Cowley, R. E. Davis, P. E. Riley, *J. Am. Chem. Soc.* **1981**, *103*, 1699.

44. V. R. Richter, J. Kaiser, J. Sieler, U. H. Hartung, C. Peter, *Acta Cryst.* **1977**, *B33*, 1887.

45. V. G. Becker, O. Mundt, M. Rössler, *Z. Anorg. Allg. Chem.* **1980**, *468*, 55.

46. O. Mundt, H. Riffel, G. Becker, A. Simon, *Z. Naturforsch.* **1988**, *43b*, 952.

47. H. L. Carrell, J. Donohue, J. *Acta Cryst.* **1968**, *B24*, 699.

48. H. Schmidbaur, T. Wimmer, A. Grohmann, O. Steigelmann, G. Müller, *Chem. Ber.* **1989**, *122*, 1607.

49. (a) S. Aime, R. K. Harris, E. M. McVicker, *J. Chem. Soc., Chem. Commun.* **1974**, 426. (b) J. A. Brunell, C. H. Bushweller, A. D. English, *J. Phys. Chem.* **1976**, 80, 2598.

50. A. H. Cowley, M. J. S. Dewar, D. W. Goodman, M. C. Padolina, *J. Am. Chem. Soc.* **1974**, 2648.

Chapter 8

Investigation of molecular mechanics and semi-empirical methods for initial conformation determination of large molecules.

8.1 Introduction

Chapters 2, 3 and 4 described the gas-phase electron diffraction studies of a series of sterically crowded disilanes. Some incredibly surprising results were obtained from the GED study of these bulky molecules, especially for 1,1,2-tri-*tert*-butyldisilane, for which the *syn* conformer was ultimately found to be more than 10 kJ mol^{-1} more stable than either of the staggered (*gauche* and *antiperiplanar*) alternatives. The initial GED refinement, however, was carried out using a model describing the two staggered conformations, which were found to describe the vapour just as well as the single *syn* conformer model. This was attributed to the large number of refinable parameters needed to describe both conformers, and to the similarity of many of the very large number of interatomic distances in the two models. 1,1,2,2-tetra-*tert*-butyldisilane also gave an unexpected result with an almost *eclipsed* structure again being obtained. In this case, two of the butyl groups at opposite ends of the molecule were almost eclipsed, whereas in the tri-*tert*-butyl case, all the butyls eclipsed hydrogen atoms. For all the disilanes investigated, all but one yielded more than one minimum on the potential energy surface, and most were found to possess three.

It was decided to investigate the possibility of a more systematic and cheaper method to locate minima on the potential energy surface. If a suitable method could be found, it would save much expense and time when performing calculations on these large molecules. The two most obvious methods to try are molecular mechanics (MM) and semi-empirical calculations. As described in Chapter 1, both these methods are very quick and economical to use, and have been found to give reliable results for smaller molecules. Their application to these unusual larger molecules would indicate whether their use as a tool in the search for conformers as a precursor to higher level *ab initio* calculations would be valid. A requirement for these conformer searches is a unique torsion angle that can be varied stepwise. If there are two or more torsion angles, a two dimensional search can be performed.

8.2 Experimental

8.2.1 Molecular mechanics calculations

(*Calculations carried out by A. Parkin, Edinburgh*)

Conformer analyses were performed using the commercially available software Cerius[2] from MSI with a demonstration licence on a SGI Indigo[2] workstation. The molecules $Bu^tX_2SiSiX_2Bu^t$ (X = F, Cl, Br, I) and $Bu^t_2HSiSiH_2Bu^t$ were analysed using the Conformer Search and Conformer Analysis modules. The Conformer Search was performed using a Grid Scan method with the torsion angle ϕ(CSiSiC) the only one defined. This was analysed from –180 to 180° at 1° intervals, giving a total of 361 conformers. The "absolute" (see below) energy values were measured for each conformer after minimisation using the Universal Force Field version 1.02 (UFF1.02).[1] Atom force-field types were calculated using the default values of the UFF1.02 and no charges were calculated as this was purely a steric study. The grid [i.e. ϕ(CSiSiC)] torsion angle was restrained with a large force constant of 10000 kcal mol^{-1} during minimisation and the minimised geometry was retained for the start of the following cycle.

False minima were seen to be a problem by the incontinuous shape of the curve in certain regions, particularly when the hydrogen atoms on one *tert*-butyl group might be interacting with the hydrogen atoms on the other group. The non-continuous areas of the curves were studied further using the same parameters for the conformer search, but also contorting the minimised structure and reminimising to test whether a true minimum had been reached. Once a smooth curve had been created around half a dozen random points on the curve were selected and contorted minimisations performed to ensure the true minimum had been reached.

8.2.2 Semi-empirical calculations

All calculations were performed on a Dec Alpha 1000 4/200 workstation using the Gaussian 98[2] program. An 10° stepwise search of the torsional potential of the molecules $Bu^tX_2SiSiX_2Bu^t$ (X = F, Cl, Br, I) and $Bu^t_2HSiSiH_2Bu^t$ was carried out using AM1 semi-empirical calculations.[3-7] The models used allowed the butyl groups to

distort and twist away from the SiSiCC plane as previously observed in the higher level *ab initio* calculations. The unique torsion angles ϕ(CSiSiC) in the halogenated species and ϕ(CSiSiH) in the tri-*tert*-butyldisilane were fixed at 10° intervals and the remaining structural parameters of the molecules allowed to optimise at each geometry.

8.2.3 *Ab initio* calculations

All calculations at the HF level were performed on a Dec Alpha 1000 4/200 workstation using the Gaussian 98[2] program. A search of the torsional potential of 1,2-di-*tert*-butyltetrachlorodisilane was performed on the unique torsion angle ϕ(CSiSiC), as described in Section 8.2.2, at the HF/3-21G*[8-10] level.

8.3 Results

The results of the conformational analyses for each molecule studied are shown in Figures 1-5. It was found that at some torsion angles the AM1 calculations did not reach convergence. In these cases, the point on the graph has been left blank and as continuous a line as possible has been plotted. It should be noted that there are "spikes" present on some of the MM plots. As mentioned previously, this is probably due to the butyl groups passing at that point, when the molecule flips from one conformation before crossover into the next conformation after crossover. At these positions, more data need to be collected, perhaps at every 0.2° rather than every 1°, to smooth out the spikes present on the curves. However, for our purposes, the plots were deemed satisfactory with any further smoothing being purely cosmetic. Values between 0 and 180° were used to plot the graphs, as the plots were found to be symmetric over the 360° range used for the MM investigation, and only a torsion angle range of 180° was used for the AM1 calculations. The vertical black lines on Figures 1-5 indicate where the final *ab initio* minima were found in all cases, using either the HF/6-31G* or MP2/6-31G* levels of theory, with the arrow indicating the relative energies of the *ab initio* minima.

Figure 1 MM and semi-empirical potential energy surface plots for 1,2-di-*tert*-butyltetrafluorodisilane.

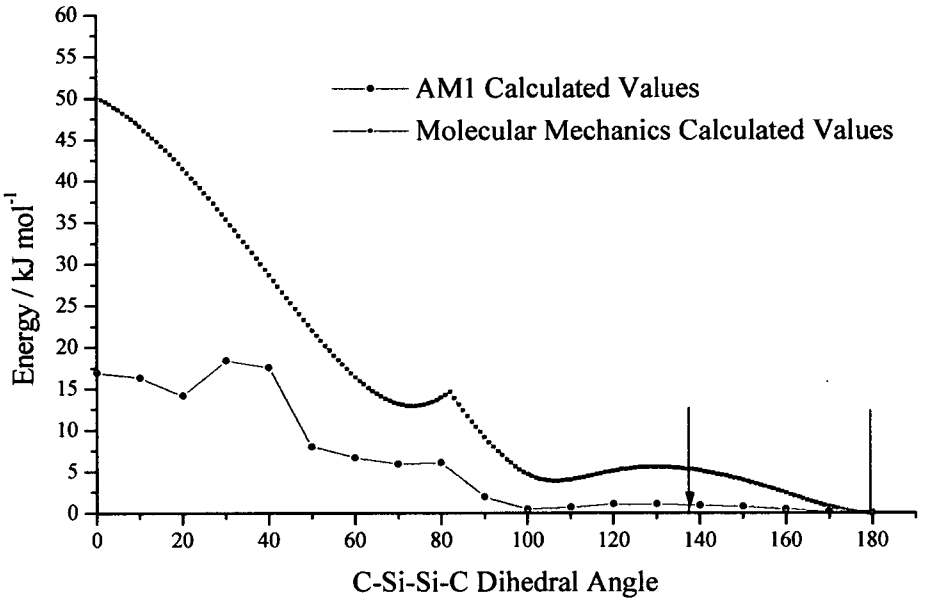

Figure 2 MM, semi-empirical and *ab initio* potential energy surface plots for 1,2-di-*tert*-butyltetrachlorodisilane.

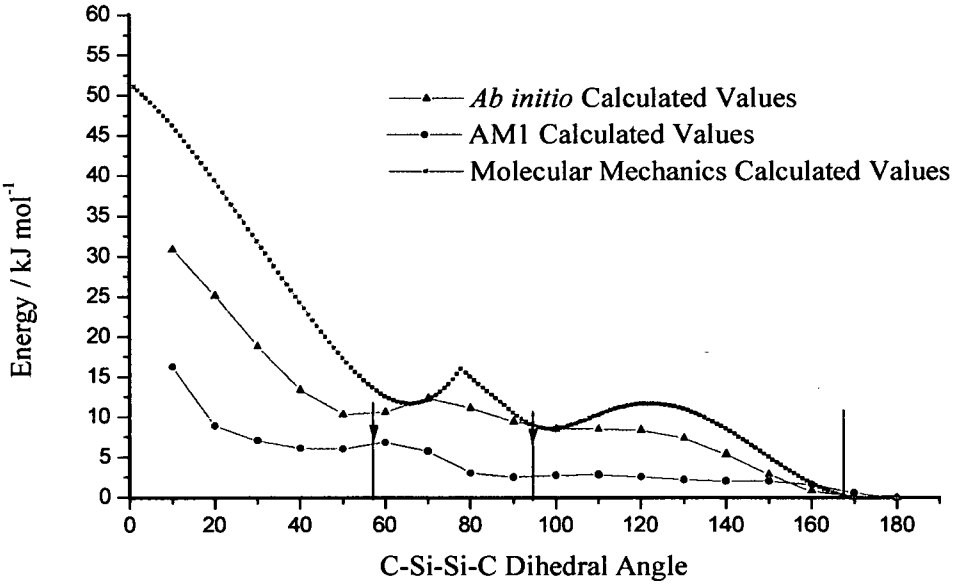

Figure 3 MM and semi-empirical potential energy surface plots for 1,2-di-*tert*-butyltetrabromodisilane.

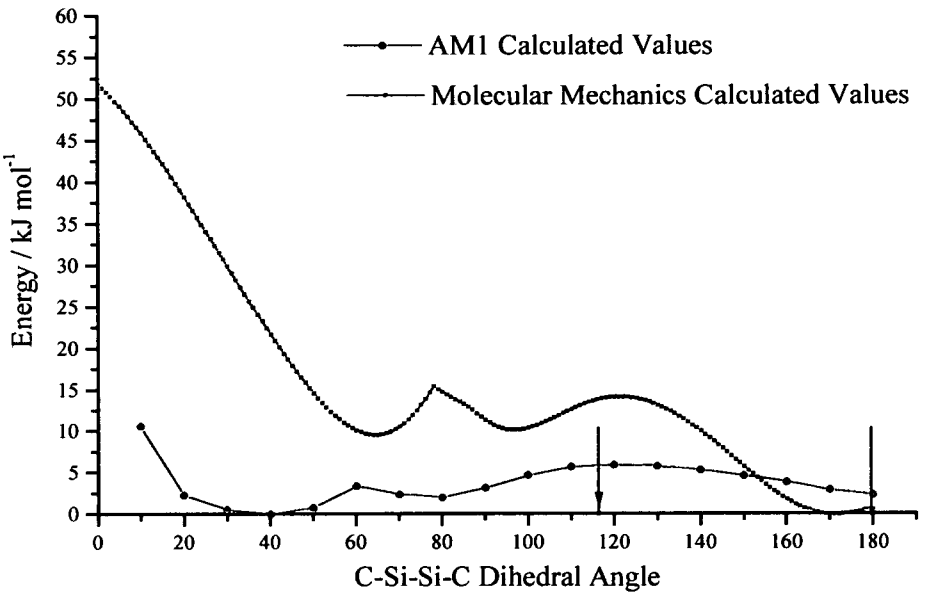

Figure 4 MM and semi-empirical potential energy surface plots for 1,2-di-*tert*-butyltetraiododisilane.

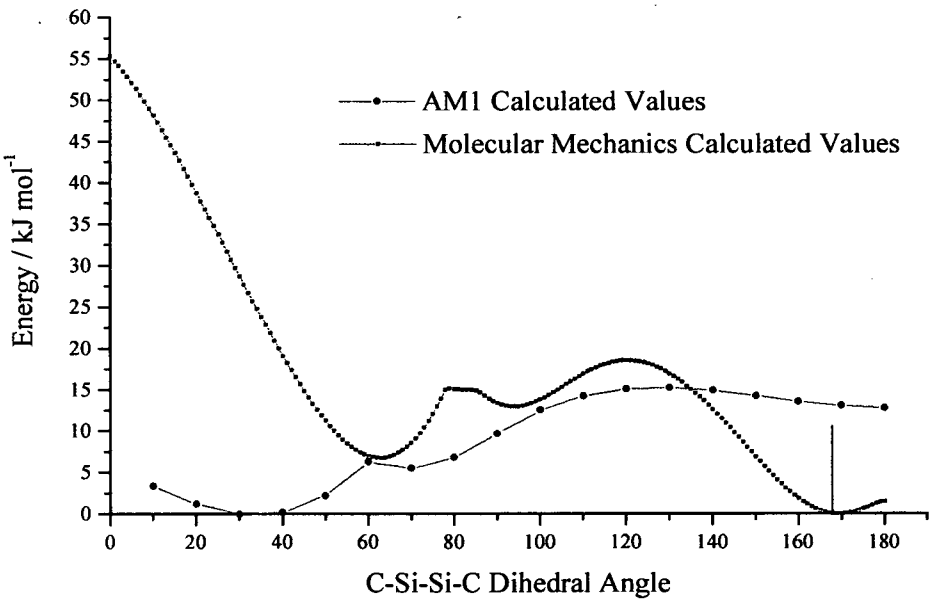

Figure 5 MM and semi-empirical potential energy surface plots for 1,1,2-tri-*tert*-butyldisilane.

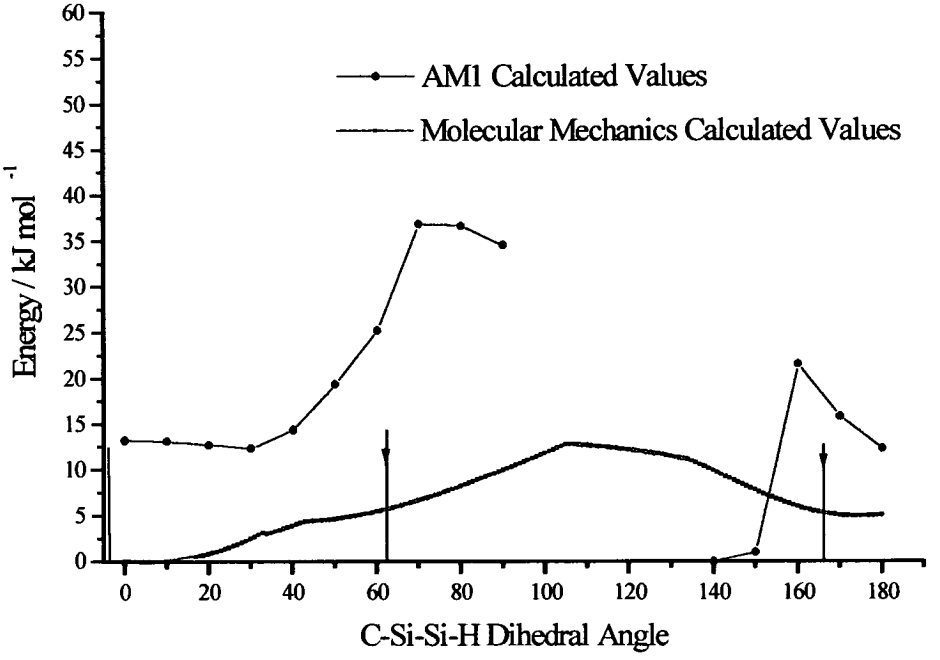

8.4 Discussion

Molecular mechanics and semi-empirical calculations were performed on a range of disilanes with bulky alkyl ligands and, in all but one case, with halogen atoms. Figure 1 shows the MM potential energy surface (PES) plot obtained for 1,2-di-*tert*-butyltetrafluorodisilane compared to the AM1 PES plot for the same molecule. Both agree that the global minimum lies at 180° as found *ab initio* at the HF/6-31G*[11-13] level. However, both methods failed to predict another minimum found *ab initio* (HF/6-31G*) at 138°. The very low barrier to large-amplitude torsion about the Si-Si bond observed by the AM1 method would have prompted further investigation of the region, but MM clearly gives a minimum at 105° which is over 30° different. It is possible that further, higher level calculations in this area may have yielded the final minimum observed *ab initio* but further investigation would be needed to confirm this. The energy differences between the minima also vary quite widely, up to 5 kJ mol^{-1} in the case of MM, whereas the difference calculated *ab initio* was just 0.68 kJ mol^{-1}. The AM1 calculations are much closer to the correct energy difference although, again, the minimum is predicted to be over 30° away from the highest level *ab initio* value.

As can be seen from Figure 2, all three techniques used predict the global minimum of 1,2-di-*tert*-butyltetrachlorodisilane to be between 170 and 180° as compared to 168° found at the MP2/6-31G* level. Two other higher energy minima were also found at the MP2/6-31G* level, ϕ(CSiSiC) 56 and 94°. The HF/3-21G* level also finds both these minima. The AM1 calculations show that there are possibly two minima around 45 and 90° whilst MM predicts minima at 65 and 100°. We can be confident that further investigation of the minima found by both MM and AM1 by higher level calculations would give the minima found eventually *ab initio*. Again there are large variations in the predicted energy differences between the three conformers. At the MP2/6-31G* level, both the *gauche* and *ortho* conformers were found to lie ~8 kJ mol^{-1} above the *transoid* conformer. Both HF/3-21G* and MM predict energy differences of ~12 and 9 kJ mol^{-1} for the *gauche* and *ortho* conformers with respect to the *transoid* conformer. AM1 predicted energy differences of 6 and 3 kJ mol^{-1} respectively.

For 1,2-di-*tert*-butyltetrabromodisilane [Figure 3], MM predicts the global minimum to be 170° compared to 180° at the MP2/6-31G* level (See Chapter 2). However, AM1 predicts it to be ~40° but also has a minimum (~3 kJ mol^{-1} higher in energy) at 180°, which is obviously not correct. This (the 40° minimum) was eventually found to correspond to a transition state on the potential energy surface at the MP2/6-31G* level. Again, further higher levels may resolve these observed anomalies. AM1 also fails for 1,2-di-*tert*-butyltetraiododisilane [Figure 4], with MM predicting 170° and AM1 predicting 35°, nowhere near the eventual minimum from the MP2/DZP calculation of 168° (See Chapter 2), although another AM1 minimum was found at ~170°, albeit 13 kJ mol^{-1} higher in energy. In the case of 1,2-di-*tert*-butyltetrabromodisilane, both AM1 and MM fail to predict the other minimum found *ab initio* (MP2/6-31G*) at 116°, MM giving two minima at 65 and 95°, and AM1 giving one at 80°. However, HF/3-21G* and HF/6-31G* calculations also predict two minima at approximately 80° and 121°, both collapsing to the 116° structure at the MP2 level. Thus justification for both methods not predicting the eventual minimum found on the potential energy surface is provided.

From Figure 5 it can be seen that the AM1 calculation for 1,1,2-tri-*tert*-butyldisilane failed to converge between 100 and 130°. Three minima were found at the MP2/6-31G* level (see Chapter 3) with ϕ(CSiSiH) torsion angles of –4, 63 and 164°. AM1 failed to find minima even vaguely close to these observed minima, with minima at ϕ(CSiSiH) torsion angles of 30 and 140°. MM predicts minima at ϕ(CSiSiH) torsion angles of approximately 5, 50 and 170°, in good agreement with those found *ab initio*. The region between 100 and 130° was found to be quite difficult to minimise because of the numerous H...H interactions. A more sophisticated dynamics model would handle these interactions perfectly adequately. Simulated annealing dynamics simulates heating from "room temperature" to a specified higher temperature and then cooling down again, eventually falling into the lowest minimum. However, it was felt that for the purpose of this exercise the extra work involved was not really justified. Energy differences between the conformers predicted *ab initio* were ~10 kJ mol^{-1} each for the *gauche* (63°) and *antiperiplanar* (164°) conformers above the *syn* (–4°) structure. MM predicts that the energy differences should be 4.5 and 5.0 kJ mol^{-1}. Thus the energy differences between the three conformers calculated by MM are consistent, if very underestimated.

It can be concluded from the above observations that molecular mechanics could be a possible method for locating the global minimum and other minima on the potential energy surface of a molecule. AM1 appeared to work reasonably for the smaller halogen atoms like fluorine and chlorine, but was very poor for the larger halogens and completely hopeless for the bulky 1,1,2-tri-*tert*-butyldisilane. Overall, molecular mechanics appears to be the better system to use, although it would be fair to conclude that the UFF needs to be optimised more carefully for use on these big systems. However, differences between energies of different conformers were not well reproduced by either AM1 or MM.

It must be stressed, however, that it is important for us to find all possible structures when investigating the potential energy surface of a molecule, as those close in energy (<5 kJ mol^{-1}) are more than likely to co-exist in the gas phase. Neither molecular mechanics nor AM1 performed very well in this task and it can be concluded that more

time-consuming searches of the PES, perhaps at the HF/3-21G* level as done for 1,2-di-*tert*-butyltetrachlorodisilane, may well prove to be prudent in the overall search for minima.

8.5 References

1. A. K. Tappe, C. J. Caséwit, K. S. Colwell, W. A. Goddard III and W. M. Skiff, *J. Am. Chem. Soc.*, 1992, **114**, 10024.
2. Gaussian 98, Revision A.7, M. J. Frisch, G. W. Trucks, H. B. Schlegel, G. E. Scuseria, M. A. Robb, J. R. Cheeseman, V. G. Zakrzewski, J. A. Montgomery, R. E. Stratmann Jr, J. C. Burant, S. Dapprich, J. M. Millam, A. D. Daniels, K. N. Kudin, M. C. Strain, O. Farkas, J. Tomasi, V. Barone, M. Cossi, R. Cammi, B. Mennucci, C. Pomelli, C. Adamo, S. Clifford, J. Ochterski, G. A. Petersson, P. Y. Ayala, Q. Cui, K. Morokuma, D. K. Malick, A. D. Rabuck, K. Raghavachari, J. B. Foresman, J. Cioslowski, J. V. Ortiz, A. G. Baboul, B. B. Stefanov, G. Liu, A. Liashenko, P. Piskorz, I. Komaromi, R. Gomperts, R. L. Martin, D. J. Fox, T. Keith, M. A. Al-Laham, C. Y. Peng, A. Nanayakkara, C. Gonzalez, M. Challacombe, P. M. W. Gill, B. Johnson, W. Chen, M. W. Wong, J. L. Andres, C. Gonzalez, M. Head-Gordon, E. S. Replogle and J. A. Pople, Gaussian, Inc., Pittsburgh PA, 1998.
3. M. J. S. Dewar, E. G. Zoebisch and E. F. Healy, *J. Am. Chem. Soc.*, 1985, **107**, 3902.
4. M. Dewar and W. Thiel, *J. Am. Chem. Soc.*, 1977, **99**, 4499.
5. L. P. Davis, R. M. Guidry, J. R. Williams, M. J. S. Dewar, H. S. Rzepa, *J. Comp. Chem.*, 1981, **2**, 433.
6. M. J. S. Dewar, M. L. McKee and H. S. Rzepa, *J. Am. Chem. Soc.*, 1978, **100**, 3607.
7. M. S. Dewar and C. H. Reynolds, *J. Comp. Chem.*, 1986, **2**, 140.
8. J. S. Binkley, J. A. Pople and W. J. Hehre, *J. Am. Chem. Soc.*, 1980, **102**, 939.
9. M. S. Gordon, J. S. Binkley, J. A. Pople, W. J. Pietro and W. J. Hehre, *J. Am. Chem. Soc.*, 1982, **104**, 2797.
10. W. J. Pietro, M. M. Francl, W. J. Hehre, D. J. DeFrees, J. A. Pople and J. S. Binkley, *J. Am. Chem. Soc.*, 1982, **104**, 5039.
11. W. J. Hehre, R. Ditchfield and J. A. Pople, *J. Chem. Phys.*, 1972, **56**, 2257.
12. P. C. Hariharan and J. A. Pople, *Theor. Chim. Acta*, 1973, **28**, 213.
13. M. S. Gordon, *Chem. Phys. Lett.*, 1980, **76**, 163.

Chapter 9

Future Developments

Gas-phase structures by dynamic interaction of theoretical and experimental data.

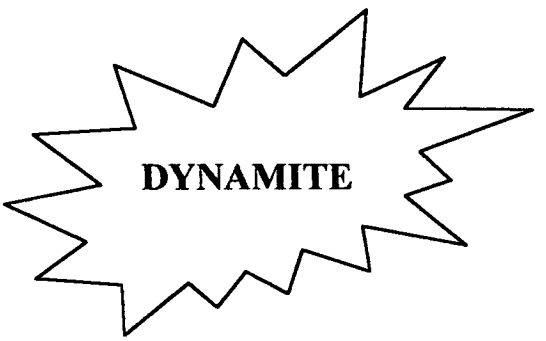

9.1 Introduction

Determination of molecular structures continues to play a central and vital role in chemistry. Increasingly powerful diffractometers can yield many hundreds of crystal structures per year, reflecting the striking recent developments in both hardware and software. Non-crystalline materials are just as important, but necessarily present more challenging structural problems. Studies of gas-phase molecules are naturally fewer in number, but here too developments in both experimental technique and data analysis have hugely extended the range of species that can be studied. This thesis has demonstrated that recent advances in computational and gas-phase techniques can now allow the study of very large, crowded, asymmetric molecules.

Electron diffraction is effectively the only experimental technique for determining structures of gas-phase molecules that are not *very* small. However, GED also has its limitations, most importantly the one-dimensional nature of the data and the consequent overlap of peaks in the radial distribution curve. Structures of relatively large and/or asymmetric molecules, which are defined by many geometrical parameters, can not therefore be completely determined, as discussed in Chapter 1.

Theoretical methods also have their limitations. For all methods, all reasonable structures must be explored, to ensure that the true potential minimum is found. Chapter 8 has shown that the results of very low-level calculations to investigate the potential energy surfaces of molecules are not really satisfactory for locating all possible minima of these bulky inorganic molecules. The global minimum (predicted by high level *ab initio* calculations) was located in all cases, but it was not necessarily calculated to be the global minimum. Accurate *ab initio* calculations require both large basis sets and high levels of theory, and the size of the calculation scales at up to the sixth power of the number of basis functions. High quality calculations for all but very small molecules are impracticably expensive, so compromises must be made. The computational demands of Density Functional Theory (DFT) calculations are lower, scaling with only about the fourth power of the number of basis functions, but

the accuracy of these calculations is unpredictable, unless a similar system has already been studied, and the calculations calibrated against some known structure. But how are computational methods calibrated? Against experimental data - which must come from accurate gas-phase work, until very recently impossible for more complex molecules.

Less sophisticated computational methods are useful for larger molecules, but accuracy is limited. Semi-empirical methods, such as AM1, are of some value for big organic molecules, but are inadequate for many inorganic systems, and particularly so for transition metal complexes, while empirical force-field (molecular mechanics) methods can be very reliable for organic and simple inorganic molecules, with minimal computational requirements. Considerable effort has therefore been made to develop hybrid techniques, such as ONIOM,[1] in which key parts of a molecule are computed at a high level, for example using coupled-cluster theory, while other parts are modelled at lower levels, perhaps Hartree-Fock or molecular mechanics. Such methods promise relatively cheap computation for some types of molecule, but are certainly not a panacea.

9.2 Hybrid Techniques

Hybrid experimental/computational methods have been introduced into the study of gas phase molecules. The MOCED (Molecular Orbital Constrained Electron Diffraction) method[2] used parameters calculated *ab initio* as fixed constraints in refinements of structures based on electron diffraction data. The SARACEN method[3] uses computed flexible restraints, which allows all significant geometrical parameters to be refined, giving meaningful estimates of errors, and a single structure which represents the best interpretation of all available information, experimental and theoretical. This method has probably doubled the number of gas-phase structures that can be determined with confidence, and permitted the study of much larger, more complex molecules.

However, for large molecules, even with the SARACEN method, assumptions are still made about apparently less important parts of molecules (such as peripheral alkyl groups) having high local symmetry, even in the presence of steric crowding. But this is not true, and these parts are not unimportant! For example, in $Bu^t_2HSiSiH_2Bu^t$ (Chapter 3) around 31% of the molecular scattering arises from long-range distances involving the hydrogen atoms, and a further 35% from the methyl group carbon atoms. These atoms clearly need to be placed accurately; otherwise the parameters for the remaining atoms may be seriously in error. Figure 1 shows the radial distribution curve for $Bu^t_2HSiSiH_2Bu^t$, (a) in full, (b) omitting contributions from non-bonded atom pairs including a hydrogen atom, and (c) also omitting contributions from pairs including a methyl group carbon atom.

Figure 1 Radial distribution curve of the final GED refined structure of 1,1,2-tri-*tert*-butyldisilane: (a) in full [blue], (b) omitting contributions from non-bonded atom pairs including a H atom [purple] and (c) also omitting contributions from pairs including a methyl group carbon atom [pink].

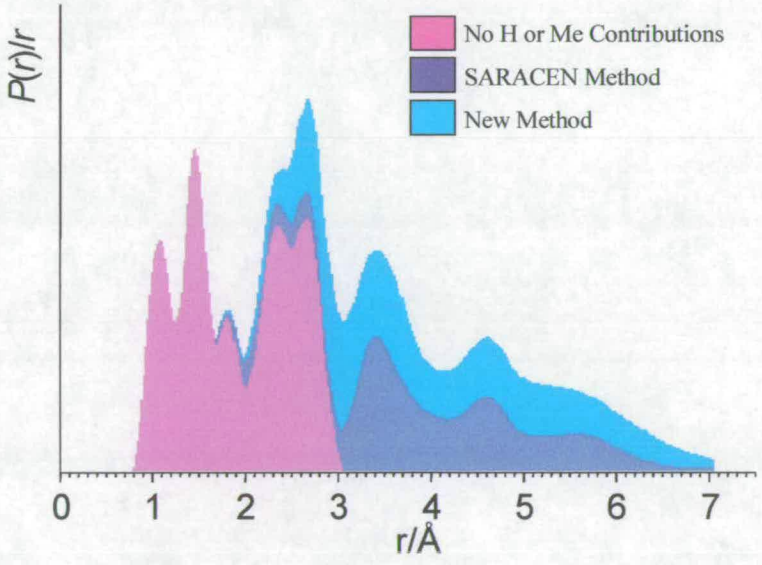

The difference between (b) and (c) effectively represents the scattering that is modelled properly using the SARACEN method. The difference between (a) and (b) is the scattering that we aim to model properly with a new method to be developed in Edinburgh. The consequence will be that the refined parameters, which define the

primary structure of the molecule, will be much more accurate than was possible previously. In many cases, structures that were impossible to determine will become accessible.

9.3 The dynamic interaction of theory and experiment: DYNAMITE

9.3.1 Initial DYNAMITE development

A new method that will lead to structures for large molecules that are as accurate as those currently obtained for much smaller molecules is outlined here. The method will find particular application in studies of transition metal complexes and of molecules suffering from extreme steric effects.

Following the introduction of hybrid methods and extensive use of computational methods to support GED data, a more advanced program combining all methods is proposed. The program will refine key parts of a molecular structure using gas electron diffraction and other experimental data, while simultaneously and continually optimising the remaining parts of the structures using molecular mechanics calculations. Eventually, the aim is to study compounds that exhibit severe steric strain, including $Si_2Bu^t_6$, and restudying $Bu^t_2HSiSiHBu^t_2$ [Chapter 4] and stable radicals $P/As[CH(SiMe_3)_2]_2$ and $P/As[N(SiMe_3)_2]_2$ [Chapter 7]. We also plan to extend the technique to allow partial structure optimisation by other computational techniques, including AM1 and possibly even DFT and low-level *ab initio* methods.

The method would then be applied to very crowded silyl compounds, particularly $Bu^t_2HSiSiHBu^t_2$. Chapter 3 has shown that $Bu^t_2HSiSiH_2Bu^t$ has an unusual eclipsed structure, which avoids strong Bu...Bu interactions. These cannot be avoided in the tetrabutyl compound and significant distortions are observed. In $Bu^t_3SiSiBu^t_3$ the strain will be much greater, and an exceptionally long Si-Si bond will be inevitable, so allowing for the effects of compression of crowded methyl groups will be very important. Thus we will be able to determine accurately structures of molecules for which high level *ab initio* calculations would be prohibitively expensive, and

extremely expensive even for DFT methods with large basis sets. With the proposed method the core structure will come from experiment, and the periphery will be defined by relatively undemanding calculations.

The radicals $P[CH(SiMe_3)_2]_2$, $P[N(SiMe_3)_2]_2$, $As[CH(SiMe_3)_2]_2$ and $As[N(SiMe_3)_2]_2$ will also be studied. Chapter 7 has revealed that accurate structures are needed to explain the remarkable dissociation of R_2PPR_2 and R_2AsAsR_2 on vaporisation, despite the fact that the P-P and As-As bonds are not particularly long. Energy redistribution from the crowded ligands in the dimers is critically important, and all atoms are involved, so must be located accurately. The present technique employed of constraining the methyl groups to C_{3v} local symmetry is particularly undesirable in this case.

9.3.2 Advanced DYNAMITE

There are of course many potential subjects for study, which require more sophisticated calculations than molecular mechanics. We therefore plan to introduce other computational methods, such as AM1, as partners of the GED refinement program. For situations where such calculations are too time-consuming to be used continually, or even higher levels of calculation are called for, we would develop a further hybrid technique. In this advanced method, the procedure would be:

- parameters for atoms which will not be refined from experimental data are calculated by the high-level method, A.
- these parameters are then also calculated by a low-level method, such as molecular mechanics, B.
- during refinement of the structure, using experimental data, differential placements of non-refined atoms would be determined by method B.
- from time to time, the positions of these atoms would be updated using method A.

This will provide the accuracy attainable with the high-level computational method, while retaining the economy of the low-level method for the large majority of calculations. We can then tackle the structure of any molecule that can be persuaded

to go into the gas phase to give diffraction data, confident in the accuracy of the results of the combined experimental/theoretical study.

This method will not be restricted to the study of molecules with bulky alkyl groups on the periphery. A major area of application could be to carbonyl complexes, with continual updating of positions of the carbonyl ligands. Small clusters would also become feasible candidates for study for the first time. These exciting new areas of study for the gas-phase electron diffractionist and the synthetic chemist can hopefully be exploited by this new technique for total structure determination.

9.4 References

1. M. Svensson, S. Humbel, R. D. J. Froese, T. Matsubara, S. Sieber and K. Morokuma, *J. Phys. Chem.*, 1996, **100**, 19357.
2. V. J. Klimkowski, J. D. Ewbank. C. Vanalsenoy, J. N. Scarsdale and L. Schafer, *J. Am. Chem. Soc.*, 1982, **104**, 1476.
3. A. J. Blake, P. T. Brain, H. McNab, J. Miller, C. A. Morrison, S. Parsons, D. W. H. Rankin, H. E. Robertson and B. A. Smart, *J. Phys. Chem.*, 1996, **100**, 12280; P. T. Brain, C.A. Morrison, S. Parsons and D. W. H. Rankin, *J. Chem. Soc., Dalton Trans.*, 1996, 4589.

Appendix 1

Supplementary tables for 1,2-di-*tert*-butyltetrachlorodisilane.

Table 1 Theoretical geometrical parameters (HF/3-21G* and HF/6-31G* level) for the *anti* conformers of 1,2-di-*tert*-butyltetrachlorodisilane (C_2), 1,2-di-*tert*-butyltetrabromo-disilane (C_{2h}) and HF/DZP and HF/DZP for1,2-di-*tert*-butyltetraiododisilane (C_1).[a]

	$Bu^tCl_2SiSiCl_2Bu^t$		$Bu^tBr_2SiSiBr_2Bu^t$		$Bu^tI_2SiSiI_2Bu^t$	
Parameter	HF/3-21G*	HF/6-31G*	HF/3-21G*	HF/6-31G*	HF/DZP	HF/DZP
Si-Si	236.1	238.4	235.3	237	239	241.4
Si-C	188.4	190.8	189	191.1	191	193.4
C(3)-C(4)	155.3	154.3	155.4	154.2	155.3	154.1
C(3)-C(5)	155.3	154.2	155.2	154.1	155.3	154.2
C(3)-C(6)	155.3	154.2	155.2	154.1	155.2	154.1
Si(2)-X(16)	206.2	207.7	224.2	223.1	250.6	250.6
Si(2)-X(17)	206.4	207.9	224.2	223.1	250.5	250.6
C-H[b]	108.4	108.5	108.4	108.5	108.4	108.5
Si-Si-C	117.6	118.7	118.8	119.6	119.6	119.6
Si(2)-C(3)-C(4)	110	109.4	109.5	108.9	110.2	109.8
Si(2)-C(3)-C(5)	110.7	110.6	110.9	110.2	111.5	111
Si(2)-C(3)-C(6)	109.9	109.8	110.9	110.2	110.2	109.9
Si(1)-Si(2)-X(16)	105.7	105.5	107.1	105.9	105.5	105.5
Si(1)-Si(2)-X(17)	108.9	108	107.1	105.9	108.1	108.2
C-C-H[b]	110.7	111.2	110.2	111.1	110.4	111.1
C-Si-Si-C	167.1	169.5	180	180	169	170.3
Absolute Energy[c]	-2716.5689	-2729.5216	-11127.1379	-11171.0904	-931.4176	-936.0698

[a] All distances in pm, all angles in degrees. See Figure 2 for atom numbering.
[b] Average value.
[c] Energy in Hartrees.

Table 2 Theoretical geometrical parameters (MP2/6-21G* level) for the *gauche* and *ortho* conformers of 1,2-di-*tert*-butyltetrachlorodisilane (C_2).[a]

	$Bu^tCl_2SiSiCl_2Bu^t$	
Parameter	*gauche*	*ortho*
Si-Si	236.2	237.5
Si-C	189.1	189.3
C(11)-C(111)	153.6	153.6
C(11)-C(112)	153.6	153.5
C(11)-C(113)	153.4	153.6
Si(1)-X(12)	206.6	206.4
Si(1)-X(13)	207.0	207.6
C-H[b]	109.5	109.5
Si-Si-C	120.7	118.4
Si(1)-C(11)-C(111)	108.9	109.0
Si(1)-C(11)-C(112)	109.2	109.4
Si(1)-C(11)-C(113)	110.3	110.0
Si(2)-Si(1)-X(12)	103.4	107.4
Si(2)-Si(1)-X(13)	106.8	106.6
C-C-H[b]	110.9	110.9
C-Si-Si-C	56.4	94.6
Absolute Energy[c]	-2731.1687	-2731.1686

[a] All distances in pm, all angles in degrees. See Figure 1 for atom numbering.

[b] Average value.

[c] Energy in Hartrees.

Table 3 Geometric restraints used in the GED study of 1,2-di-*tert*-butyltetrachlorodisilane.

Parameter	Value[a]
Independent Parameters	
p_1	112.0(20)
p_6	110.9(10)
p_{10}	1.4(5)
p_{11}	178.3(20)
p_{12}	3.0(20)
p_{13}	171.1(20)
p_{16}	2.1(10)
p_{17}	168.8(10)
Dependent Parameters	
p_{18}	109.1(10)
p_{19}	110.0(10)
p_{20}	108.9(10)

[a] Distances in pm, angles in °.

Table 4 Amplitude restraints applied to 1,2-di-*tert*-butyltetrachlorodisilane.

No.	*u*/pm	No.	*u*/pm
u_1	6.6(7)	u_{25}	44.3(50)
u_6	11.6(10)	u_{26}	14.0(14)
u_7	8.2(8)	u_{27}	49.7(50)
u_8	11.5(10)	u_{28}	76.9(77)
u_{10}	21.5(20)	u_{29}	25.1(25)
u_{11}	9.1(10)	u_{30}	56.2(60)
u_{13}	13.5(13)	u_{31}	34.6(35)
u_{14}	14.4(14)	u_{32}	21.1(20)
u_{15}	10.9(11)	u_{35}	21.2(20)
u_{17}	30.4(30)	u_{36}	28.6(30)
u_{20}	27.3(30)	u_{37}	27.2(30)
u_{21}	27.9(28)	u_{38}	24.1(20)

Table 5 Least-squares correlation matrix for the GED refinement of 1,2-di-*tert*-butyl-tetrachlorodisilane.[a]

	p_3	p_4	p_{14}	p_{15}	u_2	u_{26}	k_1
p_4							-57
p_7		84					-36
u_2							68
u_7	54						
u_9						65	
u_{11}			-57				
u_{15}				50			
k_2					74		63

[a] Only elements with absolute values >50% are shown; k_1 and k_2 are scale factors.

Table 6 Experimental coordinates for 1,2-di-*tert*-butyltetrachlorodisilane from the GED analysis.

Atom	*x*	*y*	*z*
Si(1)	-1.1899	0.0000	0.0000
C(11)	-2.1208	-1.5870	-0.3458
C(111)	-3.6042	-1.4025	0.0360
C(112)	-2.0286	-1.9988	-1.8298
C(113)	-1.5096	-2.7029	0.5270
H(1111)	-4.2156	-2.3433	-0.1777
H(1112)	-3.6565	-1.1543	1.1498
H(1113)	-4.0171	-0.5287	-0.5727
H(1121)	-0.9227	-2.0637	-2.1079
H(1122)	-2.5332	-3.0056	-2.0210
H(1123)	-2.5360	-1.1891	-2.4556
H(1131)	-0.4296	-2.8648	0.1921
H(1132)	-2.0926	-3.6805	0.4321
H(1133)	-1.5269	-2.3484	1.6126
Cl(12)	-1.6674	0.7137	1.8827
Cl(13)	-1.7953	1.4756	-1.3231
Si(2)	1.1899	0.0000	0.0000
C(21)	2.1208	1.6242	0.0000
C(211)	3.6042	1.3627	0.3338
C(212)	2.0286	2.3426	-1.3624
C(213)	1.5096	2.5288	1.0903
H(2111)	4.2156	2.3274	0.3253
H(2112)	3.6565	0.8831	1.3691
H(2113)	4.0171	0.6385	-0.4471
H(2121)	0.9227	2.4651	-1.6203
H(2122)	2.5332	3.3669	-1.3348
H(2123)	2.5360	1.6846	-2.1462
H(2131)	0.4296	2.7583	0.7976
H(2132)	2.0926	3.5042	1.2057
H(2133)	1.5269	1.9512	2.0756
Cl(22)	1.6674	-1.0982	1.6876
Cl(23)	1.7953	-1.1602	-1.6069

Table 7 Geometrical parameters for the x-ray crystallographic structures of 1,2-di-*tert*-butyltetrachlorodisilane, 1,2-di-*tert*-butyltetrabromodisilane and 1,2-di-*tert*-butyl-tetra-iododisilane.[a]

Parameter	$Bu^tCl_2SiSiCl_2Bu^t$	$Bu^tBr_2SiSiBr_2Bu^t$	$Bu^tI_2SiSiI_2Bu^t$
Si-Si	236.9(1)	235.5(4)	236.6
Si-C	188.1(3)	189.7(7)	190.4
Si-X(12)	206.6(1)	221.8(2)	246.1
Si-X(13)	206.1(2)	223.2(2)	246.8
C-C[b]	154.3(3)	153.7(1)	154
SiSiC	118.2(1)	119.2(2)	120
SiSiX(12)	107.2(1)	106.1(1)	106.7
SiSiX(13)	106.4(1)	106.5(1)	105.4
X(12)SiX(13)	106.9(1)	107.6(1)	108.1
CCC[b]	109.5(2)	110.1(6)	109.2

[a] All distances in pm, angles in °. See Figure 5 for atom numbering.

[b] Mean value.

Table 8 Calculated and observed wavenumbers for $Bu^tCl_2SiSiCl_2Bu^t$.

			Transoid			*Gauche*	*Ortho*
mode	Approx. label	sym.[a]	*ab initio* (scaled by 0.92)	observed IR(s), Raman(s)	PED (> 10%)	*ab initio* (scaled by 0.92)	*ab initio* (scaled by 0.92)
1	τSiSi	$a(a_u)$	14	-	$235S_{28},129S_{27},23S_{12},21S_{23},17S_{24},12S_{13},11S_8$	31	15
2	τSiC	$b(b_g)$	41	-	$143S_{40},28S_{51},22S_{38}$	40	52
3	τSiC	$a(a_u)$	49	-	$89S_{27},20S_{25}$	63	58
4	δSiSiC	$b(b_u)$	79	-	$79S_{51},11S_{52}$	80	90
5	$\rho SiCl_2$	$a(a_u)$	85	-	$64S_{24},58S_{23}$	89	92
6	δSiSiC	$a(a_g)$	108	110	$66S_{12},40S_{13}$	107	112
7	$\tau SiCl_2$	$b(b_g)$	128	130/137	$92S_{36}$	124	119
8	$\gamma SiCl_2$	$a(a_g)$	129	130/137	$25S_{14},15S_{23},13S_{11},12S_{21},12S_{24},10S_{13}$	126	137
9	$\tau SiCl_2$	$a(a_u)$	134	-	$21S_{23},19S_{24},18S_{14},14S_{21},11S_{11}$	135	137
10	$\rho SiCl_2$	$b(b_g)$	158	158	$53S_{37},24S_{34},10S_{52}$	151	145
11	$\gamma SiCl_2$	$b(b_u)$	168	-	$48S_{53},15S_{52},12S_{37},11S_{48}$	176	177
12	$\delta SiCl_2$	$b(b_u)$	182	-	$54S_{52},26S_{48},13S_{53}$	177	182
13	$\delta SiCl_2$	$a(a_g)$	183	186	$36S_{13},30S_{14},11S_{12}$	185	185
14	ρCC_3	$a(a_g)$	224	233	$45S_8,16S_{11},12S_{15}$	218	221
15	$\tau_1 CC$	$b(b_g)$	228	-	$96S_{38}$	222	226
16	$\tau_1 CC$	$a(a_u)$	229	-	$92S_{25}$	225	226
17	ρCC_3	$a(a_u)$	254	-	$40S_{26},38S_{21},16S_{20}$	256	259
18	$\tau_2 CC$	$b(b_g)$	260	264	$48S_{39},20S_{34},13S_{33}$	262	261
19	τCC	$b(b_u)$	270	279	$44S_{54},16S_{48}$	269	269
20	τCC	$a(a_g)$	282	289	$70S_{15}$	276	279
21	ρCC_3	$b(b_u)$	289	-	$44S_{54},23S_{48}$	290	293
22	$\tau_2 CC$	$a(a_u)$	294	-	$52S_{26},23S_{21}$	292	295

Table 8 Continued

			Transoid			*Gauche*	*Ortho*
mode	Approx. label	sym.[a]	*ab initio* (scaled by 0.92)	observed IR(s), Raman(s)	PED (> 10%)	*ab initio* (scaled by 0.92)	*ab initio* (scaled by 0.92)
23	ρCC_3	$b(b_g)$	296	307	$44S_{39},26S_{34}$	295	298
24	$\nu_{sym}SiCl_2$	$a(a_g)$	303	307	$21S_8,18S_{10},14S_7,11S_{12}$	299	299
25	$\delta_{sym}CC_3$	$b(b_u)$	351	352	$40S_{47},27S_{46},14S_{49},12S_{53}$	357	357
26	$\delta_{asym}CC_3$	$a(a_g)$	379	383	$72S_7,12S_3$	376	378
27	$\delta_{asym}CC_3$	$b(b_g)$	387	391	$68S_{33},11S_{31}$	389	389
28	$\delta_{asym}CC_3$	$a(a_u)$	388	-	$70S_{20},11S_{18}$	392	390
29	$\delta_{asym}CC_3$	$b(b_u)$	395	396	$40S_{47},15S_{46},14S_{48},13S_{53}$	393	395
30	$\delta_{sym}CC_3$	$a(a_g)$	442	437	$54S_6,27S_{10},17S_{14},10S_{11}$	442	440
31	$\nu_{sym}SiCl_2$	$b(b_u)$	479	483	$77S_{50},17S_{46}$	480	480
32	$\nu_{asym}SiCl_2$	$b(b_g)$	545	548	$95S_{35},27S_{37}$	553	550
33	$\nu_{asym}SiCl_2$	$a(a_u)$	554	562	$94S_{22}$	558	551
34	$\nu SiSi$	$a(a_g)$	581	585	$49S_{10},28S_{11},16S_{12}$	579	582
35	νSiC	$b(b_u)$	596	616	$51S_{49},19S_{44},14S_{46},12S_{50}$	602	599
36	νSiC	$a(a_g)$	616	632	$45S_9,19S_4,18S_{11},13S_{14}$	613	610
37	$\nu_{sym}CC_3$	$b(b_u)$	808	815	$74S_{44},19S_{49},16S_{41}$	809	808
38	$\nu_{sym}CC_3$	$a(a_g)$	810	814	$73S_4,20S_9,17S_1$	811	810
39	$\nu_{asym}CC_3$	$b(b_u)$	942	940	$58S_{45},26S_{43}$	940	941
40	$\nu_{asym}CC_3$	$a(a_g)$	943	939	$56S_5,26S_3,10S_2$	940	942
41	$\nu_{asym}CC_3$	$b(b_g)$	946	939	$56S_{32},27S_{31},10S_{29}$	946	947
42	$\nu_{asym}CC_3$	$a(a_u)$	946	940	$55S_{19},27S_{18},10S_{16}$	946	947
43	ρ_2CH_3	$a(a_u)$	977	-	$95S_{17}$	973	976
44	ρ_2CH_3	$b(b_g)$	977	-	$95S_{30}$	974	977
45	ρ_2CH_3	$b(b_u)$	1038	1006	$81S_{42}$	1036	1038
46	ρ_1CH_3	$b(b_g)$	1040	1006	$79S_{29}$	1037	1038

Table 8 Continued

			Transoid			*Gauche*	*Ortho*
mode	Approx. label	sym.[a]	*ab initio* (scaled by 0.92)	observed IR(s), Raman(s)	PED (> 10%)	*ab initio* (scaled by 0.92)	*ab initio* (scaled by 0.92)
47	ρ_1CH_3	$a(a_u)$	1040	1006	$81S_{16}$	1039	1040
48	ρ_2CH_3	$a(a_g)$	1042	1006	$81S_2$	1041	1042
49	ρ_3CH_3	$b(b_u)$	1219	1185	$50S_{43},31S_{45},11S_{47}$	1219	1221
50	ρ_3CH_3	$a(a_g)$	1221	1188	$42S_3,27S_5,10S_7$	1219	1221
51	ρ_3CH_3	$a(a_u)$	1224	1185	$42S_{18},27S_{19},10S_{20}$	1223	1224
52	ρ_3CH_3	$b(b_g)$	1224	1188	$50S_{31},32S_{32},11S_{33}$	1223	1224
53	ρ_1CH_3	$b(b_u)$	1239	1204	$60S_{41},18S_{46},10S_{49}$	1239	1238
54	ρ_1CH_3	$a(a_g)$	1241	1202	$59S_1,18S_6,10S_9$	1241	1240

[a] The u and g symmetry species used are those for the hypothetical perfectly staggered geometry of C_{2h} symmetry.

Table 9 Calculated and observed wavenumbers for $Bu^tBr_2SiSiBr_2Bu^t$.

	Transoid					*Gauche*
mode	approx. label	sym.[a]	*ab initio* (scaled by 0.92)	observed IR(s), Raman(s)	PED (>10%)	*ab initio* (scaled by 0.92)
1	τSiSi	$a(a_u)$	17	-	$173S_{28},50S_{27,12},11S_{13},10S_{23}$	27
2	τSiC	$b(b_g)$	42	-	$140S_{40},37S_{51},17S_{38},10S_{36}$	40
3	τSiC	$a(a_u)$	50	-	$116S_{27},53S_{26},17S_{25}$	57
4	$\tau SiBr_2$	$a(a_u)$	59	-	$67S_{23},43S_{24}$	60
5	δSiSiC	$b(b_u)$	76	-	$62S_{51},21S_{52}$	72
6	$\delta SiBr_2$	$a(a_g)$	76	77	$69S_{13},27S_{12},19S_{14}$	80
7	$\tau SiBr_2$	$b(b_g)$	91	96	$97S_{36}$	85
8	$\gamma SiBr_2$	$a(a_g)$	102	114	$35S_{14},17S_{12},10S_{11}$	105
9	$\rho SiBr_2$	$a(a_u)$	110	-	$48S_{24},30S_{23}$	110
10	$\delta SiBr_2$	$b(b_u)$	115	-	$63S_{52},10S_{53}$	115
11	$\rho SiBr_2$	$b(b_g)$	130	131	$61S_{37},11S_{34}$	130
12	δSiSiC	$a(a_g)$	138	141	$39S_{12},22S_{13},22S_{14}$	131
13	$\gamma SiBr_2$	$b(b_u)$	150	-	$66S_{53},19S_{48}$	158
14	$\nu_{sym}SiBr_2$	$a(a_g)$	210	223	$20S_{25},19S_{10},16S_9$	205
15	τ_1CC	$b(b_g)$	218	223	$77S_{38},12S_{54}$	212
16	τ_1CC	$a(a_u)$	221	-	$68S_{25},14S_{15}$	215
17	ρCC_3	$b(b_u)$	230	-	$25S_{34},20S_{39},16S_{48},12S_{50},11S_{38}$	230
18	τ_2CC	$a(a_u)$	232	-	$34S_{21},27S_{26},15S_8,11S_{10}$	231
19	ρCC_3	$b(b_g)$	240	244	$28S_{34},18S_{48},10S_{35},10S_{38}$	237
20	ρCC_3	$a(a_g)$	242	244	$29S_8,23S_{21},11S_{10},11S_{15}$	239
21	τ_2CC	$b(b_g)$	280	284	$40S_{54},39S_{39}$	280
22	ρCC_3	$a(a_u)$	286	-	$17S_{15},11S_8,10S_{21}$	281
23	τCC	$b(b_u)$	291	-	$42S_{54},36S_{39}$	284

Table 9 Continued

			Transoid			*Gauche*
mode	approx. label	sym.[a]	*ab initio* (scaled by 0.92)	observed IR(s), Raman(s)	PED (>10%)	*ab initio* (scaled by 0.92)
24	τCC	$a(a_g)$	292	284	$58S_{15},20S_{26}$	286
25	$\delta_{asym}CC_3$	$b(b_u)$	338	342	$41S_{47},15S_{48},13S_{50},13S_{53},12S_{46}$	334
26	$\delta_{asym}CC_3$	$a(a_g)$	368	381	$73S_7,11S_3$	368
27	$\delta_{asym}CC_3$	$b(b_g)$	373	381	$75S_{33},12S_{35},11S_{31}$	375
28	$\delta_{asym}CC_3$	$a(a_u)$	376	390	$67S_{20},10S_{18},10S_7$	378
29	$\delta_{sym}CC_3$	$b(b_u)$	385	390	$39S_{47},24S_{46}$	384
30	$\nu_{sym}SiBr_2$	$b(b_u)$	403	407	$50S_{50},22S_{46},16S_{48},12S_{51}$	402
31	$\delta_{sym}CC_3$	$a(a_g)$	412	410	$59S_6,21S_{10},17S_{12},14S_{14}$	416
32	$\nu_{asym}SiBr_2$	$a(a_u)$	458	474	$75S_{22},18S_{21},17S_{24}$	464
33	$\nu_{asym}SiBr_2$	$b(b_g)$	463	470	$71S_{35},42S_{37},19S_{34}$	466
34	νSiSi	$a(a_g)$	528	537	$44S_{11},25S_{10},18S_{12},12S_8$	522
35	νSiC	$b(b_u)$	580	601	$56S_{49},21S_{46},19S_{44}$	586
36	νSiC	$a(a_g)$	602	622	$51S_9,18S_4,14S_{11},11S_6,11S_{14}$	598
37	$\nu_{sym}CC_3$	$b(b_u)$	810	809	$74S_{44},17S_{41},17S_{49}$	810
38	$\nu_{sym}CC_3$	$a(a_g)$	810	810	$73S_4,18S_9,17S_1$	812
39	$\nu_{asym}CC_3$	$b(b_u)$	940	939	$45S_{45},27S_{43},15S_{42}$	938
40	$\nu_{asym}CC_3$	$a(a_g)$	940	939	$44S_5,27S_3,16S_{16},15S_2$	938
41	$\nu_{asym}CC_3$	$b(b_g)$	943	939	$43S_{32},28S_{31},16S_{29}$	941
42	$\nu_{asym}CC_3$	$a(a_u)$	943	939	$43S_{19},28S_{18}$	942
43	ρ_2CH_3	$a(a_u)$	956	-	$94S_{17}$	953
44	ρ_2CH_3	$b(b_g)$	956	-	$94S_{30}$	953
45	ρ_2CH_3	$b(b_u)$	1025	1004	$75S_{42},11S_{45}$	1023
46	ρ_1CH_3	$b(b_g)$	1028	1007	$74S_{29},11S_{32}$	1024
47	ρ_1CH_3	$a(a_u)$	1028	1004	$64S_{16},10S_2,10S_{19}$	1027

Table 9 Continued

			Transoid			*Gauche*
mode	approx. label	sym.[a]	*ab initio* (scaled by 0.92)	observed IR(s), Raman(s)	PED (>10%)	*ab initio* (scaled by 0.92)
48	ρ_2CH_3	a(a_g)	1029	1007	$64S_2$	1028
49	ρ_3CH_3	b(b_u)	1211	1193	$42S_{43},32S_{45},11S_{47}$	1210
50	ρ_3CH_3	a(a_g)	1213	1186	$23S_3,20S_{18},18S_5,17S_{19}$	1210
51	ρ_3CH_3	b(b_g)	1214	1186	$41S_{31},33S_{32},11S_{33}$	1213
52	ρ_3CH_3	a(a_u)	1214	1193	$24S_{18},20S_{19},18S_3,15S_5$	1213
53	ρ_1CH_3	b(b_u)	1217	1193	$52S_{41},17S_{46}$	1217
54	ρ_1CH_3	a(a_g)	1219	1200	$54S_1,18S_6$	1220

[a] The u and g symmetry species used are those for the hypothetical perfectly staggered geometry of C_{2h} symmetry.

Table 10 Calculated and observed wavenumbers for $Bu^tI_2SiSiI_2Bu^t$.

	Transoid					*Gauche*
mode	approx. label	sym.[a]	*ab initio* (scaled by 0.92)	observed IR(s), Raman(s)	PED (>10%)	*ab initio* (scaled by 0.92)
1	τSiSi	$a(a_u)$	17	-	$176S_{28},47S_{27},25S_{12},20S_{13},13S_{15},10S_{23},10S_{24}$	26
2	τSiC	$b(b_g)$	41	-	$157S_{40},39S_{51},20S_{38},18S_{36}$	42
3	τSiC	$a(a_u)$	46	-	$71S_{27},47S_{23},30S_{24}$	51
4	τSiI_2	$a(a_u)$	50	-	$65S_{27},23S_{23},14S_{25}$	52
5	δSiI_2	$a(a_g)$	57	55	$66S_{13},22S_{14},15S_{12}$	67
6	δSiI_2	$b(b_u)$	71	-	$47S_{52},37S_{36},25S_{51}$	68
7	τSiI_2	$b(b_g)$	77	80	$54S_{36},14S_{37},10S_{52}$	70
8	δSiSiC	$b(b_u)$	92	-	$30S_{51},30S_{52},11S_{53}$	92
9	γSiI_2	$a(a_g)$	94	100	$48S_{14},17S_{13},11S_{11}$	100
10	ρSiI_2	$a(a_u)$	103	-	$56S_{24},29S_{23}$	107
11	ρSiI_2	$b(b_g)$	112	118	$48S_{37},11S_{35}$	108
12	δSiSiC	$a(a_g)$	113	118	$59S_{12},18S_{10}$	109
13	γSiI_2	$b(b_u)$	137	-	$77S_{53},15S_{51}$	144
14	$\nu_{sym}SiI_2$	$a(a_g)$	185	198	$34S_{10},18S_9,18S_{14}$	181
15	$\nu_{sym}SiI_2$	$b(b_u)$	204	-	$32S_{48},29S_{50},19S_{38},15S_{54}$	201
16	τ_1CC	$a(a_u)$	217	-	$68S_{25},14S_{15},11S_{21}$	208
17	τ_1CC	$b(b_g)$	219	230	$50S_{38},28S_{34}$	217
18	ρCC_3	$a(a_u)$	222	-	$27S_{21},28S_8,26S_{26},10S_{15}$	223
19	ρCC_3	$b(b_g)$	231	230	$31S_{34},28S_{38},14S_{35}$	228
20	ρCC_3	$a(a_g)$	234	230	$28S_8,23S_{21},22S_{25},11S_{22}$	231
21	τ_2CC	$b(b_g)$	274	276	$48S_{39},35S_{54}$	274
22	τ_2CC	$a(a_u)$	284	-	$65S_{26},10S_8$	280

Table 10 Continued

			Transoid			*Gauche*
mode	approx. label	sym.[a]	*ab initio* (scaled by 0.92)	observed IR(s), Raman(s)	PED (>10%)	*ab initio* (scaled by 0.92)
23	τCC	b(b_u)	293	-	$47S_{54},35S_{39}$	284
24	τCC	a(a_g)	295	276	$66S_{15},13S_{26}$	287
25	ρCC_3	b(b_u)	328	327	$37S_{48},30S_{47},19S_{50},13S_{53},12S_{51}$	326
26	$\delta_{asym}CC_3$	a(a_u)	360	374	$38S_{20},33S_7,23S_{22}$	362
27	$\delta_{asym}CC_3$	b(b_g)	364	375	$59S_{33},23S_{35}$	363
28	$\delta_{asym}CC_3$	a(a_g)	370	375	$48S_7,24S_{20}$	373
29	$\delta_{sym}CC_3$	b(b_u)	376	374 or 390	$49S_{46},18S_{49},18S_{50}$	381
30	$\delta_{asym}CC_3$	b(b_u)	385	390	$56S_{47},19S_{48},16S_{51}$	385
31	$\delta_{sym}CC_3$	a(a_g)	401	396	$52S_6,15S_{10},22S_{12},11S_{14}$	395
32	$\nu_{asym}SiI_2$	a(a_u)	416	424	$40S_{22},27S_{21},22S_{24},21S_{20}$	422
33	$\nu_{asym}SiI_2$	b(b_g)	424	425	$45S_{35},44S_{37},27S_{34},15S_{33}$	427
34	νSiSi	a(a_g)	495	502	$52S_{11},18S_{12},16S_8,16S_{10}$	491
35	νSiC	b(b_u)	567	584	$58S_{49},28S_{46},15S_{44}$	574
36	νSiC	a(a_g)	585	601	$55S_9,18S_6,15S_4,10S_{11}$	583
37	$\nu_{sym}CC_3$	b(b_u)	806	804	$78S_{44},16S_{49},15S_{41}$	807
38	$\nu_{sym}CC_3$	a(a_g)	806	806	$78S_4,16S_9,15S_1$	808
39	$\nu_{asym}CC_3$	b(b_u)	938	937	$45S_{45},27S_{43},15S_{42}$	937
40	$\nu_{asym}CC_3$	a(a_g)	938	940	$44S_5,27S_3,16S_2$	937
41	$\nu_{asym}CC_3$	b(b_g)	942	940	$42S_{32},27S_{31},16S_{29}$	941
42	$\nu_{asym}CC_3$	a(a_u)	942	937	$42S_{19},27S_{18},17S_{16}$	941
43	ρ_2CH_3	a(a_u)	956	-	$95S_{17}$	953
44	ρ_2CH_3	b(b_g)	956	-	$95S_{30}$	953
45	ρ_2CH_3	b(b_u)	1026	1005	$75S_{42},10S_{45}$	1023
46	ρ_1CH_3	b(b_g)	1028	1005	$74S_{29},11S_{32}$	1024

Table 10 Continued

			Transoid			*Gauche*
mode	approx. label	sym.[a]	*ab initio* (scaled by 0.92)	observed IR(s), Raman(s)	PED (>10%)	*ab initio* (scaled by 0.92)
47	ρ_1CH_3	$a(a_u)$	1028	1005	$63S_{16},10S_{19},10S_2$	1027
48	ρ_2CH_3	$a(a_g)$	1030	1005	$63S_2,10S_{16}$	1028
49	ρ_1CH_3	$b(b_u)$	1207	1169	$55S_{41},18S_{46}$	1208
50	ρ_1CH_3	$a(a_g)$	1208	1167/1182	$52S_1,16S_6$	1210
51	ρ_3CH_3	$b(b_u)$	1210	1169	$36S_{43},28S_{45}$	1210
52	ρ_3CH_3	$a(a_u)$	1212	1169	$34S_{18},28S_{19}$	1211
53	ρ_3CH_3	$b(b_g)$	1213	1167/1182	$39S_{31},31S_{32},10S_{33}$	1212
54	ρ_3CH_3	$a(a_g)$	1214	1167/1182	$30S_3,25S_5,10S_{18}$	1213

[a] The u and g symmetry species used are those for the hypothetical perfectly staggered geometry of C_{2h} symmetry.

Table 11 Heavy atom distances and amplitudes of vibration for $Bu^tCl_2SiSiCl_2Bu^t$ from the GED study.[a]

No.	Atom Pair	r_a/pm	u/pm
u_1	Si(1)...Si(2)	238.0 (7)	6.5 (6)
u_2	Si(2)...C(21)	187.2 (7)	7.1 (7)
u_3	Si(2)...Cl(22)	206.9 (1)	5.6 (3)
u_4	C(21)...C(211)	154.3 (2)	6.9 (4)
u_6	Cl(23)...Cl(22)	329.8 (17)	12.5 (9)
u_7	C(212)...C(211)	251.4 (6)	7.1 (7)
u_8	Si(1)...C(21)	368.8 (14)	10.8 (10)
u_9	Si(1)...C(211)	499.5 (11)	9.7 (20)
u_{10}	Si(1)...C(212)	420.7 (28)	22.7 (21)
u_{11}	Si(2)...C(211)	279.2 (4)	9.1 (5)
u_{12}	C(11)...C(21)	533.1(21)	14.2(fixed)
u_{13}	Si(1)...Cl(22)	349.6 (13)	13.0 (12)
u_{14}	Si(1)...Cl(23)	358.3 (15)	12.5 (10)
u_{15}	C(21)...Cl(22)	323.5 (32)	10.6 (10)
u_{16}	C(21)...Cl(23)	323.1 (34)	10.5 (tied to u_{15})
u_{17}	Si(1)...C(213)	385.6 (25)	31.5 (32)
u_{18}	Si(2)...C(212)	283.7 (14)	9.3 (tied to u_{11})
u_{19}	Si(2)...C(213)	277.2 (10)	9.7 (tied to u_{11})
u_{20}	C(11)...Cl(22)	432.7 (32)	29.1 (32)
u_{21}	C(11)...Cl(23)	413.6 (31)	30.7 (29)
u_{22}	C(11)...C(211)	647.6 (14)	13.7 (fixed)
u_{23}	C(11)...C(212)	580.5 (31)	24.3 (fixed)
u_{24}	C(11)...C(213)	567.3 (25)	24.1 (fixed)
u_{25}	Cl(12)...Cl(22)	380.0 (66)	47.2 (53)
u_{26}	Cl(12)...Cl(23)	526.1 (16)	14.9 (10)
u_{27}	Cl(13)...Cl(23)	446.3 (62)	45.5 (54)
u_{28}	C(21)...Cl(23)	422.6 (75)	74.7 (85)
u_{29}	C(111)...Cl(22)	553.3 (29)	29.9 (26)
u_{30}	C(112)...Cl(22)	518.1 (57)	58.9 (65)

Table 11 Continued

No.	Atom Pair	r_a/pm	u/pm
u_{31}	C(113)...Cl(22)	374.4 (47)	35.1 (38)
u_{32}	Cl(22)...C(211)	341.2 (41)	20.5 (22)
u_{33}	Cl(22)...C(212)	461.2 (25)	12.3 (9)
u_{34}	Cl(22)...C(213)	367.9 (46)	22.3 (tied to u_{37})
u_{35}	Cl(23)...C(111)	564.9 (26)	24.1 (20)
u_{36}	Cl(23)...C(112)	392.1 (35)	30.7 (32)
u_{37}	Cl(23)...C(211)	366.1 (42)	22.8 (24)
u_{38}	Cl(23)...C(212)	351.9 (48)	23.0 (22)
u_{39}	Cl(23)...C(213)	457.9 (26)	12.3 (tied to u_{33})
u_{40}	C(111)...C(211)	772.6 (16)	13.4 (fixed)
u_{41}	C(111)...C(212)	690.7 (34)	24.1 (fixed)
u_{42}	C(111)...C(213)	653.6 (30)	30.1 (fixed)
u_{43}	C(112)...C(212)	596.1 (54)	46.8 (fixed)
u_{44}	C(112)...C(213)	644.6 (26)	33.9 (fixed)

[a] Distances in pm. See Figure 2 for atom numbering.

Table 12 Atomic coordinates (x 10^4) and equivalent isotropic displacement parameters ($Å^2$ x 10^3) for 1,2-di-*tert*-butyltetrachlorodisilane. U(eq) is defined as one third of the trace of the orthogonalized U_{ij} tensor.

	x	*y*	*z*	*U(eq)*
Si(1)	4841(1)	4800(1)	8610(1)	25(1)
Cl(12)	2117(1)	5394(1)	7341(1)	39(1)
Cl(13)	7804(1)	6981(1)	8551(1)	38(1)
C(11)	4400(5)	2347(4)	7509(3)	31(1)
C(111)	4362(6)	2462(5)	5752(3)	45(1)
C(112)	6408(6)	1850(5)	8418(3)	47(1)
C(113)	2085(5)	736(4)	7423(3)	46(1)
H(1111)	5857	3453	5808	67
H(1112)	3135	2833	5179	67
H(1113)	4070	1172	5157	67
H(1121)	6208	603	7809	70
H(1122)	6412	1723	9520	70
H(1123)	7878	2907	8504	70
H(1131)	1853	-540	6844	68
H(1132)	820	1057	6833	68
H(1133)	2109	667	8536	68

Table 13 Anisotropic displacement parameters ($Å^2$ x 10^3) for 1,2-di-*tert*-butyltetrachlorodisilane. The anisotropic displacement factor exponent takes the form: $-2\ pi^2\ [\ h2\ a^{*2}\ U11 + ... + 2\ h\ k\ a^*\ b^*\ U12\ ]$.

	U11	U22	U33	U23	U13	U12
Si(1)	29(1)	28(1)	22(1)	11(1)	12(1)	13(1)
Cl(12)	42(1)	51(1)	32(1)	14(1)	11(1)	29(1)
Cl(13)	38(1)	39(1)	36(1)	14(1)	20(1)	8(1)
C(11)	41(2)	32(2)	23(1)	8(1)	14(1)	18(1)
C(111)	69(2)	43(2)	28(1)	8(1)	21(2)	29(2)
C(112)	65(2)	50(2)	40(2)	14(2)	19(2)	39(2)
C(113)	55(2)	30(2)	42(2)	4(1)	16(2)	11(2)

Appendix 2

Supplementary tables for 1,1,2-tri-*tert*-butyldisilane.

Table 1 Theoretical geometrical parameters (HF/3-21G*, HF/6-31G* and MP2/6-31G* levels) for the *syn* conformer of 1,1,2-tri-*tert*-butyldisilane.[a]

Parameter	HF/3-21G*	HF/6-31G*	MP2/6-31G*
Si(1)-Si(2)	237.2	239.2	237.1
Si(1)-C(11)	191.8	193.8	192.3
C(11)-C(111)	154.9	153.9	153.3
C(11)-C(112)	155.1	154.2	153.5
C(11)-C(113)	155.5	154.2	153.6
Si(1)-C(12)	191.8	193.9	192.2
C(12)-C(121)	155.5	154.2	153.7
C(12)-C(122)	155.1	154.0	153.5
C(12)-C(123)	155.0	154.0	153.3
Si(2)-C(21)	190.6	192.3	191.2
C(21)-C(211)	155.0	153.9	153.4
C(21)-C(212)	155.1	154.1	153.4
C(21)-C(213)	154.9	153.9	153.2
Si(1)-H(13)	148.7	148.7	150.2
Si(2)-H(22)	148.4	148.3	149.5
Si(2)-H(23)	148.4	148.4	149.7
C-H[b]	108.6	108.7	109.6
C(11)-Si(1)-C(12)	118.8	118.2	118.7
Si(1)-Si(2)-C(21)	114.6	115.7	113.7
Si(2)-C(21)-C(211)	110.7	110.3	109.6

Table 1 Continued

Parameter	HF/3-21G*	HF/6-31G*	MP2/6-31G*
Si(2)-C(21)-C(212)	109.4	108.3	108.5
Si(2)-C(21)-C(213)	110.8	111.3	110.6
Si(2)-Si(1)-C(11)	109.6	111.1	110.4
Si(1)-C(11)-C(111)	112.9	112.7	112.2
Si(1)-C(11)-C(112)	112.5	111.1	111.1
Si(1)-C(11)-C(113)	107.4	108.1	107.3
Si(2)-Si(1)-C(12)	109.5	109.3	108.9
Si(1)-C(12)-C(121)	107.3	107.0	106.5
Si(1)-C(12)-C(122)	112.6	112.0	111.6
Si(1)-C(12)-C(123)	113.0	112.9	112.6
Si(1)-Si(2)-H(22)	110.2	109.5	110.4
Si(1)-Si(2)-H(23)	110.2	110.0	110.7
Si(2)-Si(1)-H(13)	107.7	107.3	107.8
C-C-H[b]	110.9	111.4	111.1
C(21)-Si(2)-Si(1)-H(13)	-0.4	-5.4	-3.9
Absolute energy[c]	-1044.2921	-1049.7166	-1051.4868

[a] All distances in pm, all angles in degrees.

[b] Average of all values.

[c] Energy in Hartrees. Absolute energy at the MP2/D95* level for the *syn* conformation is -1051.514558 Hartrees.

Table 2 Theoretical geometrical parameters (HF/3-21G*, HF/6-31G*, MP2/6-31G* and MP2/D95* levels) for the *antiperiplanar* (*app*) and *gauche* conformers of 1,1,2-tri-*tert*-butyldisilane.[a]

	HF/3-21G*		HF/6-31G*		MP2/6-31G*		MP2/D95*	
Parameter	*app*	*gauche*	*app*	*gauche*	*app*	*gauche*	*app*	*gauche*
Si(1)-Si(2)	237.4	237.5	239.4	239.5	237.6	237.3	238.1	237.8
Si(1)-C(11)	192.1	192.4	194.0	194.4	192.5	193.0	192.8	193.1
C(11)-C(111)	154.9	155.0	153.9	154.0	153.6	153.3	153.7	153.9
C(11)-C(112)	155.1	155.3	154.0	154.2	153.4	153.6	153.9	154.2
C(11)-C(113)	155.5	155.5	154.3	154.3	153.7	153.7	154.2	154.2
Si(1)-C(12)	191.9	192.2	193.8	194.1	192.3	192.6	192.5	192.7
C(12)-C(121)	155.5	155.4	154.3	154.2	153.7	153.6	154.2	154.1
C(12)-C(122)	155.4	155.1	154.3	154.0	153.6	153.4	154.2	154.0
C(12)-C(123)	154.8	155.1	153.9	154.1	153.2	153.5	153.8	154.0
Si(2)-C(21)	191.4	191.1	193.0	192.7	192.1	191.7	192.5	192.1
C(21)-C(211)	154.7	154.8	153.7	153.8	153.1	153.2	153.7	153.8
C(21)-C(212)	155.5	155.5	154.3	154.3	153.7	153.7	154.3	154.3

Table 2 Continued

	HF/3-21G*		HF/6-31G*		MP2/6-31G*		MP2/D95*	
Parameter	*app*	*gauche*	*app*	*gauche*	*app*	*gauche*	*app*	*gauche*
C(21)-C(213)	154.8	155.0	153.8	153.9	153.2	153.3	153.8	153.9
Si(1)-H(13)	148.9	148.7	148.8	148.7	150.3	150.2	150.5	150.4
Si(2)-H(22)	148.4	148.6	148.4	148.6	149.7	149.8	150.0	150.1
Si(2)-H(23)	148.5	148.3	148.4	148.2	149.7	149.5	149.9	149.8
C-H[b]	108.5	108.5	108.6	108.6	109.6	109.6	110.1	110.1
C(11)-Si(1)-C(12)	118.0	116.1	117.8	116.4	117.5	115.8	117.4	115.9
Si(1)-Si(2)-C(21)	125.6	122.2	126.1	122.5	124.7	122.0	124.4	121.5
Si(2)-C(21)-C(211)	112.7	113.2	112.4	112.6	112.1	112.6	112.3	112.9
Si(2)-C(21)-C(212)	107.1	107.4	106.4	106.7	106.1	106.5	106.4	106.9
Si(2)-C(21)-C(213)	112.4	111.0	112.0	111.0	111.9	110.4	112.1	110.4
Si(2)-Si(1)-C(11)	112.2	107.2	112.6	107.7	111.5	107.2	111.2	106.9
Si(1)-C(11)-C(111)	113.4	112.3	113.1	112.5	112.5	111.9	112.4	112.0
Si(1)-C(11)-C(112)	112.1	111.3	111.7	110.6	111.3	110.5	111.6	110.7

Table 2 Continued

	HF/3-21G*		HF/6-31G*		MP2/6-31G*		MP2/D95*	
Parameter	*app*	*gauche*	*app*	*gauche*	*app*	*gauche*	*app*	*gauche*
Si(1)-C(11)-C(123)	107.9	109.7	107.6	109.2	107.4	108.7	107.7	109.0
Si(2)-Si(1)-C(12)	114.4	113.9	114.3	114.1	113.7	113.4	113.4	113.1
Si(1)-C(12)-C(121)	108.1	108.3	108.1	108.0	107.5	107.8	107.6	108.2
Si(1)-C(12)-C(122)	111.5	113.0	110.7	112.5	110.8	112.0	111.1	112.3
Si(1)-C(12)-C(123)	113.3	112.1	113.0	111.9	112.4	111.4	112.4	111.2
Si(1)-Si(2)-H(22)	105.9	109.2	105.5	109.0	106.1	108.8	105.9	109.1
Si(1)-Si(2)-H(23)	105.5	105.1	105.1	105.1	106.4	105.7	106.4	105.6
Si(2)-Si(1)-H(13)	100.5	106.9	100.3	106.6	102.4	107.5	102.4	107.5
C-C-H[b]	110.8	110.9	111.4	111.4	111.1	111.6	111.1	111.1
C(21)-Si(2)-Si(1)-H(13)	165.6	62.3	166.5	60.6	163.8	63.4	163.4	63.5
Absolute energy[c]	-1044.2865	-1044.2873	-1049.7120	-1049.7124	-1051.4830	-1051.4830	-1051.5106	-1051.5104

[a] All distances in pm, all angles in degrees. [b] Average of all values. [c] Energy in Hartrees.

Table 3 Restraints on parameters and single amplitudes (distances and amplitudes in pm; angles in degrees).

Data	Computed value[a]	Refined value[b]	Data	Computed value[a]	Refined value[b]
p_5	148.7(10)	149.7(10)	p_{25}	0.3(10)	-0.3(11)
p_6	110.0(10)	110.1(6)	p_{26}	122.0(10)	122.0(11)
p_8	108.9(10)	109.3(11)	p_{27}	-5.4(10)	-6.2(11)
p_{10}	4.7(10)	4.8(10)	u_4	6.7(7)	7.2(6)
p_{11}	6.4(10)	7.3(11)	u_5	5.9(6)	6.1(7)
p_{12}	58.5(20)	58.4(22)	u_{17}	11.9(12)	12.8(9)
p_{13}	-3.0(20)	-4.4(11)	u_{20}	11.8(12)	12.8(11)
p_{14}	3.0(20)	2.0(21)	u_{22}	23.7(24)	27.9(23)
p_{15}	65.9(20)	62.0(14)	u_{25}	33.5(34)	35.5(37)
p_{16}	-10.0(20)	-12.3(20)	u_{26}	24.0(24)	26.1(18)
p_{17}	-1.8(15)	-0.3(16)	u_{29}	10.9(11)	8.2(10)
p_{18}	2.0(10)	2.4(11)	u_{32}	12.4(12)	14.4(13)
p_{19}	2.0(10)	4.0(10)	u_{35}	19.4(19)	18.7(21)
p_{20}	-3.0(10)	-4.7(9)	u_{36}	10.5(10)	10.0(11)
p_{21}	-3.0(10)	-3.0(10)	u_{39}	10.5(10)	10.4(12)
p_{23}	-2.0(10)	-2.4(10)	u_{52}	10.9(11)	9.7(12)
p_{24}	113.9(10)	112.1(7)	u_{55}	34.2(34)	32.3(24)

[a] Value used as restraint with uncertainty in parentheses.

[b] Value observed in the refinement after restraint applied, with esd.

Table 4 Restraints on ratios of vibrational amplitudes.

Amplitude ratio	Value[a]	Uncertainty[b]
u_7[Si(1)-C(11)]/u_6[Si(1)-C(12)]	1.000	0.050
u_9[Si(1)...C(121)]/u_8[Si(2)...C(211)]	0.946	0.047
u_{10}[Si(1)...C(111)]/u_8[Si(2)...C(211)]	0.968	0.048
u_{11}[Si(2)...C(213)]/u_8[Si(2)...C(211)]	1.006	0.050
u_{12}[Si(1)...C(122)]/u_8[Si(2)...C(211)]	0.975	0.049
u_{13}[Si(1)...C(122)]/u_8[Si(2)...C(211)]	0.962	0.048
u_{14}[Si(2)...C(212)]/u_8[Si(2)...C(211)]	0.967	0.048
u_{15}[Si(1)...C(123)]/u_8[Si(2)...C(211)]	0.946	0.047
u_{16}[Si(1)...C(113)]/u_8[Si(2)...C(211)]	1.015	0.051
u_{18}[Si(2)...C(11)]/u_{17}[Si(2)...C(12)]	1.089	0.055
u_{19}[Si(1)...C(21)]/u_{17}[Si(2)...C(12)]	1.083	0.054
u_{21}[Si(2)...C(122)]/u_{20}[Si(2)...C(112)]	0.976	0.049
u_{23}[Si(1)...C(213)]/u_{22}[Si(2)...C(121)]	1.074	0.054
u_{24}[Si(1)...C(211)]/u_{22}[Si(2)...C(121)]	1.045	0.052
u_{27}[Si(2)...C(113)]/u_{26}[Si(2)...C(123)]	0.787	0.039
u_{28}[Si(1)...C(212)]/u_{26}[Si(2)...C(123)]	0.478	0.024
u_{56}[C(111)...C(12)]/u_{55}[C(112)...C(123)]	0.795	0.040
u_{57}[C(11)...C(122)]/u_{55}[C(112)...C(123)]	0.629	0.031
u_{58}[C(213)...C(11)]/u_{55}[C(112)...C(123)]	0.947	0.047
u_{59}[C(21)...C(111)]/u_{55}[C(112)...C(123)]	0.925	0.046
u_{60}[C(21)...C(122)]/u_{55}[C(112)...C(123)]	0.713	0.036
u_{61}[C(211)...C(12)]/u_{55}[C(112)...C(123)]	1.114	0.056
u_{62}[C(21)...C(11)]/u_{55}[C(112)...C(123)]	0.555	0.028

[a] Values taken from HF/6-31G* scaled force field.

[b] Uncertainties are 5% of the amplitude ratio.

Table 5 Least-squares correlation matrix (×100) for 1,1,2-tri-*tert*-butyldisilane.[a]

	p_2	p_4	p_6	p_7	u_2	u_3	u_5	u_6	u_8	u_{17}	u_{18}	u_{20}	u_{22}	u_{23}	u_{26}	u_{27}	u_{55}	u_{56}	u_{57}	u_{58}	u_{59}	u_{61}	k_1
p_5	-52																						
p_6		68																					
p_7		70	70																				
u_4						61																	
u_6							-59																
u_7							-59	80															
u_9									64														
u_{10}									53														
u_{11}									59														
u_{12}									62														
u_{13}									53														
u_{14}									54														
u_{15}									53														
u_{16}									53														
u_{18}										75													
u_{19}										77	58												
u_{21}												80											
u_{23}													82										
u_{24}													82	67									
u_{27}															74								
u_{28}															73	52							
u_{43}	-62																						
u_{56}																	82						
u_{57}																	82	68					
u_{58}																	82	68	68				
u_{59}																	82	68	68	68			
u_{61}																	82	68	68	68	68		
u_{62}																	83	69	69	69	68	69	
k_1					59																		
k_2			-59	-52	67																		58

[a] Only elements with absolute values >50% are shown; k_1 and k_2 are scale factors.

Table 6 Experimental coordinates from GED analysis for the *syn* conformer of 1,1,2-tri-*tert*-butyldisilane.

Atom Number	*x*	*y*	*z*
Si(1)	0.0000	0.0000	0.0000
Si(2)	2.3634	0.0000	0.0000
C(11)	-0.6934	-0.4856	-1.7197
C(111)	-0.4150	0.6942	-2.6778
C(112)	-0.0801	-1.7663	-2.3288
C(113)	-2.2226	-0.6784	-1.6115
H(1111)	0.6761	0.9119	-2.8338
H(1112)	-0.8707	0.4017	-3.6623
H(1113)	-0.9212	1.6263	-2.3069
H(1121)	-0.2372	-2.6906	-1.7095
H(1122)	-0.5874	-1.9049	-3.3218
H(1123)	1.0216	-1.6282	-2.5008
H(1131)	-2.7685	0.2069	-1.1865
H(1132)	-2.5825	-0.8566	-2.6608
H(1133)	-2.4590	-1.5832	-0.9887
C(12)	-0.6132	-0.8653	1.5920
C(121)	-0.1289	-2.3183	1.7953
C(122)	-0.1339	-0.0169	2.7911
C(123)	-2.1582	-0.8616	1.5758
H(1211)	0.9886	-2.4294	1.8320
H(1212)	-0.5585	-2.6480	2.7798
H(1213)	-0.5326	-2.9818	0.9833
H(1221)	-0.4451	1.0617	2.7446
H(1222)	-0.5943	-0.4880	3.7014
H(1223)	0.9847	-0.0678	2.8832
H(1231)	-2.6105	-1.4632	0.7415
H(1232)	-2.4745	-1.3080	2.5573
H(1233)	-2.5457	0.1913	1.5149

Table 6 Continued

Atom Number	*x*	*y*	*z*
H(13)	-0.5287	1.3955	0.1527
C(21)	3.1975	1.7113	0.0000
C(211)	2.7590	2.5132	1.2458
C(212)	4.7231	1.4791	0.0790
C(213)	2.8952	2.5562	-1.2578
H(2111)	2.9870	1.9406	2.1853
H(2112)	3.3764	3.4518	1.2345
H(2113)	1.6713	2.7949	1.2479
H(2121)	5.0854	0.9193	-0.8253
H(2122)	5.1855	2.5031	0.0808
H(2123)	5.0542	0.9302	1.0018
H(2131)	1.7947	2.7687	-1.3365
H(2132)	3.4419	3.5265	-1.1094
H(2133)	3.2433	2.0871	-2.2176
H(22)	2.9237	-0.7961	1.1371
H(23)	2.8466	-0.6742	-1.2415

Appendix 3

Supplementary tables for 1,1,2,2-tetra-*tert*-butyldisilane.

Table 1 Experimental coordinates from GED analysis for the *syn* conformer of 1,1,2,2-tetra-*tert*-butyldisilane.

Atom Number	*x*	*y*	*z*
Si(1)	1.1969	0.0000	0.0000
Si(2)	-1.1969	0.0000	0.0000
C(3)	-1.6872	1.8719	-0.0648
C(4)	-1.1502	2.5615	-1.3293
C(5)	-3.2110	2.0673	-0.0111
C(6)	-1.0797	2.5867	1.1530
H(7)	-1.5057	1.9900	-2.2180
H(8)	-1.5413	3.6052	-1.3523
H(9)	-0.0364	2.5610	-1.2827
H(10)	-3.6537	1.6256	-0.9340
H(11)	-3.5991	1.5494	0.8966
H(12)	-3.4226	3.1606	0.0407
H(13)	0.0189	2.3974	1.1585
H(14)	-1.2890	3.6777	1.0595
H(15)	-1.5533	2.1742	2.0740
C(16)	-2.3412	-1.1555	-1.0507
C(17)	-1.6694	-2.5305	-1.1958
C(18)	-3.6800	-1.3377	-0.3176
C(19)	-2.6489	-0.6339	-2.4635
H(20)	-0.7001	-2.3924	-1.7290
H(21)	-1.4999	-2.9472	-0.1758
H(22)	-2.3485	-3.1923	-1.7819
H(23)	-3.4778	-1.8201	0.6669
H(24)	-4.1410	-0.3328	-0.1745
H(25)	-4.3372	-1.9850	-0.9436
H(26)	-1.6842	-0.5014	-3.0061
H(27)	-3.2906	-1.3837	-2.9820
H(28)	-3.1826	0.3404	-2.3690

Table 1 Continued

Atom Number	*x*	*y*	*z*
H(29)	-1.7189	-0.4509	1.3354
H(30)	1.7189	1.4095	0.0000
C(31)	1.6872	-0.6603	1.7528
C(32)	1.1502	-2.0790	2.0015
C(33)	3.2110	-0.6720	1.9551
C(34)	1.0797	0.2648	2.8197
H(35)	1.5057	-2.7381	1.1757
H(36)	1.5413	-2.4347	2.9830
H(37)	0.0364	-2.0347	2.0160
H(38)	3.6537	-1.4050	1.2413
H(39)	3.5991	0.3537	1.7548
H(40)	3.4226	-0.9726	3.0075
H(41)	-0.0189	0.3306	2.6421
H(42)	1.2890	-0.1728	3.8234
H(43)	1.5533	1.2694	2.7234
C(44)	2.3412	-0.6257	-1.4309
C(45)	1.6694	-0.3234	-2.7800
C(46)	3.6800	0.1271	-1.3690
C(47)	2.6489	-2.1312	-1.3887
H(48)	0.7001	-0.8727	-2.8199
H(49)	1.4999	0.7763	-2.8486
H(50)	2.3485	-0.6669	-3.5946
H(51)	3.4778	1.2142	-1.5110
H(52)	4.1410	-0.0588	-0.3712
H(53)	4.3372	-0.2589	-2.1826
H(54)	1.6842	-2.6877	-1.4368
H(55)	3.2906	-2.3826	-2.2650
H(56)	3.1826	-2.3534	-0.4355

Table 2 Experimental coordinates from GED analysis for the *anti* conformer of 1,1,2,2-tetra-*tert*-butyldisilane.

Atom Number	*x*	*y*	*z*
Si(1)	1.2068	0.0000	0.0000
Si(2)	-1.2068	0.0000	0.0000
C(3)	-2.1184	0.3807	1.6807
C(4)	-3.0149	1.6378	1.5938
C(5)	-2.9853	-0.8055	2.1633
C(6)	-1.0093	0.6380	2.7272
H(7)	-2.7911	2.3215	2.4583
H(8)	-2.8132	2.1793	0.6289
H(9)	-4.0969	1.3330	1.6306
H(10)	-2.5181	-1.2677	3.0760
H(11)	-4.0177	-0.4393	2.4183
H(12)	-3.0549	-1.5781	1.3489
H(13)	-1.2040	0.0166	3.6441
H(14)	-0.0095	0.3593	2.2939
H(15)	-1.0022	1.7266	3.0097
C(16)	-2.1184	0.8729	-1.4858
C(17)	-3.5137	1.3280	-0.9985
C(18)	-1.3062	2.1275	-1.8832
C(19)	-2.2999	-0.0138	-2.7397
H(20)	-4.2387	1.3083	-1.8580
H(21)	-3.8757	0.6350	-0.1900
H(22)	-3.4483	2.3741	-0.5904
H(23)	-2.0007	2.9142	-2.2877
H(24)	-0.7707	2.5319	-0.9807
H(25)	-0.5525	1.8549	-2.6722
H(26)	-1.4603	-0.7598	-2.7992
H(27)	-3.2804	-0.5610	-2.6764
H(28)	-2.2918	0.6302	-3.6618

Table 2 Continued

Atom Number	*x*	*y*	*z*
H(29)	-1.7243	-1.4042	-0.2183
H(30)	1.7243	1.4210	0.0000
C(31)	2.1184	-0.6343	1.6023
C(32)	3.0149	-1.8631	1.3233
C(33)	2.9853	0.4637	2.2614
C(34)	1.0093	-1.0494	2.5968
H(35)	2.7911	-2.6715	2.0726
H(36)	2.8132	-2.2500	0.2867
H(37)	4.0969	-1.5677	1.4065
H(38)	2.5181	0.7801	3.2343
H(39)	4.0177	0.0627	2.4571
H(40)	3.0549	1.3522	1.5753
H(41)	1.2040	-0.5761	3.5983
H(42)	0.0095	-0.7074	2.2115
H(43)	1.0022	-2.1684	2.7088
C(44)	2.1184	-0.6343	-1.6023
C(45)	3.5137	-1.1589	-1.1906
C(46)	1.3062	-1.8129	-2.1876
C(47)	2.2999	0.4344	-2.7051
H(48)	4.2387	-1.0074	-2.0369
H(49)	3.8757	-0.5983	-0.2853
H(50)	3.4483	-2.2552	-0.9481
H(51)	2.0007	-2.5282	-2.7082
H(52)	0.7707	-2.3513	-1.3579
H(53)	0.5525	-1.4224	-2.9254
H(54)	1.4603	1.1807	-2.6493
H(55)	3.2804	0.9654	-2.5584
H(56)	2.2918	-0.0603	-3.7151

Appendix 4

Supplementary tables for tris(*tert*-butyl)sulfurtriimide.

Table 1 Theoretical geometrical parameters (HF/3-21G* and HF/6-31G*) for the C_{3h} molecular structure of tris(*tert*-butyl)sulfurtriimide.[a]

Geometrical parameter	HF/3-21G*	HF/6-31G*
S(1)=N(2)	147.2	147.7
N(2)-C(5)	149.1	147.6
C-C (mean)	154.5	153.9
C-H (mean)	108.1	108.2
S(1)-N(2)-C(5)	139.1	137.7
C-C-C (mean)	110.1	109.7
H-C-H (mean)	108.3	107.7
N(2)=S(1)=N(3)-C(5)	0.0	0.0
Absolute energy[b]	-1025.4571	-1030.7739

[a] All distances in pm, angles in degrees.
[b] Energy in Hartrees.

Table 2 Experimental coordinates from GED analysis for $S(NBu^t)_3$.

Atom Number	*x*	*y*	*z*
S(1)	0.0000	0.0000	0.0000
N(2)	1.5291	0.0000	0.0000
N(3)	-0.7646	1.3242	0.0000
N(4)	-0.7646	-1.3242	0.0000
C(5)	2.3845	1.1133	-0.4524
C(6)	-2.1564	1.5084	-0.4524
C(7)	-0.2281	-2.6217	-0.4524
C(8)	2.0900	2.3893	0.3210
C(9)	-3.1142	0.6153	0.3210
C(10)	1.0242	-3.0046	0.3210
C(11)	3.7962	0.6458	-0.1334
C(12)	2.2554	1.3389	-1.9510
C(13)	-2.4574	2.9648	-0.1334
C(14)	-2.2872	1.2838	-1.9510
C(15)	-1.3389	-3.6105	-0.1334
C(16)	0.0318	-2.6227	-1.9510
H(17)	2.2701	2.1305	1.3947
H(18)	2.8086	3.1481	-0.0790
H(19)	1.0204	2.6293	0.0959
H(20)	-2.9801	0.9007	1.3947
H(21)	-4.1306	0.8583	-0.0790
H(22)	-2.7872	-0.4309	0.0959
H(23)	0.7100	-3.0312	1.3947
H(24)	1.3220	-4.0064	-0.0790
H(25)	1.7668	-2.1983	0.0959
H(26)	4.4664	1.4646	-0.4975
H(27)	2.9154	2.2146	-2.1743
H(28)	3.8187	0.5151	0.9777
H(29)	1.1695	1.5460	-2.1246
H(30)	3.9223	-0.3136	-0.6956
H(31)	2.6065	0.3869	-2.4229
H(32)	-3.5016	3.1357	-0.4975
H(33)	-3.3755	1.4175	-2.1743
H(34)	-2.3555	3.0495	0.9777
H(35)	-1.9236	0.2399	-2.1246
H(36)	-1.6896	3.5536	-0.6956
H(37)	-1.6384	2.0639	-2.4229
H(38)	-0.9648	-4.6003	-0.4975
H(39)	0.4602	-3.6321	-2.1743
H(40)	-1.4632	-3.5647	0.9777
H(41)	0.7541	-1.7858	-2.1246
H(42)	-2.2327	-3.2400	-0.6956
H(43)	-0.9682	-2.4508	-2.4229

Appendix 5

Supplementary tables for bis(trichlorosilyl)*tert*-butylphosphine.

Table 1 Theoretical geometrical parameters (HF/6-31G*) for the C_1 and C_s molecular structures of bis(trichlorosilyl)*tert*-butylphosphine.[a]

Geometrical parameter	HF/6-31G* / C_1	HF/6-31G* / C_s
P-C	191.9	192.6
C-C (mean)	153.7	154.5
P-Si (mean)	225.9	226.5
C-H (mean)	108.4	108.4
Si-Cl (mean)	204.7	204.7
P-C(1)-C(2)	106.2	116.3
P-C(1)-C(4)	114.9	106.6
P-C(1)-C(5)	108.1	106.6
C-C-C (mean)	109.1	109.0
H-C-H (mean)	107.8	107.6
C-P-Si(7)	109.5	109.0
C-P-Si(8)	108.7	109.0
P-Si(7)-Cl(17)	116.4	108.7
P-Si(7)-Cl(19)	108.4	116.7
P-Si(7)-Cl(21)	109.7	109.9
P-Si(8)-Cl(18)	116.9	108.7
P-Si(8)-Cl(20)	109.3	116.7
P-Si(8)-Cl(22)	108.3	109.9
C-P-Si(7)-Cl(17)	74.0	-67.9
C-P-Si(8)-Cl(18)	-40.7	67.9
Absolute energy[b]	-3832.4832	-3832.4730

[a] All distances in pm, angles in degrees.
[b] Energy in Hartrees.

Table 2 Experimental coordinates from GED analysis for $PBu^t(SiCl_3)_2$.

Atom	*x*	*y*	*z*
C(1)	1.9059	0.0000	0.0000
C(2)	2.3348	1.5047	0.0000
H(3)	2.0015	2.0353	-0.9389
C(4)	2.5691	-0.7383	-1.2095
C(5)	2.3887	-0.6400	1.3436
P(6)	0.0000	0.0000	0.0000
Si(7)	-0.5717	0.1111	-2.1320
Si(8)	-0.5522	-2.0953	0.4352
H(9)	1.8918	2.0665	0.8730
H(10)	3.4557	1.6207	0.0658
H(11)	3.6942	-0.6487	-1.1891
H(12)	3.5130	-0.7320	1.3836
H(13)	2.3246	-1.8403	-1.2128
H(14)	1.9662	-1.6765	1.4894
H(15)	2.2213	-0.3189	-2.1981
H(16)	2.0746	-0.0256	2.2369
Cl(17)	-0.1543	-1.5239	-3.2639
Cl(18)	0.5991	-3.5552	-0.3845
Cl(19)	-2.5696	0.4729	-2.2128
Cl(20)	-2.4446	-2.3587	-0.2567
Cl(21)	0.3424	1.7079	-2.9943
Cl(22)	-0.5517	-2.3855	2.4463

Appendix 6

Supplementary tables for Z_2R_4 and ZR_2.

Table 1 Atomic coordinates (x 10^4) and equivalent isotropic displacement parameters ($Å^2$ x 10^3) for tetra(disyl)diphosphine **(1)**. U(eq) is defined as one third of the trace of the orthogonalized Uij tensor.

	x	*y*	*z*	U(eq)
P(1)	2041(1)	9568(1)	2830(1)	21(1)
P(2)	2965(1)	10480(1)	2540(1)	23(1)
Si(1)	2935(1)	9615(1)	4693(1)	33(1)
Si(2)	1095(1)	9831(1)	3917(1)	36(1)
Si(3)	1627(1)	7281(1)	2518(1)	31(1)
Si(4)	3390(1)	7837(1)	2896(1)	35(1)
Si(5)	1485(1)	10403(1)	884(1)	44(1)
Si(6)	3204(1)	10736(1)	973(1)	44(1)
Si(7)	4075(1)	12273(1)	3263(1)	37(1)
Si(8)	2256(1)	12714(1)	2736(1)	36(1)
C(1)	2088(1)	9946(2)	3803(1)	26(1)
C(2)	2428(1)	8246(1)	2963(1)	25(1)
C(3)	2492(1)	10809(2)	1511(1)	30(1)
C(4)	3047(1)	11728(1)	3023(1)	26(1)
C(5)	3834(1)	10251(2)	4698(1)	49(1)
C(6)	2774(2)	10095(2)	5547(1)	56(1)
C(7)	3115(2)	8244(2)	4884(1)	43(1)
C(8)	968(2)	10824(2)	4557(2)	60(1)
C(9)	968(2)	8597(2)	4316(2)	53(1)
C(10)	246(1)	10021(2)	3033(2)	46(1)
C(11)	631(1)	7825(2)	2136(2)	46(1)
C(12)	1637(2)	6387(2)	3274(1)	46(1)
C(13)	1725(2)	6538(2)	1722(2)	51(1)
C(14)	4285(1)	8462(2)	3538(1)	47(1)
C(15)	3550(2)	6495(2)	3186(2)	63(1)
C(16)	3392(2)	7969(2)	1924(2)	50(1)
C(17)	673(1)	10802(2)	1195(2)	61(1)
C(18)	1415(2)	9034(2)	741(2)	57(1)
C(19)	1241(2)	11034(2)	-56(2)	70(1)
C(20)	4242(2)	10569(2)	1567(2)	64(1)
C(21)	3016(2)	9713(2)	259(2)	64(1)
C(22)	3134(2)	11961(2)	480(2)	65(1)
C(23)	4845(1)	11293(2)	3453(2)	54(1)
C(24)	4126(2)	13131(2)	2509(1)	49(1)
C(25)	4392(2)	13007(2)	4152(2)	70(1)
C(26)	1970(2)	13234(2)	1764(1)	50(1)
C(27)	2560(2)	13836(2)	3348(2)	72(1)
C(28)	1361(2)	12267(2)	2880(2)	67(1)

Table 2 Anisotropic displacement parameters ($Å^2$ x 10^3) for tetra(disyl)diphosphine **(1)**. The anisotropic displacement factor exponent takes the form: $-2\,p^2\,[\,h^2\,a^{*2}\,U11 + ... + 2\,h\,k\,a^*\,b^*\,U12]$.

	U11	U22	U33	U23	U13	U12
P(1)	21(1)	18(1)	26(1)	1(1)	10(1)	1(1)
P(2)	24(1)	20(1)	26(1)	1(1)	11(1)	0(1)
Si(1)	42(1)	30(1)	26(1)	2(1)	12(1)	-5(1)
Si(2)	40(1)	30(1)	49(1)	0(1)	30(1)	2(1)
Si(3)	35(1)	19(1)	43(1)	-4(1)	16(1)	-4(1)
Si(4)	30(1)	26(1)	51(1)	2(1)	20(1)	7(1)
Si(5)	48(1)	42(1)	31(1)	7(1)	0(1)	-10(1)
Si(6)	67(1)	37(1)	39(1)	-7(1)	35(1)	-11(1)
Si(7)	39(1)	38(1)	35(1)	-1(1)	13(1)	-17(1)
Si(8)	51(1)	21(1)	45(1)	7(1)	28(1)	6(1)
C(1)	34(1)	20(1)	30(1)	0(1)	17(1)	1(1)
C(2)	27(1)	19(1)	32(1)	1(1)	12(1)	1(1)
C(3)	39(1)	26(1)	25(1)	1(1)	12(1)	-2(1)
C(4)	34(1)	20(1)	26(1)	0(1)	14(1)	-4(1)
C(5)	41(1)	54(2)	42(1)	14(1)	3(1)	-9(1)
C(6)	83(2)	56(2)	33(1)	-7(1)	25(1)	-9(2)
C(7)	54(2)	38(1)	32(1)	10(1)	7(1)	-1(1)
C(8)	73(2)	55(2)	70(2)	-10(1)	48(2)	6(2)
C(9)	54(2)	50(2)	70(2)	10(1)	39(1)	-6(1)
C(10)	33(1)	38(1)	73(2)	4(1)	28(1)	6(1)
C(11)	33(1)	33(1)	67(2)	-5(1)	11(1)	-8(1)
C(12)	53(2)	25(1)	63(2)	6(1)	25(1)	-4(1)
C(13)	64(2)	36(1)	60(2)	-19(1)	28(1)	-11(1)
C(14)	30(1)	50(2)	60(2)	9(1)	15(1)	6(1)
C(15)	52(2)	31(1)	109(2)	12(2)	34(2)	16(1)
C(16)	52(2)	50(2)	61(2)	-10(1)	36(1)	2(1)
C(17)	38(1)	63(2)	68(2)	21(2)	2(1)	-1(1)
C(18)	69(2)	47(2)	46(1)	-1(1)	7(1)	-21(1)
C(19)	81(2)	68(2)	39(1)	15(1)	-5(1)	-17(2)
C(20)	59(2)	75(2)	78(2)	-17(2)	49(2)	-9(2)
C(21)	116(3)	46(2)	47(2)	-9(1)	50(2)	-6(2)
C(22)	114(3)	49(2)	51(2)	-4(1)	53(2)	-25(2)
C(23)	30(1)	63(2)	62(2)	19(1)	9(1)	-9(1)
C(24)	52(2)	44(2)	57(2)	6(1)	28(1)	-12(1)
C(25)	79(2)	78(2)	51(2)	-19(2)	21(2)	-39(2)
C(26)	61(2)	38(1)	54(2)	20(1)	23(1)	16(1)
C(27)	121(3)	33(1)	74(2)	-10(1)	50(2)	7(2)
C(28)	56(2)	56(2)	109(3)	37(2)	52(2)	27(1)

Table 3 Hydrogen coordinates (x 10^4) and isotropic displacement parameters ($Å^2$ x 10^3) for tetra(disyl)diphosphine **(1)**.

	x	*y*	*z*	U(eq)
H(5A)	3956(1)	10040(2)	4270(1)	73
H(5B)	4257(1)	10084(2)	5149(1)	73
H(5C)	3753(1)	10959(2)	4676(1)	73
H(6A)	2314(2)	9796(2)	5584(1)	84
H(6B)	2712(2)	10805(2)	5511(1)	84
H(6C)	3215(2)	9931(2)	5985(1)	84
H(7A)	2644(2)	7929(2)	4879(1)	65
H(7B)	3515(2)	8152(2)	5367(1)	65
H(7C)	3279(2)	7952(2)	4504(1)	65
H(8A)	1385(2)	10783(2)	5034(2)	90
H(8B)	479(2)	10731(2)	4627(2)	90
H(8C)	975(2)	11466(2)	4338(2)	90
H(9A)	1398(2)	8479(2)	4773(2)	80
H(9B)	949(2)	8080(2)	3961(2)	80
H(9C)	491(2)	8598(2)	4418(2)	80
H(10A)	296(1)	10651(2)	2815(2)	69
H(10B)	-227(1)	10014(2)	3142(2)	69
H(10C)	231(1)	9497(2)	2685(2)	69
H(11A)	603(1)	8290(2)	1745(2)	69
H(11B)	518(1)	8163(2)	2531(2)	69
H(11C)	257(1)	7303(2)	1937(2)	69
H(12A)	2144(2)	6090(2)	3485(1)	68
H(12B)	1255(2)	5876(2)	3066(1)	68
H(12C)	1516(2)	6736(2)	3660(1)	68
H(13A)	2231(2)	6232(2)	1879(2)	77
H(13B)	1665(2)	6970(2)	1303(2)	77
H(13C)	1331(2)	6031(2)	1576(2)	77
H(14A)	4302(1)	8407(2)	4046(1)	70
H(14B)	4277(1)	9152(2)	3405(1)	70
H(14C)	4737(1)	8148(2)	3494(1)	70
H(15A)	3549(2)	6423(2)	3687(2)	94
H(15B)	4042(2)	6277(2)	3169(2)	94
H(15C)	3139(2)	6098(2)	2849(2)	94
H(16A)	2936(2)	7654(2)	1579(2)	75
H(16B)	3850(2)	7658(2)	1891(2)	75
H(16C)	3390(2)	8663(2)	1802(2)	75
H(17A)	698(1)	11510(2)	1272(2)	91
H(17B)	719(1)	10471(2)	1655(2)	91
H(17C)	183(1)	10631(2)	816(2)	91
H(18A)	1829(2)	8812(2)	580(2)	86
H(18B)	923(2)	8870(2)	364(2)	86
H(18C)	1459(2)	8710(2)	1204(2)	86
H(19A)	1276(2)	11743(2)	13(2)	105
H(19B)	721(2)	10858(2)	-372(2)	105

Table 3 Continued

	x	*y*	*z*	U(eq)
H(19C)	1602(2)	10823(2)	-289(2)	105
H(20A)	4305(2)	9948(2)	1832(2)	96
H(20B)	4403(2)	11106(2)	1922(2)	96
H(20C)	4556(2)	10568(2)	1256(2)	96
H(21A)	2484(2)	9745(2)	-76(2)	96
H(21B)	3111(2)	9080(2)	510(2)	96
H(21C)	3356(2)	9791(2)	-21(2)	96
H(22A)	2603(2)	12079(2)	164(2)	98
H(22B)	3458(2)	11947(2)	179(2)	98
H(22C)	3305(2)	12485(2)	845(2)	98
H(23A)	4733(1)	10869(2)	3022(2)	81
H(23B)	4854(1)	10903(2)	3879(2)	81
H(23C)	5343(1)	11604(2)	3556(2)	81
H(24A)	3966(2)	12782(2)	2039(1)	73
H(24B)	4651(2)	13364(2)	2631(1)	73
H(24C)	3787(2)	13690(2)	2471(1)	73
H(25A)	4375(2)	12592(2)	4557(2)	104
H(25B)	4051(2)	13566(2)	4099(2)	104
H(25C)	4915(2)	13240(2)	4259(2)	104
H(26A)	2425(2)	13470(2)	1678(1)	76
H(26B)	1612(2)	13776(2)	1709(1)	76
H(26C)	1724(2)	12723(2)	1406(1)	76
H(27A)	3025(2)	14110(2)	3302(2)	107
H(27B)	2661(2)	13651(2)	3861(2)	107
H(27C)	2152(2)	14324(2)	3196(2)	107
H(28A)	1169(2)	11684(2)	2580(2)	101
H(28B)	971(2)	12779(2)	2735(2)	101
H(28C)	1480(2)	12106(2)	3400(2)	101
H(4)	3006(13)	11551(18)	3463(13)	40(6)
H(2)	2460(13)	8142(18)	3439(13)	40(6)
H(3)	2373(13)	11451(19)	1470(12)	36(6)
H(1)	2110(14)	10628(21)	3797(14)	49(7)

Table 4 Atomic coordinates (x 10^4) and equivalent isotropic displacement parameters ($Å^2$ x 10^3) for bis(disyl)chlorophosphine **(2)**. U(eq) is defined as one third of the trace of the orthogonalized Uij tensor.

	x	*y*	*z*	U(eq)
P(1)	5240(1)	7290(1)	3063(1)	27(1)
Cl(1)	7018(1)	8277(1)	2887(1)	40(1)
C(1)	5333(2)	6144(2)	2499(1)	26(1)
C(2)	5926(2)	6785(2)	3882(1)	27(1)
Si(1)	5680(1)	6556(1)	1627(1)	34(1)
C(11)	7643(3)	6727(3)	1546(1)	55(1)
C(12)	5101(3)	5503(2)	1006(1)	53(1)
C(13)	4688(3)	7830(2)	1409(1)	48(1)
Si(2)	3614(1)	5304(1)	2529(1)	33(1)
C(21)	2981(3)	5220(2)	3372(1)	55(1)
C(22)	2061(3)	5864(2)	1999(1)	52(1)
C(23)	4012(3)	3890(2)	2294(1)	51(1)
Si(3)	7831(1)	6256(1)	4057(1)	31(1)
C(31)	7741(3)	5089(2)	4632(2)	64(1)
C(32)	8700(3)	5741(2)	3333(1)	52(1)
C(33)	9093(2)	7291(2)	4436(1)	44(1)
Si(4)	5299(1)	7760(1)	4519(1)	37(1)
C(41)	6111(3)	9120(2)	4441(2)	67(1)
C(42)	5752(3)	7211(3)	5364(1)	63(1)
C(43)	3298(3)	7890(3)	4423(1)	55(1)

Table 5 Anisotropic displacement parameters ($Å^2$ x 10^3) for bis(disyl)chlorophosphine **(2)**. The anisotropic displacement factor exponent takes the form: $-2\,p^2\,[\,h^2\,a^{*2}\,U11 + ... + 2\,h\,k\,a^*\,b^*\,U12\,]$.

	U11	U22	U33	U23	U13	U12
P(1)	28(1)	26(1)	28(1)	0(1)	2(1)	1(1)
Cl(1)	50(1)	35(1)	37(1)	4(1)	4(1)	-14(1)
C(1)	26(1)	25(1)	27(1)	0(1)	1(1)	1(1)
C(2)	25(1)	28(1)	28(1)	2(1)	5(1)	-2(1)
Si(1)	41(1)	33(1)	27(1)	-3(1)	4(1)	-2(1)
C(11)	53(2)	74(2)	41(1)	-8(1)	19(1)	-12(2)
C(12)	68(2)	51(2)	39(1)	-14(1)	5(1)	-2(1)
C(13)	66(2)	37(1)	36(1)	6(1)	-8(1)	0(1)
Si(2)	27(1)	30(1)	42(1)	-1(1)	0(1)	-4(1)
C(21)	41(1)	66(2)	59(2)	-1(1)	11(1)	-25(1)
C(22)	35(1)	51(2)	66(2)	-4(1)	-8(1)	2(1)
C(23)	49(2)	30(1)	74(2)	-2(1)	2(1)	-5(1)
Si(3)	26(1)	31(1)	36(1)	4(1)	-1(1)	2(1)
C(31)	52(2)	54(2)	82(2)	33(2)	-5(2)	1(1)
C(32)	35(1)	59(2)	60(2)	-18(1)	-2(1)	18(1)
C(33)	31(1)	51(2)	49(1)	-5(1)	0(1)	-5(1)
Si(4)	31(1)	49(1)	32(1)	-7(1)	9(1)	0(1)
C(41)	69(2)	50(2)	87(2)	-30(2)	37(2)	-5(2)
C(42)	45(2)	113(3)	32(1)	-4(2)	5(1)	3(2)
C(43)	37(1)	83(2)	46(1)	-9(1)	10(1)	17(1)

Table 6 Hydrogen coordinates (x 10^4) and isotropic displacement parameters ($Å^2$ x 10^3) for bis(disyl)chlorophosphine **(2)**.

	x	*y*	*z*	U(eq)
H(1)	6160(2)	5682(2)	2673(1)	35(4)
H(2)	5320(2)	6132(2)	3938(1)	35(4)
H(11A)	8159(4)	6075(6)	1704(9)	82(2)
H(11B)	8005(5)	7347(9)	1807(8)	82(2)
H(11C)	7798(3)	6847(15)	1084(2)	82(2)
H(12A)	4054(4)	5414(11)	985(7)	82(2)
H(12B)	5570(16)	4817(4)	1131(5)	82(2)
H(12C)	5377(18)	5725(7)	574(2)	82(2)
H(13A)	3650(3)	7706(4)	1412(9)	82(2)
H(13B)	4904(17)	8065(9)	971(4)	82(2)
H(13C)	4990(16)	8390(5)	1731(6)	82(2)
H(21A)	3728(9)	4881(14)	3670(2)	82(2)
H(21B)	2098(12)	4788(13)	3356(2)	82(2)
H(21C)	2786(19)	5947(3)	3529(4)	82(2)
H(22A)	1864(13)	6600(6)	2140(6)	82(2)
H(22B)	1209(6)	5413(9)	2038(7)	82(2)
H(22C)	2295(8)	5873(14)	1541(2)	82(2)
H(23A)	4750(15)	3588(5)	2612(5)	82(2)
H(23B)	4362(19)	3884(2)	1856(4)	82(2)
H(23C)	3132(5)	3457(4)	2289(9)	82(2)
H(31A)	7346(19)	5331(4)	5035(4)	82(2)
H(31B)	8711(4)	4798(10)	4739(8)	82(2)
H(31C)	7119(17)	4528(7)	4423(4)	82(2)
H(32A)	8687(18)	6304(5)	2997(4)	82(2)
H(32B)	8172(12)	5109(9)	3154(6)	82(2)
H(32C)	9699(7)	5538(14)	3469(2)	82(2)
H(33A)	8694(10)	7598(11)	4822(6)	82(2)
H(33B)	9223(16)	7864(8)	4116(3)	82(2)
H(33C)	10025(7)	6955(4)	4568(9)	82(2)
H(41A)	7149(4)	9047(3)	4410(9)	82(2)
H(41B)	5942(17)	9554(5)	4828(4)	82(2)
H(41C)	5668(14)	9475(6)	4045(5)	82(2)
H(42A)	5323(17)	6494(7)	5396(3)	82(2)
H(42B)	5370(18)	7693(8)	5686(1)	82(2)
H(42C)	6800(3)	7158(14)	5452(4)	82(2)
H(43A)	2860(3)	7189(4)	4504(9)	82(2)
H(43B)	2987(3)	8129(15)	3976(3)	82(2)
H(43C)	2993(3)	8418(12)	4739(7)	82(2)

Table 7 Atomic coordinates [x 10^4] and equivalent isotropic displacement parameters [$Å^2$ x 10^3] for bis(disyl)chloroarsine **(3)**. U(eq) is defined as one third of the trace of the orthogonalized U_{ij} tensor.

	x	*y*	*z*	U(eq)
As(1)	9319(1)	3493(1)	1090(1)	28(1)
Si(4)	11177(1)	1376(1)	1841(1)	30(1)
Si(2)	7499(1)	3628(1)	2164(1)	35(1)
Si(1)	6724(1)	2450(1)	461(1)	35(1)
Cl(1)	10583(1)	4109(1)	2247(1)	43(1)
Si(3)	11259(1)	2752(1)	312(1)	39(1)
C(1)	8006(3)	2799(3)	1417(2)	25(1)
C(2)	10327(3)	2255(3)	964(2)	27(1)
C(43)	10442(4)	1232(4)	2645(3)	50(1)
C(23)	5945(4)	3248(4)	2185(3)	56(1)
C(22)	7500(4)	5097(3)	1916(3)	48(1)
C(21)	8496(5)	3384(4)	3213(3)	51(1)
C(42)	11199(5)	-18(3)	1438(3)	56(1)
C(13)	5728(4)	3630(4)	56(3)	50(1)
C(41)	12767(4)	1863(4)	2339(3)	49(1)
C(33)	10226(5)	3176(5)	-685(3)	59(1)
C(32)	12230(5)	1651(5)	112(4)	71(2)
C(12)	7297(4)	1973(5)	-363(3)	71(2)
C(31)	12243(4)	3923(4)	784(3)	59(1)
C(11)	5830(5)	1305(4)	682(4)	71(2)

Table 8 Anisotropic displacement parameters ($Å^2 \times 10^3$) for bis(disyl)chloroarsine **(3)**. The anisotropic displacement factor exponent takes the form: $-2\,p^2\,[\,h^2\,a^{*2}\,U11 + ... + 2\,h\,k\,a^*\,b^*\,U12]$.

	U11	U22	U33	U23	U13	U12
As(1)	26(1)	24(1)	34(1)	1(1)	9(1)	2(1)
Si(4)	27(1)	27(1)	32(1)	0(1)	6(1)	5(1)
Si(2)	36(1)	32(1)	42(1)	-2(1)	20(1)	5(1)
Si(1)	24(1)	30(1)	45(1)	-7(1)	3(1)	2(1)
Cl(1)	38(1)	38(1)	49(1)	-15(1)	8(1)	-9(1)
Si(3)	33(1)	53(1)	34(1)	3(1)	15(1)	1(1)
C(1)	18(1)	24(1)	30(2)	-1(1)	3(1)	1(1)
C(2)	23(1)	27(2)	31(2)	-3(1)	9(1)	1(1)
C(43)	57(3)	48(2)	48(3)	20(2)	23(2)	15(2)
C(23)	48(2)	58(3)	73(3)	1(2)	36(3)	2(2)
C(22)	51(2)	33(2)	66(3)	-6(2)	28(2)	8(2)
C(21)	66(3)	56(3)	38(2)	-6(2)	23(2)	6(2)
C(42)	65(3)	32(2)	64(3)	-8(2)	10(2)	10(2)
C(13)	43(2)	50(3)	51(3)	9(2)	6(2)	15(2)
C(41)	34(2)	45(2)	57(3)	0(2)	-3(2)	3(2)
C(33)	62(3)	77(3)	39(2)	19(2)	16(2)	1(3)
C(32)	60(3)	100(5)	69(4)	1(3)	43(3)	23(3)
C(12)	43(2)	101(4)	57(3)	-46(3)	-1(2)	8(3)
C(31)	49(3)	66(3)	65(3)	11(3)	21(2)	-17(2)
C(11)	49(3)	47(3)	97(5)	-1(3)	-4(3)	-19(2)

Table 9 Hydrogen coordinates (x 10^4) and isotropic displacement parameters ($Å^2$ x 10^3) for bis(disyl)chloroarsine (**3**).

	x	*y*	*z*	U(eq)
H(1A)	8331(3)	2117(3)	1681(2)	30
H(2A)	9736(3)	1761(3)	610(2)	32
H(43A)	10400(4)	1925(4)	2880(3)	74
H(43B)	10913(4)	748(4)	3051(3)	74
H(43C)	9634(4)	949(4)	2417(3)	74
H(23A)	5366(4)	3351(4)	1662(3)	84
H(23B)	5727(4)	3694(4)	2566(3)	84
H(23C)	5944(4)	2505(4)	2339(3)	84
H(22A)	6985(4)	5216(3)	1375(3)	72
H(22B)	8315(4)	5322(3)	1966(3)	72
H(22C)	7201(4)	5506(3)	2279(3)	72
H(21A)	9323(5)	3561(4)	3256(3)	77
H(21B)	8449(5)	2638(4)	3347(3)	77
H(21C)	8231(5)	3827(4)	3575(3)	77
H(42A)	11569(5)	-2(3)	1018(3)	84
H(42B)	10380(5)	-283(3)	1227(3)	84
H(42C)	11660(5)	-484(3)	1861(3)	84
H(13A)	5409(4)	3906(4)	460(3)	76
H(13B)	5068(4)	3411(4)	-404(3)	76
H(13C)	6194(4)	4182(4)	-98(3)	76
H(41A)	12744(4)	2578(4)	2543(3)	74
H(41B)	13205(4)	1872(4)	1956(3)	74
H(41C)	13169(4)	1388(4)	2774(3)	74
H(33A)	9704(5)	3744(5)	-617(3)	88
H(33B)	9740(5)	2572(5)	-944(3)	88
H(33C)	10701(5)	3430(5)	-1010(3)	88
H(32A)	12784(5)	1401(5)	611(4)	106
H(32B)	12682(5)	1923(5)	-222(4)	106
H(32C)	11721(5)	1065(5)	-156(4)	106
H(12A)	7819(4)	1360(5)	-181(3)	106
H(12B)	7747(4)	2541(5)	-512(3)	106
H(12C)	6621(4)	1771(5)	-819(3)	106
H(31A)	12782(4)	3714(4)	1300(3)	89
H(31B)	11740(4)	4511(4)	847(3)	89
H(31C)	12713(4)	4145(4)	447(3)	89
H(11D)	6364(5)	708(4)	890(4)	106
H(11E)	5213(5)	1090(4)	198(4)	106
H(11F)	5454(5)	1529(4)	1073(4)	106

Table 10 Nozzle-to-plate distances (mm), weighting functions (nm^{-1}), correlation parameters, scale factors and electron wavelengths (pm) used in the electron diffraction study for both radicals.

	$P[CH(SiMe_3)_2]_2$		$As[CH(SiMe_3)_2]_2$	
Nozzle-to-plate distance[a]	247.93	497.94	247.93	497.94
Δs	4	2	4	2
s_{min}	40	16	40	20
s_{w1}	60	36	60	40
s_{w2}	244	122	228	94
s_{max}	284	142	268	114
Correlation parameter	0.161	0.436	0.32	0.317
Scale factor[b]	0.797(11)	0.665(7)	0.799(17)	0.746(12)
Electron wavelength	5.896	5.896	5.9	5.9

[a] Determined by reference to the scattering pattern of benzene vapour.

[b] Values in parentheses are the estimated standard deviations.

Table 11 Parameter and amplitude restraints for bis(disyl)phosphinyl (distances and amplitudes in Å; angles in degrees).

Data	Observed Value[a]	Computed Value[b]
p_2	0.002(1)	0.002(1)
p_4	-0.020(10)	-0.021(11)
p_5	108.1(10)	108.1(13)
p_6	105.2(10)	103.9(10)
p_7	109.6(10)	111.1(6)
p_8	111.3(10)	111.7(3)
p_9	0.2(10)	0.2(1)
p_{10}	0.5(10)	0.5(1)
p_{11}	2.5(10)	2.5(1)
p_{12}	2.2(10)	2.1(1)
p_{13}	-0.7(10)	-0.7(1)
p_{14}	111.4(5)	109.4(4)
p_{15}	1.6(10)	0.7(9)
p_{16}	17.0(10)	16.8(13)
p_{17}	1.0(10)	0.7(12)
p_{18}	1.0(10)	1.2(13)
p_{19}	121.5(10)	121.5(6)
p_{20}	1.2(10)	1.9(11)
p_{21}	36.8(10)	37.3(11)
p_{22}	118.6(10)	119.4(6)
p_{23}	-2.7(10)	-2.4(11)
p_{24}	49.9(10)	50.9(12)
p_{25}	114.2(10)	115.0(5)
p_{26}	0.4(1)	0.4(1)
p_{27}	-27.0(10)	-26.4(8)
u_1	0.055(6)	0.057(7)
u_2	0.055(6)	0.050(6)
u_4	0.078(8)	0.078(10)
u_{12}	0.087(9)	0.111(8)
u_{14}	0.080(8)	0.087(8)
u_{19}	0.101(10)	0.125(11)
u_{22}	0.144(15)	0.150(17)
u_{26}	0.101(10)	0.120(11)
u_{27}	0.213(20)	0.227(24)
u_{28}	0.155(15)	0.157(18)
u_{29}	0.172(17)	0.151(20)
u_{30}	0.165(16)	0.165(19)
u_{31}	0.114(11)	0.122(13)
u_{32}	0.301(30)	0.301(38)
u_{33}	0.106(11)	0.098(13)
u_{34}	0.161(16)	0.149(19)
u_{35}	0.289(29)	0.301(36)
u_{36}	0.251(25)	0.226(31)

Table 11 Continued

Data	Observed Value[a]	Computed Value[b]
u_{37}	0.102(10)	0.107(12)
u_{38}	0.343(34)	0.323(42)
u_{39}	0.376(38)	0.367(48)
u_{40}	0.196(20)	0.225(22)
u_{41}	0.234(23)	0.249(26)
u_{42}	0.103(10)	0.105(13)
u_{43}	0.259(26)	0.238(32)
u_{44}	0.176(17)	0.185(21)
u_{45}	0.124(12)	0.121(15)
u_{46}	0.218(22)	0.193(25)
u_{47}	0.268(27)	0.267(34)
u_{48}	0.447(45)	0.453(57)
u_{49}	0.181(18)	0.199(22)
u_{50}	0.514(50)	0.526(64)
u_{51}	0.186(18)	0.177(23)
u_{52}	0.195(20)	0.208(20)
u_{53}	0.115(11)	0.115(14)
u_{54}	0.089(9)	0.086(11)
u_{55}	0.362(36)	0.373(46)
u_{56}	0.121(12)	0.122(15)
u_{57}	0.112(11)	0.116(14)
u_{58}	0.120(12)	0.134(14)
u_{59}	0.119(11)	0.131(13)
u_{60}	0.120(12)	0.130(13)
u_{61}	0.431(43)	0.463(53)

[a] Value used as restraint with uncertainty in parentheses.

[b] Value observed in the refinement after restraint applied, with esd.

Table 12 Parameter and amplitude restraints for bis(disyl)arsinyl (distances and amplitudes in Å; angles in degrees).

Data	Observed Value[a]	Computed Value[b]
p_2	0.003(10)	0.003(12)
p_4	0.112(10)	0.107(9)
p_5	106.1(10)	106.4(12)
p_6	101.8(10)	100.6(10)
p_7	111.4(10)	110.4(6)
p_9	0.2(1)	0.1(1)
p_{10}	-2.3(10)	-3.0(9)
p_{11}	-2.6(10)	-0.6(9)
p_{12}	2.2(10)	1.5(9)
p_{13}	0.1(1)	0.1(1)
p_{15}	0.6(10)	0.6(11)
p_{16}	183.3(10)	183.5(12)
p_{17}	-2.0(10)	-4.2(11)
p_{18}	3.0(10)	4.2(11)
p_{19}	119.2(10)	120.2(6)
p_{20}	3.5(10)	2.3(11)
p_{21}	-72.0(20)	-72.9(19)
p_{22}	119.1(10)	119.6(6)
p_{23}	-2.2(10)	-1.2(11)
p_{24}	39.0(20)	41.5(17)
p_{26}	0.03(1)	0.04(1)
p_{27}	-25.0(10)	-25.3(9)
u_1	0.047(5)	0.042(6)
u_2	0.054(5)	0.052(6)
u_7	0.053(5)	0.053(6)
u_{12}	0.089(9)	0.120(9)
u_{13}	0.091(9)	0.120(9)
u_{14}	0.080(8)	0.095(9)
u_{23}	0.161(16)	0.162(20)
u_{24}	0.150(15)	0.157(18)
u_{25}	0.147(15)	0.131(18)
u_{26}	0.102(10)	0.099(12)
u_{27}	0.191(20)	0.192(23)
u_{28}	0.157(16)	0.159(19)
u_{29}	0.256(26)	0.255(30)
u_{30}	0.092(10)	0.097(11)
u_{31}	0.182(20)	0.159(22)
u_{32}	0.113(10)	0.118(12)
u_{33}	0.278(30)	0.283(34)
u_{34}	0.168(17)	0.164(20)
u_{35}	0.174(17)	0.169(20)
u_{36}	0.119(12)	0.114(14)
u_{37}	0.366(40)	0.368(48)

Table 12 Continued

Data	Observed Value[a]	Computed Value[b]
u_{38}	0.105(12)	0.105(14)
u_{39}	0.124(12)	0.123(15)
u_{40}	0.116(10)	0.119(12)

[a] Value used as restraint with uncertainty in parentheses.

[b] Value observed in the refinement after restraint applied, with esd.

Table 13 Least-squares correlation matrix (×100) for $P[CH(SiMe_3)_2]_2$.

	p_2	p_{19}	u_2	u_6
p_{11}	-76			
p_{29}		-70		
u_{12}				-60
u_{43}			-59	
k_2				50

[a] Only elements with absolute values >50% are shown; k_2 is a scale factor.

Table 14 Least-squares correlation matrix (×100) for $As[CH(SiMe_3)_2]_2$.[a]

	p_{11}
p_{19}	-51

[a] Only elements with absolute values >50% are shown.

Table 15 Experimental coordinates from the GED analysis for bis(disyl)phosphinyl and arsinyl radicals.

	Bis(disyl)phosphinyl			Bis(disyl)arsinyl		
Atom	*x*	*y*	*z*	*x*	*y*	*z*
Z(1)[a]	0.0000	0.0000	0.0000	0.0000	0.0000	0.0000
C(2)	1.4624	0.0000	1.1435	1.5344	0.0000	1.2611
C(3)	-1.4624	0.0000	1.1435	-1.5344	0.0000	1.2611
Si(4)	1.9219	-1.7999	1.5667	2.0311	-1.7563	1.7621
Si(5)	-1.9219	1.7999	1.5667	-2.0311	1.7563	1.7621
Si(6)	2.8331	1.1124	0.4350	2.9147	1.1645	0.7003
Si(7)	-2.8331	-1.1124	0.4350	-2.9147	-1.1645	0.7003
H(8)	1.1509	0.4704	2.1025	1.1649	0.4551	2.2022
H(9)	-1.1509	-0.4704	2.1025	-1.1649	-0.4551	2.2022
C(10)	2.1401	-2.7935	-0.0122	0.8896	-2.4505	3.0714
C(11)	-2.1401	2.7935	-0.0122	-0.8896	2.4505	3.0714
C(12)	3.5507	-1.9133	2.4951	2.0003	-2.8950	0.2757
C(13)	-3.5507	1.9133	2.4951	-2.0003	2.8950	0.2757
C(14)	0.6300	-2.6475	2.6308	3.7697	-1.8162	2.4558
C(15)	-0.6300	2.6475	2.6308	-3.7697	1.8162	2.4558
H(16)	2.4016	-3.8516	0.1996	1.2740	-3.4561	3.3266
H(17)	1.2195	-2.7896	-0.6332	0.7929	-1.8675	4.0068
H(18)	2.9606	-2.3565	-0.6196	-0.1173	-2.5653	2.6275
H(19)	-2.4016	3.8516	0.1996	-1.2740	3.4561	3.3266
H(20)	-1.2195	2.7896	-0.6332	-0.7929	1.8675	4.0068
H(21)	-2.9606	2.3565	-0.6196	0.1173	2.5653	2.6275
H(22)	3.4750	-1.3581	3.4537	2.7872	-2.5660	-0.4292
H(23)	3.8173	-2.9648	2.7324	2.2633	-3.9047	0.6440
H(24)	4.3888	-1.4739	1.9141	1.0447	-2.9647	-0.2778
H(25)	-3.4750	1.3581	3.4537	-2.7872	2.5660	-0.4292
H(26)	-3.8173	2.9648	2.7324	-2.2633	3.9047	0.6440
H(27)	-4.3888	1.4739	1.9141	-1.0447	2.9647	-0.2778
H(28)	-0.3390	-2.6797	2.0895	3.9835	-2.8774	2.6847
H(29)	0.9172	-3.6922	2.8740	4.5781	-1.4308	1.8060
H(30)	0.4657	-2.1095	3.5882	3.7842	-1.2461	3.4040
H(31)	0.3390	2.6797	2.0895	-3.9835	2.8774	2.6847
H(32)	-0.9172	3.6922	2.8740	-4.5781	1.4308	1.8060
H(33)	-0.4657	2.1095	3.5882	-3.7842	1.2461	3.4040
C(34)	2.0844	2.6353	-0.3747	2.2844	2.8067	0.0677
C(35)	-2.0844	-2.6353	-0.3747	-2.2844	-2.8067	0.0677
C(36)	3.9723	1.7790	1.7727	4.1003	1.4972	2.1120
C(37)	-3.9723	-1.7790	1.7727	-4.1003	-1.4972	2.1120
C(38)	3.8861	0.2391	-0.8476	3.8986	0.4000	-0.7008
C(39)	-3.8861	-0.2391	-0.8476	-3.8986	-0.4000	-0.7008
H(40)	1.5185	3.2210	0.3802	1.8142	3.3457	0.9119
H(41)	2.8641	3.2992	-0.8040	3.1709	3.3813	-0.2612
H(42)	1.3816	2.3657	-1.1910	1.5616	2.7730	-0.7693

Table 15 Continued

	Bis(disyl)phosphinyl			Bis(disyl)arsinyl		
Atom	*x*	*y*	*z*	*x*	*y*	*z*
H(43)	-1.5185	-3.2210	0.3802	-1.8142	-3.3457	0.9119
H(44)	-2.8641	-3.2992	-0.8040	-3.1709	-3.3813	-0.2612
H(45)	-1.3816	-2.3657	-1.1910	-1.5616	-2.7730	-0.7693
H(46)	3.4165	2.3668	2.5333	3.6652	1.9169	3.0387
H(47)	4.4713	0.9353	2.2945	4.6112	0.5491	2.3661
H(48)	4.7644	2.4330	1.3511	4.8570	2.2083	1.7300
H(49)	-3.4165	-2.3668	2.5333	-3.6652	-1.9169	3.0387
H(50)	-4.4713	-0.9353	2.2945	-4.6112	-0.5491	2.3661
H(51)	-4.7644	-2.4330	1.3511	-4.8570	-2.2083	1.7300
H(52)	4.3723	-0.6694	-0.4337	4.3587	-0.5869	-0.5048
H(53)	3.2510	-0.0759	-1.7024	3.2332	0.3051	-1.5798
H(54)	4.6850	0.9003	-1.2444	4.7043	1.1161	-0.9503
H(55)	-4.3723	0.6694	-0.4337	-4.3587	0.5869	-0.5048
H(56)	-3.2510	0.0759	-1.7024	-3.2332	-0.3051	-1.5798
H(57)	-4.6850	-0.9003	-1.2444	-4.7043	-1.1161	-0.9503

[a] Where Z = P or As.

Table 16 Theoretical geometrical parameters for bis(disyl)phosphinyl and bis(disyl)-arsinyl[a] at the 6-31G*/UHF and UHF/DZP levels.

	6-31G*/UHF		UHF/DZP	
Parameter	PCS	ASCS	PCS	ASCS
Z(1)-C(2)[b]	1.876	1.984	1.873	2.004
C(2)-Si(4)	1.92	1.909	1.92	1.915
C(2)-Si(6)	1.924	1.914	1.924	1.917
Si(4)-C(10)	1.893	1.898	1.893	1.898
Si(4)-C(12)	1.898	1.893	1.898	1.894
Si(4)-C(14)	1.897	1.897	1.897	1.898
Si(6)-C(34)	1.895	1.897	1.895	1.897
Si(6)-C(36)	1.896	1.895	1.897	1.897
Si(6)-C(38)	1.895	1.895	1.894	1.895
C(2)-H(8)	1.09	1.089	1.09	1.09
C-H[c]	1.087	1.087	1.087	1.087
C(2)-Z(1)-C(3)	105.2	102	105.2	102.9
Z(1)-C(2)-H(8)	108.1	107.2	108	106.2
Si(4)-C(2)-Si(6)	116.3	117.5	116.3	117.1
C(2)-Si(4)-C(10)	112.4	110.4	112.5	109.9
C(2)-Si(4)-C(12)	111.9	112.2	111.9	112.5
C(2)-Si(4)-C(14)	109.9	112.1	109.9	112.1
C(2)-Si(6)-C(34)	111.8	111.4	111.8	112
C(2)-Si(6)-C(36)	109.6	109.8	109.5	109.7
C(2)-Si(6)-C(38)	112.3	112.1	112.4	112
SiCH[c]	111.4	111.5	111.5	111.5
H(8)-C(2)-Z(1)-C(3)	-27	-26.5	-26.9	-26.4
Z(1)-C(2)-Si(4)-C(10)	49.9	-71.2	50.1	-71.2
Z(1)-C(2)-Si(6)-C(34)	36.7	36.4	36.3	37
Absolute Energy[d]	-2048.7907	-3940.0896	-2048.8	-3942.22

[a] All distances in Å, all angles in degrees. See Fig. 1 for atom numbering.

[b] Where Pn = P or As.

[c] Weighted average of all values.

[d] Energy in Hartrees.

Table 17 Extra observations used for both bis(disyl)phosphinyl and arsinyl radicals.

	Bis(disyl)phosphinyl		Bis(disyl)arsinyl	
Data	Observed Value[a]	Calculated Value[b]	Observed Value[a]	Calculated Value[b]
C(2)-Si(4)-C(10)	112.4(10)	109.9(3)	112.1(10)	111.7(4)
C(2)-Si(4)-C(12)	111.9(10)	112.1(3)	110.4(10)	111.6(4)
C(2)-Si(4)-C(14)	109.9(10)	112.7(3)	112.2(10)	110.2(7)
C(2)-Si(6)-C(34)	111.7(10)	110.3(3)	111.4(10)	113.1(7)
C(2)-Si(6)-C(36)	109.5(10)	112.3(3)	109.8(10)	110.0(6)
C(2)-Si(6)-C(38)	112.3(10)	112.8(3)	109.8(10)	110.6(7)
Si(4)-C(2)-Si(6)	116.3(10)	117.5(5)	117.5(10)	115.2(9)
C(10)-Si(4)-C(12)	108.2(10)	106.4(7)	107.9(10)	108.7(9)
C(10)-Si(4)-C(14)	108.4(10)	108.5(10)	105.5(10)	107.4(7)
C(12)-Si(4)-C(14)	105.6(10)	106.8(7)	108.6(10)	107.2(7)
C(34)-Si(6)-C(36)	106.3(10)	105.1(10)	107.0(10)	108.4(7)
C(34)-Si(6)-C(38)	106.9(10)	107.8(7)	106.7(10)	106.6(9)
C(36)-Si(6)-C(38)	109.8(10)	108.2(7)	109.7(10)	107.9(7)

[a] Value used as restraint with uncertainty in parentheses.

[b] Value observed in the refinement after restraint applied, with esd.

Appendix 7

Publications.

1,1,2-tri-tert-butyldisilane, $Bu^t_2HSiSiH_2Bu^t$: Vibrational spectra and molecular structure in the gas phase by electron diffraction and ab initio calculations.

S. L. Hinchley, B. A. Smart, C. A. Morrison, H. E. Robertson, D. W. H. Rankin, R. Zink and K. Hassler, *J. Chem. Soc., Dalton Trans.*, 1999, 2303.

1,2-di-tert-butyltetrachlorodisilane, $Bu^tCl_2SiSiCl_2Bu^t$: Vibrational spectra and molecular structure in the gas and crystalline phases by electron diffraction, ab initio calculations and X-ray diffraction.

S. L. Hinchley, B. A. Smart, C. A. Morrison, H. E. Robertson, R. A. Coxall, S. Parsons, D. W. H. Rankin, R. Zink and K. Hassler, Manuscript in Preparation.

Persistent phosphinyl radicals from a bulky diphosphine: An example of a molecular Jack-in- the-box.

S. L. Hinchley, C. A. Morrison, D. W. H. Rankin, C. L. B. MacDonald, J. A. C. Clyburne, R. Wiacek, A. H. Cowley, M. F. Lappert, G. Gundersen, J. A. C. Clyburne and P. P. Power, *Chem. Comm*, 2000, 2045.

Breaking P-P and As-As bonds to give stable radicals: A structural study of some disyl phosphorus and arsenic compounds.

S. L. Hinchley, C. A. Morrison, D. W. H. Rankin, C. L. B. MacDonald, J. A. C. Clyburne, R. Wiacek, A. H. Cowley, M. F. Lappert, G. Gundersen, J. A. C. Clyburne and P. P. Power, Manuscript in Preparation for *J. Am. Chem. Soc.*.

Molecular structure of tris(tert-butyl)sulfurdiimide, $S(NBu^t)_3$, in the solid and gas phases.

S. Freitag, D. Stalke, M. Buhl, W. Thiel, S. L. Hinchley, H. E. Robertson, B. A. Smart, C. A. Morrison and D. W. H. Rankin, Manuscript in Preparation.

Planar 1,2λ4δ2,2,4-benzodithiadiazine and its non-planar 5,6,7,8-tetrafluoro derivative: Gas phase structures studied by electron diffraction and ab initio calculations.

F. Blockhuys, S. L. Hinchley, A. Y. Makarov, Y. V. Gatilov, A. V. Zibarev, J. D. Woollins and D. W. H. Rankin. Submitted to *Chem. Eur. J.*

Molecular structure of bis(trichlorosilyl)tert-butylphosphine, $P(SiCl_3)_2Bu^t$, in the gas phase determined by electron diffraction and ab initio calculations.

S. L. Hinchley, H. E. Robertson, D. W. H. Rankin, L. Müller, R. Martens and Wolf-W. du Mont. Manuscript in Preperation.

Appendix 8

Conferences and Courses Attended.

Courses Attended

- Unix 1, 1997
- Unix 2, 1997
- Unix 3, 1998
- Prof. S. K. Chapman: Bioinorganic Chemistry, 1998
- Introduction to HTML, 1999
- University of Edinburgh Inorganic Section Meetings, 1997 – 2000

Conferences Attended

Universities of Scotland Inorganic Club (USIC) Conference
University of Strathclyde, September, 1998
Poster Presentation: Disilane in Double Conformer Shocker!

Royal Society of Chemistry, Dalton Division Symposium
University of Strathclyde, December, 1998

8th European Symposium on Molecular Structure
Blaubauren, Germany, June, 1999
Poster Presentation: "Radically" Different Structures

Universities of Scotland Inorganic Club (USIC) Conference
University of Heriot Watt, September, 1999
Poster Presentation: Two's Company, Three's a Crowd, Four Leads To Break-ups (Poster Prize)

18th Austin Symposium on Molecular Structure
The University of Texas at Austin, Texas, USA, March, 2000
Oral Presentation: Small Molecules are Not Enough

Universities of Scotland Inorganic Club (USIC) Conference

University of Glasgow, September, 2000

Oral Presentation: *M: I3*

Highlights of Chemistry Research and R&D by Younger Chemists in 2000

Royal Society, London, November, 2000

Poster Presentation: The Conundrum of a Weak-Strong Bond; A Chemical Jack-in-the-box

(Poster Prize)